An information analysis of the interaction between sensory signals and ongoing cortical activity using a novel mechanistic cortical model, behavioural and MEG studies

Michael Dempster
MNeuro MSci

Submitted in fulfilment of the requirements for the
Degree of Doctor of Philosophy in Psychology

School of Psychology
College of Science and Engineering
University of Glasgow

April 2013

Abstract

In this work I present a novel mechanistic cortical model derived from the most current cortical anatomical data. The model is built at the cellular level representing the mean laminar distribution and connectivity of the neocortex. From this model I derive an extracellular field potential signal and simulate ongoing cortical activity using top down, local and bottom up sensory input. An information theoretic analysis is applied to the simulation data in the context of a bottom up input. This identifies a relationship between cortico-cortical oscillatory activity across a number of frequencies and the information contained in spiking neurons that have long range afferent connections. From these model predictions three auditory perception experimental paradigms are developed, implemented and analysed. I show that the behavioural data is explained by the model predictions and offer a mechanistic explanation of the effect derived from model behaviour. I perform an information analysis on magnetoencephalography data acquired from a simple 50 % auditory perception task and demonstrate prestimulus ongoing activity frequency power and phase features facilitate perception. In addition there is evidence of attention related interaction between the auditory and visual early cortices.

Contents

0.1 List of tables

List of Tables

0.2 List of figures

List of Figures

0.3 Acknowledgements

First and foremost I express my fullest and utmost gratitude to my supervisor Professor Joachim Gross. Throughout my research he has given me guidance and support through the challenges I have faced both in my work and matters outwith my work. During the time I have carried out my research under his supervision I have faced bereavement and physical illness that impacted upon my ability to consistently carry out my work. For all the patience, understanding and belief you have shown me Joachim, I am deeply thankful.

Working in Joachims lab group I have had the opportunity to meet a number of excellent people who are past and present members of his research group. I would like to thank them all for their conversation and inspiring work. In particular I would like to thank Dr Gavin Paterson for all his help with my work in the MEG and in helping me overcome any mishaps I faced with hardware. I would also like to thank Dr Jan-Mathijs Schoffelen for his help with using field trip. I would also like to thank Jo for all her help in acquiring my behavioural data.

Working within Glasgow University's psychology department has been a wonderful experience and I have found many friends, knowledgeable and kind people within both the academic and non academic staff. In particular the computing support group has been a great help in keeping my many software and hardware demands satisfied.

Through attending and presenting to the numerous research seminars, I have found a wide number of people who have influenced my work by providing questions, discussions and suggestions or by presenting their own work in an inspiring way. I would especially like to thank Dr Luisa Frei, Dr Carl Gasper and Dr Oliver Garrod for taking an interest in my research and for many conversations research related and otherwise.

Finally I would like to thank my parents, Michael Dempster, Rose Anne Dempster and Andy Smith, my brothers, Stephen and Jamie, and Rachael, my partner, for all their love and support during the period of this research.

0.4 Author's declaration

I declare that, except where explicit reference is made to the contribution of others, that this dissertation is the result of my own work and has not been submitted for any other degree at the University of Glasgow or any other institution.

Signature Michael Dempster

Printed name Michael Dempster

Chapter 1

Introduction

Measurement of magnetic and electrical field potentials provide experimental neuroscience with a unique insight into the physiological activity of the working brain. Magnetoencephalography (MEG) and electroencephalography (EEG) allow us to study the magnetic or electrical field produced by the whole brain whilst extracellular electrophysiology gives us access to local field potentials (LFP) produced by approximately one cubic millimetre of neural tissue (Kandel, 2000). All of these measurements can be resolved at the millisecond scale. However, due to the nature of these signals and the means of attaining them, a number of challenges associated with experimental design and data interpretation present themselves.

In this work I will address three of these challenges. The first of these is the question of what the signals actually represent. When measuring a field potential you are determining the potential difference in the field between a single point in space and a reference point (Mizdorf, 1985). As such any field potential measurement presents us with the inverse problem, i.e. the potential number, location and strength of the field sources are infinite. Fortunately there are a wealth of anatomical and physiological studies that present us with the opportunity to constrain the potential sources of a given signal.

A second challenge is to the integration of information from previous studies and experimental design posed by the scale and the invasiveness of the various methods of measurement. Small scale investigations into neuroelectrophysiology tend to require invasive methods, and as such are carried out in animal models. Large scale investigations tend to require a larger number of sensors that are placed outside the brain, and as such are non-invasive and thus available for use in human experimental participants. As a result of this there tends to be little communication between the two areas of research. However there is a large degree of anatomical and physiological generalities in

mammalian brains that may allow us to have a basis of comparison between the research fields(Thomson, 2003; Thomson, 2007). A further complication is the difficulty in comparing results from different scales. Metrics representing widely varying measurement regimens and physical quantities can be difficult to compare, as can statistical interpretation of results. Recent application and development of information theory techniques have been shown to provide a robust model free basis of comparison between different metrics (Panzeri et al., 2008; Magri et al., 2009).

A third challenge is from the high level of variability in a recorded field potential signal(Busch, 2009; Curto, 2009). A given neural source produces its signal in the context of a high number of neural sources that produce signals of comparable strength that are not related to the experimental paradigm. This has been termed ongoing activity. What's more is that recent work has shown that ongoing activity impacts on the perception of stimuli and may contribute to a neural coding scheme (Fries et al., 2007; Montemurro et al., 2008; Vinck et al., 2010; Vanrullen et al., 2011).

The aim of this work is to address these issues through computer modelling. A traditional approach to using modelling in neuroscience is to perform an experiment and develop a model to fit the data during the analysis phase of the experimental process and use the model for interpretation of the results (figure 1.1, top.) I have taken the approach of deriving a model from anatomical and physiological experimental data, exploring the model its self and using it as a forward model to develop an experimental paradigm to be carried out with human participants, make predictions of the results from the model and compare them to the model(figure 1.1, bottom.)

In chapter 2 I present a novel mechanistic cortical model derived from the most current cortical anatomical data. The model is built at the cellular level representing approximately three cubic millimetres of neocortex. Using this model I explore the parameter space with the aim of extracting spiking activity and, within the confined of the model, a signal representative of the extracellular field potential. The model encompasses the mean laminar distribution and connectivity of the neocortex. Due to the high number of cells in these simulations I restrict my cellular investigations to the average cell from each subpopulation.

In order to derive model behaviour that may be considered analogous to realistic extracellular signals I develop and characterise the model's response to a variety of input conditions to simulate biological ongoing activity.

In chapter 3 I then investigate the response of the model in the simulated ongoing activity state to a simple simulated sensory input. I investigate the spiking and simulated field potential response and quantify this using information theory. Lastly I investigate the response of the model to a sensory

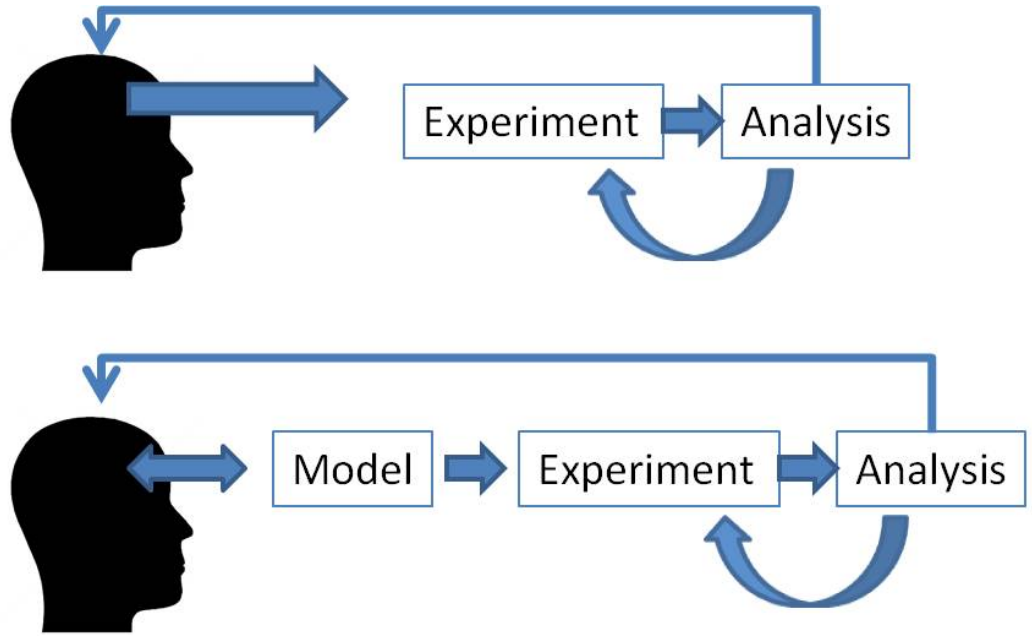

Figure 1.1: **Two experimental approaches** *(Top) an experimental paradigm is developed in the context of a theory and hypothesis, the experiment is carried out, analysis and refinement of the experiment until it addresses the theoretical issue being tested, develop a new experiment. (Bottom) a computer model is used in the context of theory to explore and develop the paradigm and make predictions before the experiment is performed.*

input in the context of ongoing activity and an inter-cortical oscillatory input. This is also quantified using information theory.

In chapter 4 from the results of the work with the model I derive a number of testable hypotheses from which I develop three experimental paradigms. Two of which relate to induced auditory steady state response (ASSR) cortical oscillations and the phase related perception of a near threshold stimulus. These were carried out as behavioural experiments. The results of the experiment most closely related to the model work are predicted by the results from the model. Next I carried out two MEG experiments derived from the model. The ASSR paradigm was unsuccessful due to problems delivering an equivalent stimulus. The second MEG experiment demonstrates that perception of a near threshold stimulus is dependent upon the power and phase of particular frequency components in preceding ongoing activity. This was shown using information theory.

In this introductory chapter I will discuss firstly cortical anatomy and the sources of the field potential signal. Secondly the role of modelling and mechanistic cortical modelling.

1.1 Cortical anatomy and the field potential signal

Some of the descriptive text and figures in this section have been adapted from (Dempster, 2007).

1.1.1 Field potentials and the field potential signal

Electrophysiological signals are obtained by measuring the potential difference between a specific spatial position and a suitable ground. In the EEG this is measured from the scalp, whilst in the LFP it is measured from within the neural tissue. The electric field for a particular spatial location is defined by the location and charge of all charged particles within the system. The electric fields of the individual charges are summed, weighted by the distance of each charged particle from the measuring location. When there is a change in the membrane conductance due to the opening of transmembrane ion channels ionic current flows across the membrane to a new equilibrium in accordance with the Nernst equation(Dayan and Abbott, 2001). Accordingly there is a change of ionic concentration in the intracellular fluid. This leads to an equal and opposite current in more distant regions of the cell in accordance with Kirchovs law(Trappenberg, 2002). A region in which the current is into the cell is know as a sink and a region in which the current

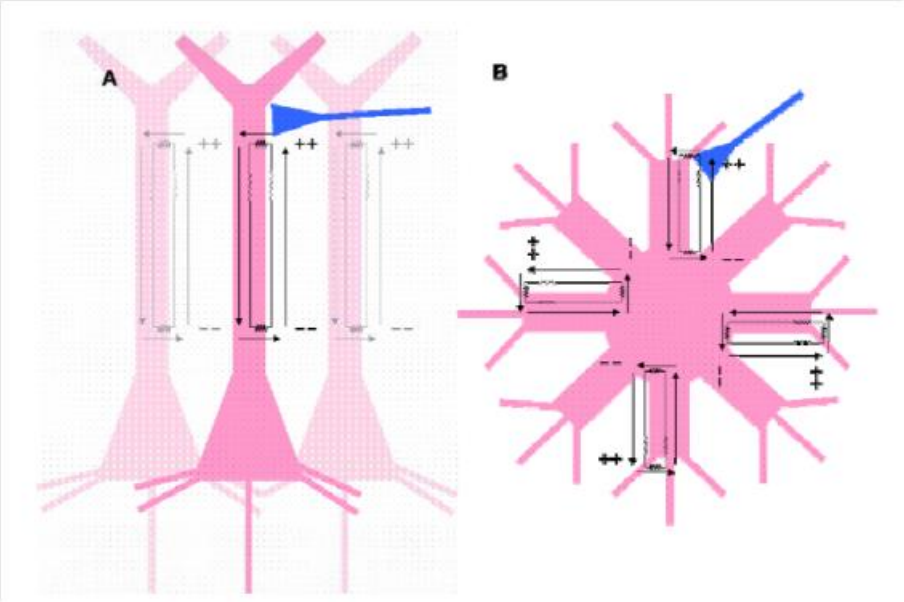

Figure 1.2: **Basic current flow in pyramidal and stellate cells.** *The blue connection represents an afferent synaptic connection to the dendrite of a cell. The small circuit diagrams show the resultant direction of current flow within and outwith the dendrite due to a synaptic event. (A) is a pyramidal cell and (B) is a stellate cell.*

is out of the cell is know as a source (Mitzdorf, 1985, , 1987). Figure 1.2 illustrates these currents.

The fast currents involved in the action potential create stereotypical biphasic or triphasic fluctuations in the measured voltage. These events have to be quite close to an extracellular measuring electrode to affect the voltage measurement due to the comparatively weak field. The fields generated by the synaptic currents tend to cancel out for cells with radial dendritic arbores(Mitzdorf, 1985, , 1987). This is known as a closed field configuration 1.2 (B). However synaptic currents in cells with dendritic extension in largely one direction, open field configuration, affect the electromagnetic field in an altogether different manner.

As mentioned above pyramidal cells have a stereotypical pattern of dendritic arbourisation. Synchronized synaptic input to the apical dendrites of a single cell results in the creation of a strong dipole along the major axis of the apical dendrites as shown in figure 1.2 (A). As the time course of synaptic ion channels opening and closing is reasonably long compared to those involved in the action potential, the dipole persists. Pyramidal cells are all orientated perpendicularly to the pial surface, whenever there is a synchronized

net current input to all cells these sum to produce a strong electromagnetic field. These slow fluctuations make up the large part of the LFP. There are other membrane phenomena that contribute to slow fluctuations in the electromagnetic field these are detailed in (Kobayashi et al., 1997; Kamondi et al., 1998a; Kamondi et al., 1998b) and will not be discussed here.

Oscillations in neural activity are a widely observed phenomenon across a variety of systems in a broad range of frequencies during many behavioural states. Oscillatory behaviour occurs in both spiking and field potentials. The frequency range has traditionally been subdivided into a number of different classes. Namely alpha (8-13 Hz), beta (13-30 Hz), delta (0.5-4 Hz), gamma (30-70 Hz) and theta (4-7 Hz)(Buzsaki, 2006). The mechanisms behind cortical oscillations are not fully understood. A variety of mechanisms have been proposed. One possibility is that activity is driven by a subpopulation of cortical cells that have intrinsic oscillatory properties(Buzsaki, 2006). Cells have been found in the rat frontal cortex that exhibit subthreshold oscillation and in cat striate cortex which fire in regular bursts in response to visual stimulation(Buzsaki, 2006). Another possibility is that the oscillations arise from the properties of the local intracortical network. Experimental evidence for this is detailed in (Steriade et al., 1993)where they also outline evidence from work done with neural networks.

1.1.2 Cortical Anatomy

The neocortex is an outgrowth of the telencephalon that makes up a significant portion of the mammalian brain. It is the most prominent feature of the primate and human brain, making up over half of the brain mass. Function can be localized, but a particular function does not have to be performed by a particular part of the cortex. For example, language areas of the brain can usually be found in the left mediotemporal cortex, but this is by no means the case for everyone. Function can be in other areas of the brain or entirely non-local (Herron, 1980). This is not limited to higher cortical areas primary sensory areas can be made to develop the response properties of another modality. It has been shown that the auditory cortex of neonatal ferrets can perform functions of the visual cortex when the normal auditory input is replaced with visual projections (Sur, 1988; Sur et al., 1988). Similar findings have been shown in visual cortex for somatosensory inputs(Schlaggar and O'Leary, 1991). This level of plasticity in function is not limited to the developing cortex, there is also much evidence of it occurring in the adult (Phillips and Singer, 1997). The ability of the cortex to adapt to a variety of computational functions strongly suggests that there may be information processing operations common to all areas of the cortex. Support for this

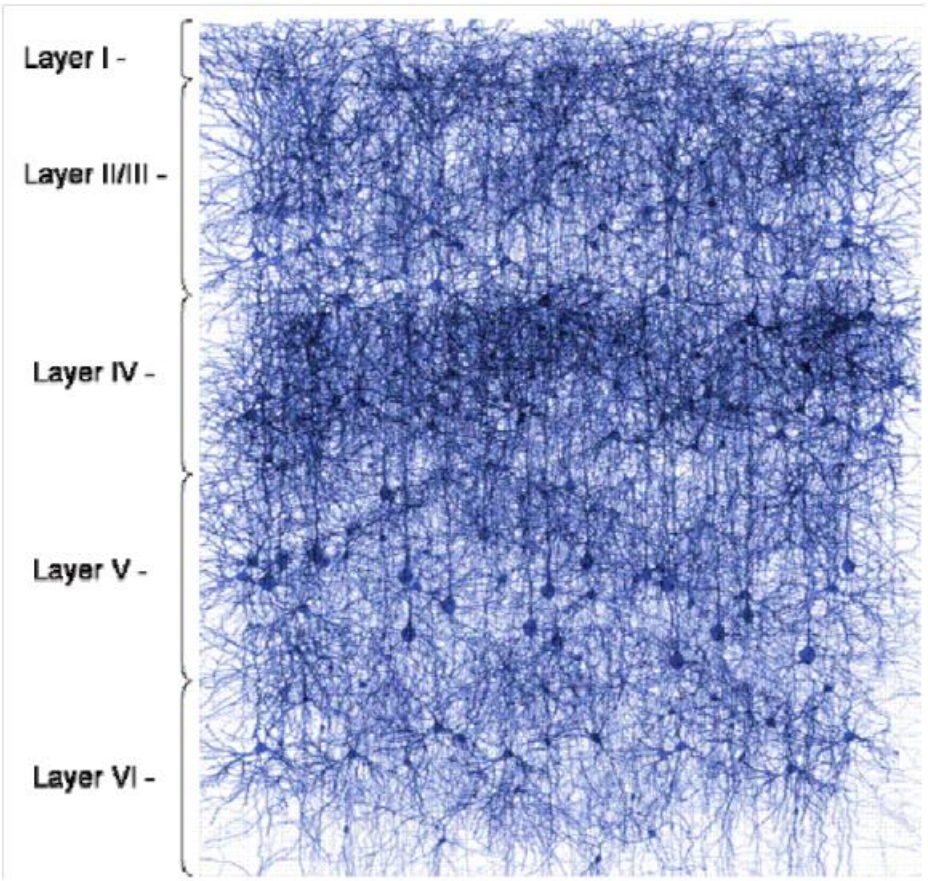

Figure 1.3: **The laminar structure of the neocortex** *(Image from IBM blue brain website: http://bluebrain.epfl.ch/)*

viewpoint comes upon closer inspection of the anatomy and physiology of the cortex. At various levels of inspection there are many features that are consistent across cortical areas, between individuals and across species.

The neocortex develops from a sheet of cells into 6 layered structure, there are some variations in the thickness of the layers depending on which part of cortex, but it is always 2-4mm thick(Kandel et al., 2000). A detail of the cortex where the layers are clearly visible is shown in figure 1.3. Each layer is composed of a particular species of cell. The cells present in the neocortex can be classified into two distinct types depending on the scope of their connections. Projection neurons synapse with neighboring cells and distant cortical and subcortical areas, and local interneurons synapse only locally.

Pyramidal cells constitute the bulk of projection neurons. Pyramidal cells make up approximately 70% of cortical neurons and their cell bodies can be

found in layers II-VI. They have a pyramid shaped cell body when viewed in cross section. Dendritic arbourisation is characterized by projections from the apex of the pyramid which extend up through the higher layers of the cortex, and basal projections which extend horizontally within the layer. The axonal projection emerges from the base of the cell. The synapses they form are excitatory and are mediated by glutamate(Kandel et al., 2000).

Local interneurons characteristically have dendritic arbourisations that project radially from the cell body. The local interneurons can be further subdivided into excitatory and inhibitory interneurons. Excitatory interneurons make up 10 percent of cortical neurons and are largely spiny stellate cells. These cells form glutamatergic synapses and their cell bodies are found in layer IV. Inhibitory interneurons, which make up the remaining 20 % of cortical neurons, are a morphological and physiological heterogeneous group that can be found in all layers of the cortex. The majority of synapses formed by interneurons are GABAergic, but many are non-GABAergic. In addition to this some interneurons have been found to contain more than one neuroactive substance(Kandel et al., 2000).

Cortical neurons can also be classified due to their spiking properties under tonic stimulation. Spiny neurons, pyramidal and spiny stellate cells, display spike rate adaptation. This is a reduction in interspike interval times when the neuron is repetitively firing. Local cortical connectivity is sparse and specific. Whilst a simple repeating microcircuit is not immediately apparent, there are some gross features of interlaminar excitatory and inhibitory connectivity that have been established in the literature. This model will account for 3 of the layers of the neocortex For a review of laminar structure see Thomson and Bannister (Thomson and Bannister, 2003).

Recent work using paired and triple intracellular recordings in association with dye filling techniques has revealed the connectivity ratios of cells of different classes within the neocortex and the post synaptic potential properties and latencies (Thomson et al., 2002; Thomson and Lamy, 2007). This work was performed in multiple regions of cortex of both the rat and the cat. Whilst this work details the major connections, it should be noted that connections which occur with low frequency but significantly affect the network behaviour may have been overlooked (Haeusler and Maass, 2007).

1.2 Neuronal modelling

In this section I will outline some of the approaches taken in cortical modelling used to gain insight into the mechanisms of external oscillatory signals. Firstly I will look at the neural mass model approach, secondly I will look at

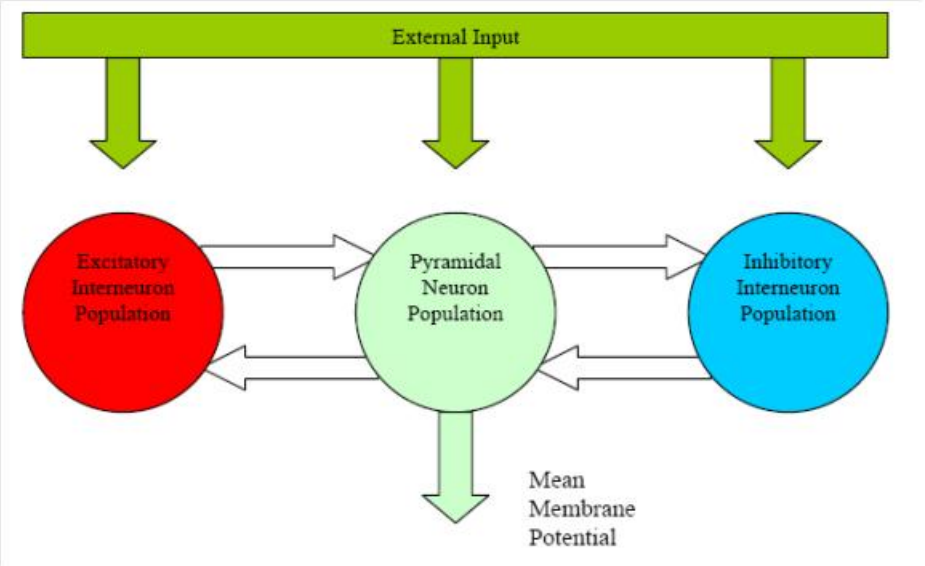

Figure 1.4: **A simplified cortical microcircuit** *The extended Jansen model showing two populations of interneurons, excitatory and inhibitory, and a population of pyramidal neurons*

the full conductance model and thirdly I will look at the leaky integrate and fire model used in this work.

Some of the descriptive text and figures in this section have been adapted from (Dempster, 2007).

1.2.1 Mass models and dynamic causal modelling

The neural mass model was introduced by Lopes da Silva et al in the (Lopes da Silva et al., 1974). They developed a mathematical model inspired by cortical biology to simulate alpha activity in the EEG. Their model consisted of two modules representing a population of excitatory neurons and a population of inhibitory interneurons. A module consists of two equations, the first representing the transformation of an input mean firing rate into a mean membrane potential and the second transforming the mean membrane potential of the population into a mean firing rate to be output to the other module. The field potential is taken as the value of the mean membrane potential of the excitatory population.

This model was extended by Jansen et al to include an additional excitatory population that is named the excitatory interneurons module (shown in figure 1.4)(Jansen et al., 1993; Jansen and Rit, 1995). This module represents the excitatory feedback within the local cortical circuit, so formally

this represents both excitatory interneurons and pyramidal cells. Each of the connections between the modules are weighted by a factor that represents the relative strength of synaptic connectivity derived from biological data available at the time. Jansen shows that this system demonstrates a wide range of oscillatory behavior when all three modules receive a random noise input by varying the connectivity constant. Jansen develops the model further by coupling two of these models together to represent two different areas of the cortex. This configuration involves taking the mean firing rate of the pyramidal cell module of one unit and using it as an additional input to all the modules of the second unit. These interunit connections are weighted by individual weighting factors. Using coupled units and varying the weights of the interconnection Jansen et al are able to elicit a wider range of oscillatory behavior. Another feature of this system is that by applying an impulse to a single unit a response similar to the evoked potential can be shown.

Jansens cortical unit has been used by a variety of researchers to study field potential activity. David et al expanded the detail of the interunit connectivity to express the whole spectrum of EEG signals and investigate the mechanisms of the event related potential (David and Friston, 2003; David et al., 2005; David et al., 2006a). Figure 1.5 shows the hierarchical connectivity utilized in this study. Dempster and Panzeri (Dempster, 2006) carried out an investigation of information propagation in each of the hierarchical arrangements using Poisson spike generated input derived from firing rates measured from the rat barrel cortex under different stimulus conditions. They also demonstrated that specific LFP features could be fitted to specific model architectures.

The neuronal mass model has and continues to prove useful in the investigation of field potential generation and compared to other mechanistic models it is not computationally intensive. Jansen mentions that the assumptions made in this model do not verify it as the mechanism behind cortical oscillations and suggests that further verification be made (Jansen et al., 1993; Jansen and Rit, 1995). One method of verification would be to compare the behaviour of a model of finer detail. Also it does not directly model individual cells so it cannot provide insight into the cellular and subcellular mechanisms responsible for field potential signals, nor can it give a spatial component to the model. The model developed in this work would provide a suitable basis of comparison for further verification of this model.

1.2.2 Hodgkin-Huxley conductance models

An approach which places a far greater emphasis on the subcellular mechanisms of the individual cells within a network are those that use models based

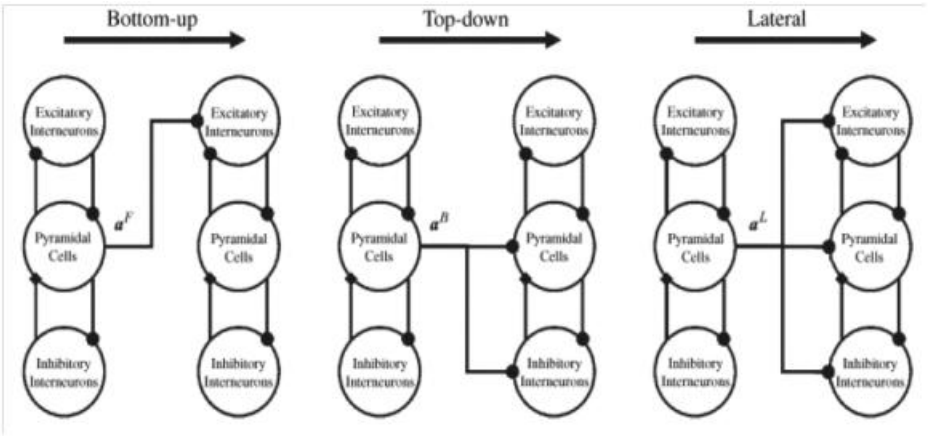

Figure 1.5: **Hierarchical connectivity in a mass model***Each of the three network models show coupled mass models in (left) a bottom up configuration, (middle) a top down configuration and (right) a lateral connection. (from David et al., 2005)*

on the dynamics of transmembrane ion channels as described by Hodgkin and Huxley in 1952 (Hodgkin and Huxley, 1952d, 1952e, 1952f, 1952a, 1952b, 1952c; Hodgkin et al., 1952).

In these models individual cells are modelled in compartments where dimensionality of the individual cells can be reproduced and internal cellular currents are directly modelled.

Wilson and Bower have explored neural oscillations in models of the piriform cortex and the visual cortex (Wilson and Bower, 1992; Koch and Davis, 1994a; Koch and Davis, 1994b). These models are identical in all aspects with the exception of the spatial extent of the association fibres, in the visual cortex model these fibres are more spatially limited. There are three cell types in the model organized in a two dimensional matrix. The largest is the five compartment pyramidal cell model with three linked compartments representing the apical dendrites and two opposite representing the basal dendrites. The other two cells types were feed forward and feed back inhibitory interneurons, these were modelled as single compartments. Connections with the pyramidal cells were compartment specific. The main findings of these models are that oscillations typical of the EEG arise from the network under both phasic and tonic external input and that inhibitory feed back is essential in the production of oscillatory behaviour.

A major advantage to this type of modelling is that due to the spatial components of the model, i.e. cell location and the apical segments extending perpendicular to the sheet of neurons the field potentials can be derived

directly from the discrete currents rather than using the mean membrane potential of the population. This also allows the measuring electrode to be placed in different places within the plane of neurons.

Due to limitations in computational power there were many reduced representations used in the implementation of the model used in this study. Due to the high computational demand of multicompartmental Hodgkin-Huxley conductance based models any approach which requires many repeated simulations of large scale networks is precluded.

1.2.3 Leaky integrate and fire models

The leaky integrate and fire model of the neuron is a widely used model for the study of neural systems(Dayan and Abbott, 2001). This model offers a simple description of the spiking behaviour of a given cell and concentrated on the subthreshold dynamics of the membrane potential. This approach allows the development of cellular models with realistic temporal characteristics.

The main features of the model are the capacitive properties of the membrane, a leak current and a current representing the synaptic input. Each current is defined by the change in conductance of each element and the difference in voltage between the instantaneous membrane potential and the reversal potential of that element(Dayan and Abbott, 2001).

Other currents can be added to this circuit to adapt the model to properties of specific neuron classes. The afterhyperpolarisation current models post spike afterhyperpolarisation by resetting a conductance that decays exponentially to a maximum value each time the neuron spikes. The spike rate adaptation current models spike rate adaptation in regular spiking neurons by increasing an exponentially decaying conductance each time the neuron spikes. This results in a polarizing current that increases with the firing rate, thus dampening the firing rate as time goes on(Dayan and Abbott, 2001). The specific equations of the leaky integrate and fire model used in this study are introduced in chapter 2.

As the leaky integrate and fire model is relatively simple it allows analytical explorations of simple networks. Oscillations in networks have largely been found to arise as the result of interactions between excitatory and inhibitory neurons. In a network of sparsely connected 80% excitatory and 20% inhibitory simple leaky integrate and fire neurons Nicolas Brunel has demonstrated a wide range of states (Brunel and Hakim, 1999). These include synchronous regular firing, asynchronous firing with no global signal, and global oscillation with irregular firing of the individual neurons. Further work has shown that detailed single-cell properties have a substantial impact on population oscillations (Brunel and Hakim, 1999; Brunel, 2000; Brunel

and Wang, 2003). In particular the synaptic dynamics and the balance between excitation and inhibition play a key role.

As the models of individual neurons become more detailed in order to characterize a particular species of neuron and network connectivity becomes more biologically inspired, current analytical techniques become limited in their scope and numerical simulation can play an important role in the discovery of the properties of the system (Burkitt, 2006b, 2006a)

Chapter 2

A novel mechanistic cortical model

2.1 Chapter introduction

The aim of this chapter is to introduce a novel mechanistic model with simulated neural signals comparable to biological extracellular signals and spiking data. This in order to be able to develop an experimental model paradigm suitable for comparison with a biological experimental paradigm.

The model will represent a laminar volume of neocortex of approximately 3 cubic millimetres, or 3000 cells. The principle signal investigated is a corollary of the electromagnetic field potential. This is interpreted as an LFP/EEG/MEG signal.

First I will run simulations with an independent Gaussian white noise stimulus applied to each cell. I will then present simulations with varying means and standard deviations of the white noise stimulus. This is within the range that best produces subthreshold responses most similar to cells in a biological cortical network(Okun et al., 2010).

Secondly I will address the question of whether or not the network can be scaled to represent a larger proportion of cortex by uniformly increasing synaptic weights.

Thirdly I will explore network activity and its impact upon network behaviour. In this section I remove all synaptic connections, only the excitatory connections and only the inhibitory connections to observe the contribution each cell type gives to the network behaviour.

Lastly I will consider the response properties of ongoing field potential and spiking activity. These investigations group the network according to three input standard deviation conditions. The first is a low input standard

deviation condition, the second is a mid range input standard deviation condition and the third is a high input standard deviation condition. In each of these conditions a range of input means.

2.2 Introduction to the model

In this section I will detail the individual cell models used in the network model, the network connectivity, the simulation environment, the inputs used for the network, the output derived from the simulations and the analysis packages used.

2.2.1 Individual cells

The basic individual neuron model employed in the modelling portion of the project is the leaky integrate and fire (LIF) model. The individual cell model is described in equations 2.1 - 2.4. This is a one dimensional description of the biophysical properties of the neuron. The equilibrium distribution of ions across the cell membrane results in a build up of negative ions on the internal surface of the lipid membrane and positive ions along the external surface. The result is a capacitive effect with a measurable membrane capacitance. This can be considered a constant as the ions available internally and externally are much larger than those involved in information processing. The membrane is semi permeable to certain ions resulting in the relaxation to a resting membrane potential if it deviates, the time course of the relaxation is dependent on the membrane capacitance (C_m) and the membrane decay constant (τ_m).

The mechanisms of the action potential are not directly modelled in the LIF neuron. A fixed value threshold (θ) is determined where, if the membrane potential approaches it from below, the membrane potential is reset to the equilibrium value (V_{reset}) for a fixed refractory period. This approximates the action potential, however it should be noted that real neurons have variable threshold levels dependent upon the previous activity of the cell. However taking this approach reduces the model by three differential equations and vastly reduces computation time in large models.

Deviation from the equilibrium membrane potential is due to any external current across the membrane. In this model it is due to synaptic input (I_{Syn}) and a noise term ($I_{Noise}+I_{AC}$). The noise term can be varied in quality to account for the contribution of a number of different processes including nondeterministic presynaptic vesicle release, somatic action potentials, ringing and most importantly, synaptic input from neurons not included in the

model. This will be addressed below in the section concerning model input.

The synaptic input to the model can take many forms. The simplest of which, employed in this model, is an alpha function ($s(t)$), a fixed current response where deviation of the membrane potential decays to zero over a fixed time. This is the function that I have applied to the model. There are some unrealistic properties of using this function including the lack of rise time (although this is much shorted than the decay time), unrealistic summation of the effect of presynaptic spiking on the postsynaptic membrane potential at high firing rates, and the independence of postsynaptic effects from the membrane potential of the post synaptic neuron. Alternative approaches to the behaviour of synapses are available, again at a slight computational cost, in particular conductance based synapses. Conductance based synapses are a term that determines the conductance of the membrane for a given ion. The effect of a presynaptic spike on the membrane potential of the postsynaptic neuron is a function of this conductance and the membrane potential of the post synaptic neuron.

The values of the fixed parameters are found in table 2.1.

$$C_m \frac{dV_m(t)}{dt} = -\frac{C_m}{\tau_m}(V_m(t) - V_{rest}) + I_{Syn}(t) + I_{Noise}(t) + I_{AC}(t) \tag{2.1}$$

where:

$$I_{syn}(t) = \sum_{k,j} w_k s(t - t_{k,j}) \tag{2.2}$$

synaptic kernal:

$$s(t) = t\frac{e}{\tau_{Syn}} e^{(\frac{-t}{\tau_{Syn}})} \tag{2.3}$$

and if:

$$V_m > \theta \qquad V_m = V_{reset} \tag{2.4}$$

2.2.2 The cortical network

As computational power has increased to the point where large scale detailed network simulations are possible, surveys of the general statistical properties of populations of neurons have been undertaken with a view to acquiring appropriate parameters. Of particular note is the work of Alex Thomson

Variable	Value
C_m	250 pF
τ_m	20 ms
τ_{syn}	2 ms
V_{rest}	-70 mV
V_{reset}	-70 mV
θ	-55 mV

Table 2.1: **Fixed parameters**

et al (Thomson et al., 2002; Thomson and Bannister, 2003; Thomson and Lamy, 2007) from whose work the model parameters have been derived.

The connectivity structure of the cortical network is the same as that used in (Haeusler and Maass, 2007), however the individual cell models are simple LIF cells, as opposed to the full Hodgkin-Huxley type used in the paper. This allows for a larger network to be simulated in a realistic time frame. The network model consists of six populations of neurons representing the excitatory and inhibitory cells of layers 2/3, 4 and 5. Layer 6 has been omitted due to the sparse statistical data and the apparent relative independence of this layer from the others.

The ratio of inhibitory to excitatory cells is 1:4. The proportion of cells between layers is layer 2/3 : 30%, layer 4 : 20%, and layer 5 : 50%. The interconnectivity is illustrated in figure 2.1. The percentage in brackets is the probability that any two cells between two populations will have a synaptic connection. The black arrows represent excitatory connections and the red arrows inhibitory connections. For example the probability that a randomly chosen cell from the layer 5 excitatory population will have an excitatory synapse on a randomly chosen cell from the layer 5 inhibitory population is 10%. It is also worth noting that there is a within group connectivity probability. The number outside the brackets is a weighting factor for the synapses derived from the average peak value of the post synaptic potential following an arriving spike.

A connectivity matrix for each cell is generated from the connectivity probabilities in this model. This is done by using the connectivity probability of each individual cell to each population and randomly selecting cells from that population of the correct proportion. This is carried out for all cells in the network during the build phase. The individual cells are connected with a weighting value (w_k) set such that the PSP elicited from a single presynaptic action potential elicits a PSP of one tenth of the experimentally measured value.

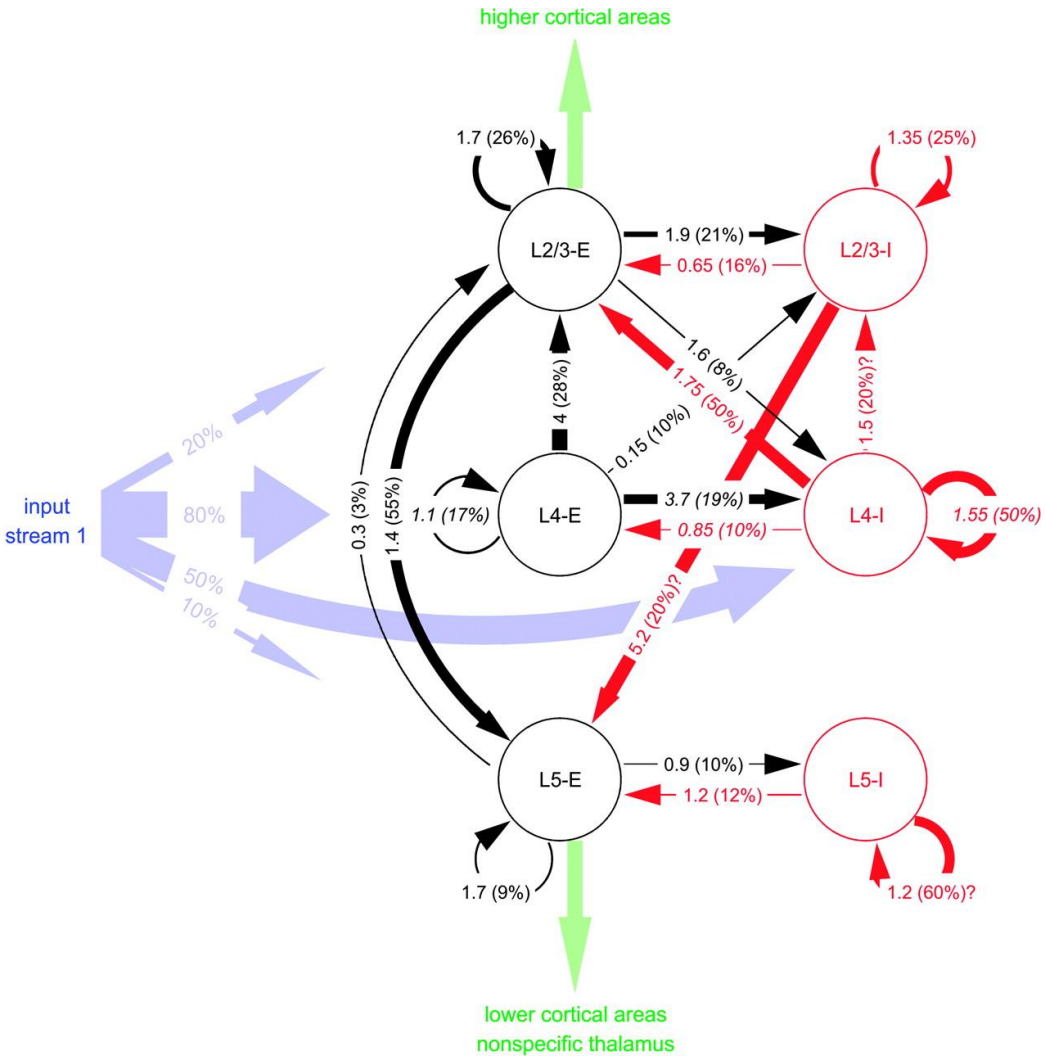

Figure 2.1: **Cortical microcircuit template.** *Numbers at arrows denote connection strengths (mean amplitude of PSPs measured at soma in mV) and connection probabilities (in parentheses) according to Thomson and others (2002), for connections between cortical neurons in 3 different layers, each consisting of an excitatory (E) and an inhibitory (I) population, with an estimated maximal horizontal distance of up to 100 m. Most of the data are from rat cortex, except for interconnections in layer 4 (italic), which are from cat. (Connections from L2/3-I to L5-E are reported in Thomson and others [2002], but are discussed only qualitatively. Hence, the entry for connections from L2/3-I to L5-E [marked by a question mark] is only an extrapolation. The same applies to connections from L4-I to L2/3-I. No data on the amplitudes of inhibitory PSPs from L5-I to L5-I are given in Thomson and others [2002], hence the corresponding entry is just a guess.) Percentages at the input stream denote connection probabilities for input neurons used in our simulations. In addition, each neuron receives background noise reflecting the synaptic inputs from a large number of more distal neurons(adapted from (Haeusler and Maass, 2007))*

2.2.3 The simulation environment

The first step undertaken was to implement the model in MATLAB (MATLAB 7.5.0, The MathWorks Inc., Natick, MA, 2000). The simulations took 7 hours to run one second. I explored methods of reducing the simulation time. These included exploring optimisation of the integration method used to solve the equations and testing of available simulation packages. I looked at Neuron(Hines and Carnevale, 2003) and Genesis(Wilson and Bower, 1992), these are appropriate for small networks of highly detailed individual neurons. Another package, NEST (Gewaltig and Diesmann 2007), is now available for the simulation of large networks of simple, one dimensional neurons with the ability to implement more detailed multicompartment models in the source code. I implemented the model in NEST and the simulation time is 4 minutes per simulated second, a vast improvement. NEST is not as widely established in the literature as the other two available packages, however its usage is increasing with a number of theoretical neuroscience courses being taught within the context of the package. It also has a growing support literature and an active users forum in which the developers regularly assist with coding questions(Nordlie et al., 2009; Hanuschkin et al., 2010; Linden et al., 2010).

An advantage of the NEST simulation environment is that it avoids using the simulation time step as the integration time step for dynamic equations. NEST integrates the dynamic equations with machine precision, using a technique termed "Exact Integration in the context of pulse coupled neuronal systems" (Rotter and Diesmann, 1999).

The limitations of the version of the NEST simulation environment version used in this work have been that there was no way to directly monitor the incoming synaptic currents individually and that the connectivity matrix returned for the generated networks only gave the afferent connectivity from each cell and not the efferent synaptic connectivity from each cell.

2.2.4 Input to the network

The model employed in this study is of an isolated cortical area, and as such is removed from sensory input by three direct synapses between sensory transduction and the cortex. This means that the known phasic and tonic responses to mechanical stimuli have been re-encoded by the nervous system before they enter the cortex. The manner of this re-encoding is still a subject of much investigation. Inputs to the cortical layer 4 from the specific thalamus are known to make up 4% of the synapses on these cells(Thomson, 2007). Other synaptic inputs not present in the model include distant cor-

tical and subcortical contributions. Given this, the input to the model from non-local connections is not trivial.

My initial approach has been to use Gaussian white noise current generated at the same sample rate as the integration time step (0.1ms) as an independent input for all individual cells. This has allowed an exploration of the behaviour of the network using the standard deviation and the mean values of the noise.

As described in the next chapter to explore the interaction between sensory input and ongoing oscillation a group of poisson generators were added to the input. To further explore sensory input in the context of oscillations I introduced a common sinusoidal current to all cells.

The direct injected current is straightforward to implement and useful in the exploration of the qualitative properties of the model, but in real neural systems all inputs are synaptic.

2.2.5 Output from the network

NEST outputs the simulation data in large text files. I have written MATLAB code to reduce the file size of this data and convert it into a number of useful formats such as the field potential signal, firing rates and membrane potentials of the individual cells and subpopulations based upon the type and layer of the cell. In this for a wide number of tools developed in computational neuroscience are available for analysis.

Deciding upon which of the model parameters from which to derive an equivalent signal to the MEG/EEG/LFP is a challenge in modelling. The physical signal is derived from the net electric or magnetic field of all currents in the brain, with a particular weight given to open field cells in the cortex, the pyramidal cells. The cortex its self is a convoluted surface so the first reduction is to consider it a flat surface. In this model where 1 mm^3 is explored this is less problematic than in intercortical models that span differently orientated surfaces.

The next issue is describing internal current flow in a one dimensional model of a highly structured pyramidal cell. In a recent paper by (Mazzoni, 2011) a difference of synaptic currents was used to express the equivalent signal. Assuming AMPA signals to be apical and GABA synapses to be perisomatic the absolute values of synaptic currents were summed. Whilst a current based approach would be preferable, in the model I present the synaptic currents are of a fixed duration and magnitude unrelated to the membrane potential, so any signal derived from the summation of these currents would be unrelated to the state of the model neuron. In addition to this the version of NEST used in simulation does not allow direct access to

incoming synaptic signals, only outgoing spikes. So any additional calculations derived from the available metrics of the simulation environment would add a significant processing time to each simulation.

In my model the signal extracted from the model to represent the EEG/MEG/LFP signal is the mean membrane potential of all the pyramidal cells, i.e. the excitatory cells of layer 2/3 and 5. As the LIF model is a one dimensional model there is no representation of the internal movement of charge carriers to give a direct equivalent of the signal. However, as the movement of charge within the cell is dependent upon the potential difference between points on the neural membrane, the membrane potential is a closer correlate of the electrophysiological signal than the firing rate that is traditionally used to explore population activity in these networks. The membrane potential allows for the integration of synaptic signals including the instantaneous state of the neuron on which the incoming signals act. The membrane potential had been used as an equivalent signal in Ursino and in neural mass modelling(Ursino, 2006; David 2003).

2.3 Initial explorations of the model using white noise input

2.3.1 Introduction

With specific connectivity to an abstract cortical area being largely unknown, the first investigation into network behaviour was carried out using independent white noise currents injected into each cell. This type of input can be thought to loosely model the intracortical post synaptic currents summed over the cell body. The initial aim was to find the parameters of an input that would illicit a membrane potential in individual cells and the simulated field potential with a 1/f like response, as has been measured electrophysiologically, and roughly realistic individual cortical cell firing rates (Okun et al., 2010).

The white noise is defined by two parameters, the mean and the standard deviation, both expressed in pA. Theoretically each of these parameters may be thought of as modelling a type of input. A high mean could be considered an asynchronous input of a number of excitatory post synaptic potentials possibly from long range cortical connections, as these are only excitatory in nature. A high standard deviation could be considered as complex local synaptic inputs as they will include positive and negative deflections of the individual cell's membrane potential.

An illustration of a typical individual simulation response is given, followed by an investigation into the firing rate and simulated field potential mean and standard deviation values. Subsequently the power spectrum of sampled parameter space is investigated in order to investigate the 1/f like properties of the network across parameter space. Finally an approximate phase diagram illustrating network behaviour across parameter space is presented in order to explain the smaller regions of parameter space chosen for further investigation in the subsequent sections of the thesis.

2.3.2 Methods

2.3.2.1 Simulations

Four hundred simulations were carried out using a single network structure. Each simulation had a unique value for the white noise parameters: White noise mean and White noise standard deviation. These parameters were taken from a 20X20 matrix where one axis contained the white noise mean values -270pA increasing in steps of 30pA to 300pA ; the second axis contained the white noise standard deviation values 580pA increasing in steps of 80pA to 2100pA. These parameters were used to drive independent white noise generators at a ratio of one noise generator to each cell. For each simulation the random number generator was set with the same seed, ensuring that the structure of the Gaussian white noise input was identical in each simulation, with only the magnitudes being influenced by the white noise parameters. All cells had a membrane potential of -70mV at t=0ms. No cells were firing at the initiation of the simulation. Each simulation lasted 1000ms.

2.3.2.2 Analysis

For each simulation analyses were performed on the simulated field potential signal and the combined spike trains of each population. Each analysis was performed on the time period 200 to 1000 ms to remove artefacts from the network's initial response to the stimulus. Each of the population firing rate means were calculated first by dividing by the number of cells in that population and then expressing the rate in Hz. The simulated field potential mean and standard deviations were calculated using the appropriate Matlab function. The power spectral density of the simulated field potential was calculated using the Matlab periodogram function.

For assessment of the 1/f like response of the simulated field potential to a given input parameter 20 simulations were carried out with differing input

seeds, the mean power spectral distribution was calculated and plotted on a log log power-frequency plot. The Matlab best fitting line algorithm was used on the data points between 3 and 40 Hz to obtain a linear function and magnitude of the PSD response.

The parameter space property diagram was produced by hand based upon the response properties of the network at a number of sampling resolutions and the specific boundaries are for illustrative purposes only.

2.3.3 Results

2.3.3.1 A single simulation

In this section I will show an example of a single simulation to determine whether or not the simulations can produce mean field potentials that are qualitatively similar to biological field potentials. I will inspect the raw signal, the power spectral density (PSD) of the signal, the spike patterns of all cells and types in each layer and the average firing rate of the average cell in each layer and cell type.

Figure 2.2 shows the mean field potential from a single simulation. Between 0-100ms the network is responding to the input mean. As the starting membrane potential values for the individual cells is -70mV, the mean of the input determines the mean of the field potential adjusting according to the membrane time constants of the individual cells. Although it is not shown in the figure, when the white noise input is turned off, the field potential will return to -70mV over a similar time period.

Once the network has reached a mean value in accordance with the input mean it behaves in a complex manner reminiscent of a biological electrophysiological signal. The similarity can be further shown in the $1/f^{\alpha}$ like characteristics of the PSD of the signal. This is shown in figure 2.3 and is similar to the power frequency content of biological electrophysiological signals which are not stimulus linked(Okun et al., 2010). This similarity will be quantified below.

Figure 2.4 shows the number of spikes per 0.1ms time sample over the whole simulation period. This can be thought of as the result of spike sorting from an idealised multiunit activity signal taken across the depth of the cortex. The spikes are grouped by both cell type and cortical layer. The inhibitory spikes (in red) are sparser than the excitatory spikes (in blue) due to the lower proportion of inhibitory cells. The spikes are relatively uniformly distributed across time reflecting the independent inputs supplied to each cell. The mean firing rate for each cell type in each layer is given in the right hand column. The firing rates fall within the range typical for

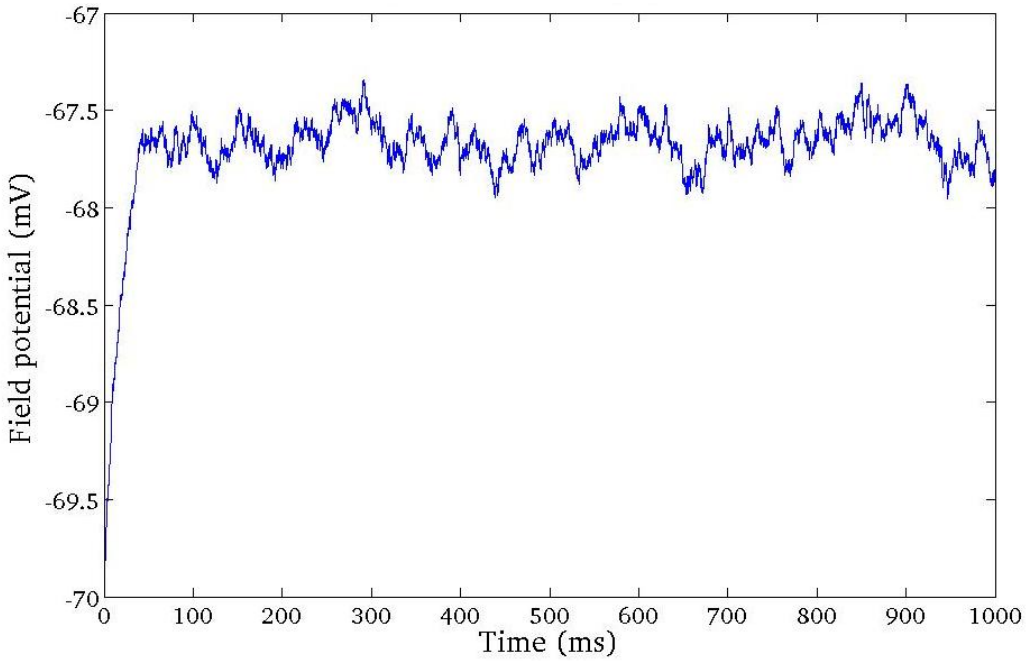

Figure 2.2: **The mean field potential from a single trial.** *Each cell in the model receives an independent white noise input generated with a mean value of 30 pA and a standard deviation of 1300pA.*

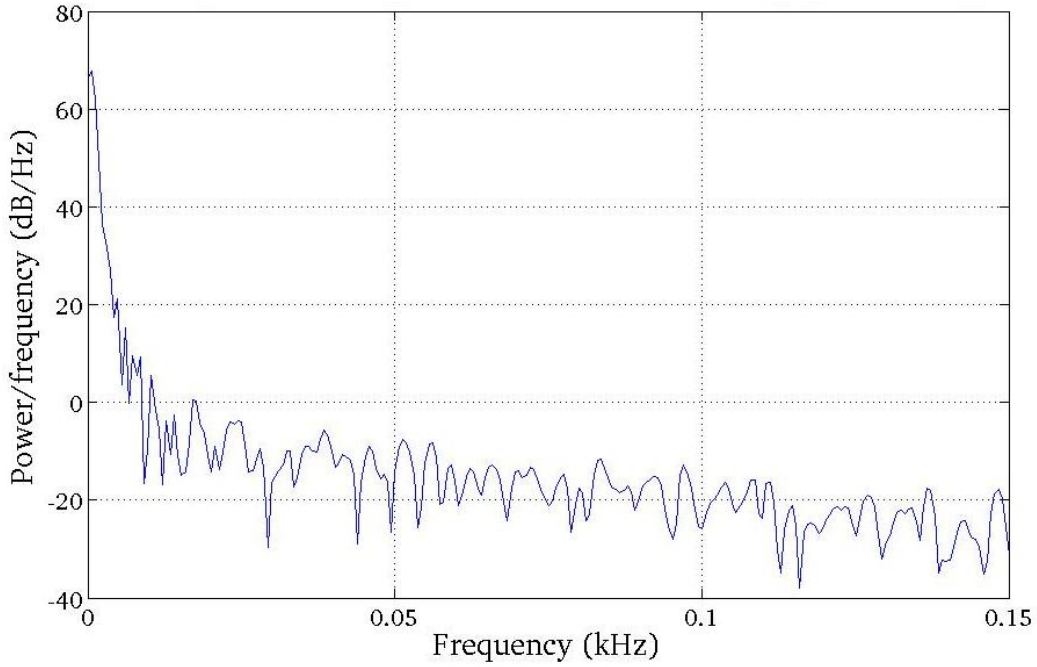

Figure 2.3: **The power spectrum of a single trial.** *The power spectral density of the mean field potential of a 1 second simulation where each cell in the model receives an independent white noise input generated with a mean value of 30 pA and a standard deviation of 1300pA.*

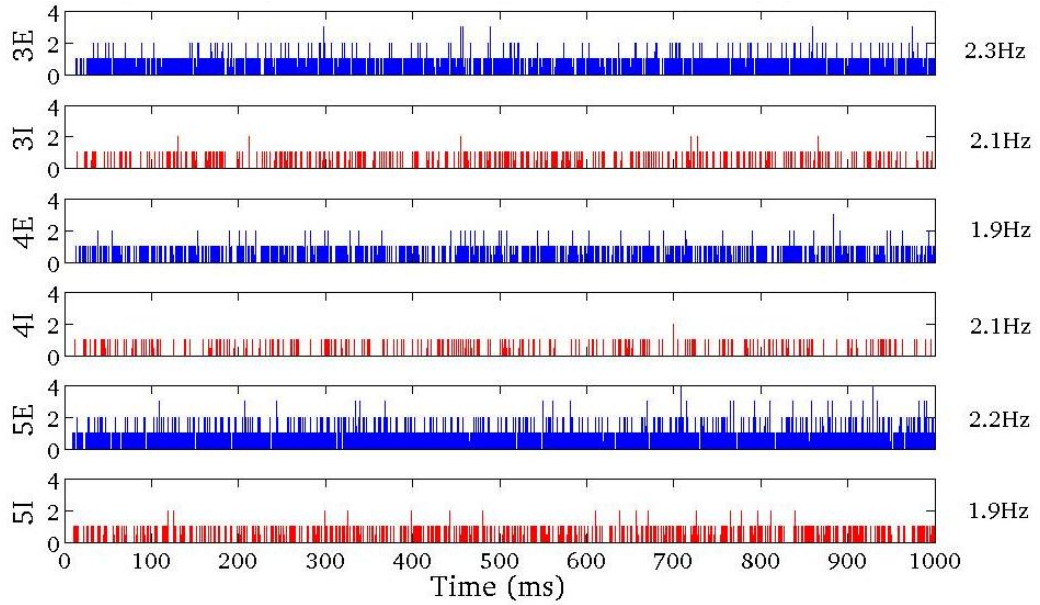

Figure 2.4: **The number of spikes per 0.1ms in each cell type and layer in a single trial with the mean firing rate of an average cell.** *Each cell in the model receives an independent white noise input generated with a mean value of 30 pA and a standard deviation of 1300pA. The subplots each represent a layer population in the model by number and type. The blue plots represent the population spike rates in the excitatory layers. The red plots represent the population spike rates in the inhibitory layers. The right hand frequency is the average spike rate for an average cell calculated over 1 second.*

cortical cells during ongoing activity(Wolfe et al., 2008).

In this section I have shown that the mean field potential and the spiking behaviour of the network has demonstrable qualitative similarities with biological electrophysiological signals.

2.3.3.2 Exploring white noise parameters

In this section I will explore the network behaviour over a range of biologically realistic parameters for the white noise input. I will demonstrate that the network behaves in a number of different modes depending upon the white noise mean and standard deviation. I will look at the mean and standard deviation of the simulated field potential, the firing rates of the cells in each layer, and the raw signal and PSD of the field potential from different sections of the parameter space. I will also demonstrate the $1/f^{\alpha}$ properties of the

simulated field potential.

The main question addressed here is whether or not the network is directly encoding the information in the input, performing a computation on the input, or obliterating the information entirely. If the information is encoded in the output there should be a one to one correspondence between the input state and the output state. If a computation is performed, some representations of the input would have the same representations in the output, i.e. there would be a reduction in the information. And if the information is obliterated there would be no representation of the input in the output.

Figure 2.5 consists of two plots. The top plot shows the mean value in mV of the mean field potential after the settling period (from 100ms after the simulation begins). The bottom plot shows the standard deviation in mV after the settling period.

In the plot of the mean, input mean values less than 0 pA are directly encoded into the field potential mean. It proportionally increases along with the input mean with a one to one relationship between the input mean and the output mean. Where the input mean is greater than 0 pA the field potential mean may hold the same value when all other parameters of the simulation remain the same. With input standard deviations less than approximately 1620 pA a given field potential mean may represent two or more input mean values. For input means above zero the field potential mean value approaches a maximum. The maximum value of the field potential mean is in the region of input mean value of 120-150 pA. The representation is not symmetrical around the maximum value. As the input mean increases beyond the maximum value of the field potential mean, the field potential mean approaches a fixed value. With input standard deviations greater than approximately 1620 pA, the field potential mean quickly approaches a fixed value as the input mean increases from zero. As the standard deviation of the input increases there is a region in the bottom left of the parameter space where the standard deviation of the input is encoded in the field potential mean up to a point where the output is uniform.

The network behaviour is such that over this parameter space there are three regions where firstly the mean of the input is directly encoded into the mean of the output, with little representation of the input standard deviation. Secondly, the mean value of the field potential may represent more than one value for the input mean and the standard deviation of the input is represented in the mean. And thirdly, a region where the information about the input mean and standard deviation of the mean is largely obliterated in the field potential mean.

In the bottom plot of figure 2.5 we can see the distribution of the standard deviation of the mean field potential. Parameter space is roughly bisected

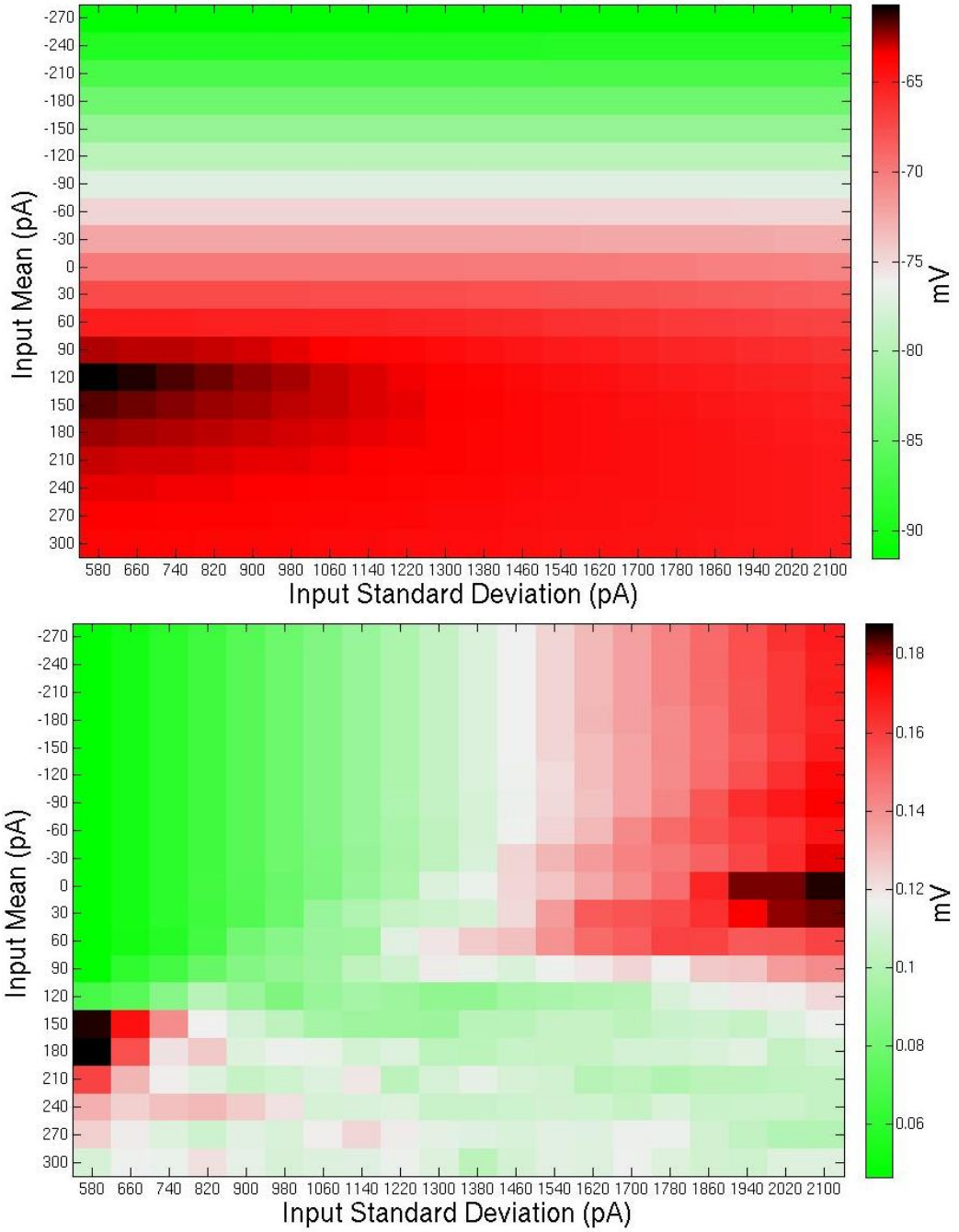

Figure 2.5: **The mean and standard deviations of the simulated field potential as a function of input mean and standard deviation.** *In both subfigures the input parameter space is represented with the white noise input mean on the y-axis ranging top to bottom from -270pA to 300pA in steps of 30pA, and the input standard deviation on the x-axis ranging from 580pA to 2100pA in steps of 80pA. (Top) The average value of the mean field potential in mV. (bottom) The standard deviation of the mean field potential in mV*

diagonally where the upper left hand side shows a direct encoding of both the mean and the standard deviation of the input in the standard deviation of the field potential. Neither of the input parameters could be read off independently from the field potential standard deviation, as the input mean could be from the output mean. However a strong component of each of the parameters appears to be represented in the standard deviation of the field potential. To the bottom right of the bisecting line of the parameter space there appears to be three regions where the network behaves in different manners. The first region is roughly perpendicular to the bisecting line where values of the standard deviation are largely identical, suggesting that the input values are not systematically encoded in the standard deviation of the field potential. Either side of this perpendicular line there is a single maxima of standard deviation around which there is a drop off of standard deviation. Around each of these there is a systematic computation dependent upon the input mean and standard deviation.

Figure 2.6 shows the mean firing rate of the average excitatory or inhibitory cell in each layer across all combinations of input mean and standard deviation values. Table 2.7 is a table of the firing rates of the average excitatory cell from layer five. The common features for all cell types are a firing rate threshold, where the firing rate is zero to the top left of the region of the diagonal line that bisects the standard deviation plot of figure 2.5. There is then a region to the bottom right of this line where there is a slight increase in firing rate according to the input mean, two or three spikes per second per unit increase of input mean, and an approximate increase of one spike per second per unit increase in input standard deviation. Below this second region the representation of the input mean sees an increase in firing rate of 12 spikes per second per unit increase in the input mean. The firing rates are within the range of recorded instantaneous firing rates for cortical cells. It should be noted that the different regions of network behaviour marked out in the mean of the field potential and the standard deviation of the field potential (figure 2.5) are not evident in the firing rates of the cells.

Although there are general trends for cell firing rates across cell types, there is some variation according to cell type and layer shown in figure 2.6. In layer 3 and layer 5 the excitatory cells have a higher firing rate than the inhibitory cells. In layer 4, the 'input layer' for bottom up connections, the inhibitory cells have higher firing rates than the excitatory cells. Layer 3 excitatory cells have a slightly lower firing rate than the layer 5 excitatory cells, whilst the layer 4 excitatory cells have a far lower firing rate than either layer 3 or layer 5 excitatory cells. Layer 3 and layer 4 inhibitory cells have a similar firing rate, whilst layer 5 inhibitory cells have a far lower firing rate than layer 3 and layer 4 inhibitory cells. This suggests that the cell types in

each layer may each have differing roles in processing information.

Returning to table 2.7 I have marked out two lines, the uppermost marks the firing threshold where cells are either firing or silent. The lower line marks the change in firing rate where the encoding of the input mean changes from 2-3 spikes per unit increase to 12-13 spikes per unit increase. I have also marked out twenty five points on the parameter space, five for each particular value of standard deviation covering all the separate regions of network behaviours identified from the field potential and firing rates.

Figure 2.8 shows the mean power spectral density of two simulated field potentials illustrative of different regions of parameter space. The top plot is typical of the response of the network with input parameters from the zero or low firing rate region. α values are typically between 1.3 and 1.4 in this region. bottom plot is typical of the response of the network in the regions in which the firing rate is unrealistically high. α values are typically around zero in this region, however at low input standard deviation near the low firing rate condition the α value tends to be less than zero.

$1/f^{\alpha}$ like behaviour has been demonstrated in biological neural networks where α takes a value between 0.5 and 1.5 at frequencies below 40 Hz (Novikov 1997). It has been hypothesized that this indicates a state of self-organized criticality(Linkenkaer-Hansen, 2001), however it has also been suggested that this is a consequence of filtering of neural signals through the cortical tissue (Bedard, 2006). In this model it seems to arise from the filtering of a white noise input through the membrane response function.

Field potential simulations from a network with a white noise standard deviation of 0pA and then from each of these points in parameter space will be looked at in detail over the subsequent six figures (2.9, 2.10, 2.11, 2.12, 2.13, 2.14)

Figure 2.9 shows the simulated field potential and the power spectral density of the simulations with an input standard deviation of 0 pA and an increasing mean. The simulated field potentials are completely flat until the input passes the threshold of the individual cells. After this the network shows oscillations at around 20 Hz modulated by a 1.5 Hz component and then increasing in the next higher simulation to an unmodulated oscillation of around 35 Hz. With no white noise the network tends to oscillate with one or two strong dominant frequencies.

Figure 2.10 shows the field potential and the power spectral density of the simulations with an input standard deviation of 580pA in table 2.7. The input mean values of 90 pA (blue) and 120 pA (green) are situated in the region where the mean value and the standard deviation of the field potential directly encode the mean and the standard deviation of the input. The blue field potential is in the region where no cells are firing. The green field

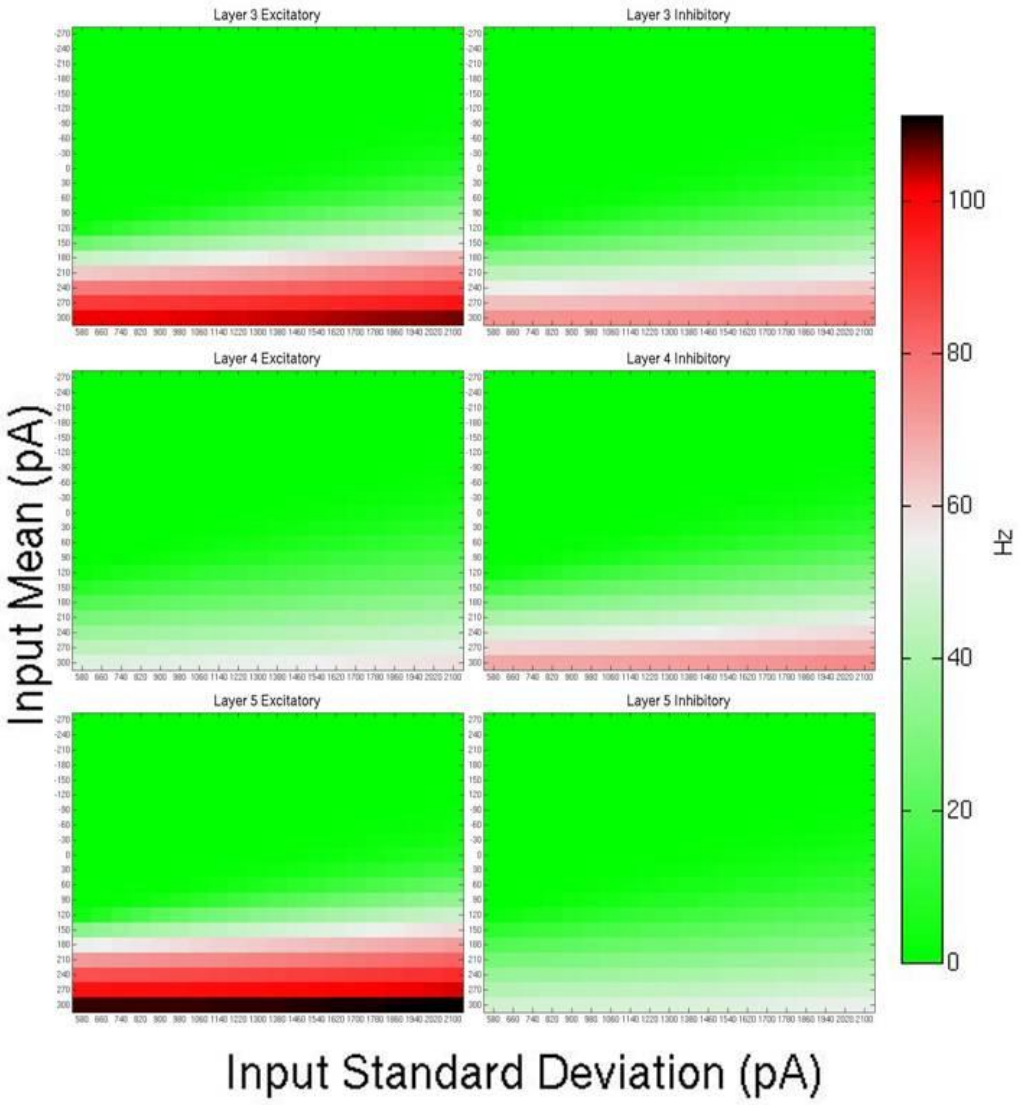

Figure 2.6: **The mean firing rate of the average cell in each cell class and layer across the input parameter space.** *In all plots the input parameter space is represented with the white noise input mean on the y-axis ranging top to bottom from -270pA to 300pA in steps of 30pA, and the input standard deviation on the x-axis ranging from 580pA to 2100pA in steps of 80pA. The left hand plots are the mean firing rates of the average excitatory cells from each population. The right hand plots are the mean firing rates of the average inhibitory cells from each population. Each layer is represented with layer 3 at the top, layer 4 in the middle and layer 5 at the bottom.*

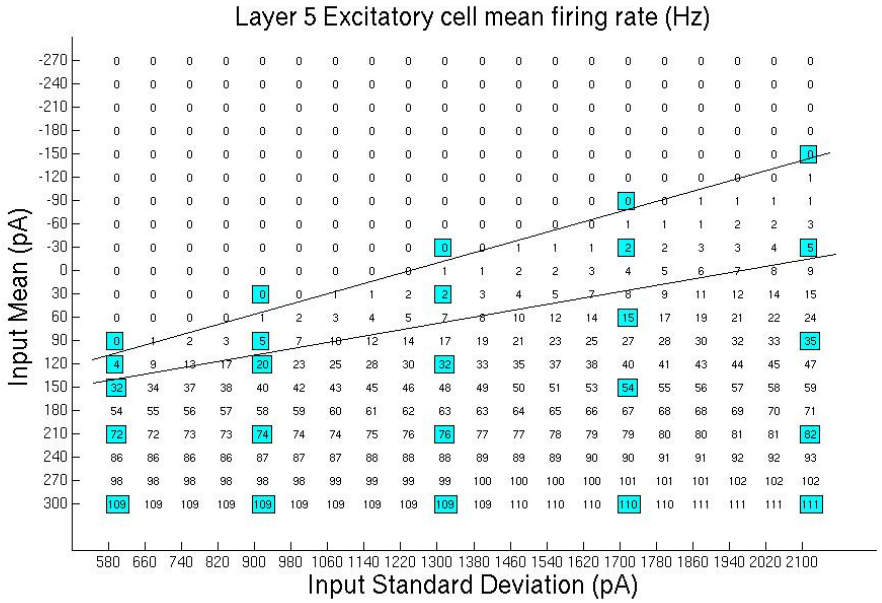

Figure 2.7: **Average layer 5 excitatory cell firing rate across input parameters** *The input parameter space is represented with the white noise input mean on the y-axis ranging top to bottom from -270pA to 300pA in steps of 30pA, and the input standard deviation on the x-axis ranging from 580pA to 2100pA in steps of 80pA. The top line across parameter space represents the threshold where the cells begin to fire. The bottom line across parameter space represents the threshold where network firing increases at a higher gradient. The blue numbers identify the parameter space sampled in subsequent figures.*

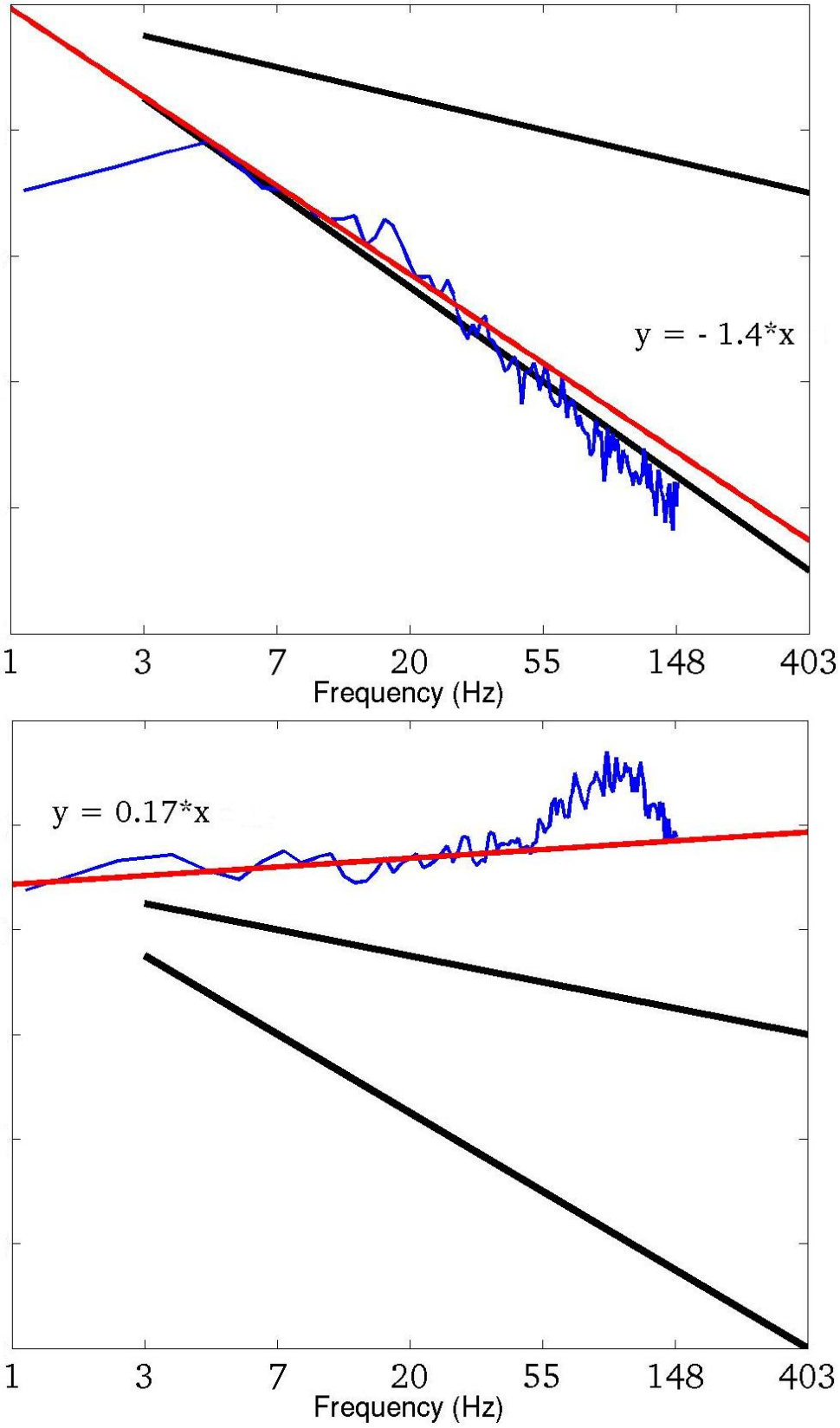

Figure 2.8: $1/f^{\alpha}$ **like properties of the power spectral density of the simulated field potential** *In both figures the PSD of the signal is in blue. The best fitting line between 3 and 40 Hz is in red with the magnitude given in the linear formula. The upper black line represents* $1/f^{-}0.5$ *and the lower black line represents* $1/f^{-}1.5$*. The top plot is an example of the low firing rate condition network. The bottom plot represents the biologically unrealistic high firing rate condition network.*

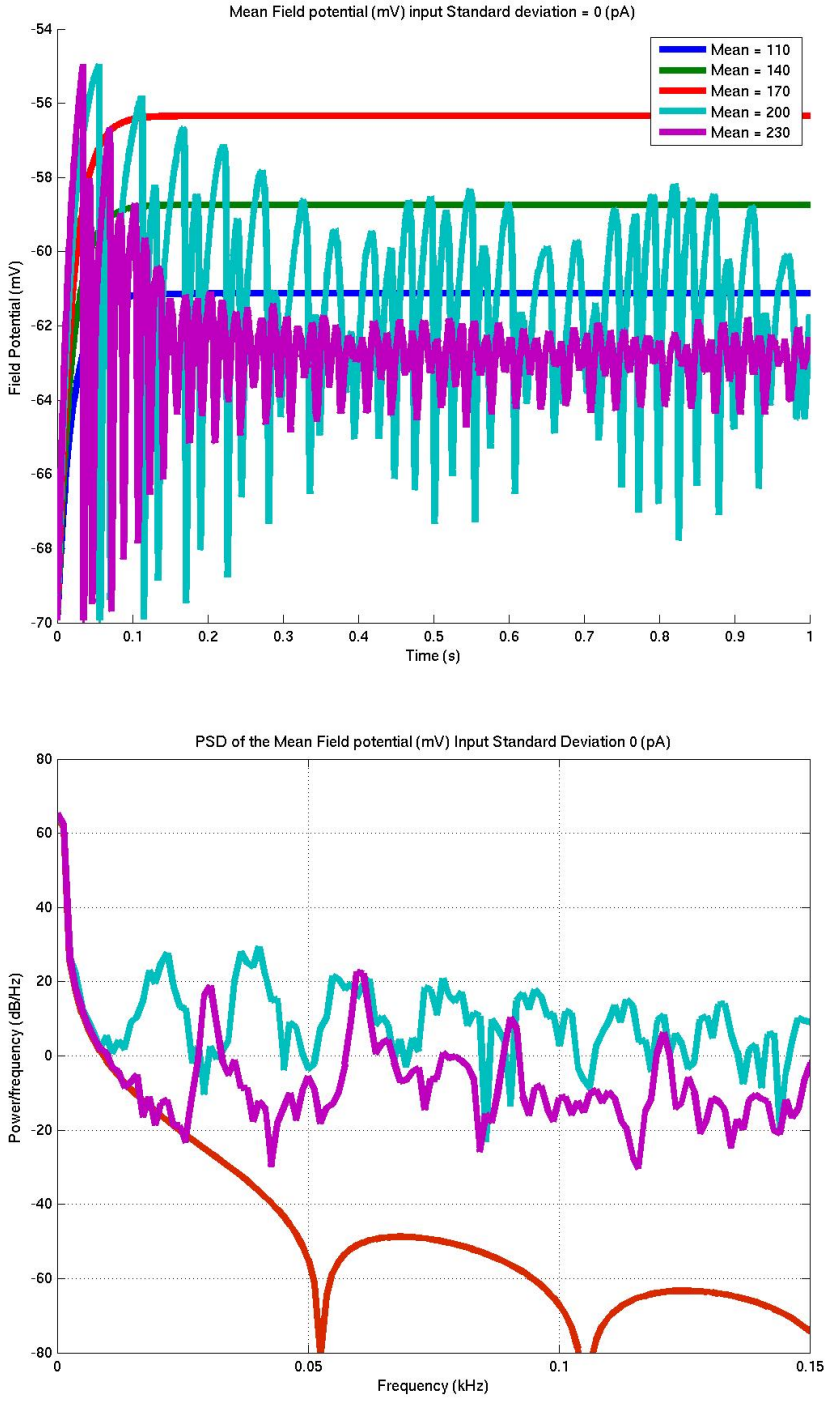

Figure 2.9: **The simulated field potentials and PSDs of a selection of input means with input standard deviation of 0 pA** *The top figure shows the simulated field potentials with input standard deviation of 0pA and five different input mean values. The bottom figure shows the Power spectral density of simulated field potentials with input standard deviation of 0pA and five different input mean values.*

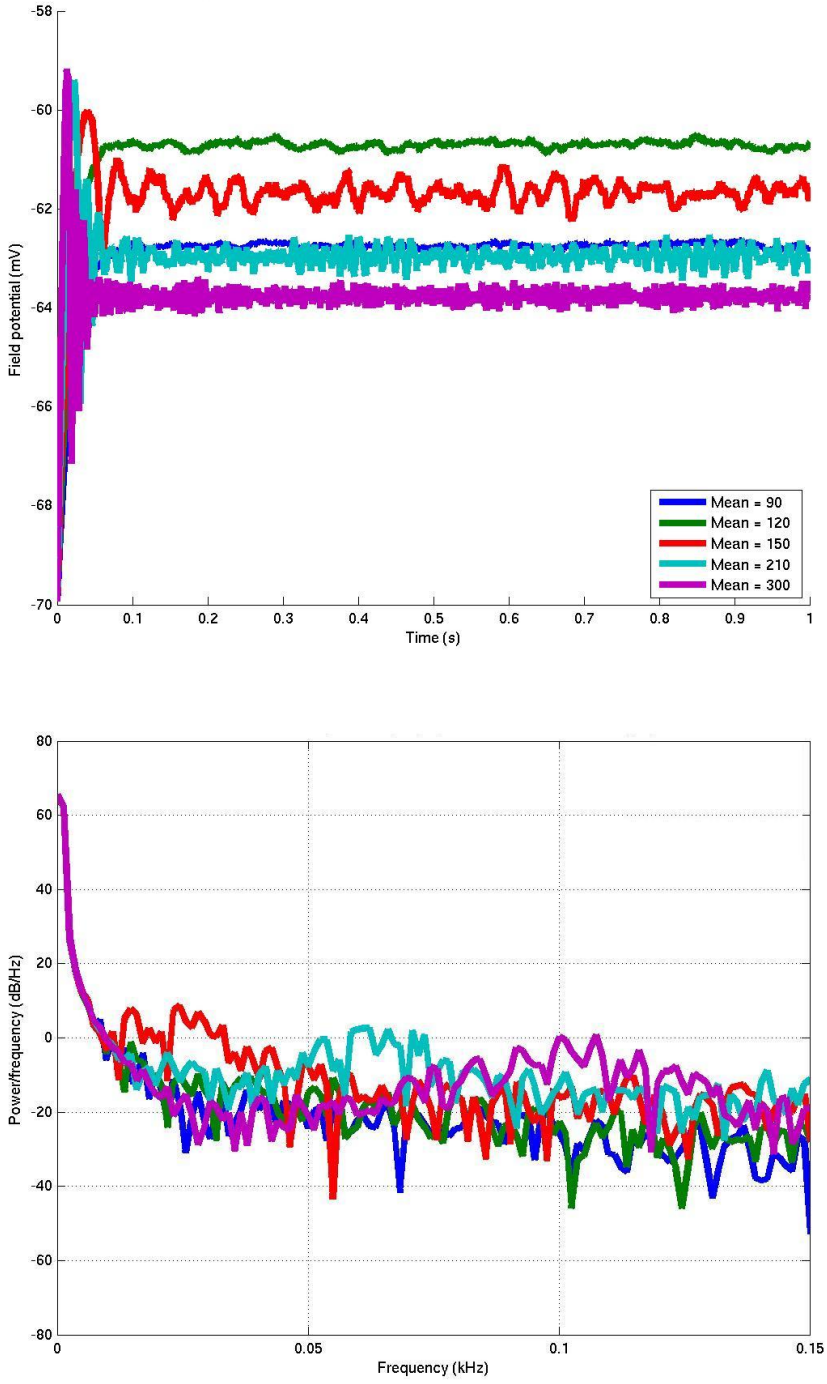

Figure 2.10: **The simulated field potentials and PSDs of a selection of input means with input standard deviation of 580 pA** *The top figure shows the simulated field potentials with input standard deviation of 580pA and five different input mean values. The bottom figure shows the Power spectral density of simulated field potentials with input standard deviation of 580pA and five different input mean values.*

potential is in the region where the cells are firing at a low rate. There is an initial rise in the field potential voltage to a mean that is dependent upon the input mean, with the green field potential higher than the blue. The initial slope of the rising phase is higher depending upon the input mean. The PSD of the blue and the green field potentials take a 1/f like shape with no particular frequency largely deviating from this.

The input mean values of 150 pA (red), 210 pA (cyan), and 300 pA (magenta) are in a different class of behaviour from the blue and green field potentials. There is the initial rise where the slope increases with the input mean, however this seems to reach a threshold point around -60 mV. This is followed by a negative deflection to settle around a mean value that does not follow the encoding of the field potentials that do not reach the -60 mV threshold. Although in this plot the mean value the field potential settles around appears inversely proportional to the input mean figure 2.5 shows that this is not the case. The next most important feature is that the field potential begins to oscillate around the mean with a single dominant frequency. This is apparent in both the field potential plots and in the PSDs. It appears that the dominant frequency increases as the input mean increases. The red plot has a dominant frequency range of 15-40 Hz, possibly with two or three major components in this range. The cyan plot has a dominant frequency range from 45-75 Hz, possibly with two or three major components in this range. The magenta plot has a dominant frequency range of 75-125 Hz, possibly with a number of components in this range. All three plots are in the region of the parameter space where the firing rate of the network increases by 12-13 Hz per cell per input mean unit. In this region there is no dominant frequency in the input, along with the -60 mV threshold, the nonlinear dependence of the field potential mean on the input mean and the 'dominant frequency' of the field potential it would suggest that the network is entering a computational state where its internal activity is dominating the input activity in the field potential signal.

Figure 2.11 shows the field potential and the power spectral density of the simulations with an input standard deviation of 900pA in table 2.7. The features noted when discussing figure 2.10 hold with three main exceptions. The network activity threshold under the higher input standard deviation is reduced to a value between -62 and -61 mV. The range of the post network threshold field potential mean is smaller than the with the smaller input standard deviation. The dominant frequency content of the post network threshold field potential, although still present is reduced. However there appears to be a clearer multiple number of frequencies in the dominant frequency range. The red plot has a peak at 20Hz and a separate peak at 35Hz. The cyan and magenta plots also appear to have separate peaks.

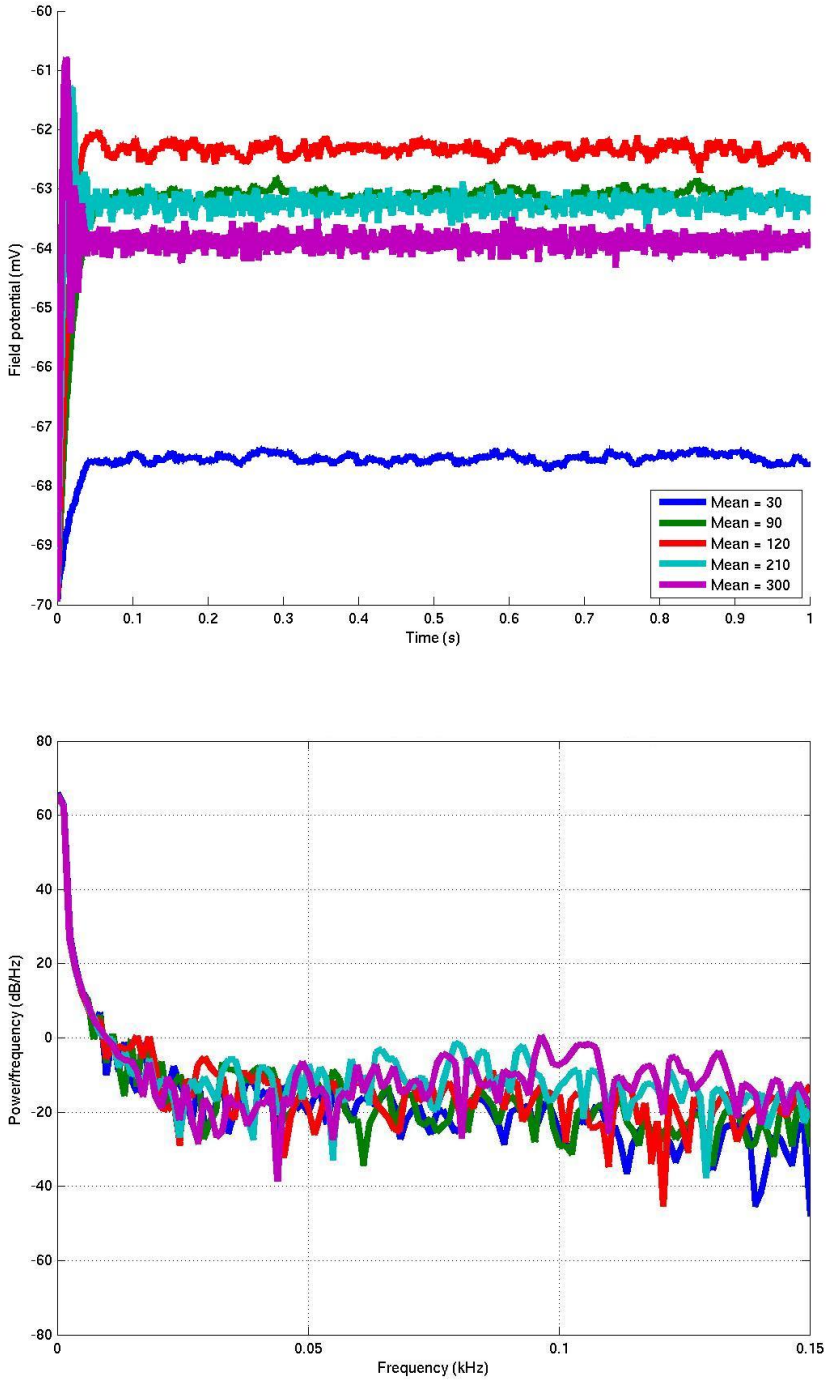

Figure 2.11: **The simulated field potentials and PSDs of a selection of input means with input standard deviation of 900 pA** *The top figure shows the simulated field potentials with input standard deviation of 900pA and five different input mean values. The bottom figure shows the Power spectral density of simulated field potentials with input standard deviation of 900pA and five different input mean values.*

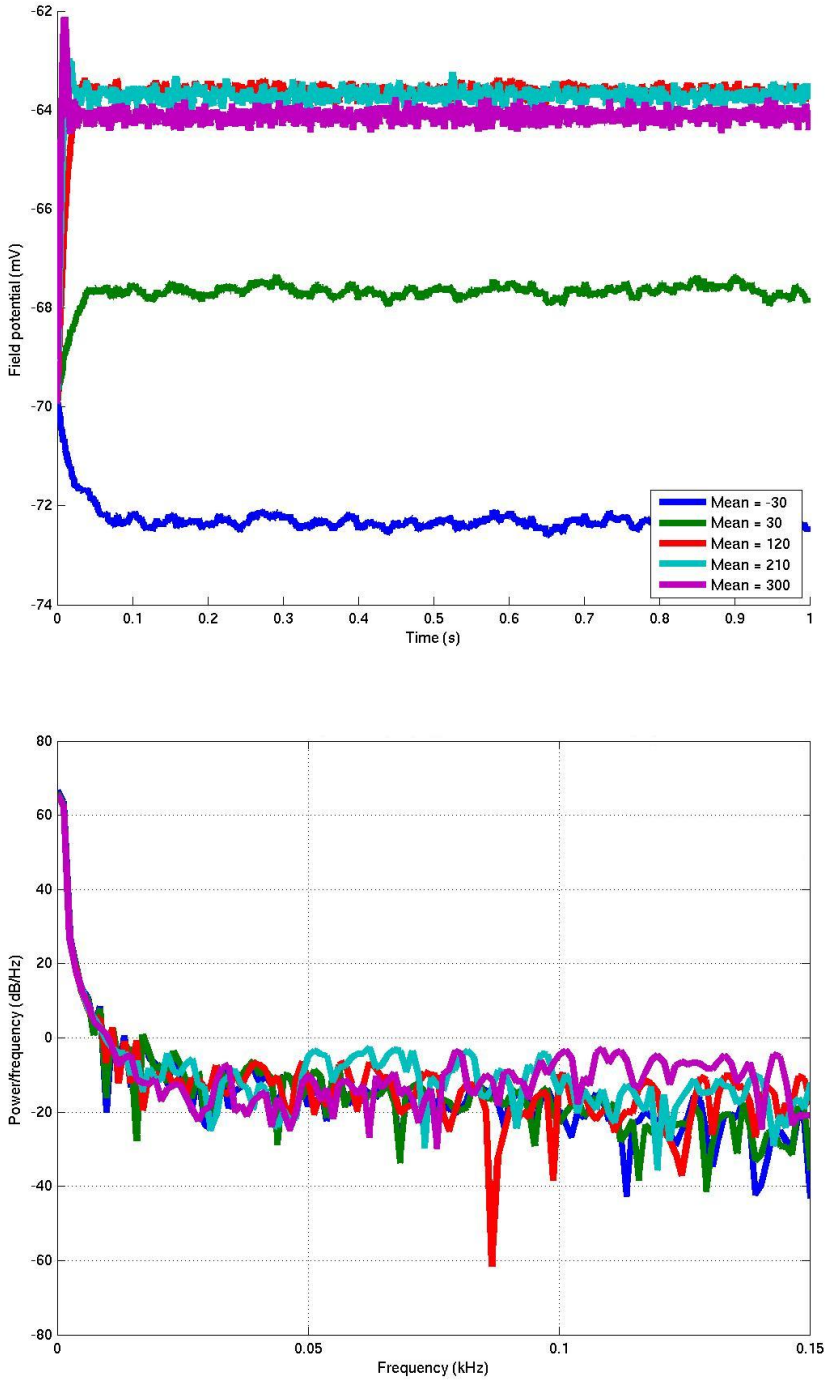

Figure 2.12: **The simulated field potentials and PSDs of a selection of input means with input standard deviation of 1300 pA** *The top figure shows the simulated field potentials with input standard deviation of 1300pA and five different input mean values. The bottom figure shows the Power spectral density of simulated field potentials with input standard deviation of 1300pA and five different input mean values.*

Figure 2.12 shows the field potential and the power spectral density of the simulations with an input standard deviation of 1300pA in table 2.7. In these plots the features of the network activity threshold are maintained. However the network activity threshold has reduced to less than -62 mV and the post network activity threshold field potential mean range has reduced again to -62 mV. The oscillatory activity of the super threshold field potentials is no longer visually apparent in the field potential, but suggests its self in the PSDs. There are no longer dominant frequencies in the red plot below 50Hz, but there are reduced frequencies at 80 Hz and 100 Hz. In the cyan plot there is increased power between 50 and 100 Hz. In the magenta plot there are increased frequencies in the >Hz range. The blue plot demonstrates the reduction in the input mean required for the network to have a zero firing rate with the increased input standard deviation.

Figure 2.13 shows the field potential and the power spectral density of the simulations with an input standard deviation of 1700pA in table 2.7. In this plot the network activity threshold has been further reduced to -64 mV. The range of post network activity threshold mean has almost approached unity(cf the discussion of encoding in the mean in figure 2.5). Increased frequency content is only apparent in the magenta plot. The cyan PSD shows a reduced power content at 40Hz. In this plot I selected three simulations that did not reach the network activity threshold: input mean -90 pA (blue), -30 pA (green), and 60 pA (red). The blue plot has a cell firing rate of zero and the red plot has a low firing rate, the features of their field potentials after 200 ms are largely identical excluding the mean. This demonstrates that the field potential is strongly determined by the input. The red plot is far less like the other two due to its higher firing rate, this shows that even in the sub network activity threshold region the network firing rate does have an impact on the characteristics of the field potential. Although this is a single trial it may also have an impact on the frequency content of the signal, as there are some reduced powers at certain frequencies when compared to the blue and green PSDs.

Figure 2.14 shows the field potential and the power spectral density of the simulations with an input standard deviation of 2100pA in table 2.7. In this region of parameter space the network activity threshold and mean have reduced to a unity of -65 mV. The sub threshold simulations have a similar representation of the input as in figure 2.13. All PSDs take a roughly 1/f form with a number of frequencies reduced in a non systematic way.

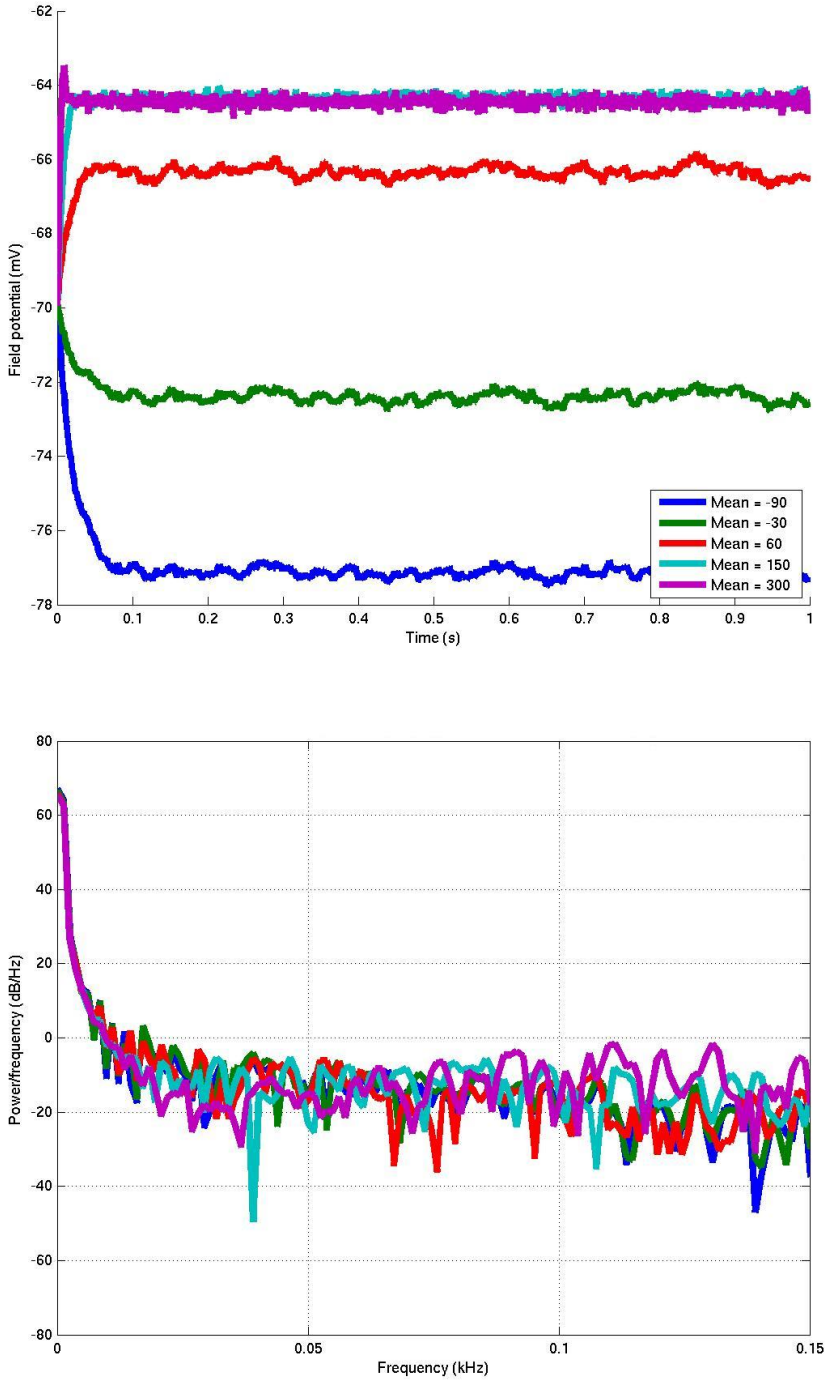

Figure 2.13: **The simulated field potentials and PSDs of a selection of input means with input standard deviation of 1700 pA** *The top figure shows the simulated field potentials with input standard deviation of 1700pA and five different input mean values. The bottom figure shows the Power spectral density of simulated field potentials with input standard deviation of 1700pA and five different input mean values.*

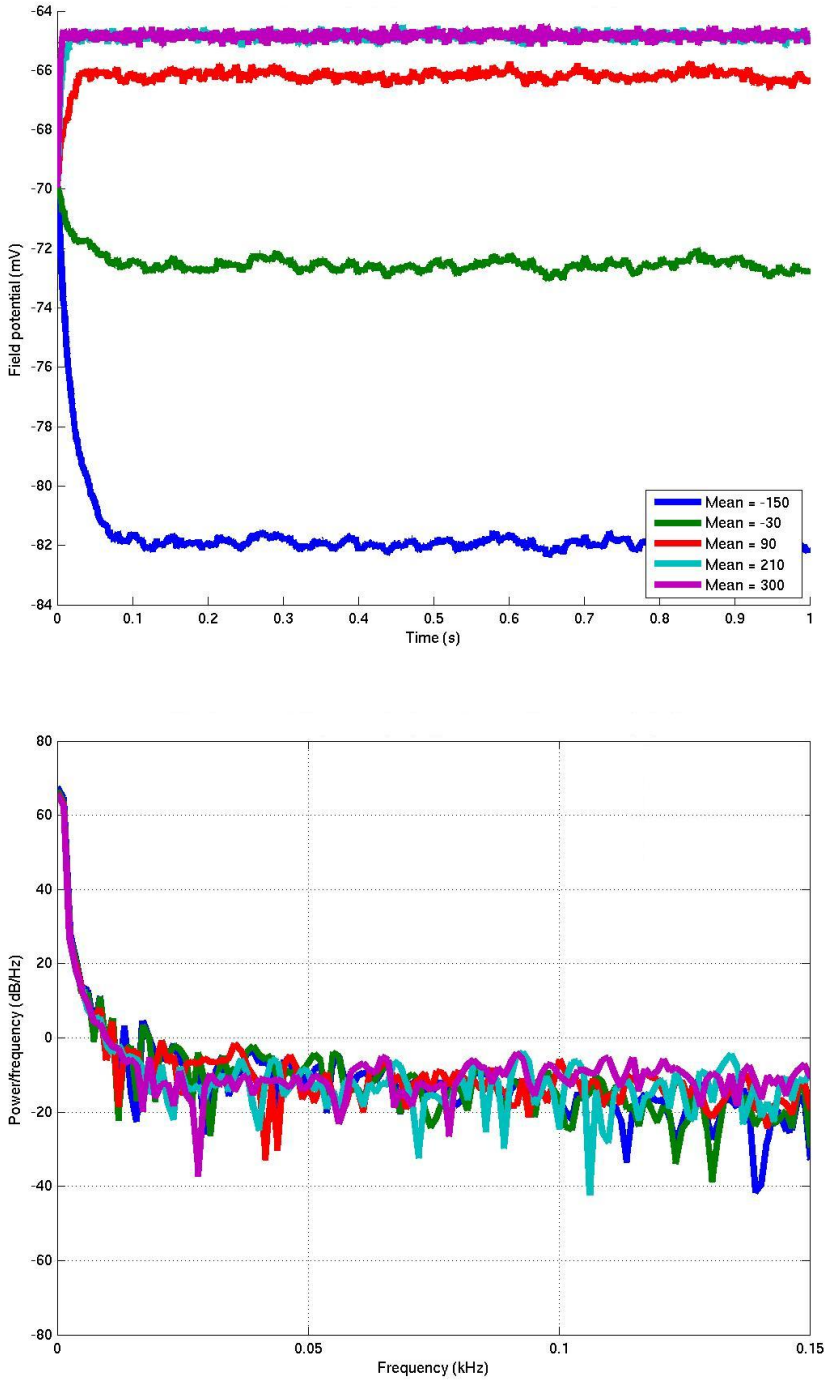

Figure 2.14: **The simulated field potentials and PSDs of a selection of input means with input standard deviation of 2100 pA** *The top figure shows the simulated field potentials with input standard deviation of 2100pA and five different input mean values. The bottom figure shows the Power spectral density of simulated field potentials with input standard deviation of 2100pA and five different input mean values.*

2.3.4 Discussion

In this section I have carried out a qualitative description of the network where each cell is driven by an independent white noise current. In each simulation the normalized white noise input to a particular cell would be identical. All white noise signals were modified by two parameters, the mean, which could be considered an additive DC current; and the standard deviation, which would be a multiplicative weighting. I have carried out the simulations included in this section using a number of white noise seeds and network connection random number generator seeds and all qualitative observations reported here hold true.

Whilst a white noise is not biologically realistic I have chosen to use it for a number of reasons. Ideally each neuron would have as its input synaptic contacts from something in the order of 1000 neurons with a small white noise component representing thermal noise, misfiring ion channels and other biological noise an order of magnitude smaller than an average post synaptic current. However, determining the origin and the firing statistics of these neurons would prove to be a task out with current anatomical and physiological knowledge. This would result in a reduction of the input neurons to a set of poisson generated action potentials. Firstly this would increase simulation time and secondly this takes no account of the dendritic location of the afferent synapse. The individual neuron models are one dimensional, so there would have to be at least a weighting of groups of synaptic inputs according to how distally they synapse from the cell body. As the LIF neuron can be considered a model of the axon hillock, rather than the whole cell I decided to model all nonthalamic input (which I introduce below) as white noise as this gives membrane potential characteristics similar to that of intracellular recordings from awake behaving animals.

Given that the input has been abstracted from biological reality the question remains: how can we interpret the parameter space investigated in terms of the biology of the cortical network? In the first instance I would posit that the mean value of the input would represent the sum of asynchronous excitatory and inhibitory postsynaptic potentials. As the regions of interest in the parameter space are all in the positive input mean space, long distance connections in the cortex are only excitatory, the connections from cortical areas higher in the cortical hierarchy are generally distributed across the cells and layers, and that spike timing contains less information for top down connections, it can be assumed that the mean parameter may roughly represent top down cortical input.

In the second instance I would posit that the standard deviation of the input would represent something like the level of synchrony of local cortical

connections. Increasing the standard deviation of the input will increase the input amplitude at all frequencies, so any local frequency content will be amplified, equivalent to increasing the number of synchronous excitatory or inhibitory post synaptic potentials, dependent upon the phase of the locally dominant frequency in the white noise. This random process is far from ideal considering that local connections have been shown to have correlations in firing times and should be dependent upon the firing of cells within the simulated network. However, it is worth further investigation along this dimension as we know that stochastic resonance is employed by the cortex and we have no biological constraint to limit this abstracted parameter.

Based on these two assumptions I will now consider the behaviours of the network across the parameter space. Figure 2.15 shows 7 areas in parameter space where the input is encoded in different ways in the field potential and mean firing rate of the cells. This figure has been assembled by eye for illustrative purposes.

In region A there is a strong negative current, where a general inhibitory signal is applied to the cells. The local synchronised signals increase only as the inhibitory signal increases. Where there is a low level of local synchronised cortical input there can be a small general excitatory current. In this region the input mean, and possibly the combined input mean and standard deviation are encoded in the field potential mean. The combined input mean and standard deviation are encoded in the field potential standard deviation. Nothing is encoded in the firing rate.

In region B there is a small contribution from local connections and a small contribution from long range connections. In this region there is an encoding of the input mean in the mean of the field potential and the combined signal is represented in both the standard deviation of the field potential and the firing rate of the cells.

In region C there is a high contributions from local synapses and no contribution from long range synapses. The input mean is directly encoded in the field potential mean. This may be thought of as local inhibitory input being encoded in the field potential mean. The combined input signal is represented in the field potential standard deviation. The combined signal is represented in the firing rate of the cells with each parameter unit increasing the firing rate by an equal amount.

In region D there is a low to medium input contribution from local cortical cells and a high contribution from distant cortical excitatory cells. This is the region where local network activity dominates the firing rate and the simulated field potential signal. The linear relationship between input mean and simulated field potential brakes down and there appears to be a linear relationship between input mean and the frequency of oscillations in the

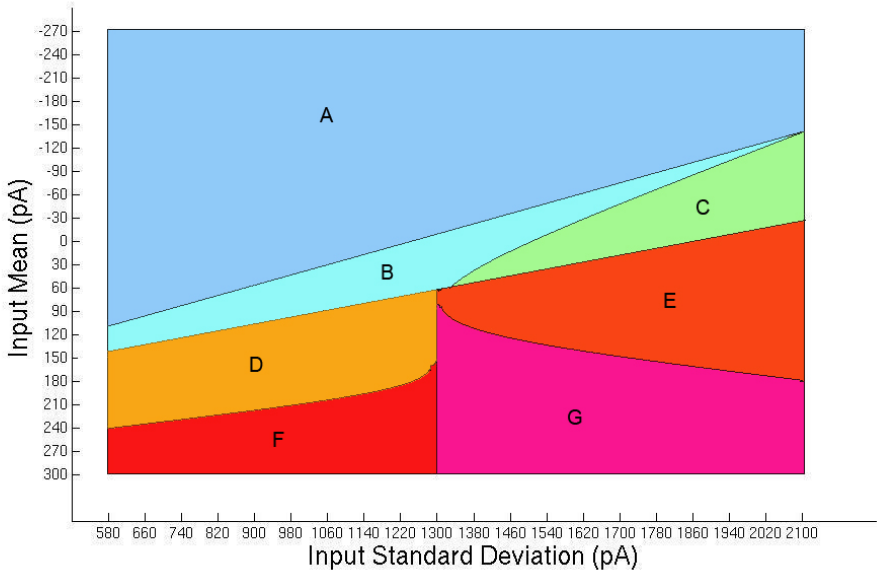

Figure 2.15: **Behaviours of the network***A - the firing rate is zero, but the simulated field potential mean represents the input mean and the input standard deviation linearly. B - as region A, but with a low firing rate. C - a low firing rate with a nonlinear representation of the input in the simulated field potential standard deviation. D - a higher rate of increase in firing rate according to input mean, oscillatory simulated field potentials and a nonlinear representation of the input mean in the simulated field potential mean. E - a higher rate of firing rate as the input mean increases, nonlinear representation of the input mean in the simulated field potential standard deviation. F - very high firing rates, flat power spectra and a small representation of the input parameters in the simulated field potential standard deviation. G - high a synchronous firing rate, no representation of the input parameters in the simulated field potential.*

simulated field potential.

In region E there is a high input contribution from local cortical cells and a medium to high contribution from distant cortical excitatory cells.

In region F there is a low input contribution from local cortical cells and a high contribution from distant cortical excitatory cells. This region produces flat power spectra and unrealistic high firing rates in the individual cells. The input standard deviation is somewhat represented in the simulated field potential standard deviation.

In region G there is a high input contribution from local cortical cells and a high contribution from distant cortical excitatory cells. This region produces flat power spectra and unrealistic high firing rates in the individual cells.

In the subsequent two sections there are investigations into synaptic weighting and network connectivity using inputs from across this parameter space. However, by the criteria of realistic firing rates and simulated field potential power spectra, in particular the prominence of oscillatory behaviour and $1/f$ like features, further investigation of the model will be carried out in the parameter space along and bisecting the two threshold lines where the network transitions from zero firing rate through low firing rate to the point where the local network activity dominates network activity signals over the input activity.

2.4 An investigation into network scaling

2.4.1 Introduction

Is it possible to scale a network by increasing the synaptic weight? If so the features identified in the previous section should be preserved.

2.4.2 Methods

2.4.2.1 Simulations

In this section the simulations carried out in section 2.3.2 were twice repeated identically, with the exception that a synaptic weight was applied uniformly to all synapses. The weighting values were 10 and 100.

2.4.2.2 Analysis

The same analysis was carried out on these simulations as in section 2.3.2.

2.4.3 Results

2.4.3.1 Scaling using synaptic weights

Figure 2.16 shows the average value of the mean field potential for synaptic weights of 10 and 100. The parameter space explored is the input Gaussian white noise mean between -270 and 300 pA and the input Gaussian white noise standard deviation between 580 and 2100 pA. With both the synaptic weights investigated the region where there is no firing preserves the encoding of input mean and standard deviation observed in the networks with a synaptic weight of 1. Where there is a synaptic weight of 10 there is a small region of low mean and high standard deviation where there is a very low firing rate in the cells and the input parameters are encoded in the mean. This region is not present where the synaptic weight is 100. In both synaptic weights there is a distinct network activity threshold where no input parameters are encoded in the mean and all parameters result in the same fixed mean. In this region the firing rate of the cells is between 417-430 Hz.

In figure 2.17 the standard deviation of the mean field potential is shown in the same parameter space as in figure 2.16. In the non firing state the encoding of the input parameters are the same as in the network with a synaptic weight of 1. Along the threshold line of network activity the standard deviation increases towards that of an individual cell firing at maximal rate. Simulations above this have a very low standard deviation approaching zero as the input parameters increase.

2.4.4 Discussion

Below the network firing threshold level the network with increased synaptic weights behaves in the same way as a network with unitary weights. This is to be expected as the field potential is determined by the subthreshold properties of the cells integrating the input. At the threshold there is a region where there is maximal synchronised firing of the network around a fixed mean, this is demonstrated by the high standard deviation. In this situation network communication allows the cells to synchronise in maximal firing. Above this threshold there is unsynchronised firing of the network as each cell initially enters maximal firing at a time determined by the white noise input.

In simulations carried out at values of synaptic weights of two or three the properties of the network described with a unitary weighting are greatly reduced or absent, with firing rates quickly reaching an unrealistic range. It has been suggested that leaky integrate and fire cells perform individually in a realistic range at a weighting of up to 3, however within a network the

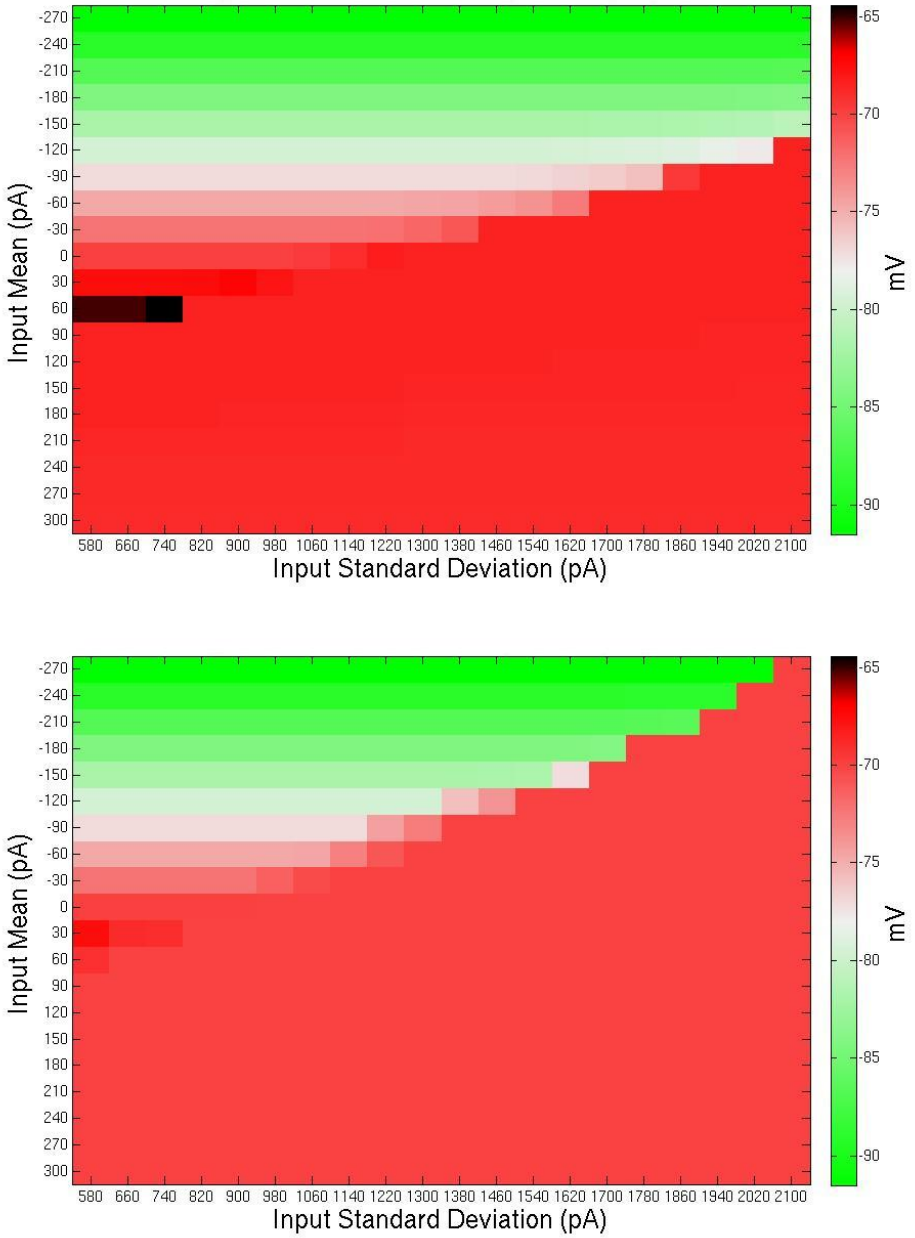

Figure 2.16: **Average values of the mean field potential for synaptic weights of 10 and 100***(Top) the average value of the mean field potential (mV) with a weighting of 10. (Bottom) the average value of the mean field potential (mV) with a weighting of 100.*

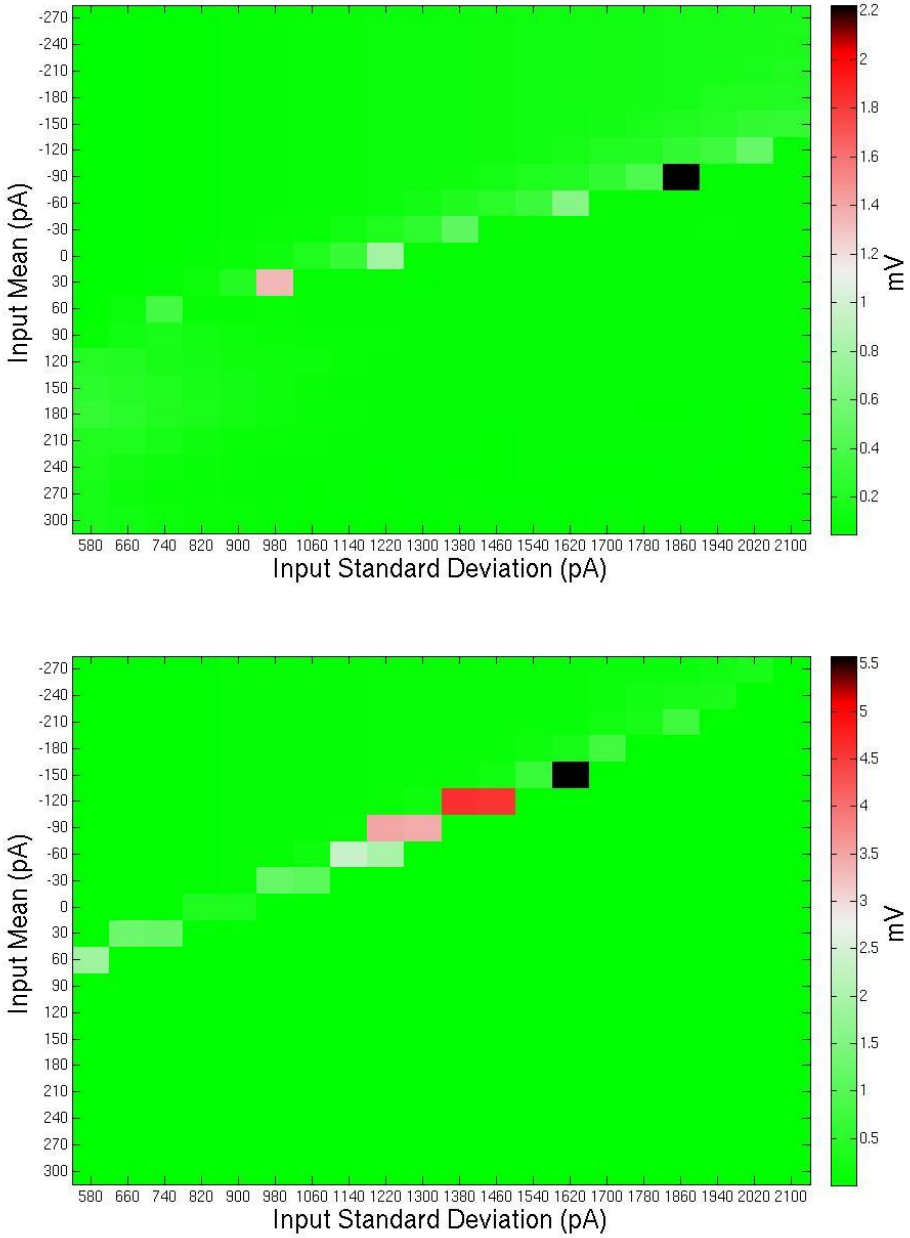

Figure 2.17: **The standard deviations of the mean field potential for synaptic weights of 10 and 100***(Top) the standard deviation of the mean field potential (mV) with a weighting of 10. (Bottom) the standard deviation of the mean field potential (mV) with a weighting of 100.*

biologically plausible activity response range is reduced and possible input encoding regions are less distinct or absent(Burkitt 2006). As such scaling of the network using increased weights was not a desirable avenue of investigation.

2.5 An investigation into network connectivity

2.5.1 Introduction

Having posited in section 2.3 a region where network activity performs a computation on the input this section will address the role of network connectivity in the behaviour of the simulated field potential and the population firing rates.

I will compare the network behaviour with that in section 2.3 in a network with the connections intact, a network with all connections severed, a network with only the excitatory connections and a network with only inhibitory connections. This will be in order to asses whether or not previous observations are down to the passive membrane properties of the neurons, full network activity or if the response properties are dominated by either the inhibitory or the excitatory synaptic connections.

2.5.2 Methods

2.5.2.1 Simulations

In this section four sets of four hundred simulations were carried out. The four sets had synaptic weights adjusted to switch the excitatory or inhibitory synapses on or off. The values were, for excitatory and inhibitory synapses (We and Wi): 1 1, 1 0, 0 1 and 0 0. The white noise parameters covered a larger range than the previous simulations. The white noise mean range was from -50 pA to 900 pA in steps of 50 pA. The white noise standard deviation range was from 0 pA to 2280 pA in steps of 120 pA. The white noise seed was the same for all simulations.

2.5.2.2 Analysis

All means and standard deviations were calculated as above. The power spectral density of the simulated field potential was calculated using the Matlab function periodogram. The instantaneous firing rate of the average cell from each population was calculated by dividing the summed firing rate for each

population by the number of cells in that population and then dividing by the duration of the simulation segment.

2.5.3 Results

2.5.3.1 The mean and standard deviation of the simulated field potential

Figure 2.18 show mean value of the simulated field potential across a larger parameter space than in the previous sections. The a comparison between the fully connected network and the disconnected network shows that the most significant differences in the mean values are at the areas where there is a low contribution from long range connections and a high contribution from local synchronised connections, the top right of the plots; and a reduced mean value for higher input means, in particular where there is a lower contribution from synchronised local connections. The similarity between the excitatory only network and the fully connected network shows a significant contribution from the excitatory synapses. However there is a contribution from the inhibitory only connections as the plots are not identical.

Figure 2.19 shows the mean values of the simulated field potential in partially and fully connected networks with the disconnected values subtracted.

Immediately apparent from this figure is that the network activity contribution to the output mean has an opposite effect depending upon whether long range or local input dominates either side of a line of equilibrium that is roughly perpendicular to the network activation threshold. The gradient of this line is not identical in the case of the excitatory only and the inhibitory only networks. The second feature of note is that the excitatory only network drives the simulated field potential toward the negative on the left hand side of this line and towards the positive on the right hand side, whilst the inhibitory only network has the opposite polarity. In the excitatory only network there is a peak in the mean for high local input and low long range input. In the inhibitory only network there is a peak in the mean at the low local input and near the network activity threshold. This is the region where the network has been shown to produce high power oscillatory field potential activity.

Figure 2.20 shows the standard deviation value of the simulated field potential. The bimodal activity identified in the subtracted mean figure is apparent in these standard deviation plots. The disconnected network shows a high standard deviation in the left hand side region that is largely absent from the excitatory only and fully connected network. This is reduced, but still present in the inhibitory only network. Whilst the excitatory network

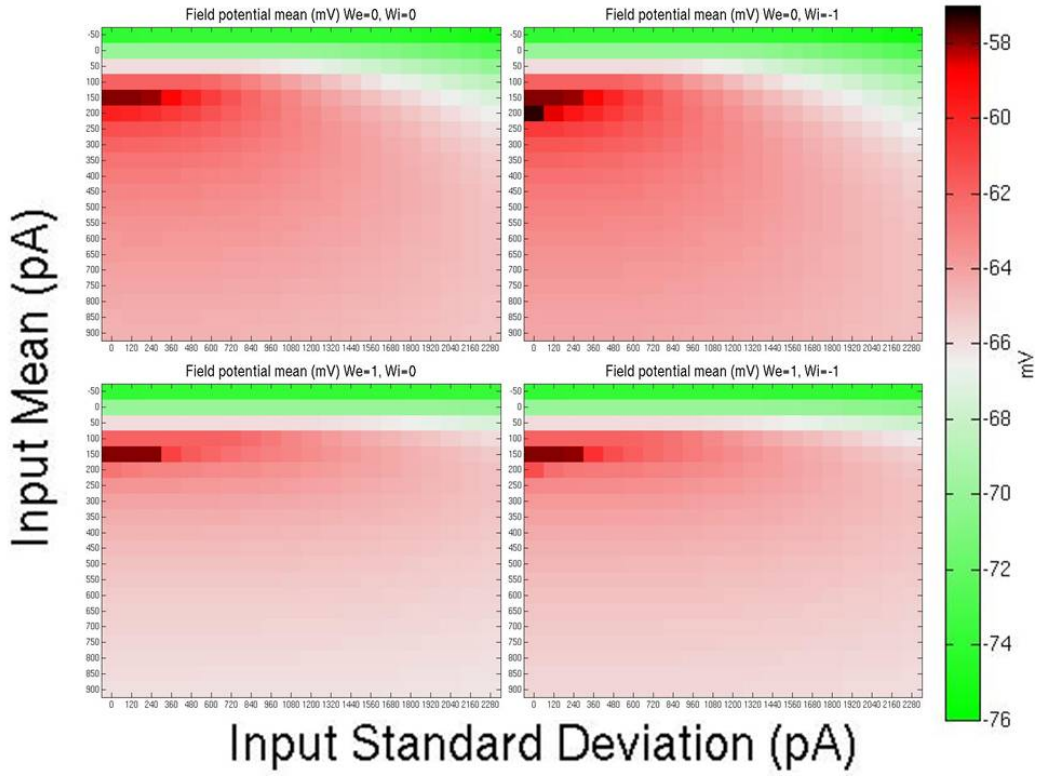

Figure 2.18: **The mean of the simulated field potential in all four connectivity states***In each of the four plots parameter space on the x-axis is the input mean, top to bottom, from -50pA to 300pA in increments of 50pA and the y axis is the input standard deviation, left to right, 0pA to 2280pA in increments of 120pA. (Top left) both excitatory and inhibitory synapses are disconnected. (Top right) the excitatory synapses are disconnected. (Bottom left) the inhibitory synapses are disconnected. (Bottom right) all synapses are connected.*

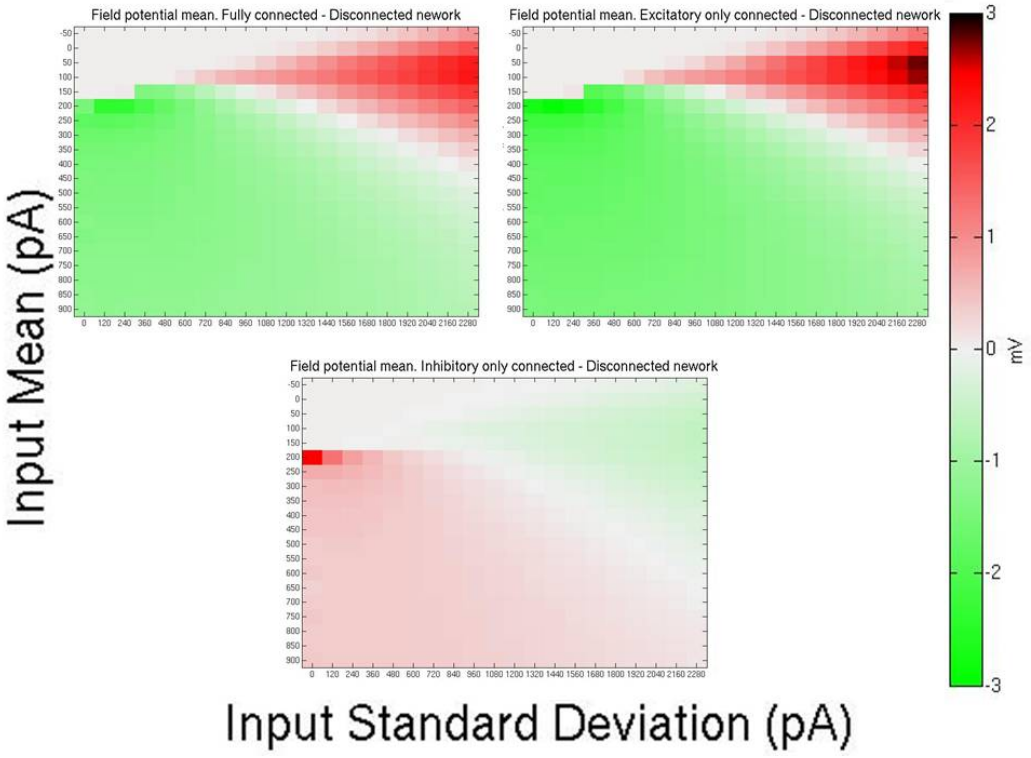

Figure 2.19: **The means of the simulated field potential in partially and fully connected networks with the disconnected values subtracted** *In each of the three plots parameter space on the x-axis is the input mean, top to bottom, from -50pA to 300pA in increments of 50pA and the y axis is the input standard deviation, left to right, 0pA to 2280pA in increments of 120pA. (Top left) the fully connected network mean values with the mean values of the disconnected network subtracted. (Top right) the excitatory connected network mean values with the mean values of the disconnected network subtracted. (Bottom) the inhibitory connected network mean values with the mean values of the disconnected network subtracted.*

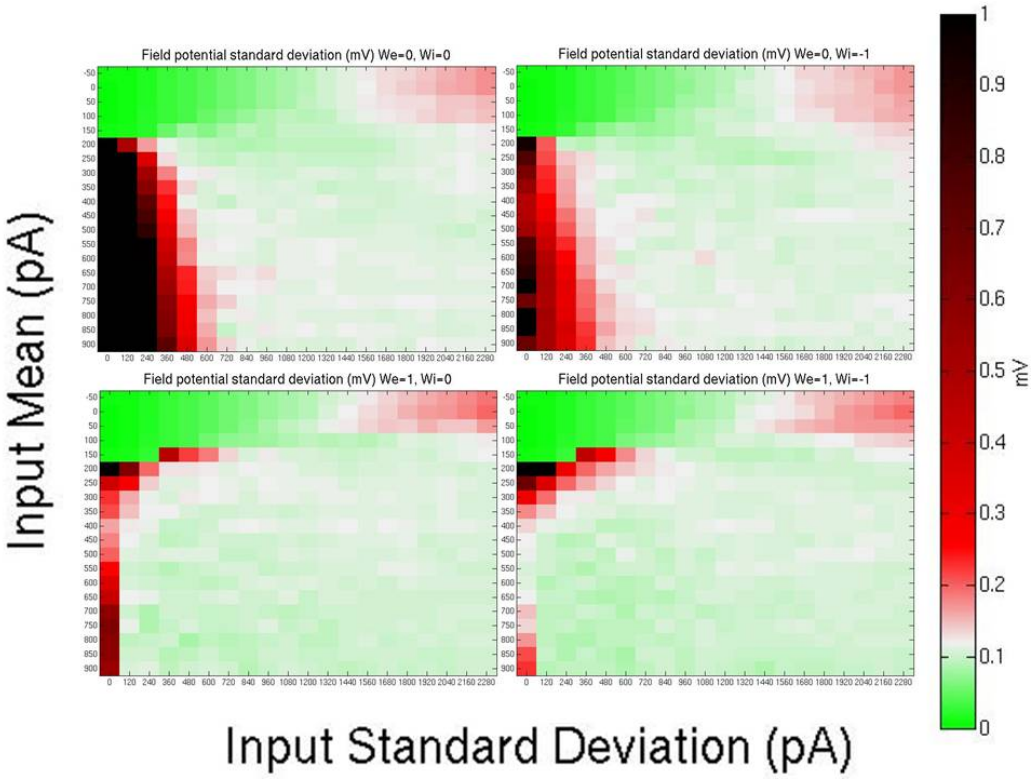

Figure 2.20: **The standard deviation of the simulated field potential in all four connectivity states** *In each of the four plots parameter space on the x-axis is the input mean, top to bottom, from -50pA to 300pA in increments of 50pA and the y axis is the input standard deviation, left to right, 0pA to 2280pA in increments of 120pA. (Top left) both excitatory and inhibitory synapses are disconnected. (Top right) the excitatory synapses are disconnected. (Bottom left) the inhibitory synapses are disconnected. (Bottom right) all synapses are connected.*

more closely reflects the standard deviation distribution of the fully connected network it should be noted that in the region of low local connection input around the network activity threshold there is a higher standard deviation. This suggests that the inhibitory cells contribute to the oscillatory nature of the simulated field potential. The right hand side of the plots are largely similar

Figure 2.21 shows the standard deviation values of the simulated field potential in partially and fully connected networks with the disconnected values subtracted. These figures are largely similar, however the higher standard deviation values around the network activity threshold on the left hand side of the plot are notable. The fully connected network has significantly higher standard deviation values in this region that in either of the partially connected networks suggesting a synergistic interaction between the two cell types.

2.5.3.2 The population firing rates

Figure 2.22 shows the mean firing rate of the average cell in each population across the whole simulation time versus the input mean. In all populations across all input mean the general trend is the lowest firing rate is in the inhibitory only connected network followed by the disconnected network, then the fully connected network and finally the highest firing rates in the excitatory only network. The only exception to this is at the high input mean in the layer 5 inhibitory cells, where the disconnected network cells fire at a slightly higher rate than the fully connected network. The reduction in firing rate between the disconnected network and the inhibitory only network is approximately equal to the reduction in firing rate between the excitatory only network and the fully connected network.

Where the input mean is less than approximately 300 pA the firing rate of the cells are more sensitive to the local input than above this, where the input mean is reflected linearly in the firing rate. It is also in this range that the cell firing rates are within a biologically realistic instantaneous firing rate range. The simulated field potential is oscillatory here too.

2.5.3.3 The simulated field potential and its power spectral density

In the figures presented in this section the simulated field potentials from all four connectivity conditions will be presented along with their power spectral densities from a named point in parameter state. In each axes the Disconnected network will be represented with a red line. The fully con-

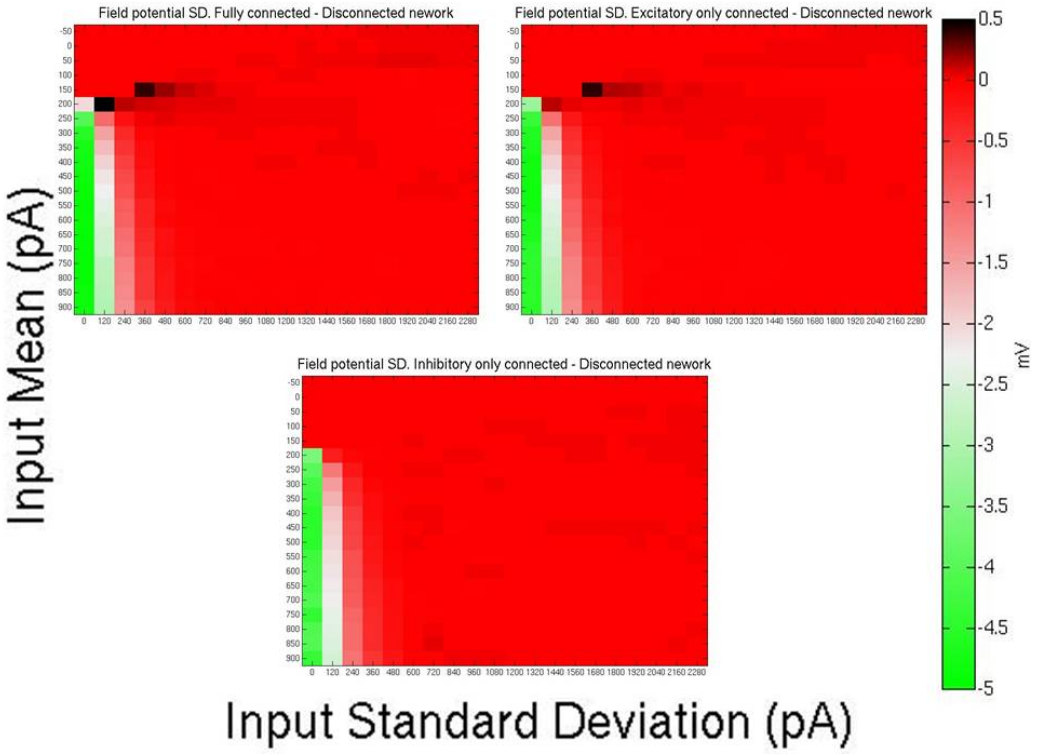

Figure 2.21: **The standard deviations of the simulated field potential in partially and fully connected networks with the disconnected values subtracted***In each of the three plots parameter space on the x-axis is the input mean, top to bottom, from -50pA to 300pA in increments of 50pA and the y axis is the input standard deviation, left to right, 0pA to 2280pA in increments of 120pA. (Top left) the fully connected network standard deviation values with the standard deviation values of the disconnected network subtracted. (Top right) the excitatory connected network standard deviation values with the standard deviation values of the disconnected network subtracted. (Bottom) the inhibitory connected network standard deviation values with the standard deviation values of the disconnected network subtracted.*

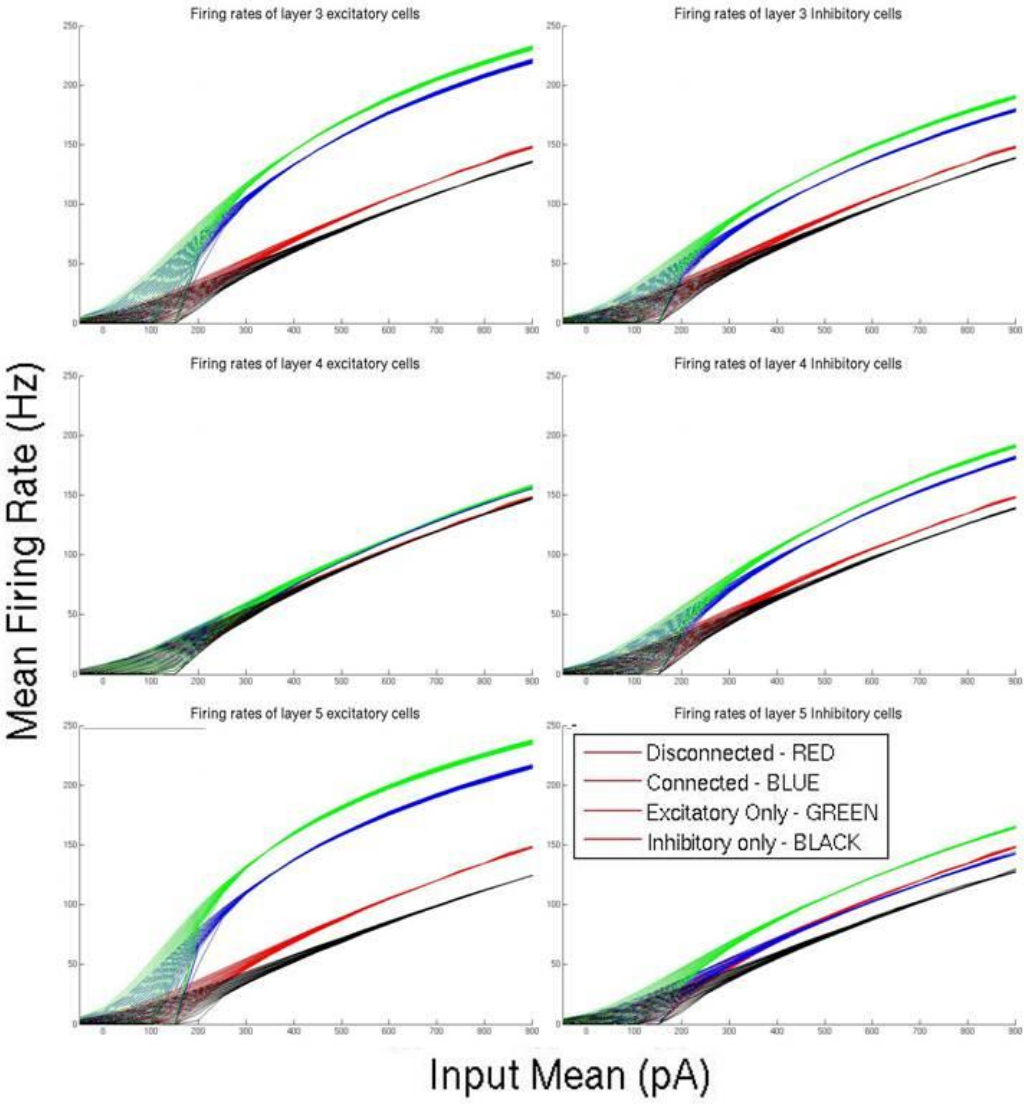

Figure 2.22: **The mean firing rate of the average cell in all populations***In each figure the y-axis is the mean firing rate from 0Hz to 250Hz in increments of 50Hz and the x-axis is the input mean from -30pA to 900pA in increments of 100pA. The left hand plots are the excitatory cells, the right hand plots are the inhibitory cells. The top plots are the layer 3 cells, the middle plots are the layer 4 cells and the bottom plots are the layer 5 cells. The red lines are the disconnected network simulations. The blue lines are the fully connected network simulations. The green lines are the excitatory only connected network simulations. The black lines are the inhibitory only connected network simulations.*

nected network with a blue line. The excitatory only by a green line and the inhibitory only network by a black line.

Figure 2.23 shows the network with a simple ramp input, i.e. the standard deviation of the input is 0pA. In the disconnected network plot it is apparent that there is a strong synchronised oscillation of around 20 Hz. This feature is present in all network connectivity conditions with the inhibitory only network damping this until it is significantly less prominent in the simulation time window. In the excitatory only network the 20Hz signal becomes dampened, and less sawtoothed in shape, but maintains its amplitude. In the fully connected network it is amplitude modulated with an envelope frequency of 1.5 Hz.

Figure 2.24 shows the simulated field potential in a region of parameter space where the cells have zero firing rate. All networks' simulated field potentials respond in the exact same way to the input. We can see from the PSDs that they have a characteristic $1/f\alpha$ power frequency relationship.

In figure 2.25 the oscillatory nature of the simulated field potential is apparent. In all networks the initialisation of the network causes the simulated field potential to rebound and oscillate. In the disconnected network the synchronisation of the cells decays until about 450 ms, where it shows a signal similar to the non firing network in figure 2.24. The inhibitory only network desynchronises by 200 ms then begins to re synchronise at around 500 ms. The excitatory only network desynchronises until about 180 ms where it reaches a persistent level of synchronisation for the remainder of the simulation. The fully connected network desynchronises until around 220 ms where it stabilizes at a slightly higher fundamental frequency than the excitatory only network and with a slightly higher amplitude. In the power spectral density plot was calculated from 200 - 1000 ms to remove the majority of the onset synchronisation oscillation. The fully connected network has a larger oscillatory power than the other networks. It has peaks that are correlated with peaks in the excitatory only network at approximately 24 Hz, 40 Hz, 60 Hz and those that are not at 30 Hz, 48 Hz, 70 Hz and 90 Hz. There is a peak in the inhibitory only network at 20 Hz and one at 30 Hz associated with the fully connected network.

In figure 2.26 all network conditions have a higher fundamental frequency. The disconnected network has a higher gain, but it still decays as it desynchronises. The inhibitory only network oscillates between 100 and 500 ms, desynchronises and the begins to oscillate between 800 and 900 ms. The excitatory only network desynchronises to a stable level of synchronisation around 100 ms. The fully connected network desynchronises to a stable level by around 150 ms. In the power spectral density plot the fully connected network has a peak around 40 Hz this is flanked at 35 Hz by the disconnected

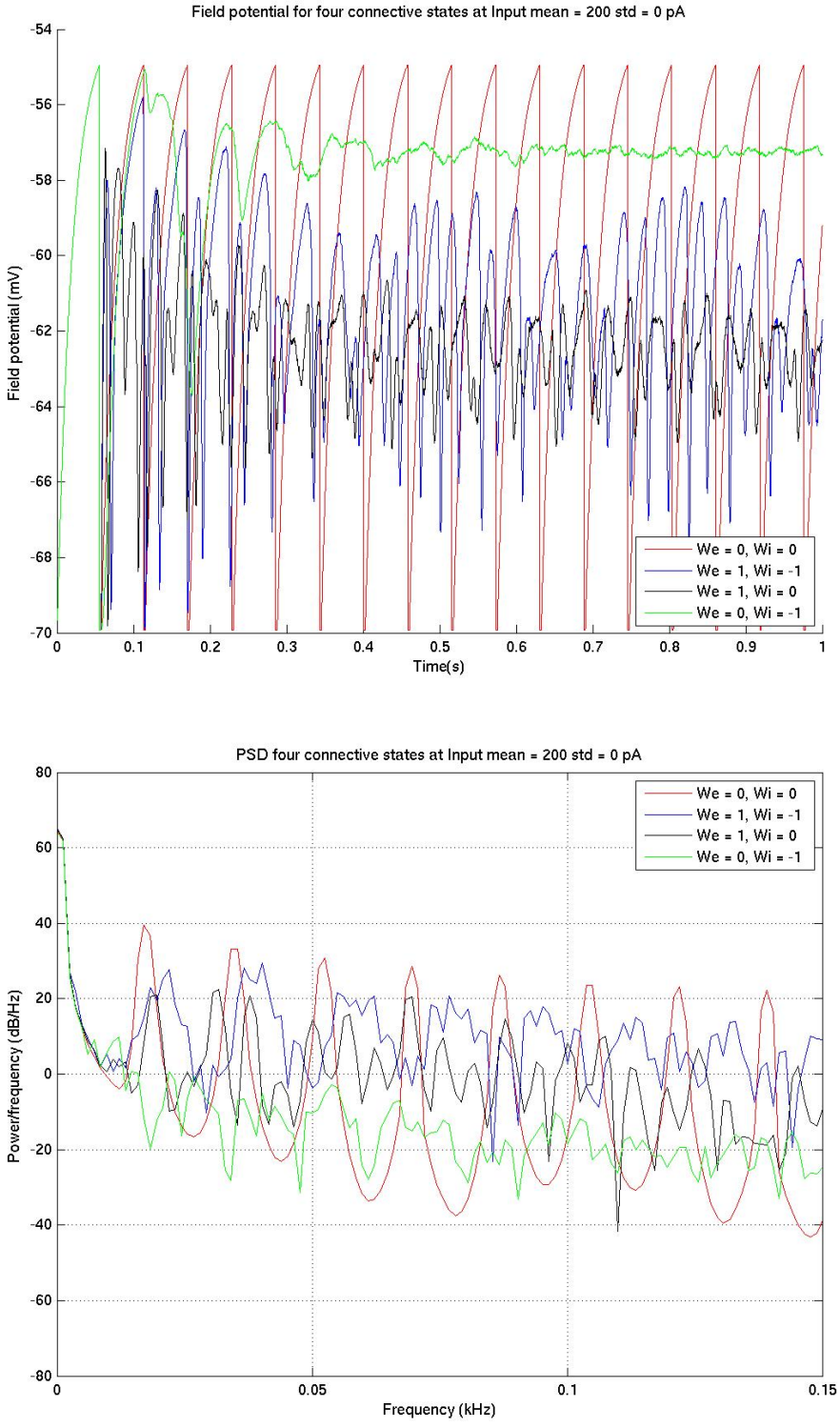

Figure 2.23: **The simulated field potential and its PSD with input mean of 200 pA and a standard deviation of 0 pA** *The top plot is the simulated field potential, the bottom plot is the corresponding power spectral density. In each plot the disconnected network is shown in red, the fully connected network is shown in blue, the excitatory only connected network is shown in green and the inhibitory only network is shown in black.*

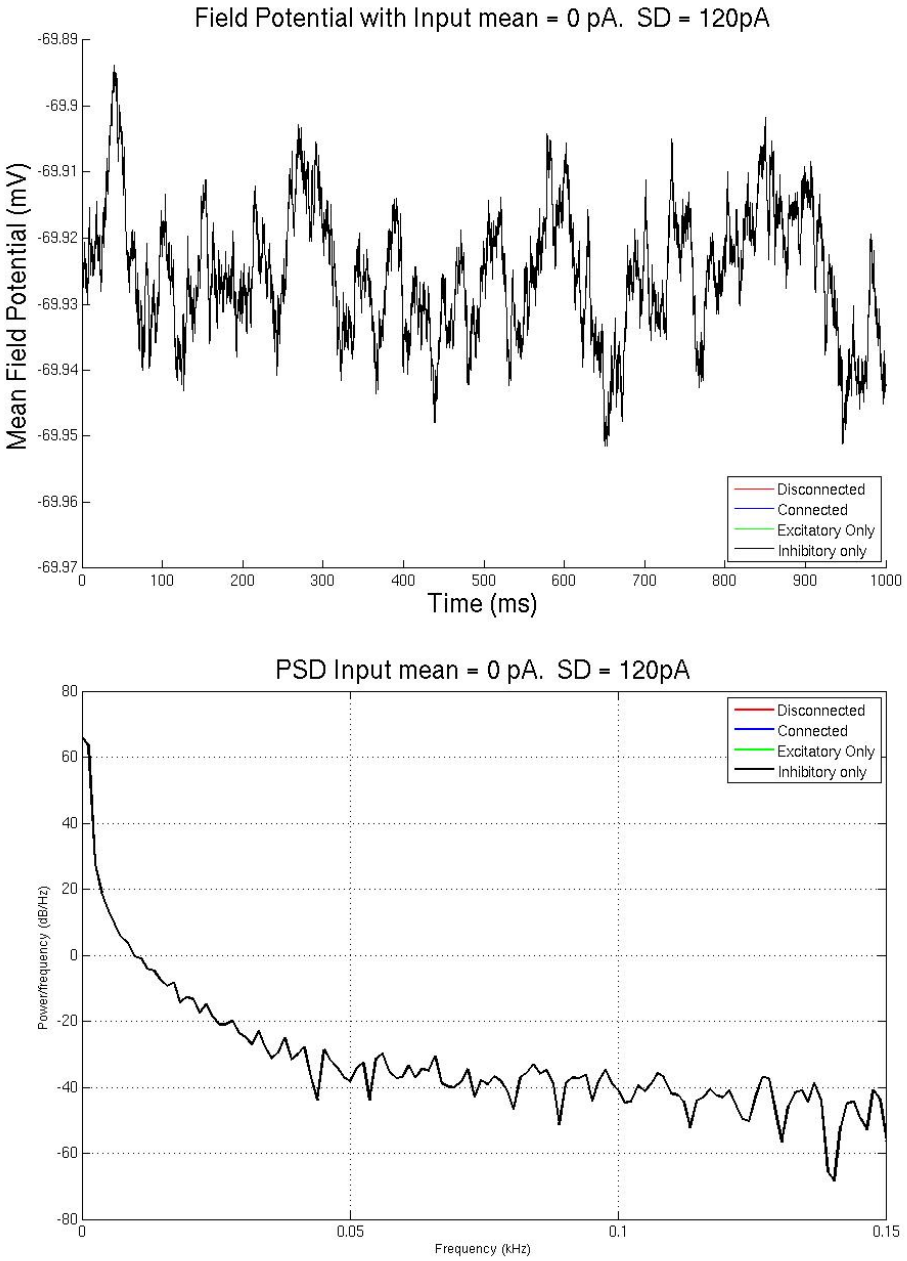

Figure 2.24: **The simulated field potential and its PSD with input mean of 0 pA and a standard deviation of 120 pA** *The top plot is the simulated field potential, the bottom plot is the corresponding power spectral density. In each plot the disconnected network is shown in red, the fully connected network is shown in blue, the excitatory only connected network is shown in green and the inhibitory only network is shown in black.*

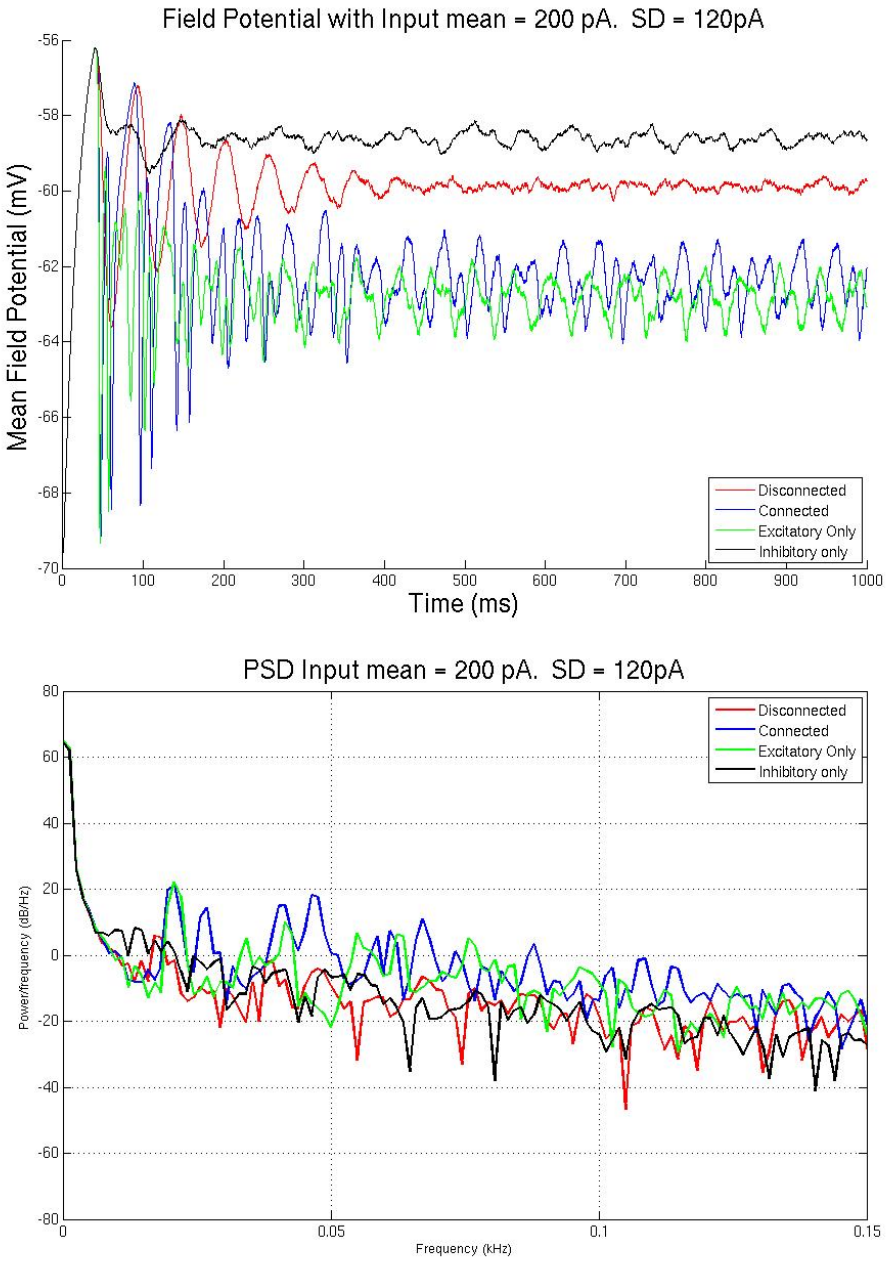

Figure 2.25: **The simulated field potential and its PSD with input mean of 200 pA and a standard deviation of 120pA** *The top plot is the simulated field potential, the bottom plot is the corresponding power spectral density. In each plot the disconnected network is shown in red, the fully connected network is shown in blue, the excitatory only connected network is shown in green and the inhibitory only network is shown in black.*

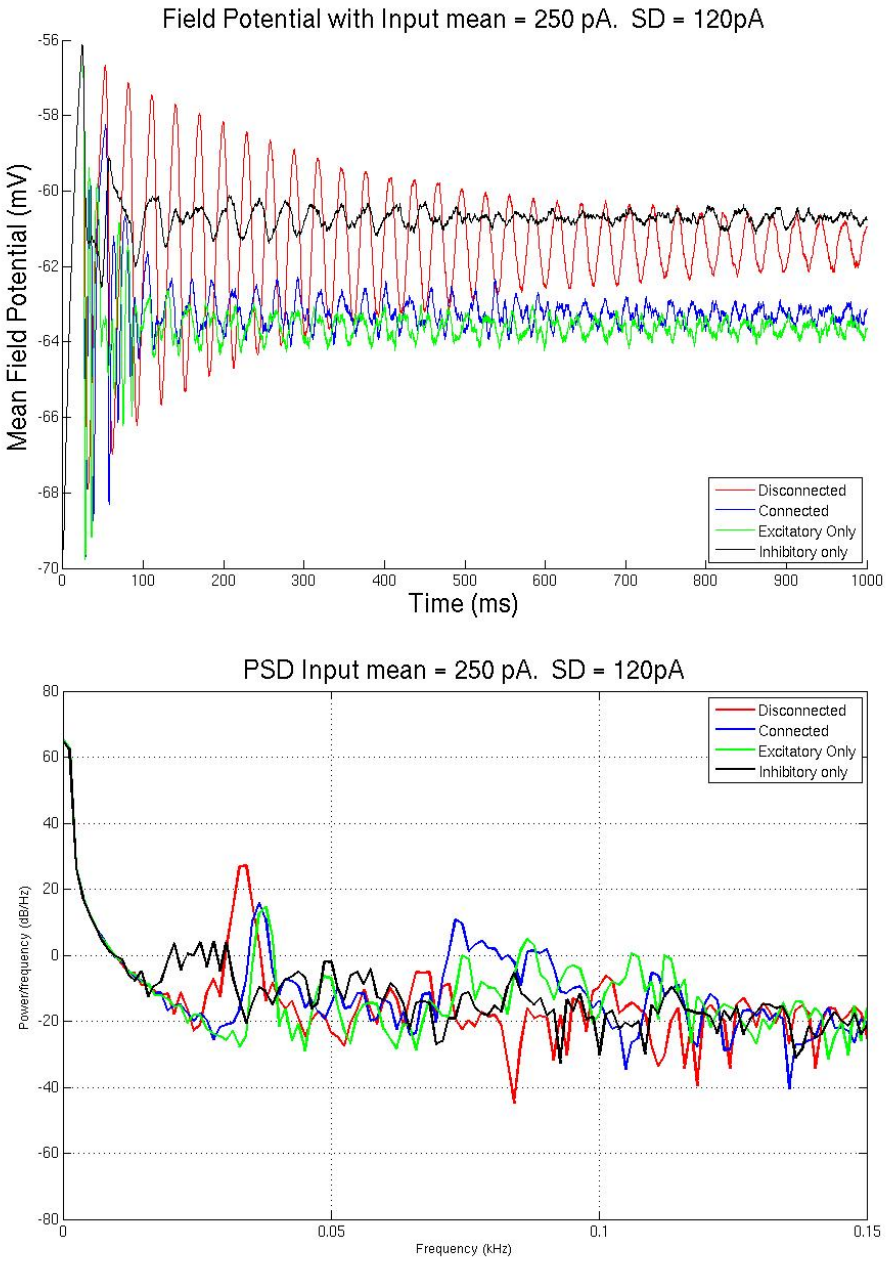

Figure 2.26: **The simulated field potential and its PSD with input mean of 250 pA and a standard deviation of 120 pA** *The top plot is the simulated field potential, the bottom plot is the corresponding power spectral density. In each plot the disconnected network is shown in red, the fully connected network is shown in blue, the excitatory only connected network is shown in green and the inhibitory only network is shown in black.*

network and at about 42 Hz by the excitatory only network. There is a peak in the inhibitory only network between 20 and 35 Hz. Around 70 to 90 Hz there is a peak in the fully connected network that is slightly correlated with a peak in the excitatory only network.

In figures 2.27 and 2.28 the characteristics noted of figure 2.26 persist, but shifted to a higher frequency band as the input mean increases. In addition there emerges a low frequency synchronisation and de-synchronisation of each of the partially or fully connected networks.

Figure 2.29 shows the simulated field potentials and their power spectral densities with an input standard deviation of 1200 pA and an input of 0, 150 and 500 pA for all four network connectivities. At an input mean of 0 pA the network has a low firing rate and the simulated field potentials vary slightly accordingly. Although they do largely follow the input. Their PSDs are strongly correlated and follow a 1/f power frequency relationship.

At an input mean of 150 pA the networks enter a higher firing rate network activation. The simulated field potentials of the fully connected and excitatory connection only networks have a higher mean value and some similarities in the low frequency high amplitude fluctuations. The disconnected and the inhibitory only networks have a slightly lower mean and share some low frequency fluctuations with the inhibitory only network amplifying the negative deflections. Their PSDs do not have any distinctive power differences other than the marginal reduction in power at 60 Hz which is absent in the excitatory only network.

At an input mean of 500 pA the simulated field potential means separate further, with the fully connected and excitatory only networks having a more negative mean. The PSDs take on a flatter white noise characteristic with a notable power increase in the inhibitory only network between 40 and 100Hz.

Figure 2.30 shows the simulated field potentials and their power spectral densities with an input standard deviation of 2280 pA and an input of 0, 150 and 400 pA for all four network connectivities. With an input mean of 0 pA the simulated field potentials are separated by their mean valued, but have highly correlated time series. The excitatory only and fully connected networks match each other especially strongly, and do the disconnected and inhibitory only networks. The PSDs are also very similar differing only slightly from each other. They maintain a 1/f power frequency relationship.

With an input mean of 150 pA the simulated field potentials maintain the correlation pattern as at 0 pA, however they are less strongly correlated. The PSDs have a higher activity between 30 and 50 Hz with a flatter power distribution above 50 Hz.

With an Input mean of 400 Hz there is little correlation between network connectivities. The PSDs are largely flat above 25 Hz with the exception of

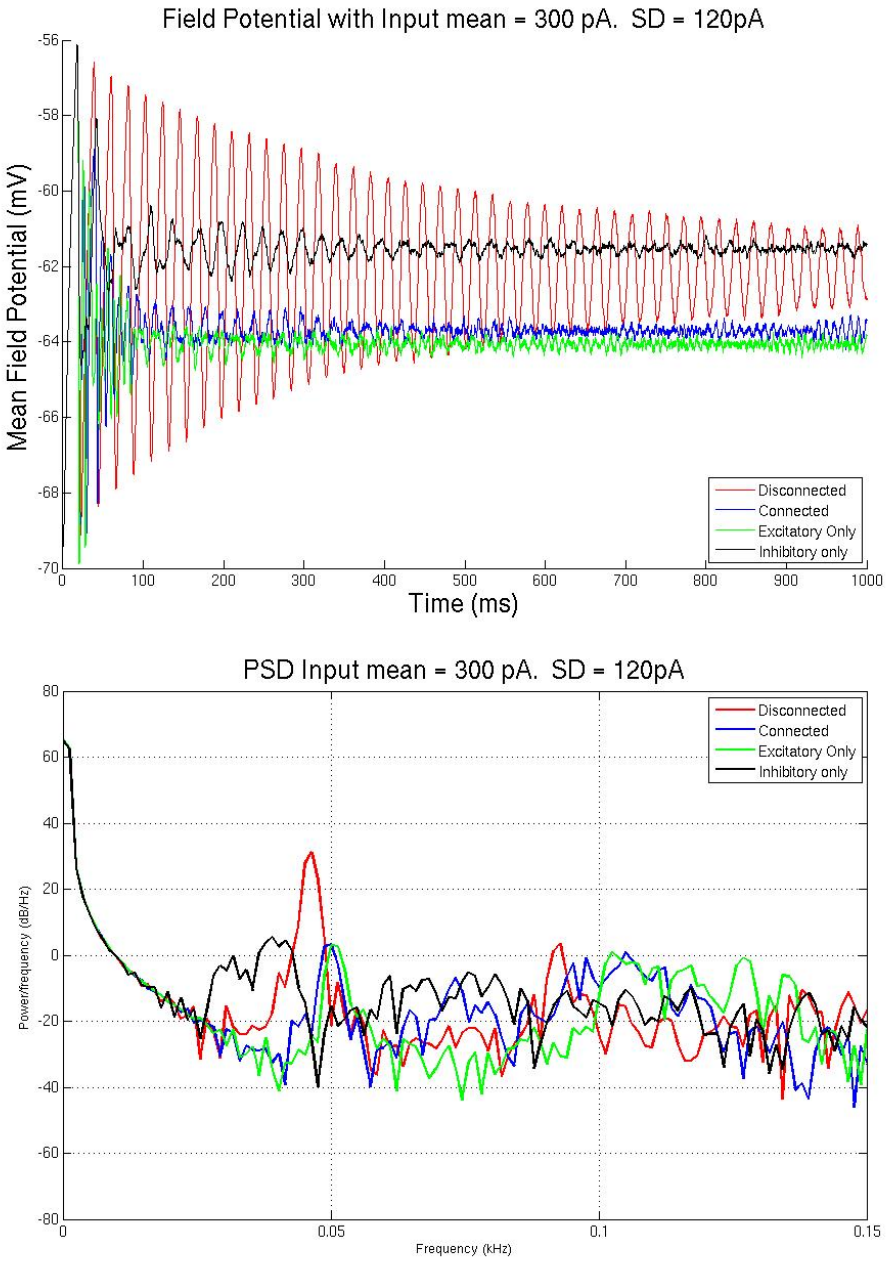

Figure 2.27: **The simulated field potential and its PSD with input mean of 300 pA and a standard deviation of 120 pA** *The top plot is the simulated field potential, the bottom plot is the corresponding power spectral density. In each plot the disconnected network is shown in red, the fully connected network is shown in blue, the excitatory only connected network is shown in green and the inhibitory only network is shown in black.*

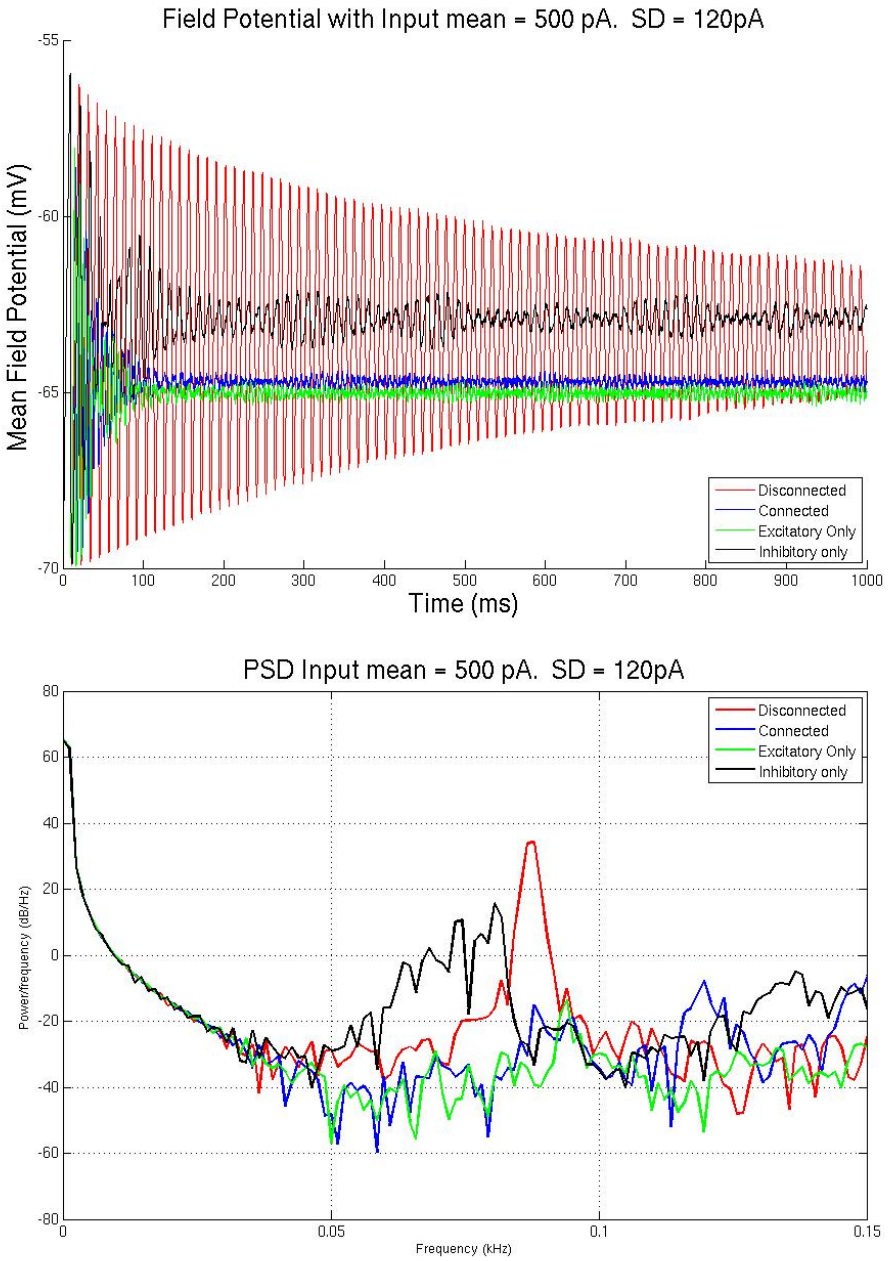

Figure 2.28: **The simulated field potential and its PSD with input mean of 500 pA and a standard deviation of 120 pA** *The top plot is the simulated field potential, the bottom plot is the corresponding power spectral density. In each plot the disconnected network is shown in red, the fully connected network is shown in blue, the excitatory only connected network is shown in green and the inhibitory only network is shown in black.*

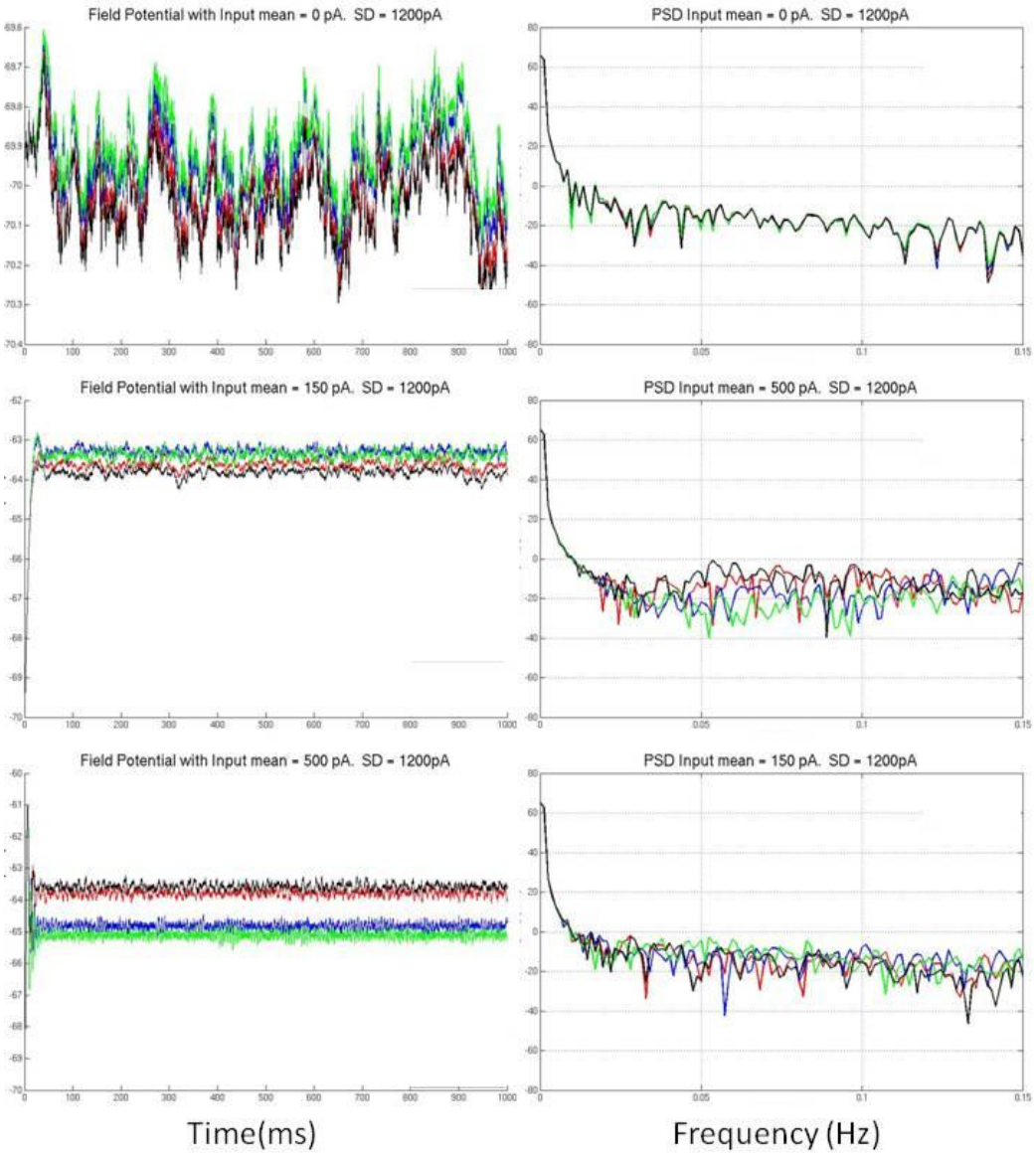

Figure 2.29: **The simulated field potentials and their PSDs with input mean from 0 to 500 pA and a standard deviation of 1200 pA** *The left hand plots are the simulated field potentials, the right hand plots are the power spectral densities. (Top) input mean 0pA, (middle) input mean 150pA and (bottom)input mean 500pA. In each plot the disconnected network is shown in red, the fully connected network is shown in blue, the excitatory only connected network is shown in green and the inhibitory only network is shown in black.*

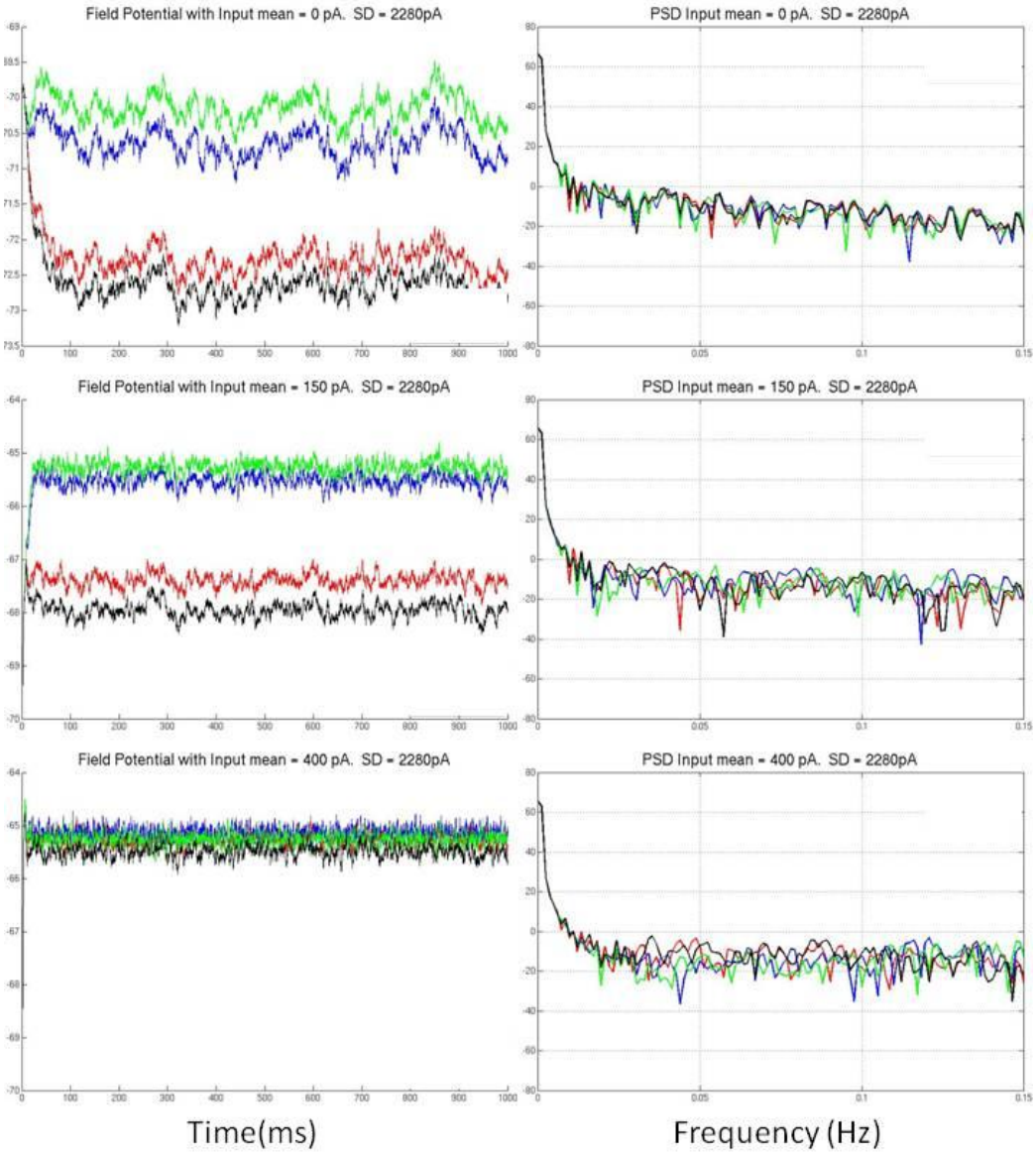

Figure 2.30: **The simulated field potentials and their PSDs with input mean from 0 to 500 pA and a standard deviation of 2280 pA** *The left hand plots are the simulated field potentials, the right hand plots are the power spectral densities. (Top) input mean 0pA, (middle) input mean 150pA and (bottom)input mean 500pA. In each plot the disconnected network is shown in red, the fully connected network is shown in blue, the excitatory only connected network is shown in green and the inhibitory only network is shown in black.*

a small peak at 40 Hz in the inhibitory only network.

2.5.4 Discussion

The primary observation from these simulations and analyses is that each aspect of the simulated signal is variable according to the network connectivity conditions. In all networks below the firing rate threshold the $1/f$ like shape of the power spectra is dependent upon the white noise nature of the input, above this the network shows oscillatory behaviour which deviates from this shape. As the standard deviation of the input decreases individual frequencies tend to dominate.

In the disconnected network synchronized oscillations tend to desynchronise over time, at a quicker rate with lower frequencies. In the inhibitory only network the oscillation amplitude is dampened and reduced in frequency but synchronization is maintained for a longer period of time. In excitatory only networks the oscillation frequency is increased and dampened, but sustained for the duration of the simulation. In the fully connected network the frequency content is slightly more complex showing influence from excitatory and inhibitory networks with some emergent new frequencies.

In the next section I will explore the relationship between input mean and network responses over a twenty trials under three input standard deviation conditions, low, medium and high, in order to obtain a more statistically robust impression of simulated field potential properties and laminar cell firing rates.

2.6 Exploring over twenty trials

2.6.1 Introduction

In this section I explore the nature of the ongoing activity in multiple trials with the same parameter conditions. Firstly I will look at the average power spectral distribution of the simulated field potential according to input mean in three input standard deviation conditions. I hypothesise from previous results that there will be a sustained relationship between input mean and the power spectral density distribution.

Secondly I explore the population firing rates under different input mean conditions. I hypothesise that there will be a relationship between input mean and population mean firing rate. A secondary hypothesis is that during network activity the different populations will have different response properties.

Thirdly I explore the power spectral distribution derived from the mean instantaneous firing rate from each population. I hypothesise that there will be a relationship between the input mean and oscillatory firing rates. A secondary hypothesis is that each cell population will have a different response profile. A tertiary hypothesis is that if there is oscillatory content in the firing rate it will relate to the oscillatory content of the ongoing simulated field potential.

2.6.2 Methods

2.6.2.1 Simulations

In this section six sets of four hundred simulations were carried out. Two sets had a Gaussian white noise input standard deviation of 580 pA, two had a standard deviation of 1300 pA and two had a standard deviation of 2100 pA. In each of these pairs one set used a fully connected network with weights We = 1 and Wi = -1. The second of the pair used a completely disconnected network with the weights We = 0 and Wi = 0. Each set of four hundred simulations consisted of twenty sets of twenty simulations with identical Gaussian white noise input parameters and a different input seed. Each of the twenty subsets had a different Gaussian white noise input mean. For the Gaussian white noise standard deviation 580 pA sets the means were drawn from the range 90 to 280 pA in steps of 10 pA. For the Gaussian white noise standard deviation 1300 pA sets the means were drawn from the range -14.5 to 280 pA in steps of 15.5 pA. For the Gaussian white noise standard deviation 2100 pA sets the means were drawn from the range -128.5 to 280 pA in steps of 21.5 pA. All simulations used the same build seed.

2.6.2.2 Analysis

Power spectral distributions for these simulations were carried out using FieldTrip(Oostenveld 2011). Either the simulated field potential or the instantaneous firing rate for the average cell of each population was analysed. The signal was downsampled at a sample rate of 2000 Hz and demeaned. The power spectrum was calculated using a multi-taper fast Fourier transform with a frequency of interest range from 0 - 150 Hz. The taper was a hanning window and the output was in units power. The firing rates of the cells were calculated as above.

2.6.3 Results

2.6.3.1 The frequency power by input mean over a selection of input standard deviations

In this analysis I seek to establish whether or not there is any regular relationship between the input mean and the frequency content of the simulated field potential. Firstly I establish the case in a network with no white noise input and then I look at the relationship between input mean and simulated field potential under three white noise conditions.

Figure 2.31 shows the average power spectral density from twenty trials at each of the twenty input mean values with an input standard deviation of 0 pA in disconnected and connected networks.

Below an input mean of 180 pA the network activity is flat, so there is no variation in the power spectral density. Above this input mean there is a clear strong fundamental frequency with the harmonic components preserved in the disconnected network, and only the first harmonic component in the connected network a significant feature.

As the input mean increases the fundamental frequency increases proportionally. This figure offers a basis of comparison with subsequent figures.

Figure 2.32 shows the average power spectral density from twenty trials at each of the twenty input mean values with an input standard deviation of 580 pA in disconnected and connected networks. The top plot shows the connected network. For input means below 130 pA the network cells have an average firing rate of less than 20 Hz and exhibit a 1/f like power frequency distribution. For values above 130 pA the network exhibits a dominant oscillatory frequency beginning around 15 Hz increasing almost linearly with the input mean to around 120 Hz. There is most power in the low gamma range with power dropping off as it approaches the higher gamma range. There is a less powerful second peak at the first harmonic of the dominant frequency.

In comparison with figure 2.31 the trend of the fundamental frequency extends to lower frequencies than in the white noise free network's threshold showing an increased range of input representation where white noise is present. The relationship between input mean and fundamental frequency shows a higher gradient in the network with a white noise component.

The bottom plot shows the disconnected network. The power range in this plot is 1/5 of the range in the top plot. There is a peak in oscillation frequency that increases with input mean in a roughly linear fashion that is of a lower gradient than in the connected network. This has maximal power around 45 Hz at input mean of 250 pA. It should be noted from the

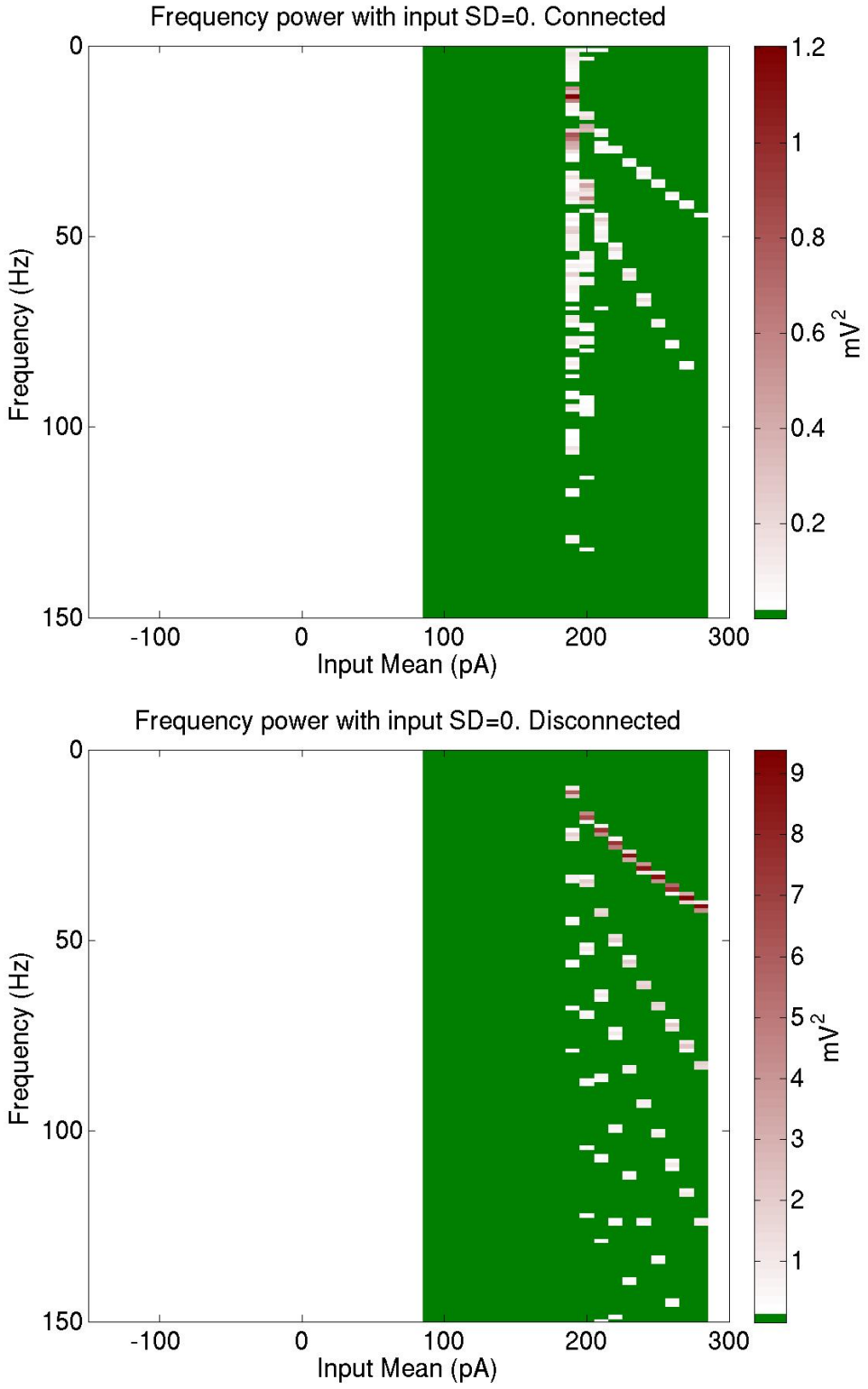

Figure 2.31: **The average power spectral density as input mean increases in a connected and disconnected network. Input standard deviation of 0 pA** *in each plot the mean power spectral density for each of the twenty input mean parameter condition is shown with power being represented by the colour intensity. The top plot is the connected model network and the bottom plot is the network with no intercellular connections.*

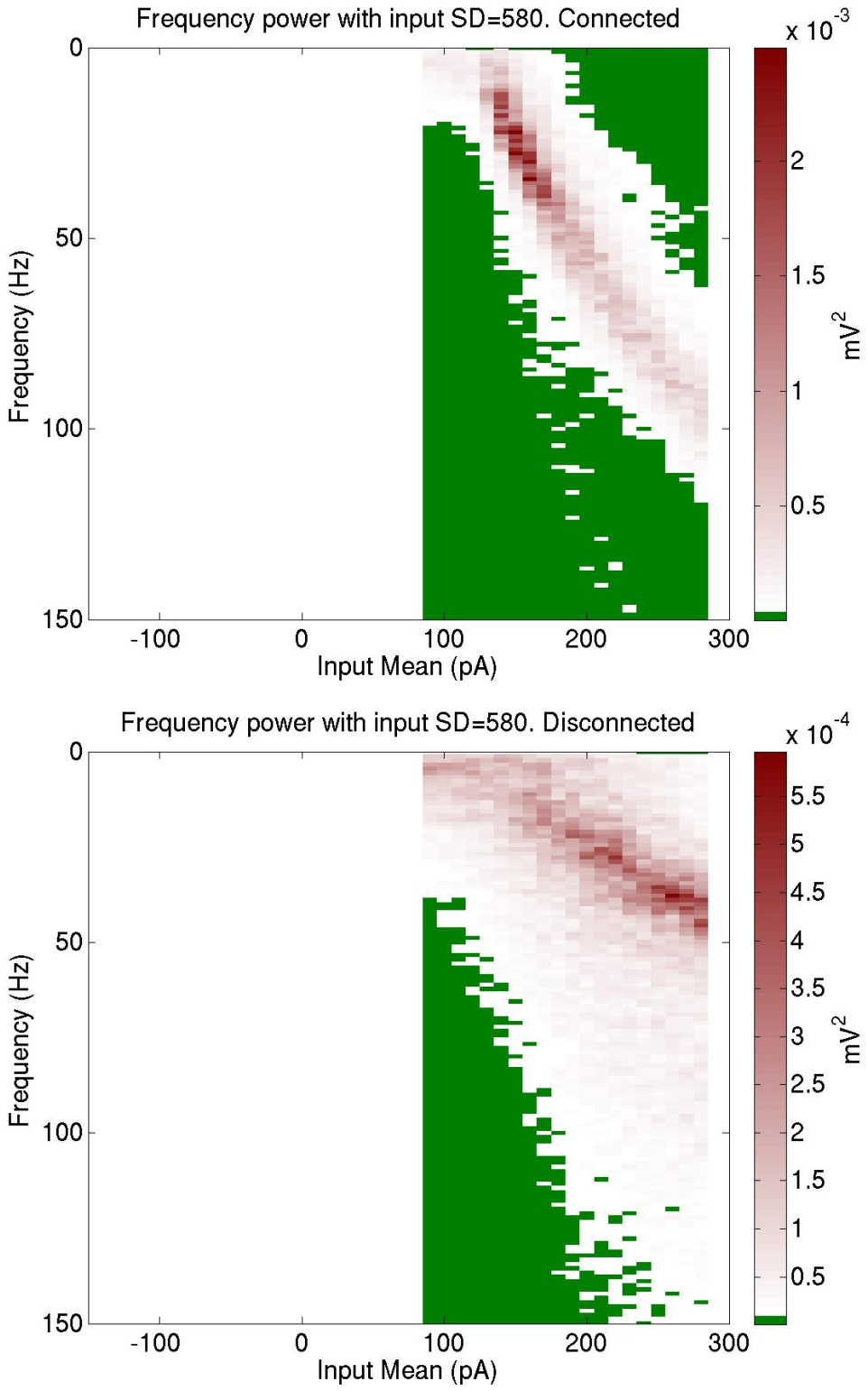

Figure 2.32: **The average power spectral density as input mean increases in a connected and disconnected network. Input standard deviation of 580 pA** *in each plot the mean power spectral density for each of the twenty input mean parameter condition is shown with power being represented by the colour intensity. The top plot is the connected model network and the bottom plot is the network with no intercellular connections.*

previous section that the oscillatory content of the disconnected network is not persistent across the whole simulation period. Rather, it is an artefact of network initialization that decays in amplitude over time as the cell firing desynchronises.

Figure 2.33 shows the average power spectral density from twenty trials at each of the twenty input mean values with an input standard deviation of 1300 pA in disconnected and connected networks. The top plot shows the connected network. As in figure 2.32 with input means below 130 pA the network cells have a low firing rate with the simulated field potential exhibiting a 1/f like power frequency distribution. However, there is a slight additional power in the frequency bands less than 10 Hz. With an input mean greater than 130 pA the relationship between a peak in the power of the frequency band and input mean shown in figure 2.32 is present, if the power is somewhat diminished. The bottom plot shows the disconnected network. Below input mean of 130 pA the network exhibits a similar distribution of power to the disconnected network, however at a two magnitude reduction in power. Above 130 pA there is a relationship between peak frequency and input mean similar to that in figure 2.32 at a vastly reduced power.

Figure 2.34 shows the average power spectral density from twenty trials at each of the twenty input mean values with an input standard deviation of 2100 pA in disconnected and connected networks. In each of the plots containing a white noise input the sub 130 pA mean characteristics shown in figure 2.33 are similar. The frequency content relationship to the mean in figure 2.32 is still marginally present at a greatly reduced power.

This analysis has shown that there is a relationship between input mean and the fundamental frequency of the simulated field potential. In the case where there is no white noise this is a linear relationship once the network passes an "activation threshold" with the addition of white noise there is an extension of this linear relationship at input means below the "activation threshold" of the ramp only network. Under the white noise condition the slope of the linear relationship is increased in the connected network, showing that local activity modulated the fundamental frequency of the input response. There is also a region between 140 pA and 200 pA where the power of the fundamental frequency is maximal. As the white noise standard deviation increases the fundamental frequency has a less strong power representation in comparison to other frequencies. and the power spectral density flattens out.

In the next section I will explore the population mean firing rates in order to determine if this linear relationship between input mean is reflected therein.

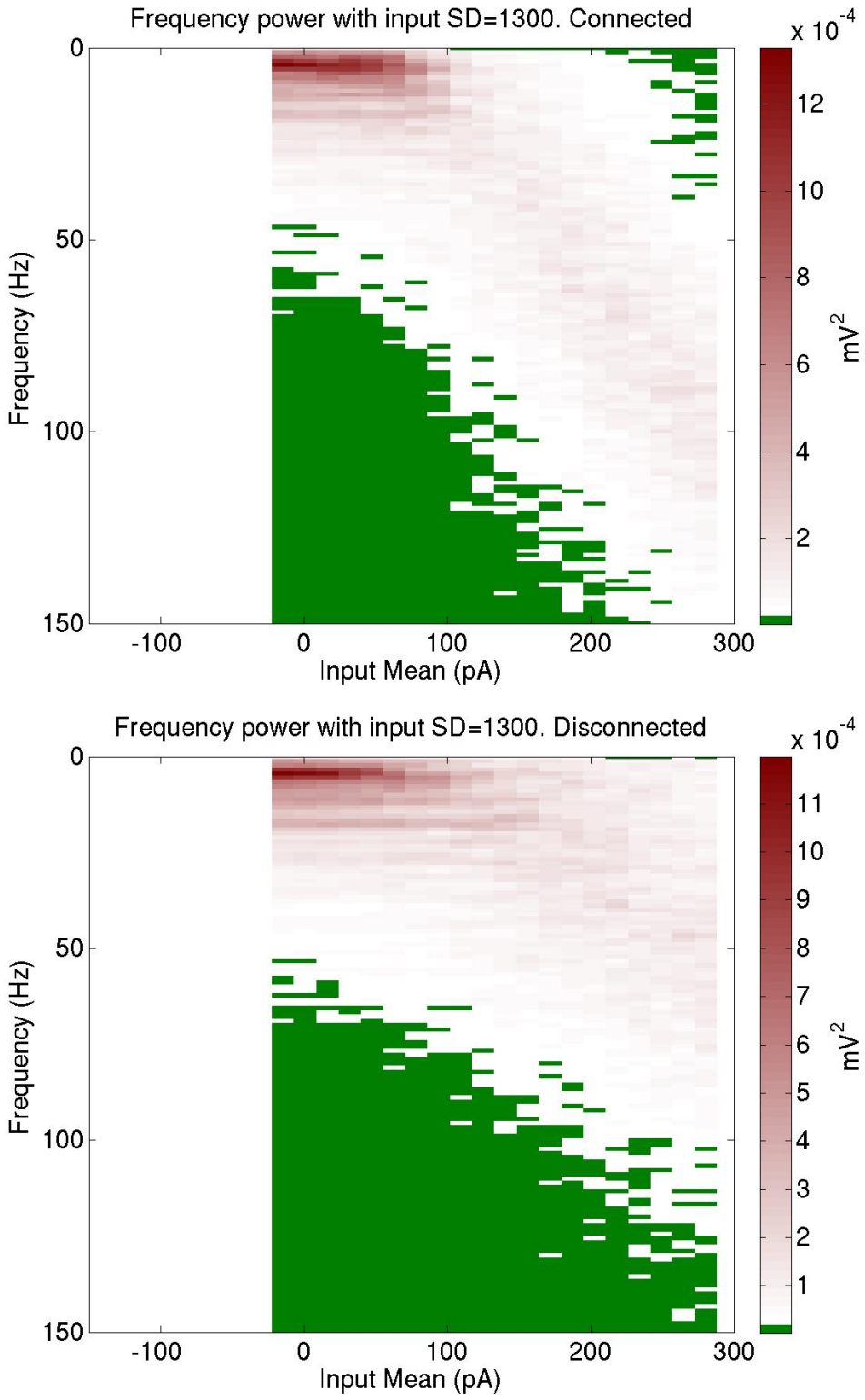

Figure 2.33: **The average power spectral density as input mean increases in a connected and disconnected network. Input standard deviation of 1300 pA** *in each plot the mean power spectral density for each of the twenty input mean parameter condition is shown with power being represented by the colour intensity. The top plot is the connected model network and the bottom plot is the network with no intercellular connections.*

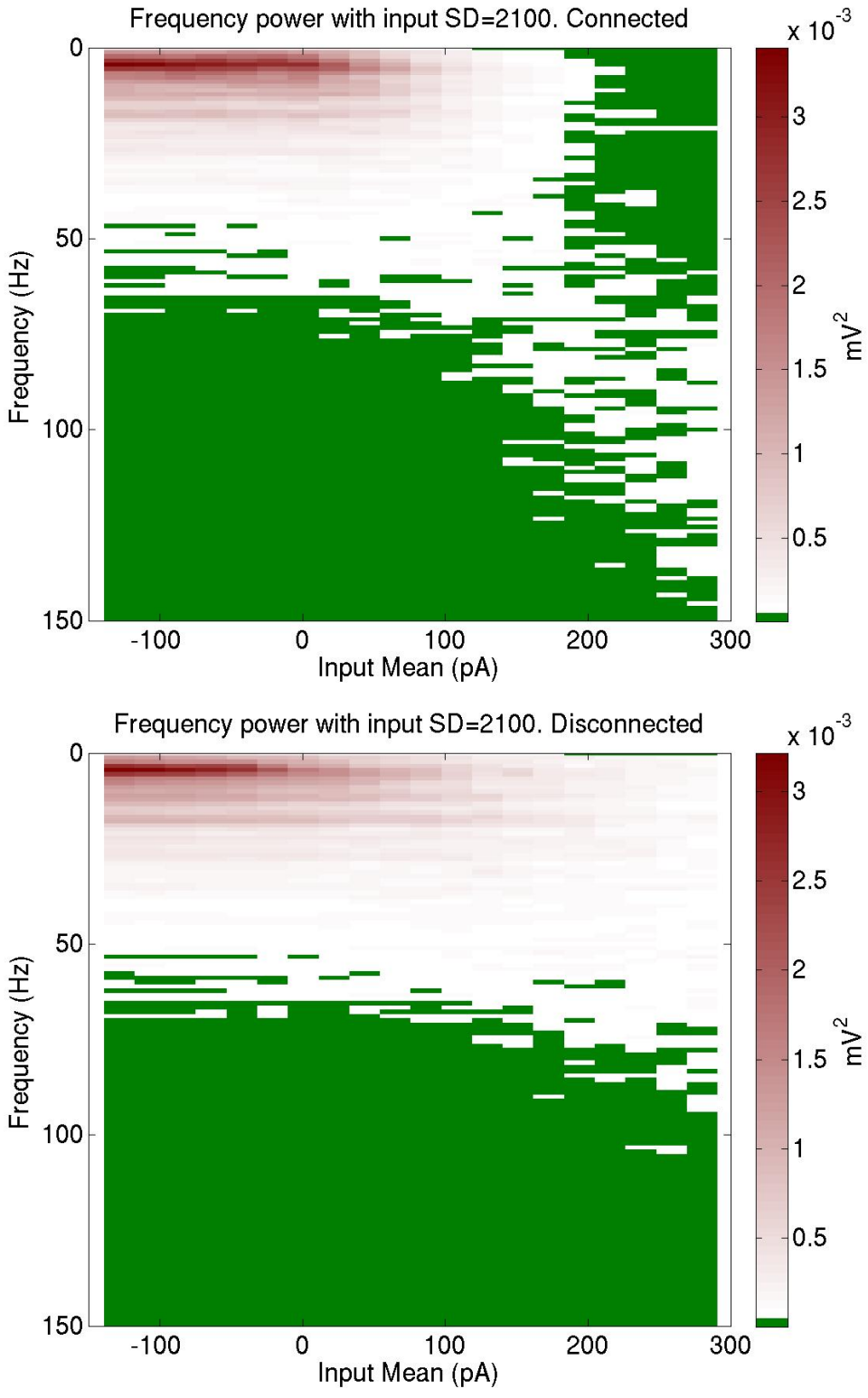

Figure 2.34: **The average power spectral density as input mean increases in a connected and disconnected network. Input standard deviation of 2100 pA** *in each plot the mean power spectral density for each of the twenty input mean parameter condition is shown with power being represented by the colour intensity. The top plot is the connected model network and the bottom plot is the network with no intercellular connections.*

2.6.3.2 The population firing rates

In this analysis I look at the relationship between the input mean and the firing rate of the average cell from each population. I wish to establish if there is any difference in response between each population that is an indicator of local network activity.

Figure 2.35 shows the mean firing rate of the average cell under a constant input in pA. Figure 2.36 shows the mean firing rate of the average cell in each population according to input mean at input standard deviations of 580, 1300 and 2100 pA.

In all plots the firing rate of each cell type reaches the same value by an input mean of 280 pA. Above this the relationship is linear as shown in figure 2.22. In the disconnected network plots all cells have the same firing rate to input mean relationship. The plots are roughly sigmoidal in shape with an increase in input standard deviation leading to in increase in firing rate and the linear relationship beginning at a lower input mean.

In the connected network the average cell from each population has a different mean firing rate. From highest to lowest we have the layer 5 excitatory cell, the layer 3 excitatory cell, the layer 3 inhibitory cell, the layer 4 inhibitory cell, the layer 4 excitatory cell and the layer 5 inhibitory cell.

As the white noise standard deviation value increases the linear phase of the sigmoid extends meaning the input mean is able to be better represented at lower population firing rates.

In this analysis I have established that there is a relationship between the input mean and the firing rate. Further to this the addition of a white noise input allows a better representation of input mean in the low firing rate condition of each cell, in particular in the less than 180 pA mean input condition. In the disconnected networks the individual cells all show the same firing rate relationship, however in the connected network each cell type has a different relationship. Of particular note is the higher slope of the projection neurons, layer 3 and 5 excitatory cells. This range would offer a finer representation of variation in the input mean whilst staying within the biologically realistic range of cell firing rate.

In the next section I will explore the power spectral distribution in each cell population in order to establish whether the individual cell populations show a relationship similar to the psd of the simulated field potential.

2.6.3.3 The oscillatory content of instantaneous cell firing rates

In this analysis I look at the power spectral density response in the firing rate of each cell type in order to establish any relationship to the input mean.

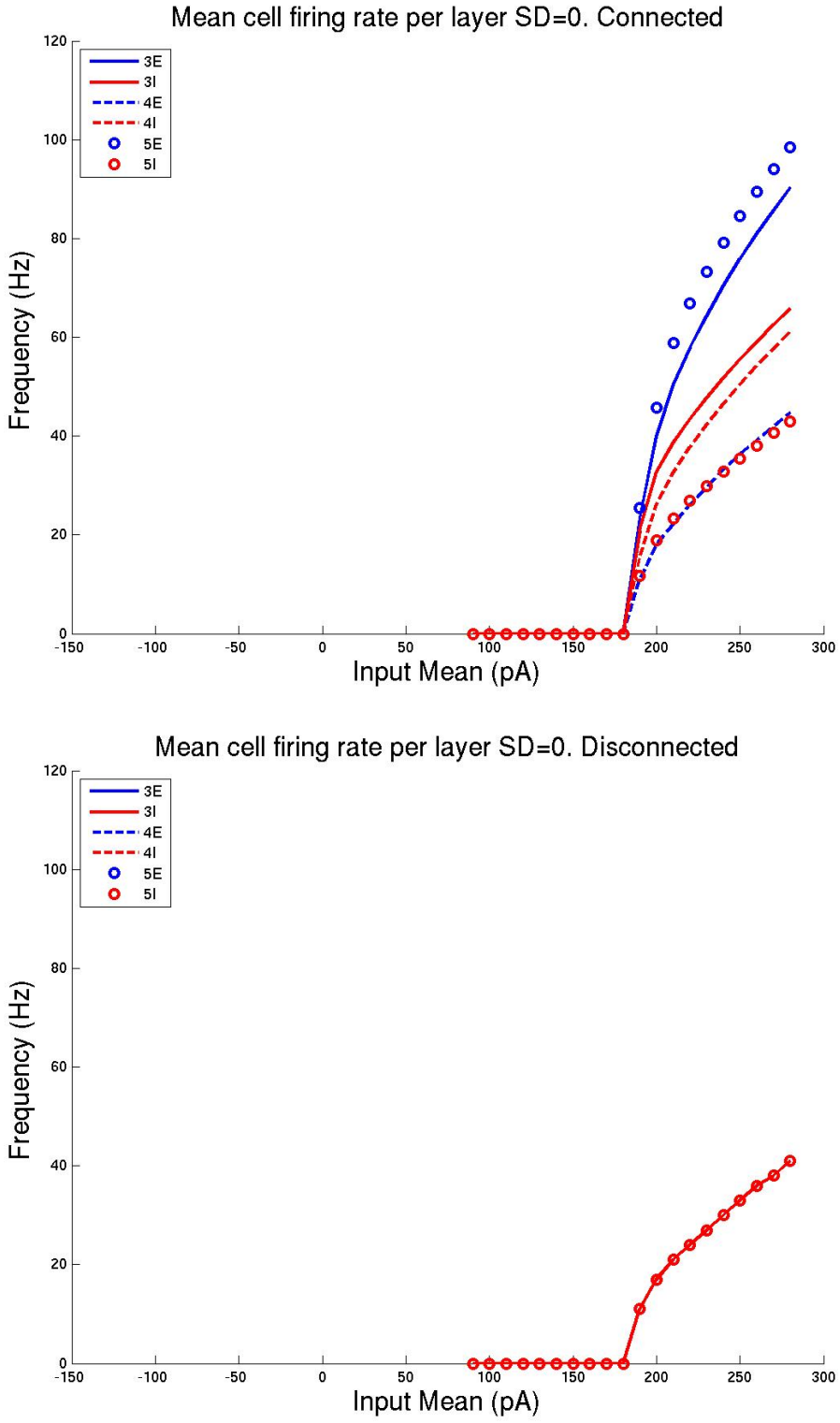

Figure 2.35: **Mean cell firing rates by population under different ramp input means** *The top plot shows the connected network and the bottom plot shows the disconnected network. The blue lines are the excitatory cell populations and the red lines are the inhibitory cell populations. The solid lines are layer 3, the dashed lines are layer 4 and the dotted lines are layer 5.*

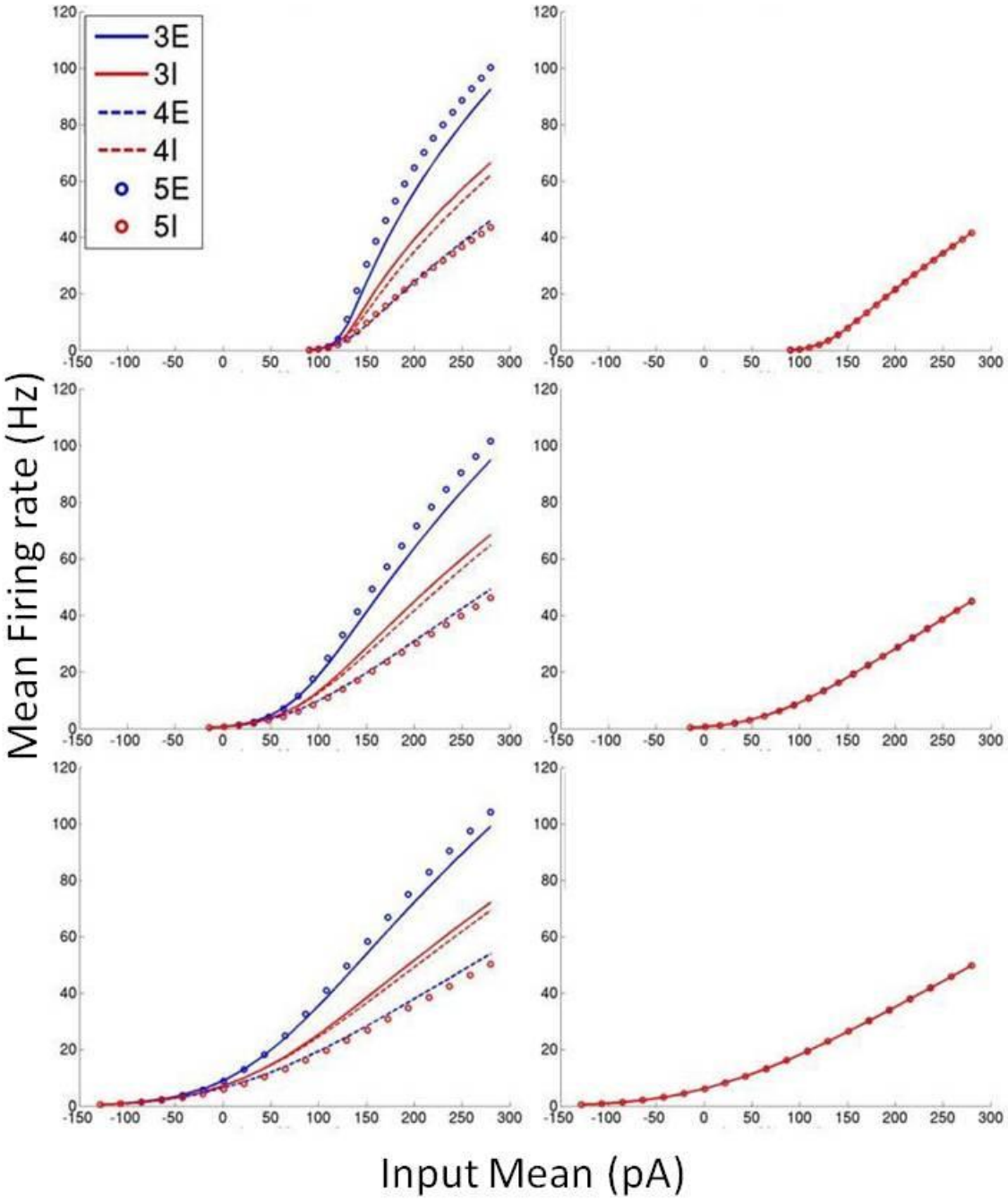

Figure 2.36: **Mean cell firing rates by population under different white noise input parameters** *The left hand plots are from the connected model the right hand plots are from the disconnected model. (Top) input standard deviation of 580pA. (Middle)input standard deviation of 1300pA. (Bottom) input standard deviation of 2100pA. In all plots the blue lines are the excitatory cell populations and the red lines are the inhibitory cell populations. The solid lines are layer 3, the dashed lines are layer 4 and the dotted lines are layer 5.*

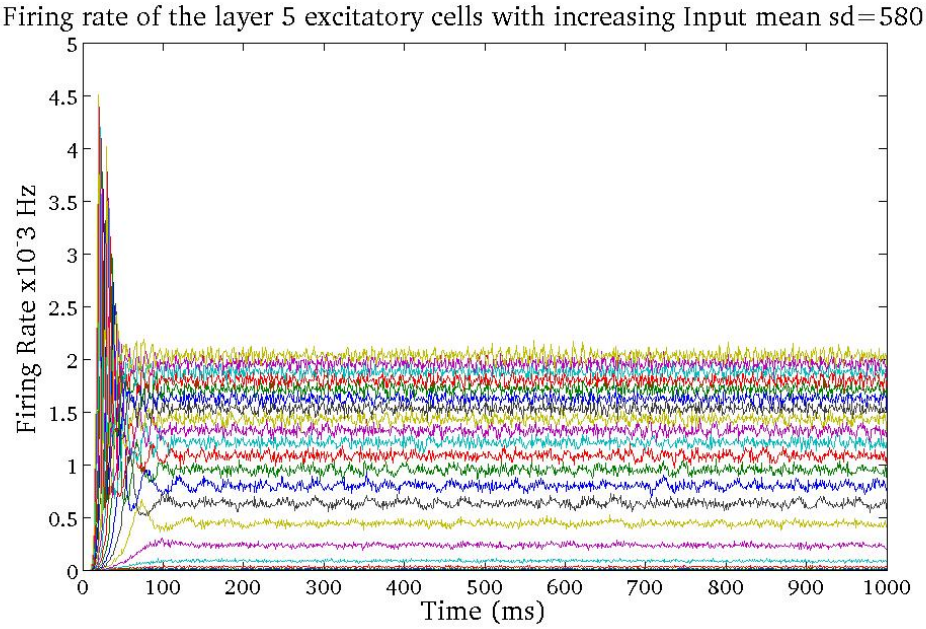

Figure 2.37: **Average layer 5 excitatory cell's instantaneous firing rates over time by increasing input mean for individual simulations** *The mean firing rate increases with the increasing input mean.*

Figure 2.37 shows the average layer 5 excitatory cell's instantaneous firing rates over time by increasing input mean for individual simulations. Each line is a simulation with a different mean. As there is an increasing relationship between mean firing rate and input mean they represent increasing input means. The bottom three lines show no initial spike at onset, and can be considered as the network operating below 'network activation.'

Figure 2.38 shows the power spectral distribution of the instantaneous firing rate of the average cell from each layer and type of population in a connected network with a d.c. current only. The figures are dominated by a single fundamental frequency and its harmonics. The maximum power is highest in the excitatory cells with layer 5 cells having the most high power. The gradient of the relationship between the fundamental frequency and the input mean value is slightly higher in the layer 5 cells with all inhibitory cells having a lower gradient than their equivalent excitatory cells. In figure 2.39 the relationship is virtually the same, however the maximum power in each plot is higher and has a more defined fundamental frequency. This is due to the synchrony of the starting states of the cells.

Figure 2.40 shows the power spectral distribution of the instantaneous firing rate of the average cell from each layer, by the input mean with input standard deviation 580 pA in a connected network. For simulations below the network activation threshold the distributions are flat. Above the threshold there is a peak frequency at each input mean. The relationship between input mean and peak frequency is reminiscent of the simulated field potential relationship in subsection 2.6.3.1. The gradient of this relationship varies according to the population layer and cell type. This is not the case in the disconnected networks of figure 2.41 which are largely the same gradient.

In the connected network as the input white noise standard deviation increases, in figures 2.42 and 2.44, the fundamental frequency becomes less distinct with a variety of other frequencies carrying a similar power value across cell types. However there is a remnant of the inter cell type fundamental frequency gradient relationships.

In this analysis I have been able to establish that the individual cell populations show a periodic relationship to the input mean. This is related to the simulated field potential, showing the same slope in the projection neurons. However in the interneurons the slope is closer to that of the neurons in the disconnected state. The layer 5 inhibitory neurons demonstrate a more complex frequency composition than the other populations. As the white noise is increased, again the psd flatten and there is less representation of the fundamental frequency.

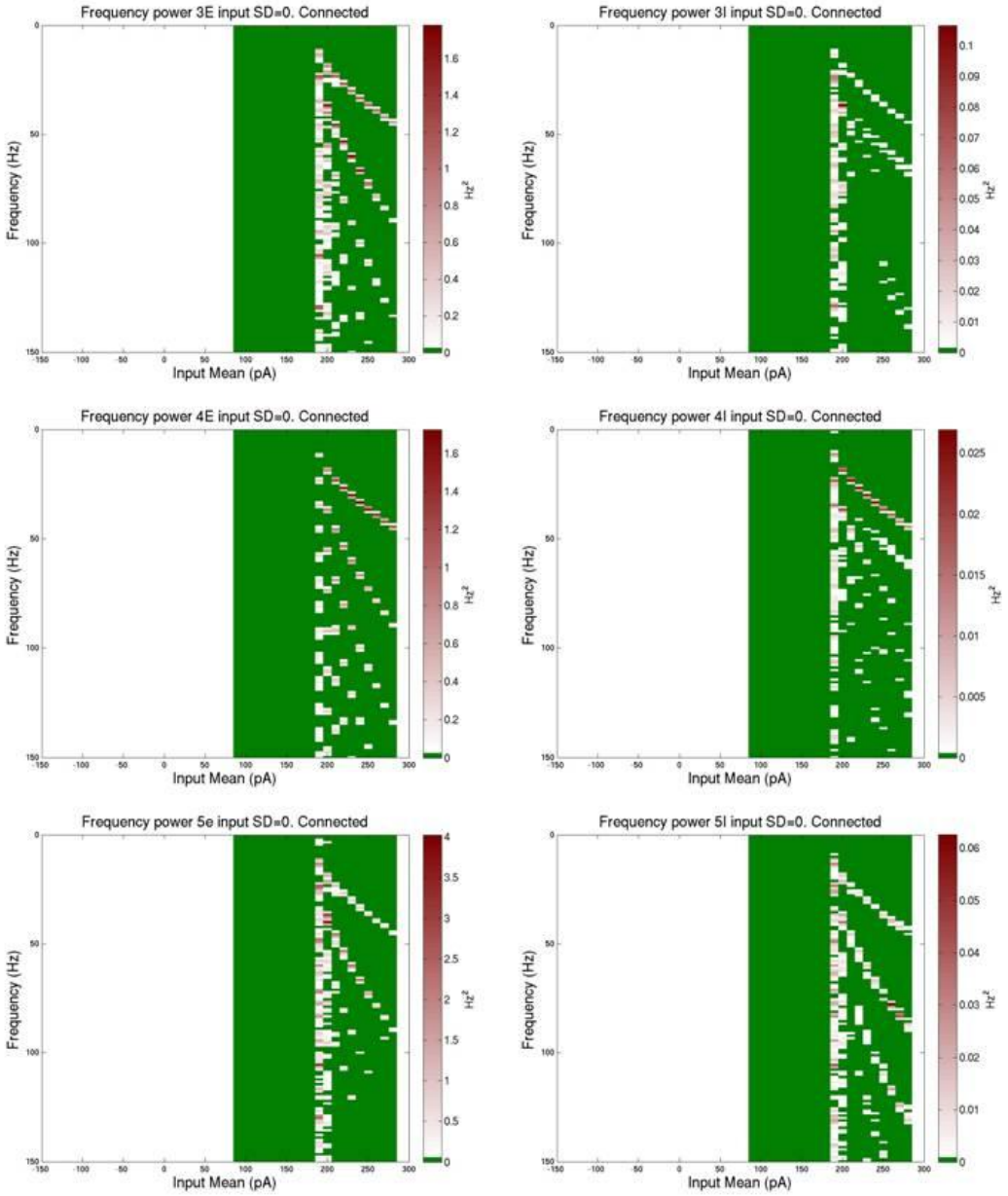

Figure 2.38: **Power spectral distribution of the instantaneous firing rate of the average cell from each layer by input mean with input standard deviation 0 pA in a connected network** *left hand plots are excitatory cells, right hand plots are inhibitory cells. Top plots are layer 3 cells, middle plots are layer 4 cells and bottom plots are layer 5 cells. Each plot has its own power range in its colour bar.*

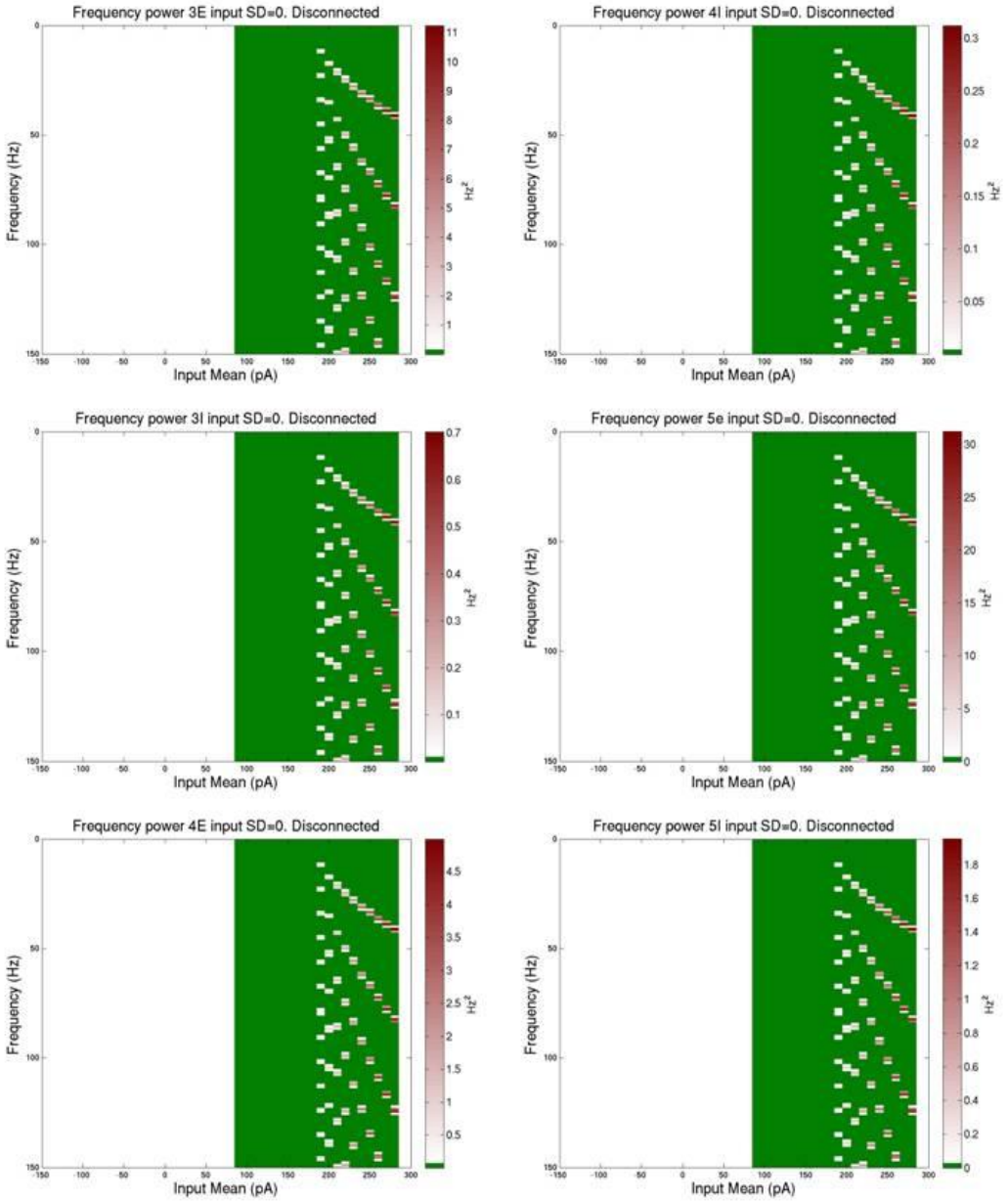

Figure 2.39: **Power spectral distribution of the instantaneous firing rate of the average cell from each layer by input mean with input standard deviation 0 pA in a disconnected network** *left hand plots are excitatory cells, right hand plots are inhibitory cells. Top plots are layer 3 cells, middle plots are layer 4 cells and bottom plots are layer 5 cells. Each plot has its own power range in its colour bar.*

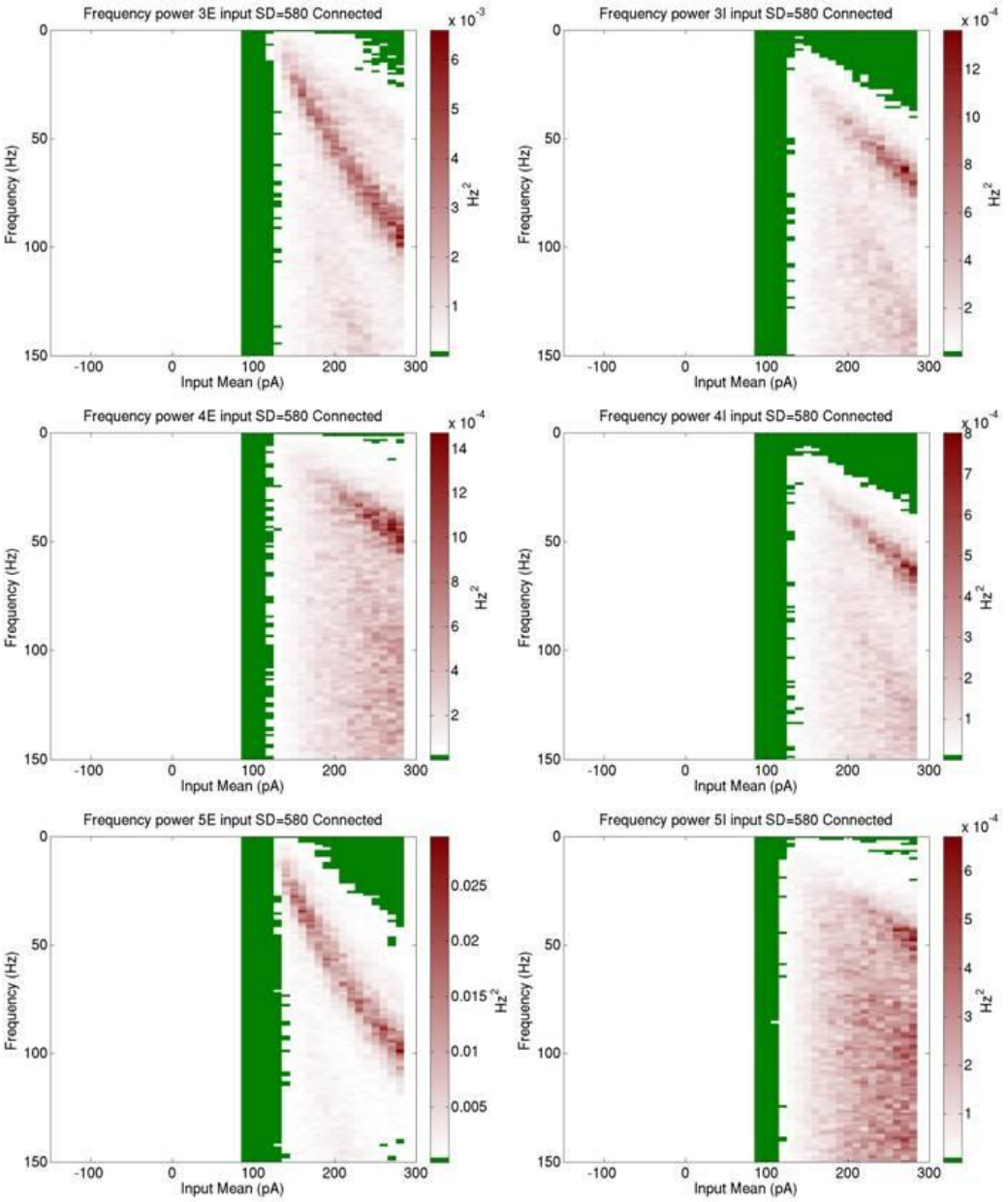

Figure 2.40: **Power spectral distribution of the instantaneous firing rate of the average cell from each layer by input mean with input standard deviation 580 pA in a connected network** *left hand plots are excitatory cells, right hand plots are inhibitory cells. Top plots are layer 3 cells, middle plots are layer 4 cells and bottom plots are layer 5 cells. Each plot has its own power range in its colour bar.*

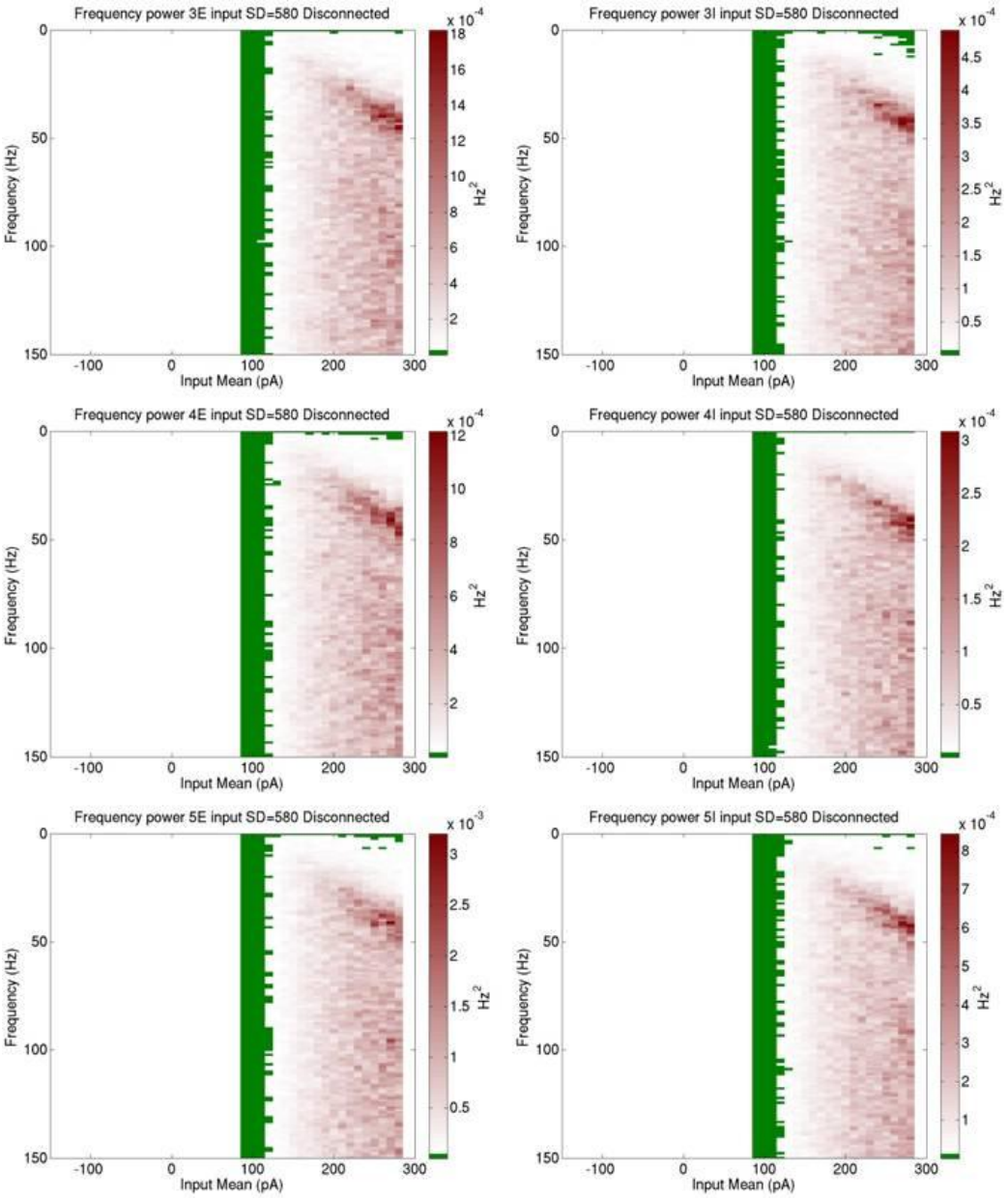

Figure 2.41: **Power spectral distribution of the instantaneous firing rate of the average cell from each layer by input mean with input standard deviation 580 pA in a disconnected network** *left hand plots are excitatory cells, right hand plots are inhibitory cells. Top plots are layer 3 cells, middle plots are layer 4 cells and bottom plots are layer 5 cells. Each plot has its own power range in its colour bar.*

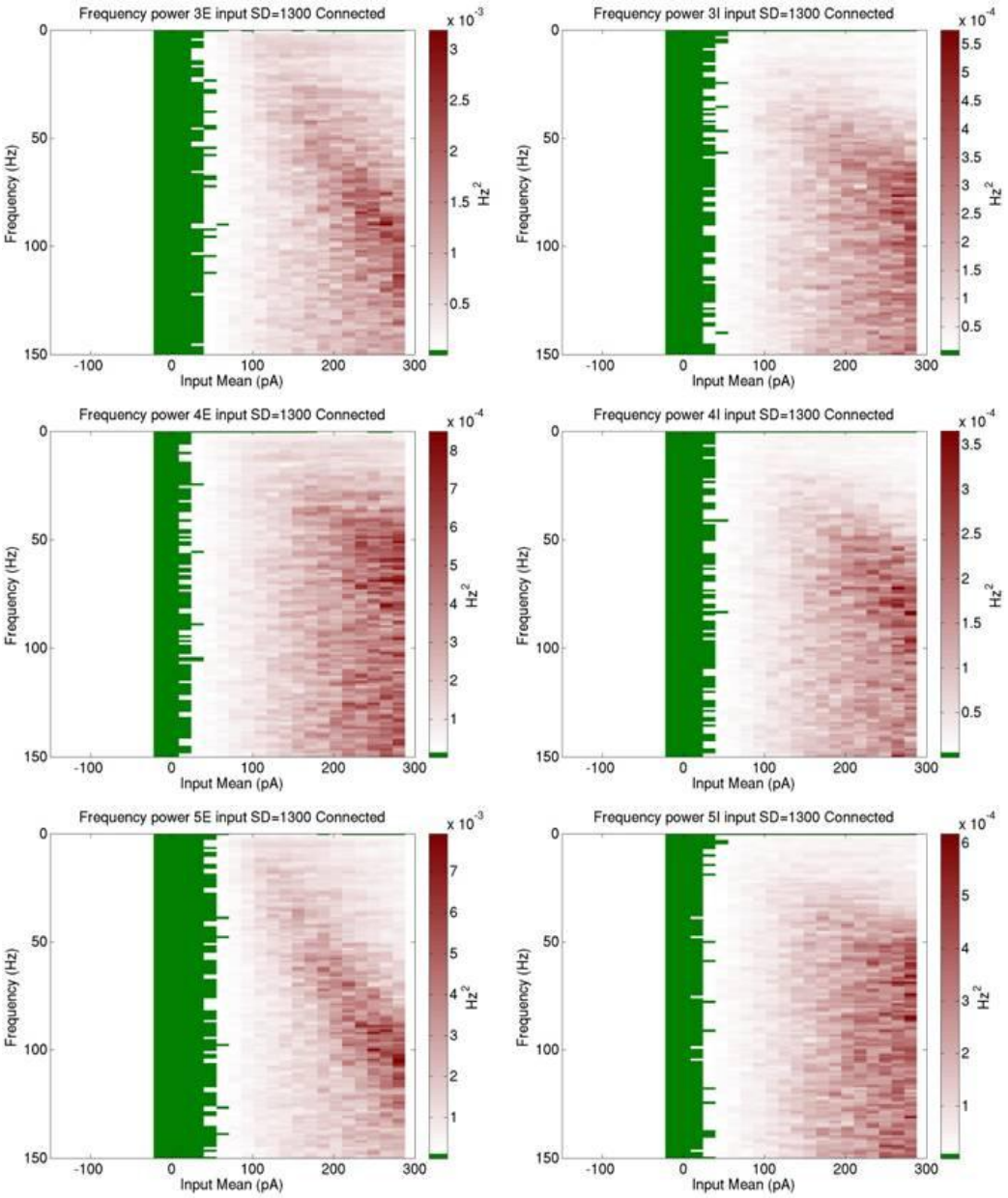

Figure 2.42: **Power spectral distribution of the instantaneous firing rate of the average cell from each layer by input mean with input standard deviation 1300 pA in a connected network** *left hand plots are excitatory cells, right hand plots are inhibitory cells. Top plots are layer 3 cells, middle plots are layer 4 cells and bottom plots are layer 5 cells. Each plot has its own power range in its colour bar.*

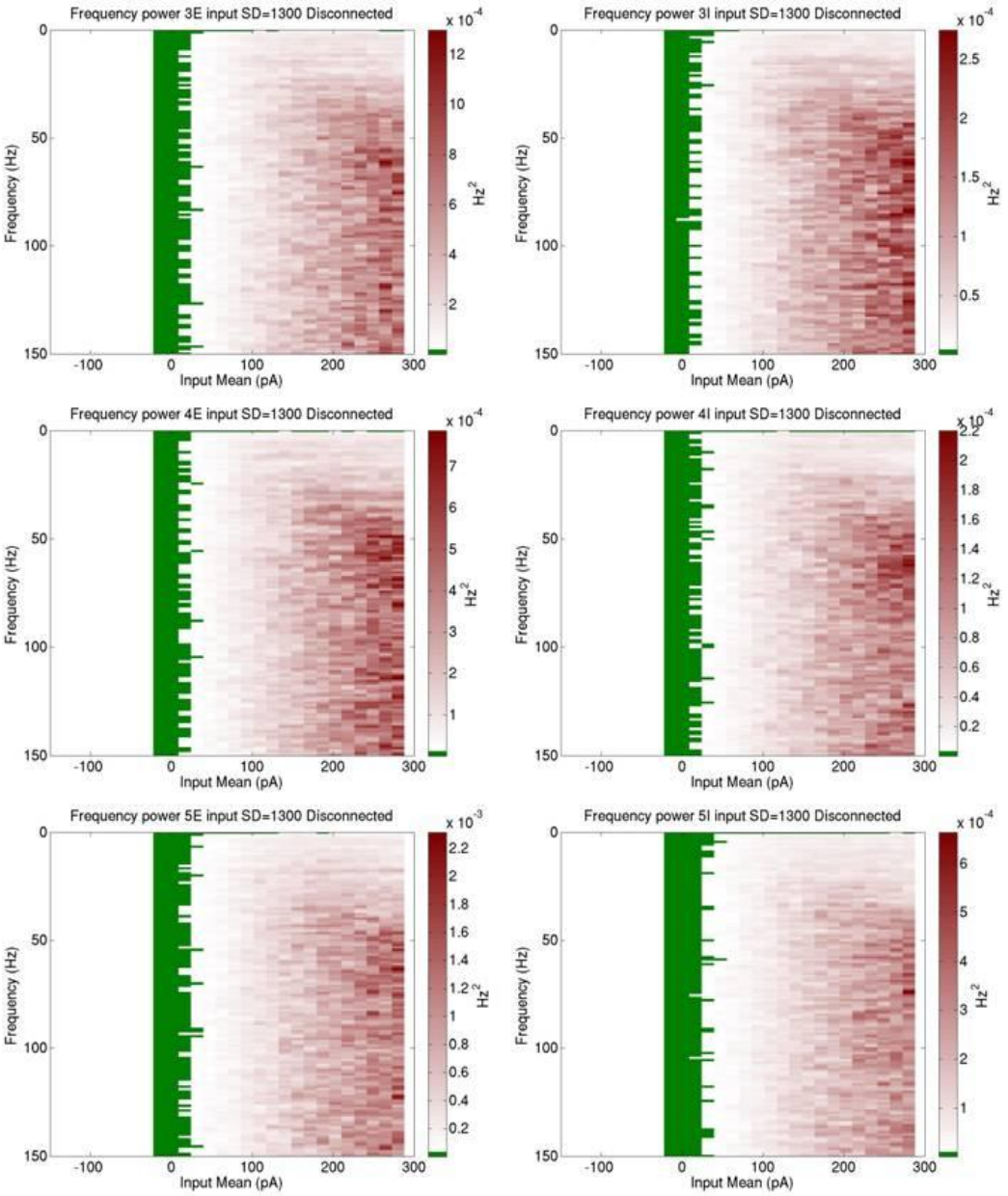

Figure 2.43: **Power spectral distribution of the instantaneous firing rate of the average cell from each layer by input mean with input standard deviation 1300 pA in a disconnected network** *left hand plots are excitatory cells, right hand plots are inhibitory cells. Top plots are layer 3 cells, middle plots are layer 4 cells and bottom plots are layer 5 cells. Each plot has its own power range in its colour bar.*

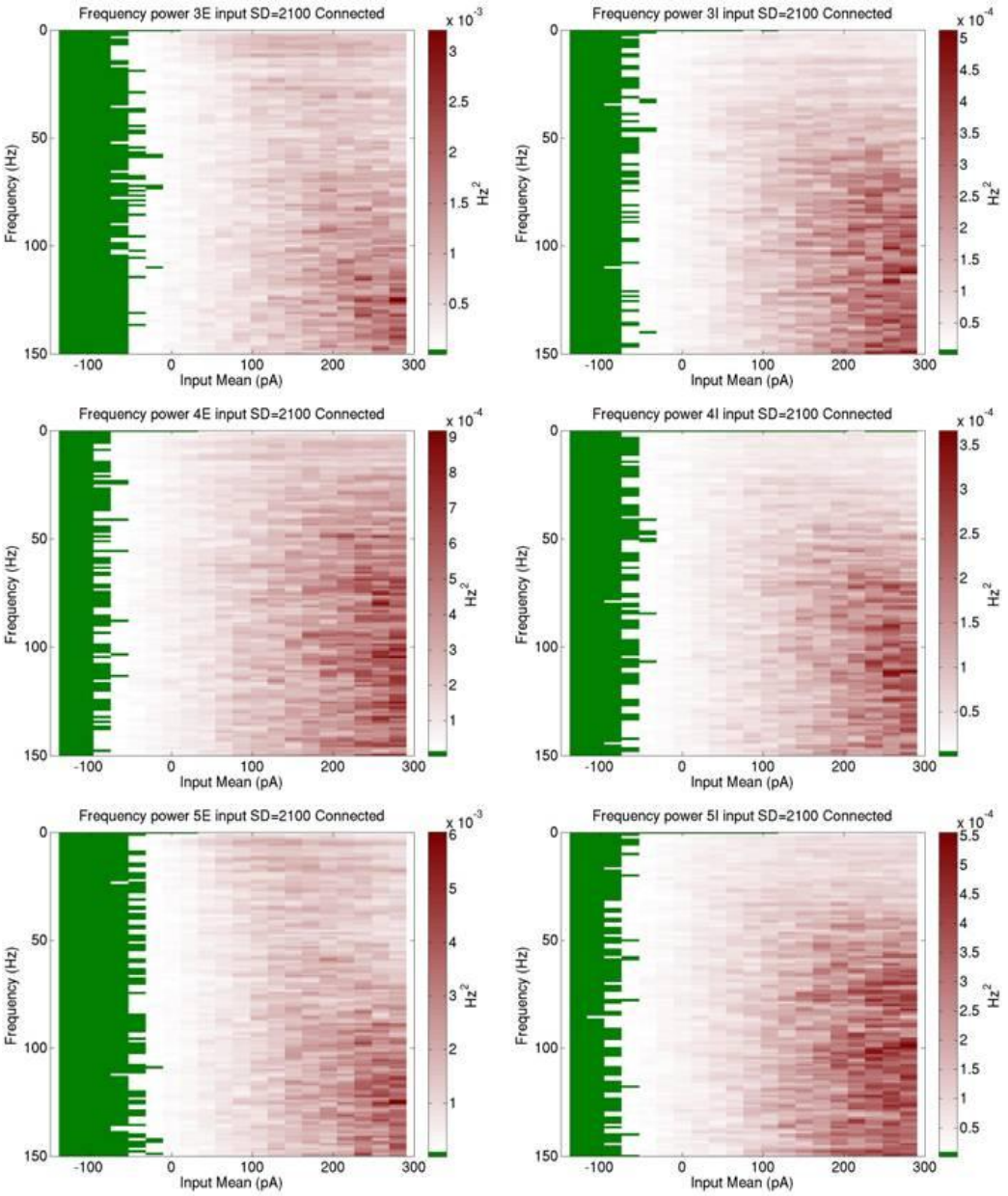

Figure 2.44: **Power spectral distribution of the instantaneous firing rate of the average cell from each layer by input mean with input standard deviation 2100 pA in a connected network** *left hand plots are excitatory cells, right hand plots are inhibitory cells. Top plots are layer 3 cells, middle plots are layer 4 cells and bottom plots are layer 5 cells. Each plot has its own power range in its colour bar.*

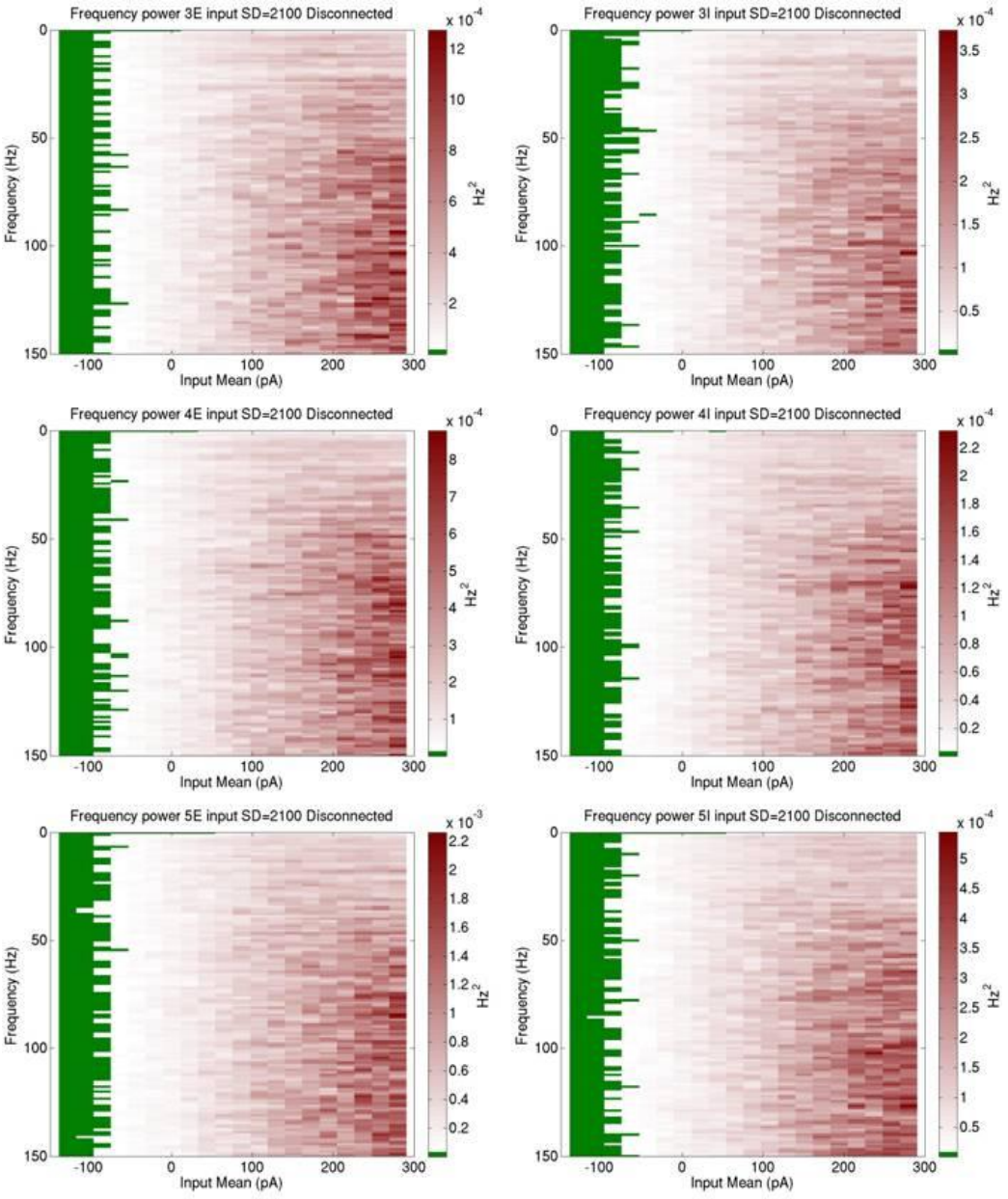

Figure 2.45: **Power spectral distribution of the instantaneous firing rate of the average cell from each layer by input mean with input standard deviation 2100 pA in a disconnected network** *left hand plots are excitatory cells, right hand plots are inhibitory cells. Top plots are layer 3 cells, middle plots are layer 4 cells and bottom plots are layer 5 cells. Each plot has its own power range in its colour bar.*

2.6.4 Discussion

In this section I have further characterised the network's response across parameter space and shown that there are regular changes in ongoing activity dependent upon the balance of local and long distant synaptic input. In particular the model suggests that during network activation there is a dominant oscillatory frequency that ranges from 25 - 100 Hz. This is the gamma range that is has been proposed as a marker for local processing in biological networks(Fries, 2005).

It is interesting to note that the frequency is dependent upon the intensity of the long distance input. This may suggest that in analysis of experimental data it may be worth investigating encoding across a wider range of frequencies than the usual narrow band.

The investigation into population firing rates and frequency content strongly support the use of laminar structure in modelling as each populations appears to have a different encoding scheme and given the frequency content disparity, suggests a different role for each population in computation.

All the regularities in the network are reduced when the synchronised local input is introduced through the increased white noise standard deviation. This suggests that there is an inhibition of encoding when a neighbouring cortical area is activated. This would suggest that any spike timing specificity is disrupted and that there is a switch to a rate coding scheme.

2.7 Chapter summary

In this chapter I have introduced a novel mechanistic cortical model. I have shown that under an independent Gaussian white noise input, in certain parameter ranges the network exhibits a number of characteristics in broad commonality with biological cortical networks. In particular that there is a threshold where the local network becomes active and performs a computation on the input. This activation of a local network has been proposed as a mechanism in neural communication(Fries, 2005).

I have demonstrated that the network behaves differently under varying input conditions, which I suggest represent a balance between local and long distant inputs to a cortical area. In particular when long range inputs impinge on the local network when there are low contributions from the surrounding cortex, the simulated network exhibits oscillatory behaviour within the same frequency range observed in biological local field potentials. When local inputs synchronise there is an inhibition of oscillatory behaviour in the network's field potential. This may be similar to centre-surround inhibition

observed in columnar organised neocortex(Kandel, 2000).

By isolating synaptic connectivity I have shown that although not all cell types generate a field potential, each cell type makes a contribution to the to the firing rate, and as such the information processing, of the network and to the oscillatory power and frequency of the network.

I believe that these initial observations support the verification of the model as being representative of a cortical network and its behaviour. When analysed on a single trial basis there are already some distinguishing features and regularities emerging in the network that merit further investigation.

In the next chapter I will introduce a sensory input and dynamically explore the input mean parameter space to explore non-static top-down cortico-cortical connections.

Chapter 3

Introducing a bottom up signal to the model

3.1 Chapter introduction

In this chapter I will explore the mean response of the network over multiple trials of a range of ongoing activity parameter conditions. The Gaussian white noise input mean will be considered as a corollary of intra cortical input. The Gaussian white noise input standard deviation will be considered as a rough representation of local synchronised synaptic input.

Firstly I will consider the introduction of a simulated bottom up, or sensory input to the network over the three input white noise conditions parameter space explored in the final section of the previous chapter, 580pA, 1300pA and 2100pA. The sensory input is provided by Poisson spike generators to the input layers of the network as detailed in figure 2.1. The mean firing rate of these cells range from 0 to 100 Hz.

This input allows an evoked potential to be derived from each stimulus condition, an 'evoked firing rate' from each population of cells and inspection of the mean time frequency response in both the power and phase dimensions. Further to this an information analysis of the relationship between sensory input and network response is carried out on the simulated field potential, the instantaneous firing rate of each population of cells and the time frequency power and phase of the simulated field potential.

In the second section I consider that the static mean representing intracortical input to the local network does not represent the oscillatory nature of long range connectivity observed experimentally. As such I introduce a sinusoidal mean to the network whilst maintaining a white noise input of 580pA. This sinusoidal input ranges across the mean levels explored in the

previous section and has 4 frequency conditions: 5 Hz, 10 Hz, 20 Hz and 40 Hz. I then investigate the relationship between a sensory input and the phase of the oscillatory intracortical input in the local network.

I then perform an analysis of the results in terms of the evoked potential, the evoked firing rate in each population and the relative mean power of the time frequency response. Subsequently I carry out an information analysis of the simulated field potential time series, the firing rate in each population, the time frequency response power and the time frequency response phase.

Information theory is the mathematical theory of communication established by Shannon. (Shannon, 1948) It has been used to quantify the amount of stimulus linked information in measurable neural signals and address questions of neural encoding. In particular spiking data and more recently LFPs and other field signals. (Arabzadeh, 2004; Montemurro, 2008; Magri 2009) Information theory results in neurophysiological data can suffer from a systematic error due to limited sampling, however a number of techniques have recently been developed to alleviate this bias. (Panzeri, 2007; Panzeri, 1996; Paninski, 2003; Nemenman 2004; Montemurro, 2007) These techniques have been packaged together in a Matlab toolbox and will be used for analysis in this and the subsequent chapter (Magri, 2009).

3.2 The introduction of a sensory input

3.2.1 Introduction

In this section I explore the response of the network to a bottom up or sensory input in the same parameter space as the previous section. The input is provided by a group of 40 Poisson spike generators feeding into the network for 100 ms according to the input connectivity described in figure 2.1. The input frequency conditions are from 0 -100 Hz in steps of 10 Hz.

Firstly I look at the evoked potentials from the simulated field potentials under different sensory input conditions, input means and connected and disconnected networks in different input standard deviations. I hypothesise that there will be a dependence on the sensory input frequency and input mean. A secondary hypothesis is that the shape of the evoked potential will be more complex as the network enters the network activity range.

Secondly I look at the evoked instantaneous firing rates of each population in response to a sensory input. I hypothesise that each population will respond differently to the input. A secondary hypothesis is that there will be evidence of information flow in the network based upon the timing of maximal firing rates.

Thirdly I look at the time frequency response power of the simulated field potential. I hypothesise that there will be input mean dependent variability in the structure of the time frequency power.

Fourthly I look at the time frequency response phase of the simulated field potential. I hypothesise that there will be evidence of phase resetting in different frequency bands associated with the sensory input. A secondary hypothesis is that there will be phase locking between frequency bands.

Next I perform an information analysis across time of a number of network output metrics. Firstly I look at the information content across time in the raw simulated field potential signal. I hypothesise that there will be a stimulus related increase in power. A secondary hypothesis is that there will be structural differences in the information content according to the white noise mean value.

Secondly I look at the information content in the instantaneous firing rate in each cell population. I hypothesise that the information will be represented differently according to the population the cell comes from. A secondary hypothesis is that there will be a different response in each population according to the input mean.

Thirdly I look at the information content in the time frequency response power. I hypothesise that different frequency bands will contain different mutual information values. A secondary hypothesis is that the information content will respond to different aspects of the stimulus. A tertiary hypothesis is that there will be evidence of different information content according to network activation state.

Lastly I look at the mutual information between sensory input and the time frequency phase. I hypothesise that there will be increased information in the phase. A secondary hypothesis is that this information will vary over the duration of the stimulus.

3.2.2 Methods

3.2.2.1 Simulations

In this section the set of six times four hundred simulations of the previous section were carried out ten times with the addition of a bottom up synaptic input with increasing firing rates. The bottom up input was provided by forty NEST spike generator models connected to the network as described in(Haeusler and Maass). The independent spike train for each spike generator was generated in Matlab using a poisson process. The firing rate of the input cells ranged from 0 to 100Hz increasing in steps of 10 Hz. In each of the twenty simulations where all parameters were identical, the spike generators

were given a different seed. The duration of the bottom up input was 100ms from simulation time 500ms to 600ms.

Combined with the simulations from the previous section the data set can be thought of as a three dimensional input parameter space: Input mean (20)X Input standard deviation (3)X bottom up input frequency (11). Each point in the parameter space has 20 simulations each with one of twenty independent randomly generated white noise and synaptic inputs.

3.2.2.2 Analysis

Evoked potentials and evoked instantaneous firing rates for each parameter space point were made using FieldTrip(Oostenveld, 2011). Each of the twenty simulation time series, from 100 to 1000 ms, were downsampled to 2000Hz and demeaned. Then they were averaged to give the evoked potential.

The mean time frequency power for each parameter space point was calculated with FieldTrip. Each of the twenty simulation time series, from 100 to 1000 ms, were downsampled to 2000Hz and demeaned. A time frequency matrix was calculated for each individual time series. This was calculated using the multi-taper convolution method with a hanning window of three times the wavelength of the frequency investigated. The frequencies of interest were integer values between one and one hundred hertz. The time steps of interest were from 100ms to 1000ms in 10 ms steps. All of the time frequency matrices were combined to give the mean time frequency power.

The mean time frequency phase was calculated using FieldTrip. Each of the twenty simulation time series, from 100 to 1000 ms, were downsampled to 2000Hz and demeaned. A time frequency matrix was calculated for each individual time series. This was calculated using the multi-taper convolution method with a hanning window of three times the wavelength of the frequency investigated. The frequencies of interest were integer values between one and one hundred hertz. The time steps of interest were from 100ms to 1000ms in 1 ms steps. The Fourier value was returned and the phase angle was computed using the Matlab 'angle' function. The phase angle means and significance were tested using the circular statistics toolbox (Berens, 2009). Where significance was tested using the parametric Watson-Williams multi-sample test for equal means with a significance of $p < 0.01$.

The mutual information between the instantaneous value of the simulated field potential or the firing rate and the frequency of bottom up synaptic input was calculated using the Information Breakdown ToolBox (ibTB)(Magri, 2009). For each time step at each input mean value and input standard deviation value, twenty trials in each of the eleven input frequency conditions were segmented into ten equal bins and the mutual information cal-

culated. The direct method and the Panzeri Treves bias correction method was used(Panzeri, 1996). In order to establish significance in the information measures the bootstrap algorithm was performed 20 time and Matlab's ttest function was carried out between the mutual information and the bootstrapped values with a significance of P <0.05.

The mutual information between the frequency power and the bottom up input frequency, and the mutual information between the frequency phase and the bottom up input frequency were calculated at each time step as above. The individual trial time frequency values were used.

3.2.3 Results

3.2.3.1 Evoked potentials

In this analysis I present the evoked potentials of a number of input parameter conditions in a connected and disconnected network. This is with the view of establishing whether or not there is a network response in the simulated field potential when a bottom up input is introduced to the network.

Figure 3.1 shows the evoked potential with input cells firing at 10 Hz and white noise standard deviation of 580 pA with a varying input mean in a connected network. Figure 3.2 shows the evoked potential in a disconnected network. Any contribution to the evoked potential from the bottom up input is of the same magnitude and standard deviation as that from the ongoing activity. In the connected network with an input mean of 140pA there is a larger overall standard deviation than in the disconnected network. This represents the network in a higher synchronized oscillatory state.

Figure 3.3 shows the evoked potential with input cells firing at 40 Hz and white noise standard deviation of 580 pA with input varying input means. Figure 3.4 shows the evoked potential in the disconnected network under the same conditions.

With the bottom up input frequency of 40 Hz there is an evoked potential at almost all conditions. When the white noise input mean is 100 pA there is an immediate positive deflection to a plateau with a return to the mean after the offset. This is present in both the connected and disconnected networks, although it is more pronounced in the connected network.

When the white noise input mean is at 120 pA there is an immediate small positive deflection during the bottom up input in the disconnected network. In the connected network after approximately 20 ms there is a positive deflection reaching a plateau with a return to the mean after the bottom up input with a slight overshoot and a return the mean.

When the white noise input mean is at 140 pA the disconnected network

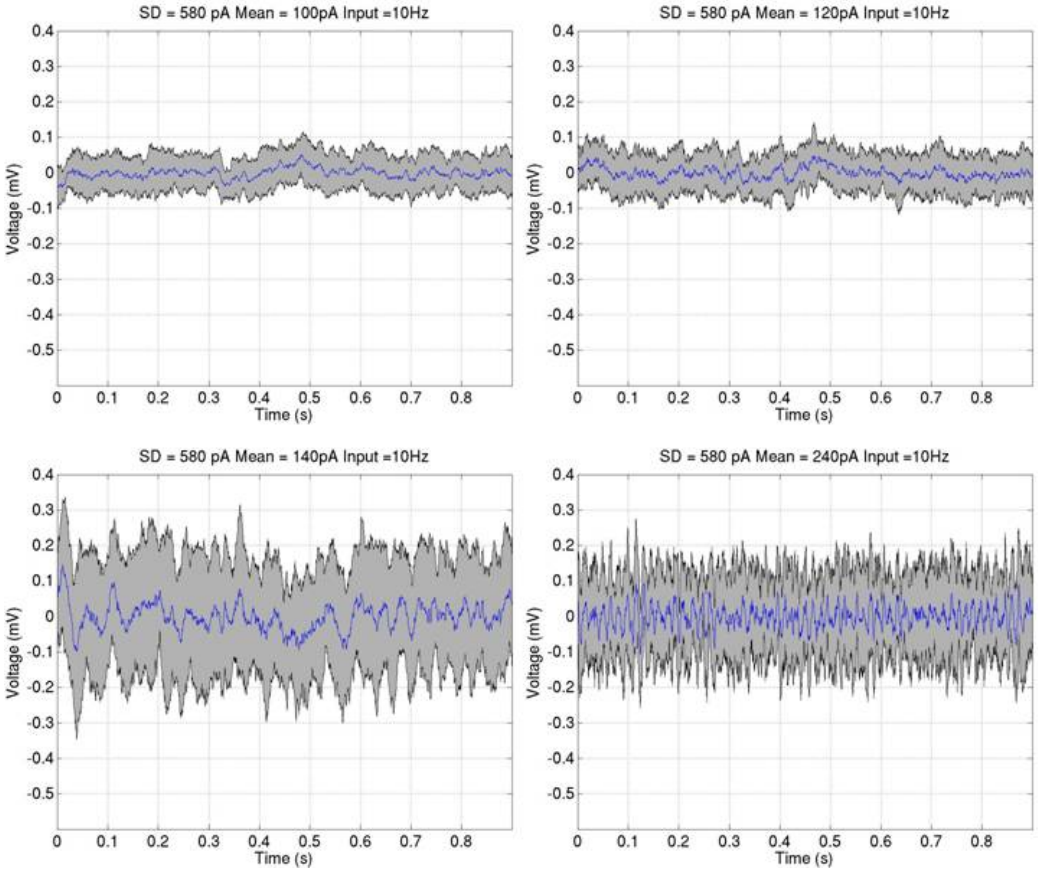

Figure 3.1: **The evoked potential with input cells firing at 10 Hz and white noise standard deviation of 580 pA in a connected network** *in all four subplots the evoked potential is shown in blue whilst the evoked potential plus and minus one standard deviation is shaded in grey. The sensory input was applied between 0.4 and 0.5 seconds. the top left subplot shows the condition with an input mean of 100pA, the top right 120pA, the bottom left 140pA and the bottom right 240pA*

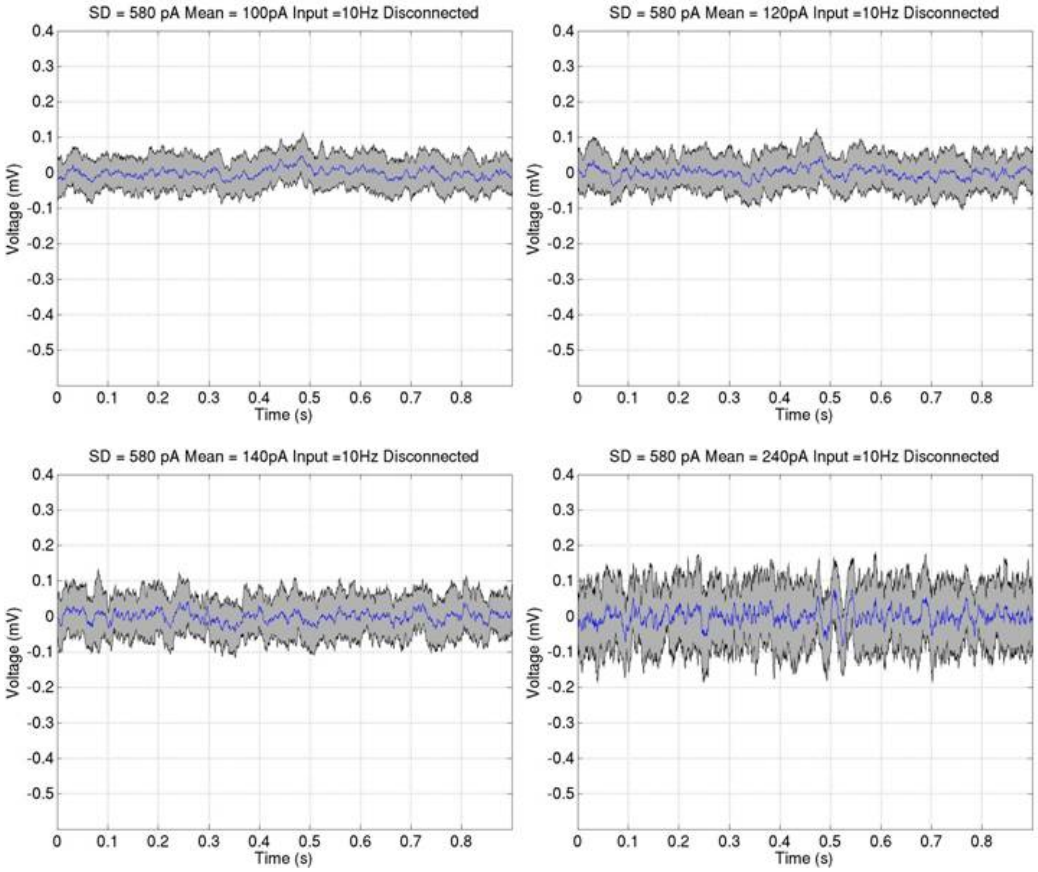

Figure 3.2: **The evoked potential with input cells firing at 10 Hz and white noise standard deviation of 580 pA in a disconnected network** *in all four subplots the evoked potential is shown in blue whilst the evoked potential plus and minus one standard deviation is shaded in grey. The sensory input was applied between 0.4 and 0.5 seconds. the top left subplot shows the condition with an input mean of 100pA, the top right 120pA, the bottom left 140pA and the bottom right 240pA*

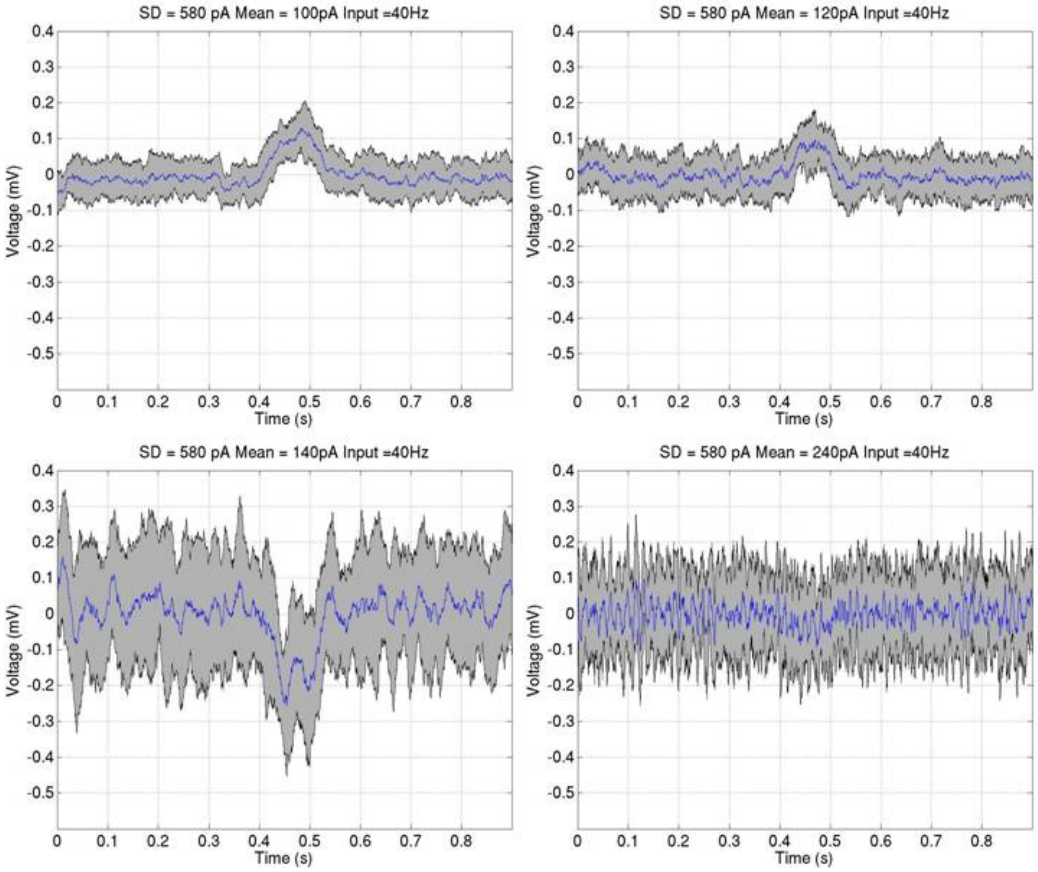

Figure 3.3: **The evoked potential with input cells firing at 40 Hz and white noise standard deviation of 580 pA** *in all four subplots the evoked potential is shown in blue whilst the evoked potential plus and minus one standard deviation is shaded in grey. The sensory input was applied between 0.4 and 0.5 seconds. the top left subplot shows the condition with an input mean of 100pA, the top right 120pA, the bottom left 140pA and the bottom right 240pA*

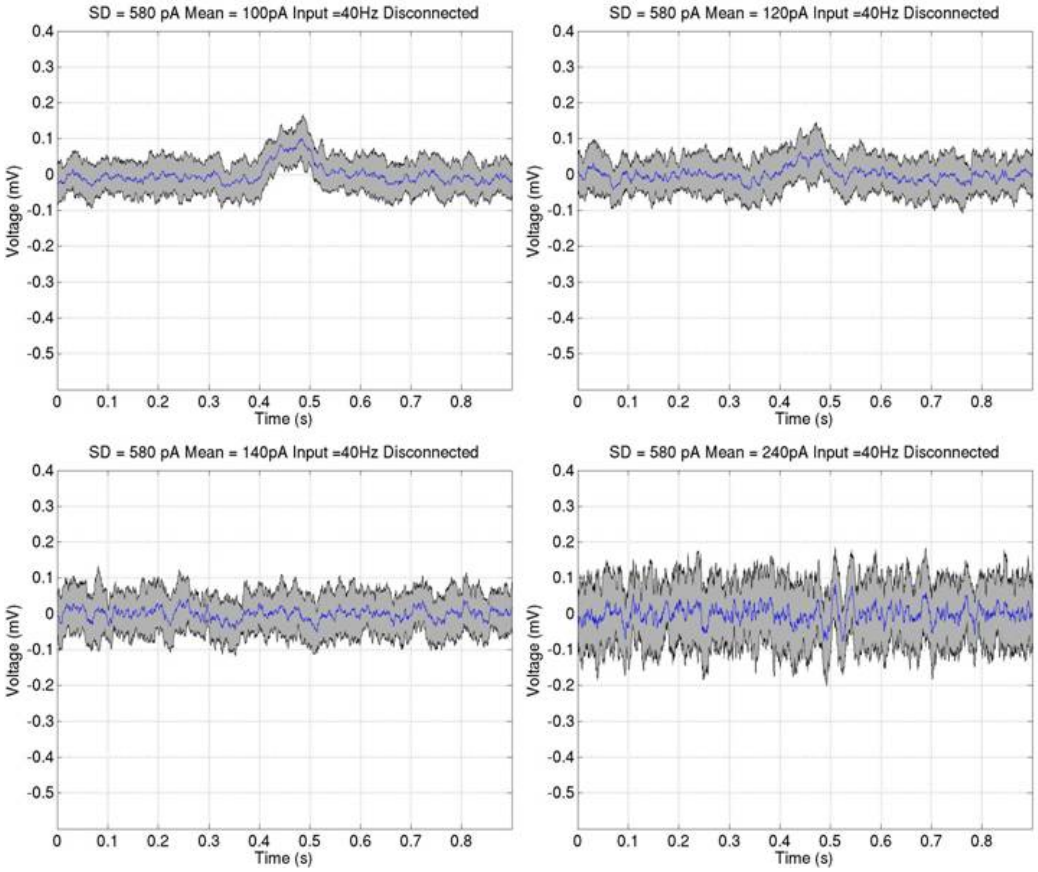

Figure 3.4: **The evoked potential with input cells firing at 40 Hz and white noise standard deviation of 580 pA in a disconnected network** *in all four subplots the evoked potential is shown in blue whilst the evoked potential plus and minus one standard deviation is shaded in grey. The sensory input was applied between 0.4 and 0.5 seconds. the top left subplot shows the condition with an input mean of 100pA, the top right 120pA, the bottom left 140pA and the bottom right 240pA*

has a very small positive deflection with a sharper post stimulus return to the mean, however this is within the range of the preceding standard deviation. In the connected network after approximately 30 ms there is a large negative deflection to a plateau where there is a short period of oscillation. About 15 ms after stimulus offset there is a return to mean with a slight positive overshoot.

When the white noise input mean is 240 pA there is a slight stimulus related offset effect in the disconnected network. In the connected network there is a slight negative deflection within the standard deviation range of the prestimulus condition.

Figure 3.5 shows the evoked potential with input cells firing at 100 Hz and white noise standard deviation of 580 pA with varying input mean. Figure 3.6 shows the evoked potentials in the disconnected networks.

When the white noise input mean is 100 pA there is an immediate positive deflection to a plateau with a return to the mean at stimulus offset in the disconnected network. In the connected network there is an immediate positive deflection with a sharp gradient until about 40 ms then there is a continued positive deflection at a lower gradient until stimulus offset when there is a decay to the mean.

When the white noise input mean is 120 pA there is an immediate positive deflection to a plateau with a return to the mean at stimulus offset in the disconnected network. In the connected network after approximately 15 ms there is a positive deflection to a peak after which there is a negative deflection to a plateau less than the mean value. At stimulus offset there is a negative deflection to a plateau for approximately 40 ms then there is a return to the mean value.

When the white noise input mean is 140 pA there is no noticeable effect in the disconnected network. In the connected network after approximately 15 ms there is a large sharp negative deflection until a peak around 45 ms when there is a smaller sharp positive deflection to a peak followed by a negative deflection to a peak immediately before stimulus offset where there is a positive deflection extending beyond stimulus offset. Approximately 10 ms post stimulus the gradient of the positive deflection increases as it returns to the mean with a small positive overshoot. The remainder of the simulation appears to have a stronger oscillatory content than those where the stimulus input was 10 or 40 Hz.

When the white noise input mean is 240 pA there is a very slight negative deflection during the stimulus period in the disconnected network. In the connected network there is a slightly larger negative deflection for the duration of the input with a reduction of ongoing oscillations.

Figure 3.7 shows the evoked potential with input cells firing at 80 Hz and

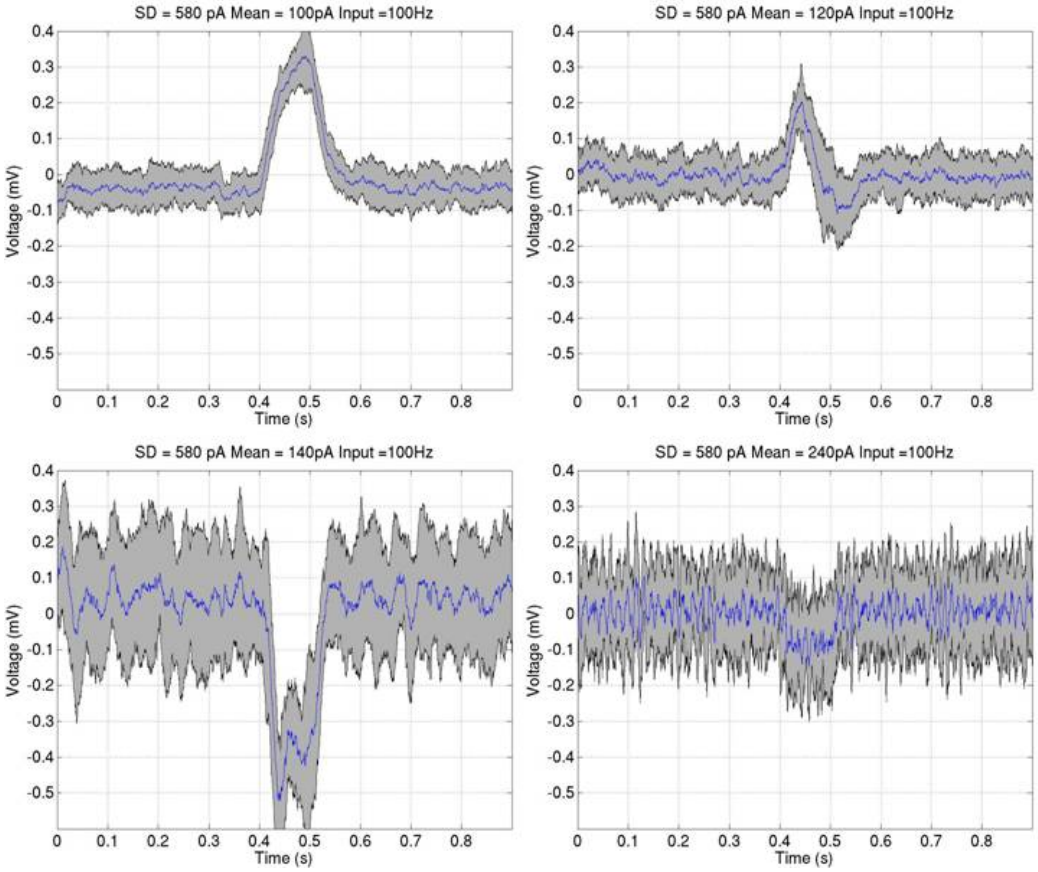

Figure 3.5: **The evoked potential with input cells firing at 100 Hz and white noise standard deviation of 580 pA** *in all four subplots the evoked potential is shown in blue whilst the evoked potential plus and minus one standard deviation is shaded in grey. The sensory input was applied between 0.4 and 0.5 seconds. the top left subplot shows the condition with an input mean of 100pA, the top right 120pA, the bottom left 140pA and the bottom right 240pA*

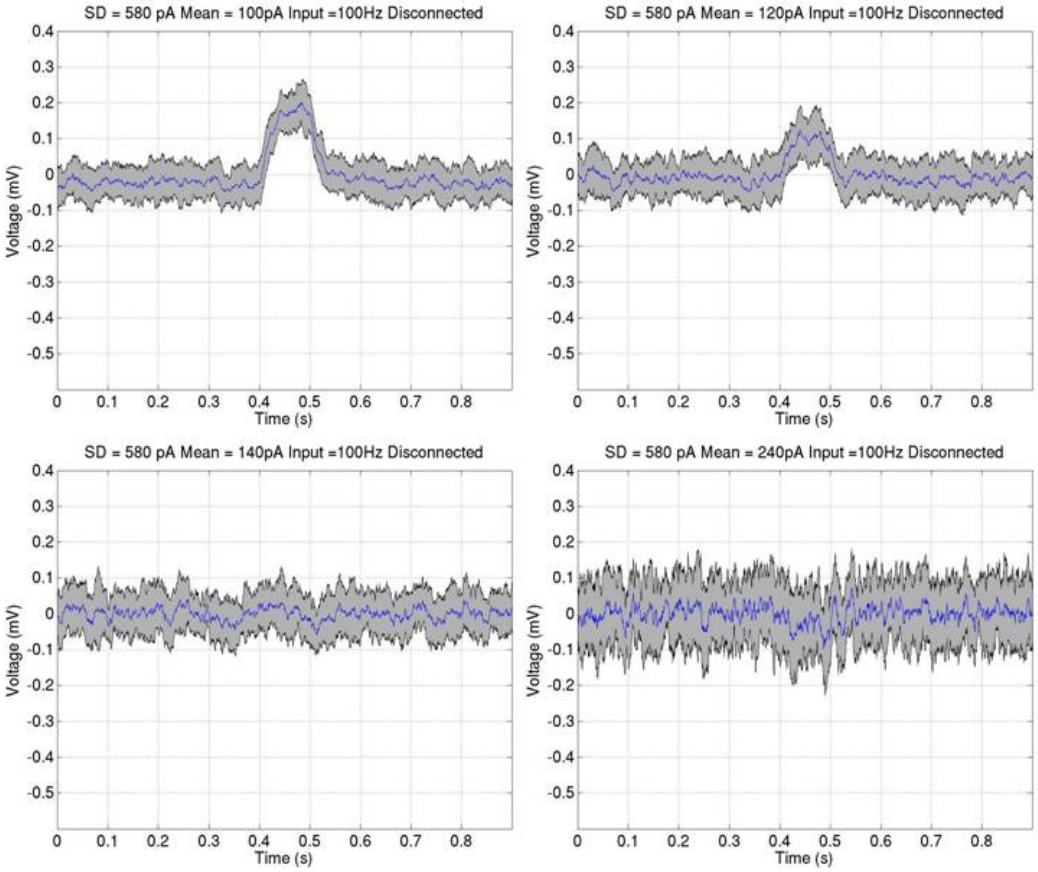

Figure 3.6: **The evoked potential with input cells firing at 100 Hz and white noise standard deviation of 580 pA in a disconnected network** *in all four subplots the evoked potential is shown in blue whilst the evoked potential plus and minus one standard deviation is shaded in grey. The sensory input was applied between 0.4 and 0.5 seconds. the top left subplot shows the condition with an input mean of 100pA, the top right 120pA, the bottom left 140pA and the bottom right 240pA*

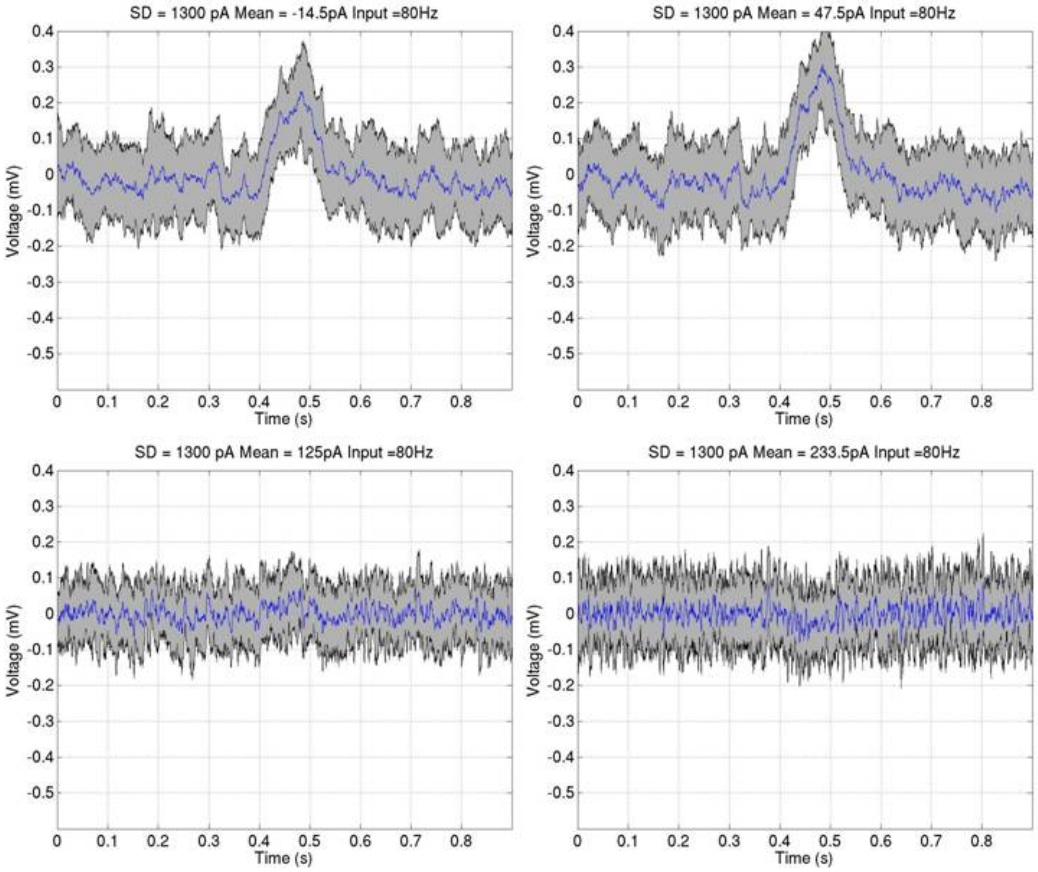

Figure 3.7: **The evoked potential with input cells firing at 80 Hz and white noise standard deviation of 1300 pA** *in all four subplots the evoked potential is shown in blue whilst the evoked potential plus and minus one standard deviation is shaded in grey. The sensory input was applied between 0.4 and 0.5 seconds. the top left subplot shows the condition with an input mean of -14.5pA, the top right 47.5pA, the bottom left 125pA and the bottom right 233.5pA*

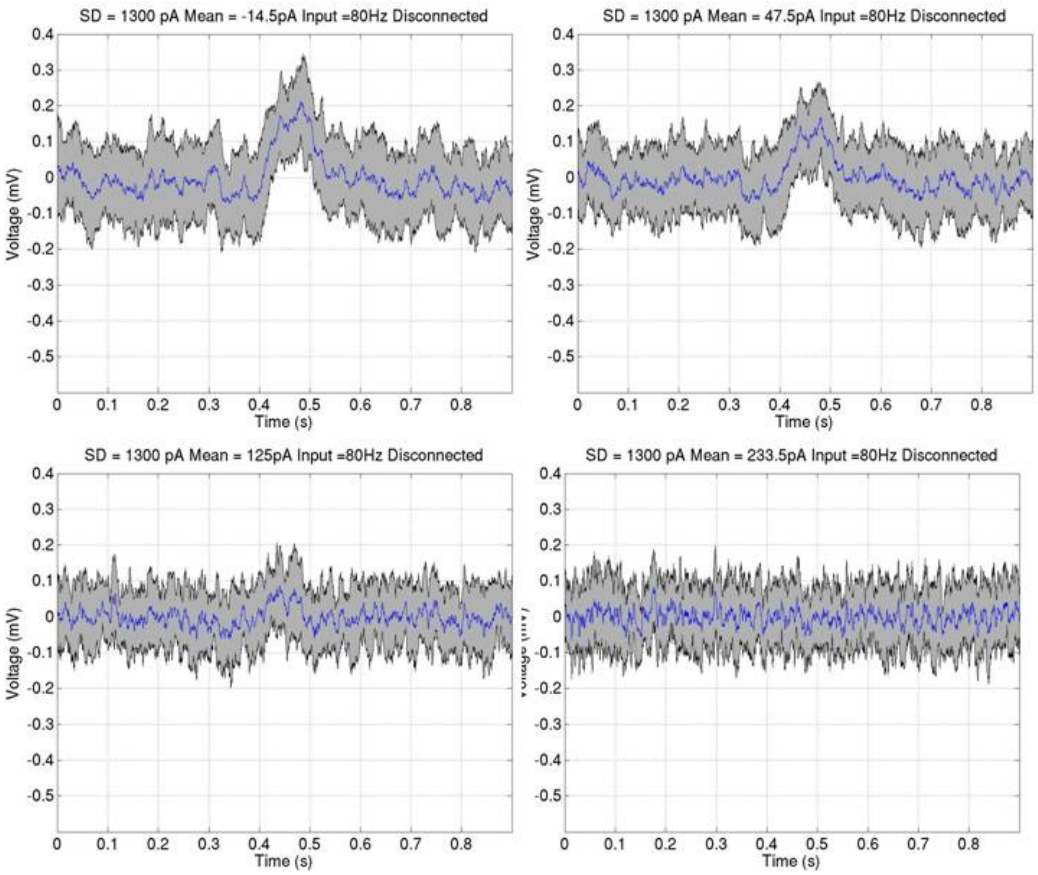

Figure 3.8: **The evoked potential with input cells firing at 80 Hz and white noise standard deviation of 1300 pA in a disconnected network** *in all four subplots the evoked potential is shown in blue whilst the evoked potential plus and minus one standard deviation is shaded in grey. The sensory input was applied between 0.4 and 0.5 seconds. the top left subplot shows the condition with an input mean of -14.5pA, the top right 47.5pA, the bottom left 125pA and the bottom right 233.5pA*

white noise standard deviation of 1300 pA with varying input means. Figure 3.8 shows the evoked potential in the disconnected network.

When the white noise input mean is -14.5 pA in both networks there is an immediate positive deflection with a reducing gradient until stimulus offset where there is a negative deflection to the mean.

When the white noise input mean is 47.5 pA in the disconnected network there is an immediate positive deflection to a plateau until stimulus offset where there is a negative deflection to the mean. In the connected network after about 10 ms there is a positive deflection to a small peak where there is a short negative deflection followed by a second positive deflection, with a lower gradient than the first, so a peak where there is a slight negative deflection until around 10 ms post stimulus where there is a decay to the mean.

When the white noise input mean is 125 pA in both networks there is a slight positive deflection to a plateau until stimulus offset when there is a return to the mean. This is more pronounce in the disconnected network. In the connected network there is a slight negative deflection 10 ms before stimulus offset followed by a positive peak and an apparent reduction in oscillation until 90 ms post stimulus offset. These are within the range of the prestimulus standard deviation.

When the white noise mean is 233.5 pA there is no noticeable effect in the disconnected network. In the connected network there is a small negative deflection and return to the mean during stimulus time. These are within the range of the prestimulus standard deviation.

Figure 3.7 shows the evoked potential with input cells firing at 80 Hz and white noise standard deviation of 2100 pA with varying input means. Figure 3.8 shows the evoked potential in the disconnected network.

When the white noise input mean is -128 pA there is a virtually identical positive deflection towards a plateaux and the a return to the mean in both the connected and the disconnected networks.

When the white noise input mean is 22 pA there is an immediate slight positive deflection and a return to the mean at stimulus offset in the disconnected network. In the connected network after about 10 ms there is a sharp positive deflection with a reduction in gradient to a plateau until stimulus offset where there is a decay to the mean over up to 200 ms.

When the white noise input mean is 151 pA there is no noticeable effect in the disconnected network. In the connected network there is a positive deflection to a plateau with a quick deflection to the mean at stimulus offset. This is within the prestimulus standard deviation range.

When the white noise input mean is 237 pA there is no noticeable effect in either network.

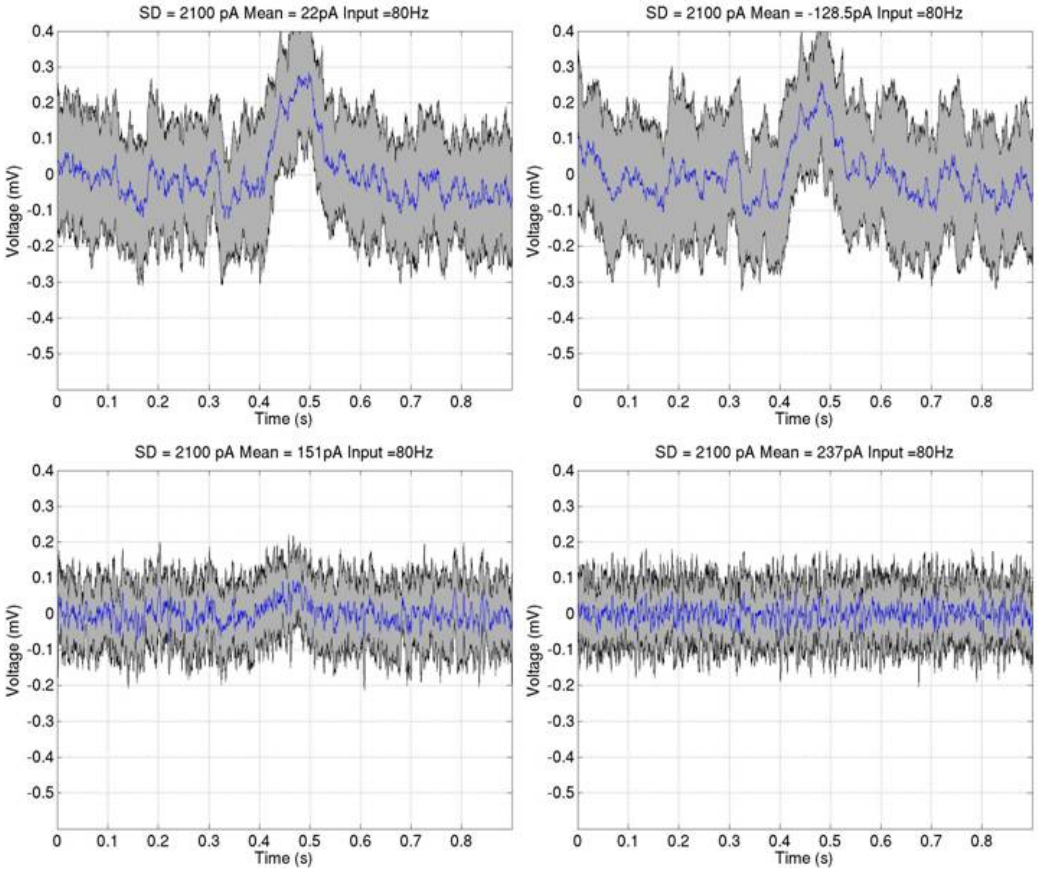

Figure 3.9: **The evoked potential with input cells firing at 80 Hz and white noise standard deviation of 2100 pA** *in all four subplots the evoked potential is shown in blue whilst the evoked potential plus and minus one standard deviation is shaded in grey. The sensory input was applied between 0.4 and 0.5 seconds. the top left subplot shows the condition with an input mean of 22pA, the top right 128.5pA, the bottom left 151pA and the bottom right 237pA*

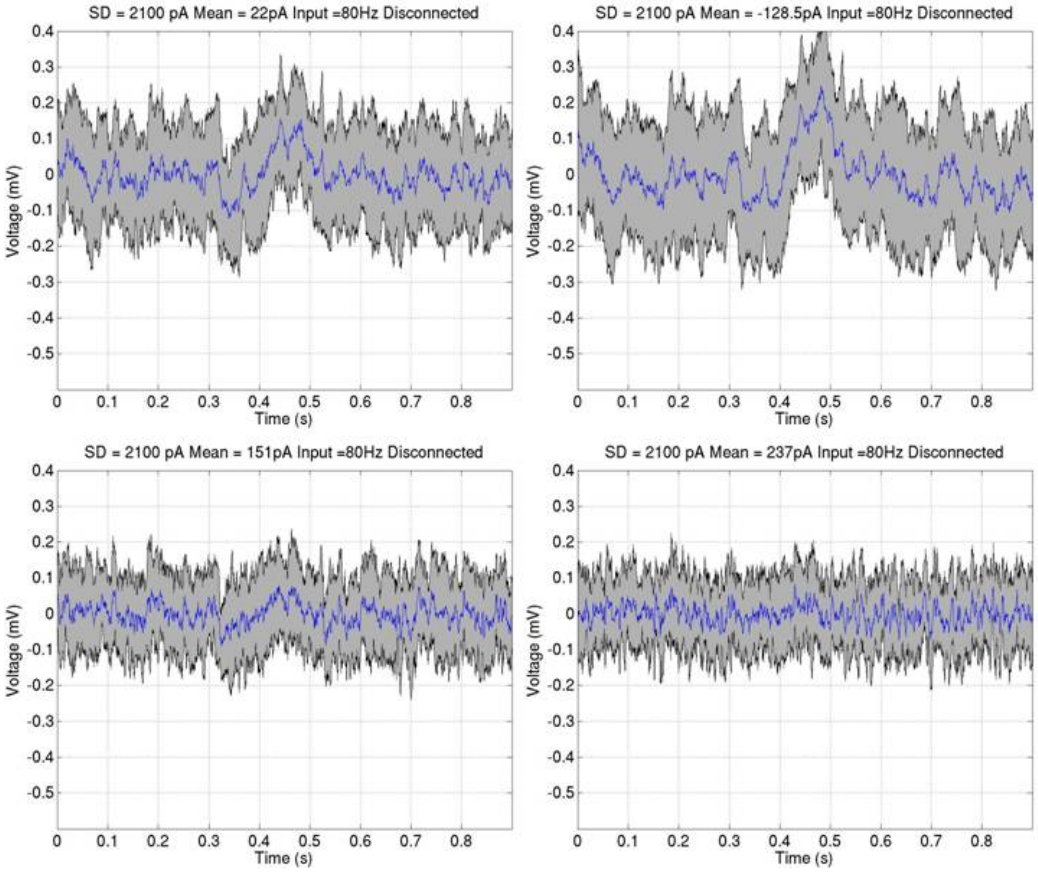

Figure 3.10: **The evoked potential with input cells firing at 80 Hz and white noise standard deviation of 2100 pA in a disconnected network** *in all four subplots the evoked potential is shown in blue whilst the evoked potential plus and minus one standard deviation is shaded in grey. The sensory input was applied between 0.4 and 0.5 seconds. the top left subplot shows the condition with an input mean of 22pA, the top right -128.5pA, the bottom left 151pA and the bottom right 237pA*

Overall each of the network inputs conditions produce a response to bottom up input, with differences between the disconnected and connected networks. However it is only under certain conditions that the amplitude changes in the evoked potential are larger than one standard deviation. In the connected networks this tends to be in the conditions where the white noise input mean is round the "network activation" threshold. In the conditions where the white noise standard deviation is 1300 and 2100 pA this produces a deflection from the stimulus mean and a return to that mean. In the 580 pA condition there are more complex responses, particularly at 120 pA input mean where the response is biphasic and at 140 pA where the evoked potential deflects in a direction opposite to all other conditions. In the next analysis I will look for similar features in the evoked firing rate.

3.2.3.2 Evoked firing rate

In this section I will present the evoked firing rates across each of the six population cell types in order to establish whether individual cell types have varying responses to a bottom up input.

Figure 3.11 shows the evoked firing rate of the average cell from each population with input cells firing at 100 Hz and white noise standard deviation of 580 pA. Figure 3.12 shows the evoked firing rate in the disconnected network. These plots correspond with the evoked potentials presented in figure 3.5.

All disconnected networks show a rise to a new mean value with a return to the original mean value post stimulus.

When the white noise input mean is 100 pA the average firing rate of all cell populations is less than 2 Hz as shown in figure 2.36. The strongest bottom up input is to the layer 4 excitatory cells which see an increase in firing rate to about 8 Hz after about 10 ms. This is roughly sustained until about 70 ms where its reduced to about 4 Hz for 10 ms then returning to about 8 Hz until about 10 ms after stimulus offset. Layer 4 inhibitory cells see a doubling of firing rate to about 4 Hz after about 10 ms. This is roughly sustained until about 60 ms where there is a short increase to about 10 Hz followed by a reduction to about 2 Hz for 10 ms followed by a return to about 4 Hz until a return to the mean at stimulus offset. Layer 3 and 5 excitatory cells have a ramped increase in firing rate until stimulus offset. Layer 3 reaches about 8 Hz and layer 5 reaches about 4 Hz. Layer 3 and 5 inhibitory cells maintain their firing rate during the stimulus but have a reduced standard deviation of instantaneous firing rates. Layer 5 inhibitory cells double in firing rate for about 20 ms post stimulus.

When the white noise input mean is 120 pA the average firing rate of all

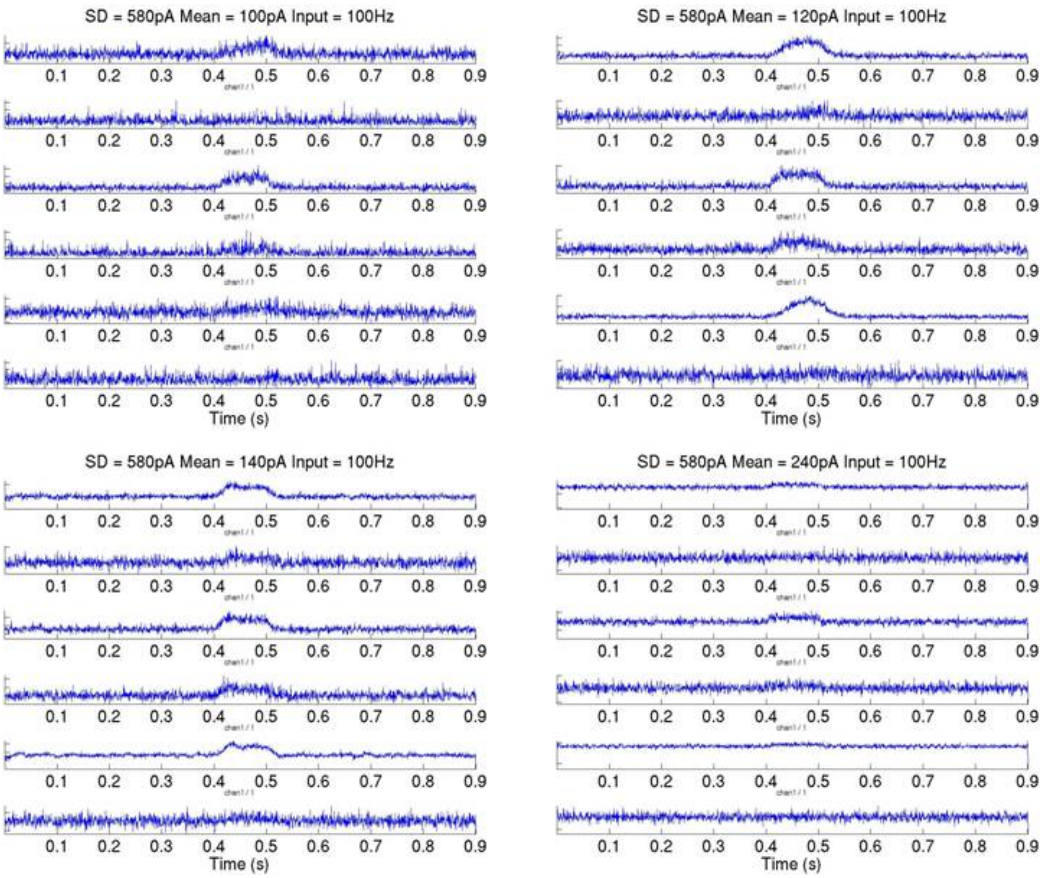

Figure 3.11: **The evoked firing rate of the average cell from each population with input cells firing at 100 Hz and white noise standard deviation of 580 pA** *in each of the four plots the subplots from top to bottom are the excitatory layer 3 cells, the inhibitory layer 3 cells, the excitatory layer 4 cells, the inhibitory layer 4 cells, the excitatory layer 5 cells and the inhibitory layer 5 cells. Each plot has been normalized. The input was delivered between 0.4 and 0.5 seconds. The top left plot is the condition where the white noise input mean is 100pA, the top right 120 pA, the bottom left 140pA and the bottom right 240pA.*

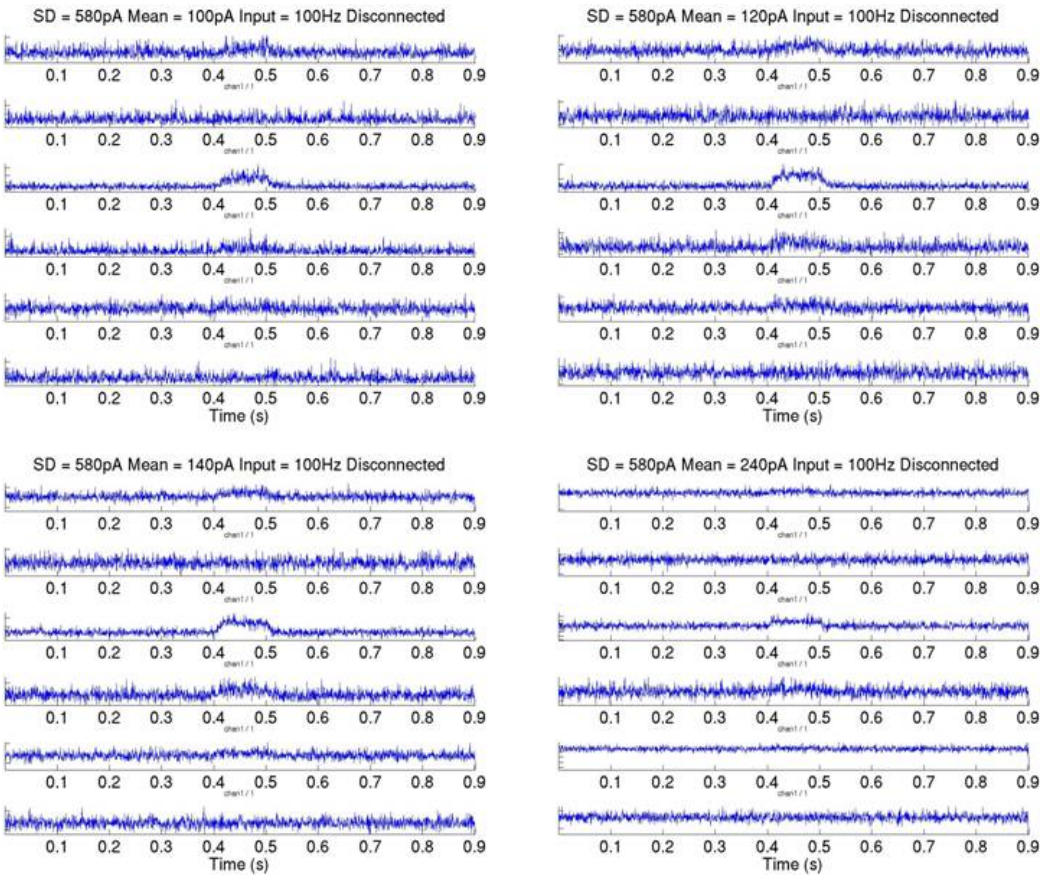

Figure 3.12: **The evoked firing rate of the average cell from each population with input cells firing at 100 Hz and white noise standard deviation of 580 pA in a disconnected network** *in each of the four plots the subplots from top to bottom are the excitatory layer 3 cells, the inhibitory layer 3 cells, the excitatory layer 4 cells, the inhibitory layer 4 cells, the excitatory layer 5 cells and the inhibitory layer 5 cells. Each plot has been normalized. The input was delivered between 0.4 and 0.5 seconds. The top left plot is the condition where the white noise input mean is 100pA, the top right 120 pA, the bottom left 140pA and the bottom right 240pA.*

cell populations is less than 5 Hz as shown in figure 2.36. Layer 4 excitatory cells rise to a firing rate of about 17 Hz by 20 ms, maintain this with some fluctuations until stimulus offset then return to the mean value over 20 ms. Layer 4 inhibitory cells rise to a firing rate of about 12 Hz and reduce slowly, with some fluctuations, to about 8 Hz by stimulus offset. There is a slight reduction of firing rate to about 6 Hz for 20 ms, then a drop below mean for about 10 ms returning to mean firing rate about 35 ms post stimulus. The layer 3 excitatory cells have a slow rise in firing rate from mean at 10 ms from stimulus onset to about 20 Hz at around 50 ms. This rate is maintained until stimulus offset when there is a decay to mean over about 35 ms. The layer 3 inhibitory cells have a ramped increase in firing rate to about 10 Hz at stimulus offset, where it decays to mean over about 30 ms. The layer 5 excitatory cells have a ramped increase in firing rate to about 25 Hz at about 80 ms followed by a ramped decrease to about 18 Hz at 20 ms post stimulus followed by a decay to mean over about 10 ms. The layer 5 inhibitory cells have a slight ramped increase to about 7 Hz at stimulus offset after which there is a decay back to mean over about 20 ms.

When the white noise input mean is 140 pA the average firing rate of all cell populations ranges from 15 - 5 Hz as shown in figure 2.36. There is a common structure to five of the six cell populations with a latency according to cell population. In layer 3, 4 and 5 excitatory there is an initial sharp rise in firing rate to a peak followed by a drop to a plateau for the duration of the stimulus followed by a decay back to the mean. This may be the case in layer 5 inhibitory cells too, but the increase in firing rate is slight. The onset in this structure is layer 4 excitatory cells about 5 ms, layer 4 inhibitory cells about 10 ms, layer 3 excitatory cells about 15 ms, layer 3 inhibitory cells about 20 ms, layer 5 excitatory cells about 25 ms and layer 5 inhibitory cells reach a maximum firing rate about 50 ms. The offset decay also follow the layer 4, 3 then 5 pattern, with inhibitory cell firing rates taking longer to decay than the excitatory cells of the same layer.

When the white noise input mean is 240 pA the average firing rate of all cell populations ranges from 90 - 35 Hz as shown in figure 2.36. All cell layers show a slight increase in firing rate during stimulus onset with layer 4 excitatory cells reaching their plateau slightly earlier than the other populations.

Figure 3.13 shows the evoked firing rate of the average cell from each population with input cells firing at 80 Hz and white noise standard deviation of 1300 pA. Figure 3.14 shows the evoked firing rate in the disconnected network. These plots correspond with the evoked potentials presented in figure 3.7.

All disconnected networks show a rise to a new mean value with a return

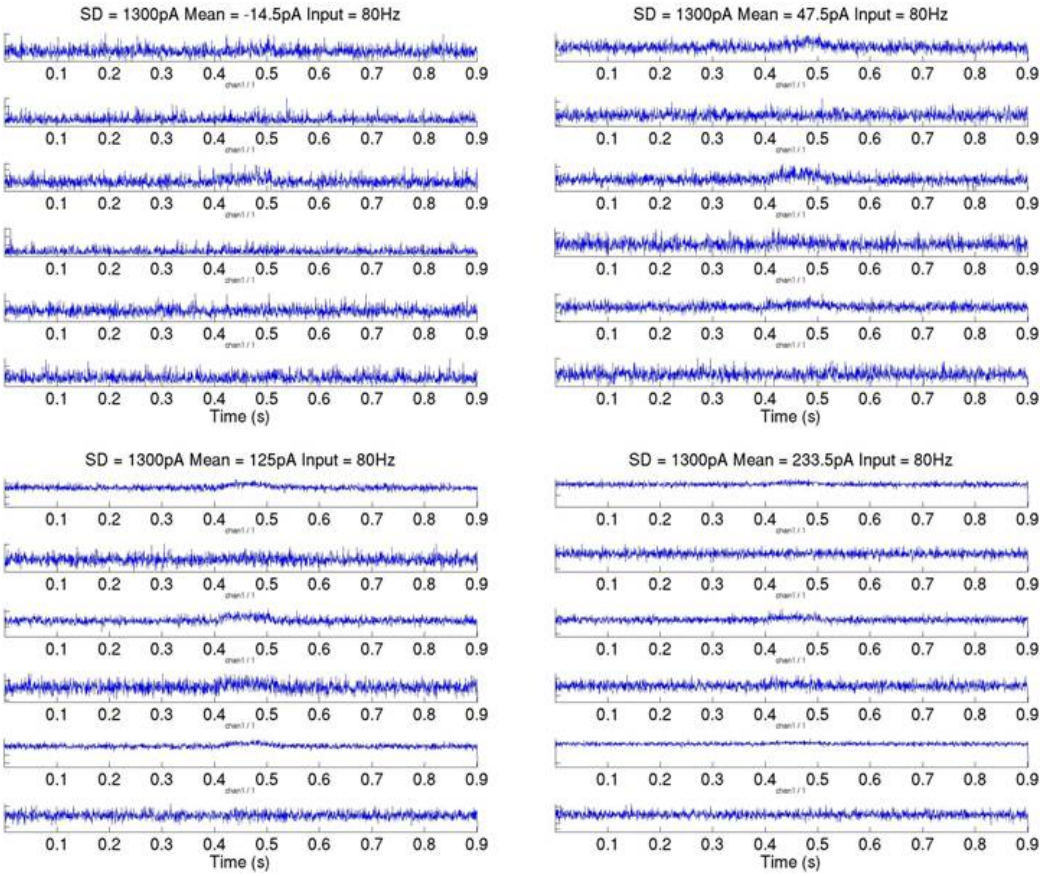

Figure 3.13: **The evoked firing rate of the average cell from each population with input cells firing at 80 Hz and white noise standard deviation of 1300 pA** *in each of the four plots the subplots from top to bottom are the excitatory layer 3 cells, the inhibitory layer 3 cells, the excitatory layer 4 cells, the inhibitory layer 4 cells, the excitatory layer 5 cells and the inhibitory layer 5 cells. Each plot has been normalized. The input was delivered between 0.4 and 0.5 seconds. The top left plot is the condition where the white noise input mean is -14.5pA, the top right 47.5pA, the bottom left 125pA and the bottom right 233.5pA.*

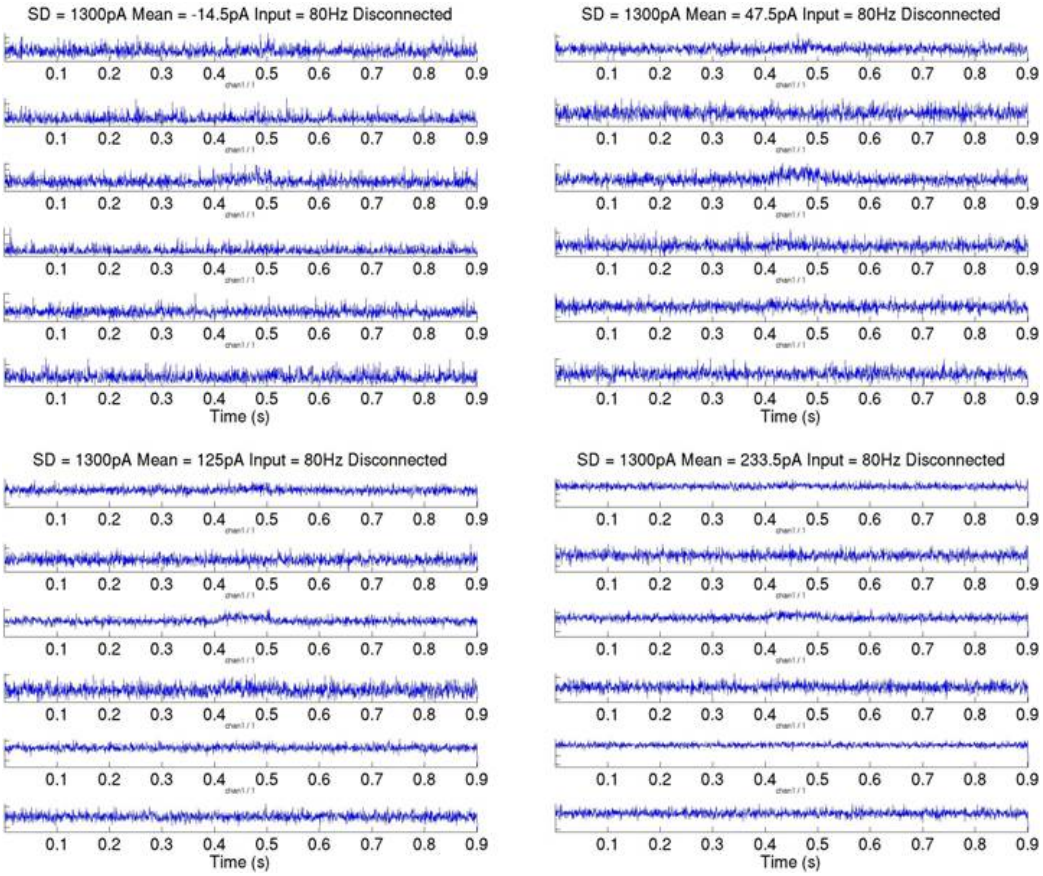

Figure 3.14: **The evoked firing rate of the average cell from each population with input cells firing at 80 Hz and white noise standard deviation of 1300 pA in a disconnected network** *in each of the four plots the subplots from top to bottom are the excitatory layer 3 cells, the inhibitory layer 3 cells, the excitatory layer 4 cells, the inhibitory layer 4 cells, the excitatory layer 5 cells and the inhibitory layer 5 cells. Each plot has been normalized. The input was delivered between 0.4 and 0.5 seconds. The top left plot is the condition where the white noise input mean is -14.5pA, the top right 47.5pA, the bottom left 125pA and the bottom right 233.5pA.*

to the original mean value post stimulus.

When the white noise input mean is -14.5 pA the average firing rate of all cell populations is less than 2 Hz as shown in figure 2.36. There is very little structure to the stimulus response, with firing rates being largely identical to the disconnected network.

When the white noise input mean is 47.5 pA the average firing rate of all cell populations is less than 5 Hz as shown in figure 2.36. There is a small increase in firing rate in all populations. In this instance the layer 4 inhibitory cells have a slight peak at 10 ms whilst the excitatory cells to not reach their plateau until 30 ms. Layer 3 excitatory cells has a ramped response peaking at about 90 ms. Layer 5 excitatory cells reach a plateau around 10 ms and maintain this rate for the duration of the stimulus. All cells decay back to the mean at stimulus offset, except layer 3 and 5 inhibitory cells which have a short and slightly longer post stimulus peak on firing rate.

When the white noise input mean is 125 pA the average firing rate of all cell populations ranges from 40 - 10 Hz as shown in figure 2.36. The patterns of increased firing rates are similar to when ther input mean is 47.5 Hz with the exceptions that Layer 5 excitatory cells do not reach their plateau until around 30 ms and inhibitory cells don't have offset peaks.

When the white noise input mean is 233.5 pA the average firing rate of all cell populations ranges from 90 - 35 Hz as shown in figure 2.36. All layers show a slight increase in firing rate with the exception of layer 5 inhibitory cells, which have a slight decrease. Both layer 4 populations reach their plateau in about 10 ms. layer 3 excitatory cells reach a maximum about 80 ms and layer 5 excitatory cells around the same time.

Figure 3.15 shows the evoked firing rate of the average cell from each population with input cells firing at 80 Hz and white noise standard deviation of 2100 pA. Figure 3.15 shows the evoked firing rate in the disconnected network. These plots correspond with the evoked potentials presented in figure 3.9.

All disconnected networks show a rise to a new mean value with a return to the original mean value post stimulus.

With the exception of the network with an input white noise mean of -128.5 pA, all connected networks demonstrate slight increases in firing rate with maxima being reached in layer 4 first followed by layer 3 excitatory cells then layer 5 excitatory cells.

The overall picture that emerges from this analysis is that the input is reflected by an increased firing rate in the populations according to the bottom up connectivity. In the cases where the input white noise is 1300 to 2100 pA there are minor differences between the connected and disconnected networks, with the inputs being of the same order of magnitude to the on-

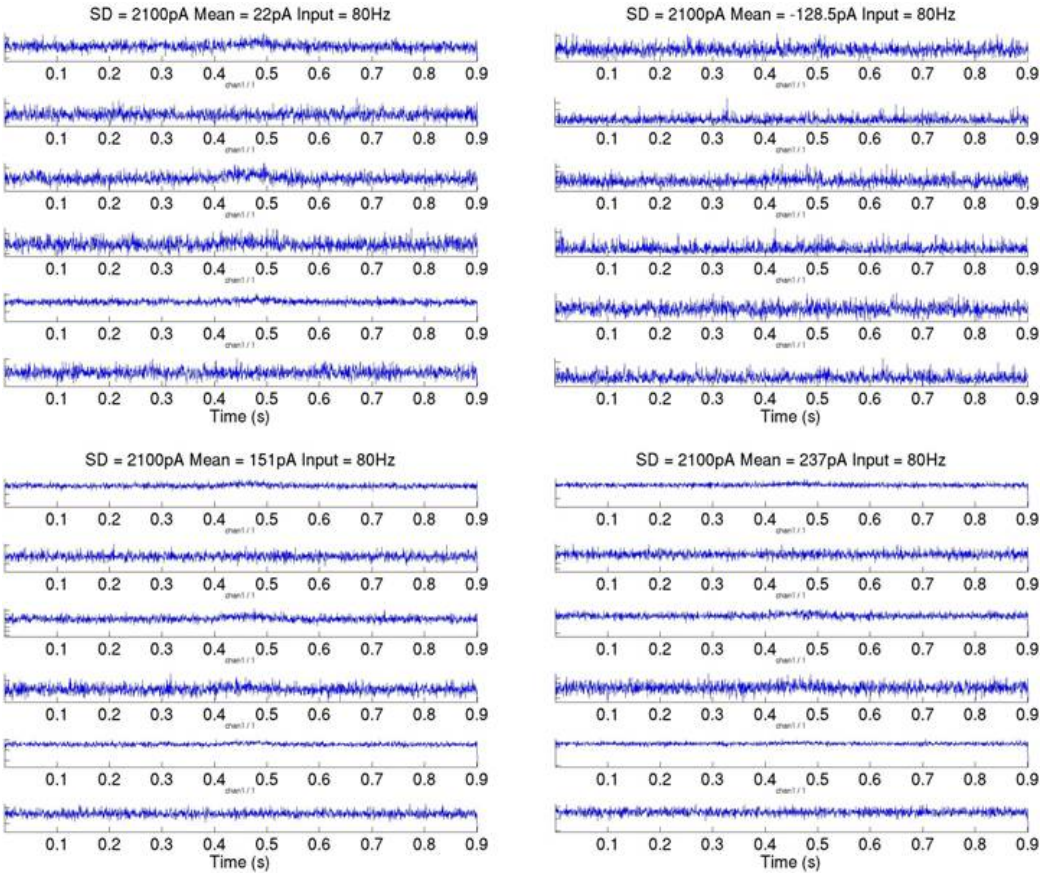

Figure 3.15: **The evoked firing rate of the average cell from each population with input cells firing at 80 Hz and white noise standard deviation of 2100 pA** *in each of the four plots the subplots from top to bottom are the excitatory layer 3 cells, the inhibitory layer 3 cells, the excitatory layer 4 cells, the inhibitory layer 4 cells, the excitatory layer 5 cells and the inhibitory layer 5 cells. Each plot has been normalized. The input was delivered between 0.4 and 0.5 seconds. The top left plot is the condition where the white noise input mean is 22pA, the top right -128.5pA, the bottom left 151pA and the bottom right 237pA.*

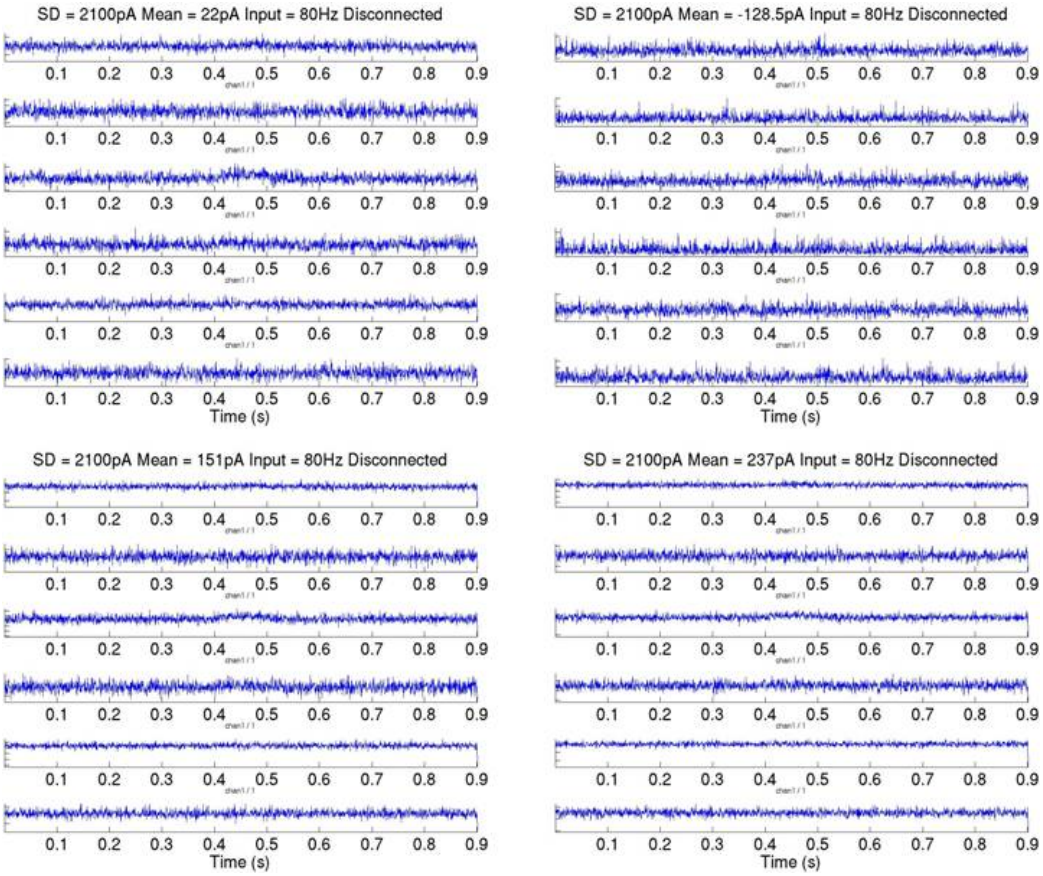

Figure 3.16: **The evoked firing rate of the average cell from each population with input cells firing at 80 Hz and white noise standard deviation of 2100 pA in a disconnected network** *in each of the four plots the subplots from top to bottom are the excitatory layer 3 cells, the inhibitory layer 3 cells, the excitatory layer 4 cells, the inhibitory layer 4 cells, the excitatory layer 5 cells and the inhibitory layer 5 cells. Each plot has been normalized. The input was delivered between 0.4 and 0.5 seconds. The top left plot is the condition where the white noise input mean is 22pA, the top right -128.5pA, the bottom left 151pA and the bottom right 237pA.*

going firing rates. However in the case where the input white noise standard deviation is 580 pA there is noticeable stimulus related increases in firing rate which evolves in structure over the duration of the input. The features, particularly in the projection neurons relate to the biphasic and negative deflection of the simulated field potential evoked potential.

3.2.3.3 Time frequency analysis

In this analysis I present an exploration of the time frequency power changes in the simulated field potential between identical simulations with and without a bottom up stimulus. This is with a view to establishing whether there are any frequency bands that can be associated with features of the bottom up stimulus.

Figure 3.17 show regions of significant increases and decreases in the time frequency power average over twenty trials between 0 and 100 Hz bottom up input. The network white noise input standard deviation is 580 pA with various input mean values. The connected network power range is approximately fifty times that of the disconnected network(figure 3.18).

When the white noise input mean is 120 pA the connected network shows an increase in power at the onset in the frequency range 5 - 15 Hz. This lasts for the duration of the input and extends to 0.1 after the bottom up input off set. Mid stimulus there is a significant increase in power in the 15 - 35 Hz range. This extends for the duration of the stimulus with increased power in the 15-20 Hz range extending 50 ms after stimulus offset. Stimulus onset is marked by an increase in power in the 45 - 65 Hz range. This does not extend beyond the mid stimulus point. The stimulus offset is marked by an increase in power in the >70 Hz range. In the disconnected network there is a stimulus related increase in power in the <10 Hz range from stimulus onset extending 0.1 seconds beyond stimulus offset.

When the white noise input mean is 130 pA the connected network shows a <10 Hz increase in power for the duration of the stimulus extending 0.1 seconds beyond stimulus offset. In the 10 Hz range there is an onset increase in power at stimulus onset with no significant change in power mid stimulus and an increase post stimulus. in the 12-45 Hz range there is an increase in power for the duration of the stimulus extending 50 ms beyond stimulus offset. Both stimulus onset and offset are marked by a short increase in power in the 50 -90 Hz range. In the disconnected network there is a stimulus related increase in power in the <10 Hz range from stimulus onset extending 0.1 seconds beyond stimulus offset.

When the white noise input mean is 140 pA the connected network shows an increase in power in the 5 Hz range throughout the stimulus. There is a

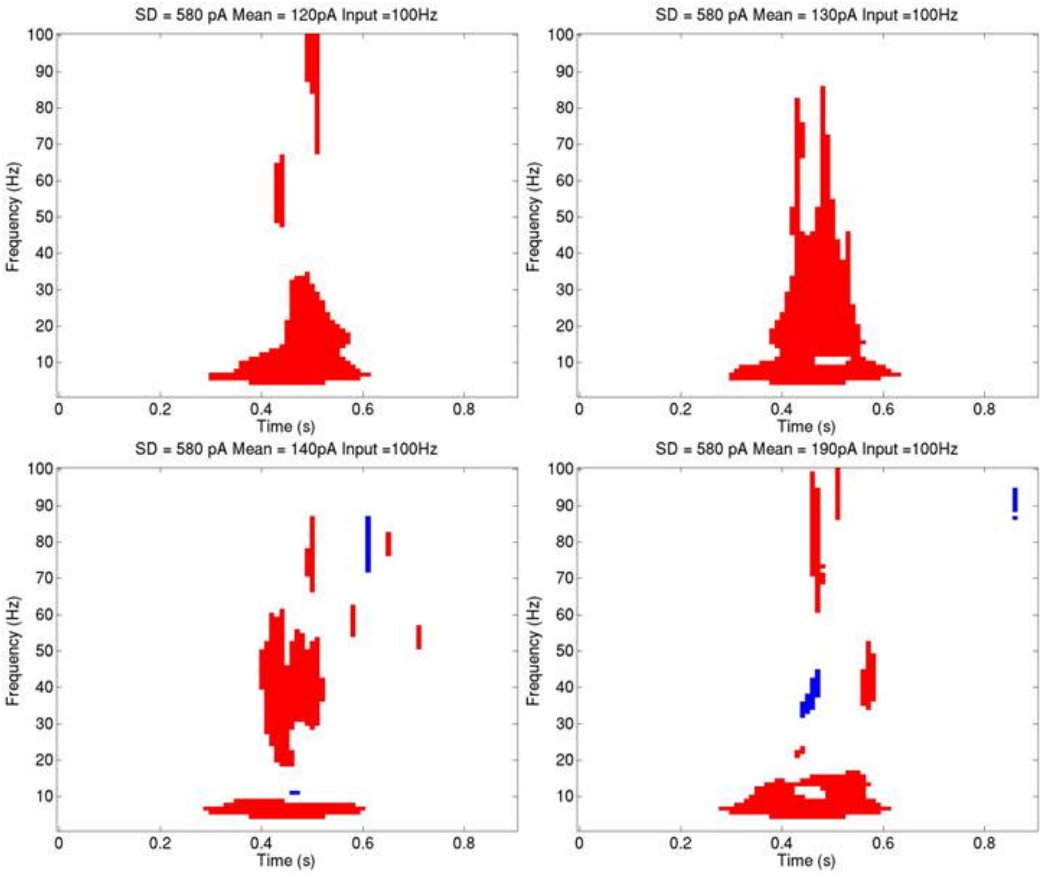

Figure 3.17: **Significant changes in the time frequency power between 0 and 100 Hz bottom up input with a white noise input standard deviation of 580 pA** *in all plots red means a significant increase in power and blue mean a significant decrease in power with $p < 0.05$. The top left plot has an input white noise mean of 120 pA, top right has 130 pA, bottom left has 140 pA and the bottom right 190 pA*

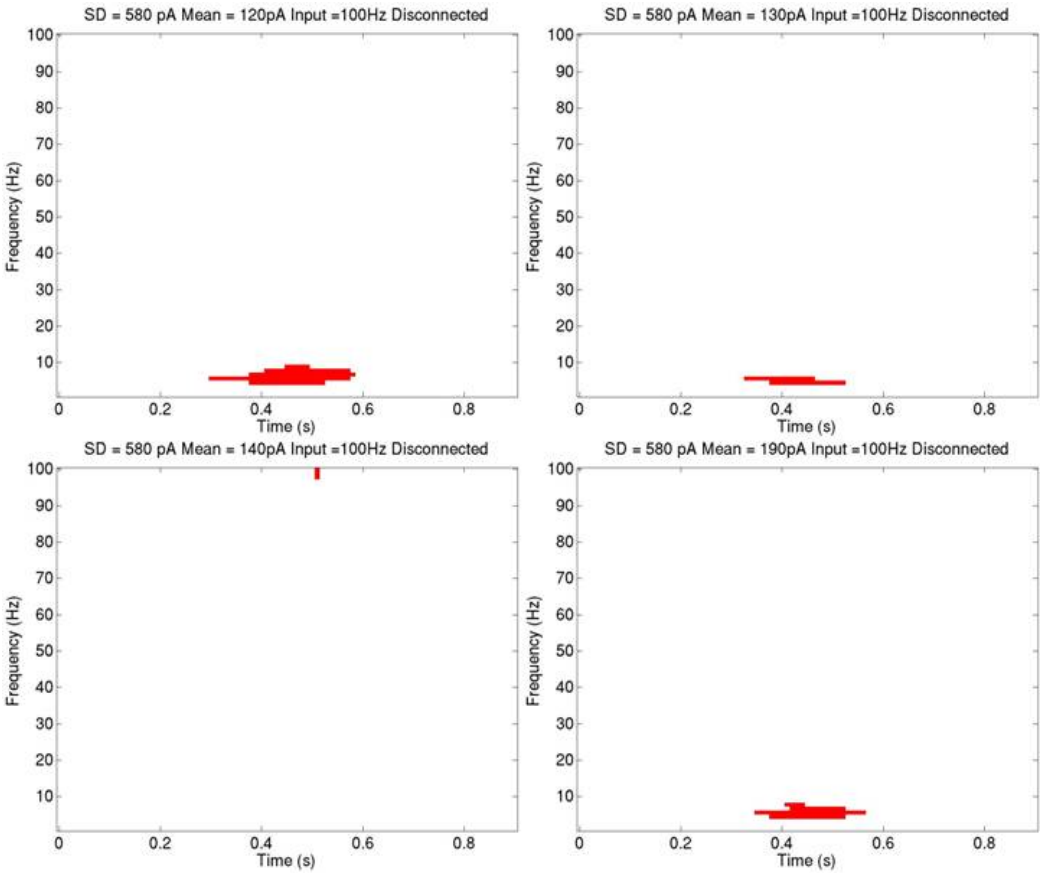

Figure 3.18: **Significant changes in the time frequency power between 0 and 100 Hz bottom up input with a white noise input standard deviation of 580 pA in a disconnected network** *in all plots red means a significant increase in power with $p < 0.05$. The top left plot has an input white noise mean of 120 pA, top right has 130 pA, bottom left has 140 pA and the bottom right 190 pA*

midstimulus decrease in power in the 10 Hz range. There is a midstimulus increase in power in the 20 Hz range. There is an onset increase in power in the 30 - 60 Hz range lasting the duration of the input. Stimulus offset is marked by an increase in power in the 65 -85 Hz range. There are brief increases and decreases in the >50Hz range that may be associated with the 5 Hz oscillation offset. There is no significant power changes in the disconnected network.

When the white noise input mean is 190 pA the connected network shows an increase in power in the 5 -15 Hz range throughout the stimulus. There is a midstimulus lack of significance of the power in the 10 Hz range. There is a brief midstimulus increase in power in the 20 Hz range. There is a midstimulus decrease in power in the 30 -40 Hz range. There is a 55 - 100 Hz increase in power at the stimulus off set. 100 ms after stimulus offset there is an increase in power in the 30 - 50 Hz range, this may be associated with the offset of the low frequency stimulus related oscillations. In the disconnected network there is a stimulus related increase in power in the <10 Hz range from stimulus onset extending 0.1 seconds beyond stimulus offset.

Figure 3.19 show regions of significant increases and decreases in the time frequency power average over twenty trials between 0 and 80 Hz bottom up input. The network white noise standard deviation is 1300 pA with various input mean values. The disconnected network is not shown as there are no significant changes in power.

In all input mean conditions of the network there is a stimulus related increase in power in the <10 Hz range from stimulus onset extending 0.05 - 0.1 seconds beyond stimulus offset.

Figure 3.20 show regions of significant increases and decreases in the time frequency power average over twenty trials between 0 and 80 Hz bottom up input. The network white noise standard deviation is 2100 pA with various input mean values. The disconnected network is not shown as there are no significant changes in power.

In the first three input mean conditions of the network there is a stimulus related increase in power in the <10 Hz range from stimulus onset extending slightly beyond stimulus offset. This is absent when the white noise input mean is 129.5 pA. In the bottom two subplots the stimulus offset is marked by an increase in power, respectively, in the 70 - 90 Hz and the 50 -70 Hz range.

Overall in the disconnected and medium and high white noise input standard deviation networks there is a low frequency significant increase in power associated with the bottom up input. However in the 580 pA white noise condition there is significant marking of stimulus onset, mid stimulus, stimulus offset and post stimulus markers. These occur in different frequency bands

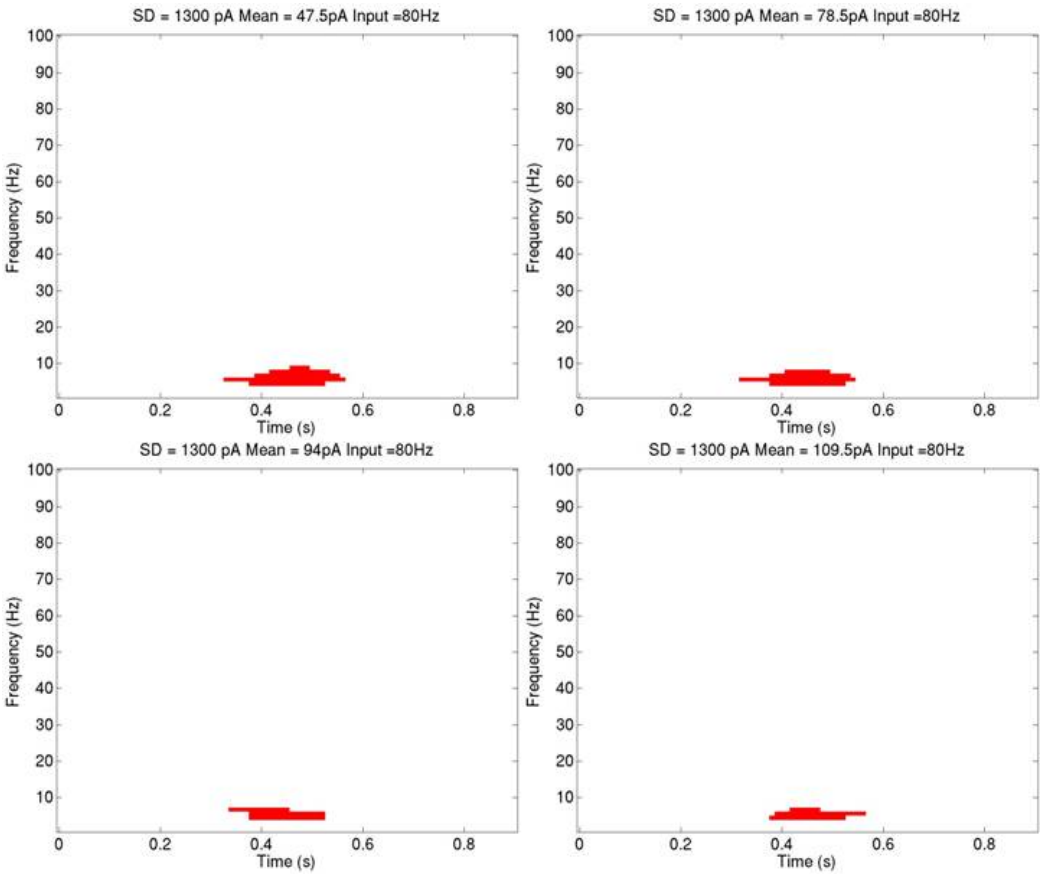

Figure 3.19: **Significant changes in the time frequency power between 0 and 80 Hz bottom up input with a white noise input standard deviation of 1300 pA** *in all plots red means a significant increase in power with $p < 0.05$. The top left plot has an input white noise mean of 47.5 pA, top right has 78.5 pA, bottom left has 94 pA and the bottom right 109.5 pA*

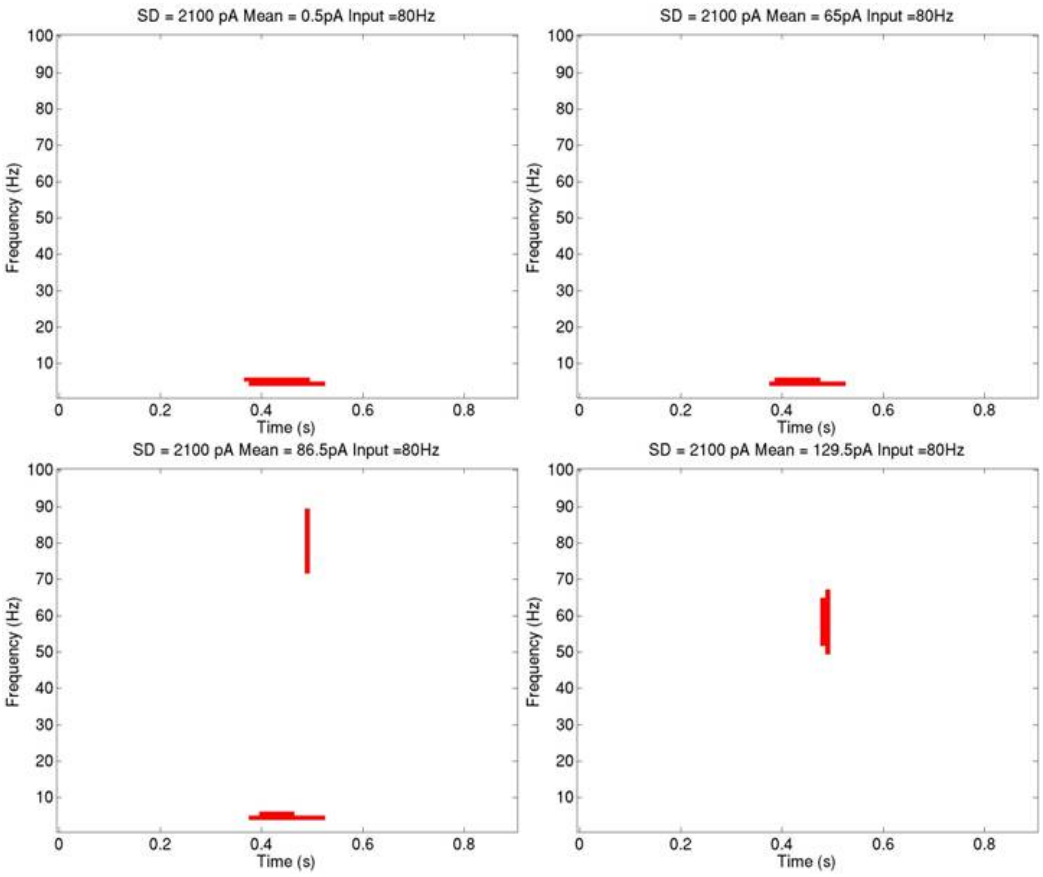

Figure 3.20: **Significant changes in the time frequency power between 0 and 80 Hz bottom up input with a white noise input standard deviation of 2100 pA** *in all plots red means a significant increase in power with $p < 0.05$. The top left plot has an input white noise mean of 0.5 pA, top right has 65 pA, bottom left has 86.5 pA and the bottom right 129.5 pA*

and are dependent upon white noise input means. They also show both increases and decreases in power. These conditions are the same conditions in which we see more complex evoked potentials and evoked firing rates of a different order of complexity. In the next section the significant mean time frequency phase of the simulated field potential will be explored in order to establish further stimulus related activity in these input conditions.

3.2.3.4 Time Frequency Phase Analysis

In this analysis I present the significant time frequency phase differences between identical simulations with and without a bottom up input.

Figure 3.21 shows the significant differences in the mean phase of the simulated field potential between a 0 Hz and a 100 Hz bottom up input in a network with a white noise input mean of 580 pA.

When the input mean is 100 pA there is an onset, mid stimulus, off set and post stimulus phase change in the >40 Hz range. There is an advance in the phase angle except in the mid stimulus period where there is a lag. Between 20 and 40 Hz there is an onset and offset phase difference with no significant change mid stimulus. Each of these show an advance in phase followed by a lag in phase. Around 10 Hz stimulus onset is marked by a lag in phase. Around 5 Hz stimulus offset is marked by an advance in phase.

When the input mean is 120 pA there is an mid stimulus and post stimulus lag in phase in the frequencies >40 Hz. In the 20 - 30 Hz range stimulus onset is marked by a lag in phase and stimulus offset is marked by an advance in phase followed by a lag. Around 10 Hz the duration of the stimulus id marked by a lag in phase. Around 5 Hz a lag in phase is present for the duration of the stimulus followed by a post stimulus advance.

When the input mean is 140 pA in the >40 Hz range there are periodic advances in phase mid stimulus with a lag at stimulus offset and subsequent differences in phase for the duration of the simulation. In the 20 - 40 Hz range there is an onset and offset lag in phase with a post stimulus advance in phase. In the 5 - 10 Hz range there is a general advance in phase for the duration of the input and post stimulus. Around 10 Hz stimulus onset is marked by a lag in phase changing to an advance mid stimulus.

When the input mean is 220 pA in the >40 Hz range stimulus onset and offset are marked by significant differences in the phase, with more activity in the post stimulus region extending the whole duration of the simulation. In the 20 - 30 Hz range there is an advance in phase marking stimulus onset followed by a lag mid stimulus. There are additional lagging features at 100 and 300 ms post stimulus. in the 10 - 20 Hz range there is a lag marking stimulus onset followed by a mid stimulus advance returning to a lag 100

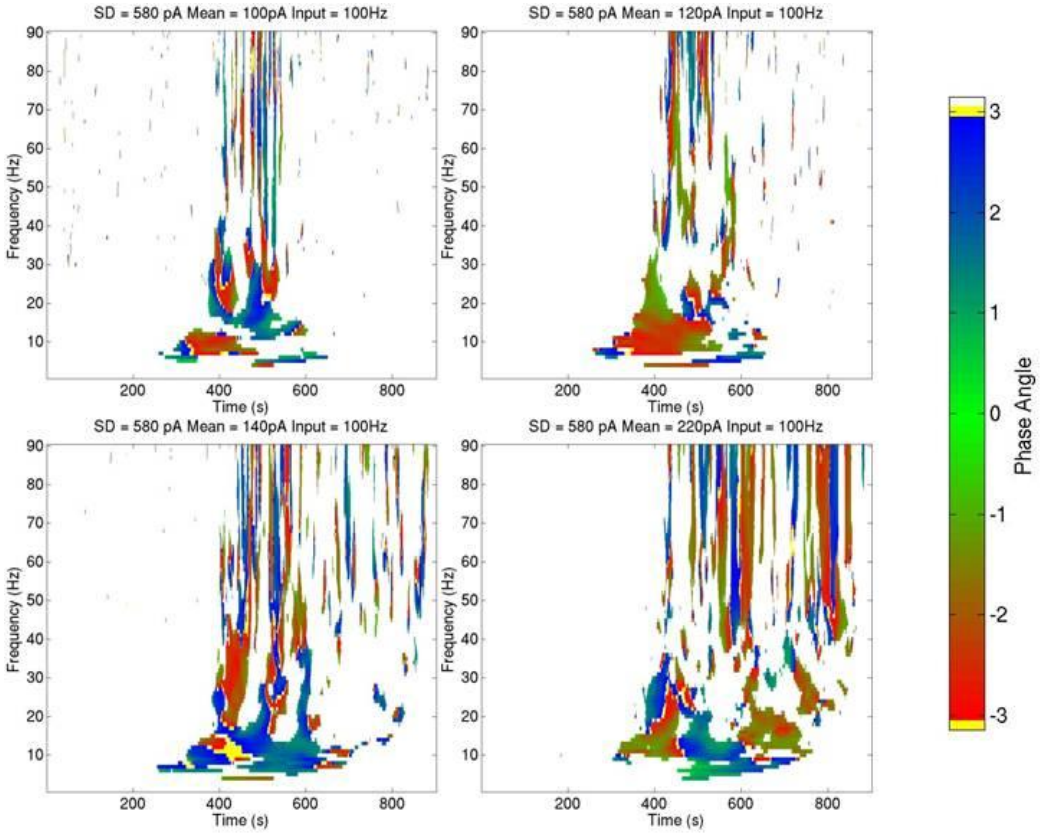

Figure 3.21: **Significant (p <0.01) simulated field potential time frequency mean phase differences between 0 and 100 Hz bottom up input in a connected network with white noise input standard deviation of 580 pA** *In all figures the colour represents the advance (blue) or lag (red) of the 100Hz input mean phase compared to the 0 Hz input. The input was delivered at 400 ms. The top left shows the input white noise mean condition of 100 pA, the top right of 120 pA, the bottom left of 140 pA and the bottom right of 220 pA.*

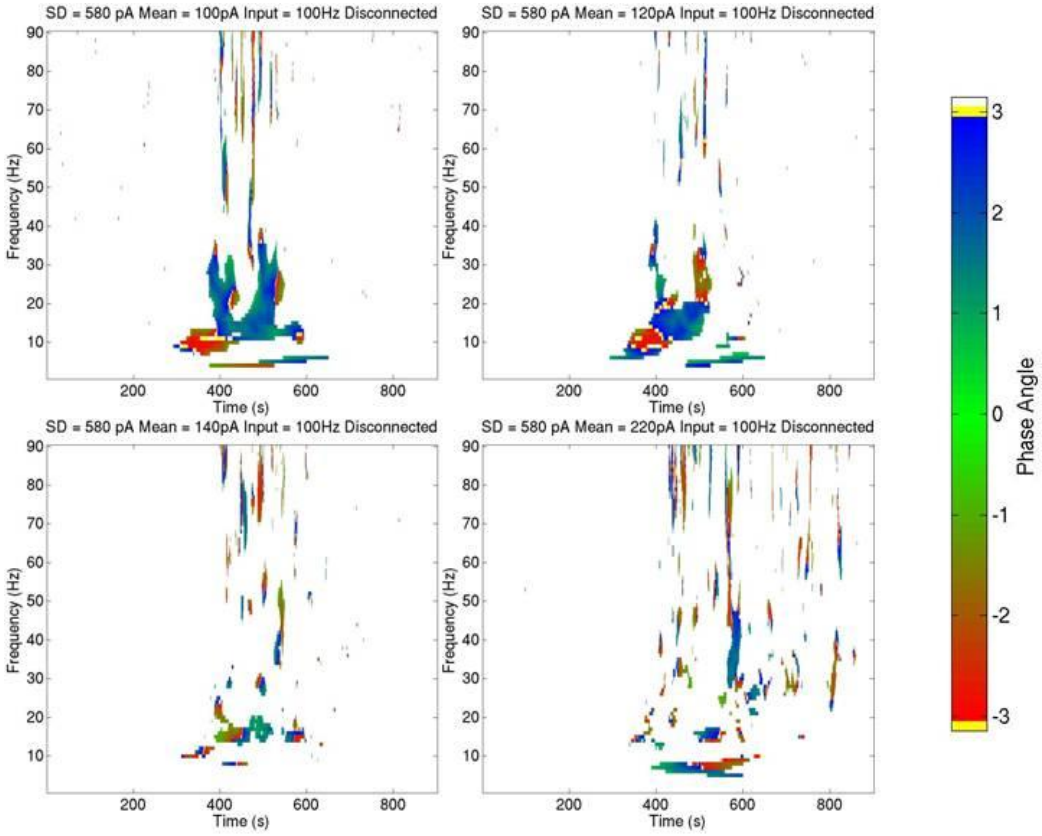

Figure 3.22: **Significant (p <0.01) simulated field potential time frequency mean phase differences between 0 and 100 Hz bottom up input in a disconnected network with white noise input standard deviation of 580 pA** *In all figures the colour represents the advance (blue) or lag (red) of the 100Hz input mean phase compared to the 0 Hz input. The input was delivered at 400 ms. The top left shows the input white noise mean condition of 100 pA, the top right of 120 pA, the bottom left of 140 pA and the bottom right of 220 pA.*

ms post stimulus. Around the 5 Hz range there is mid stimulus advance in phase extending beyond the stimulus offset.

Figure 3.22 shows the significant differences in the mean phase of the simulated field potential between a 0 Hz and a 100 Hz bottom up input in a disconnected network with a white noise input mean of 580 pA. There are some fragments of the phase behaviour observed in figure 3.21 particularly where the white noise input mean is 100 and 120 pA. Other than this being far more fragmentary than in the connected network the only major difference is with 120 pA the 10 - 20 Hz activity is more closely reltaed to the 100 pA connected network than the 120 pA connected network. This suggests that this pattern of phase changes are due to summed individual cell responses to the input rather than network responses to the input.

Figure 3.23 shows the significant differences in the mean phase of the simulated field potential between a 0 Hz and a 80 Hz bottom up input in a network with a white noise input mean of 1300 pA.

In these sub plots >40 Hz phase differences mark mid stimulus, offset and post stimulus periods of the simulation. with a mean of 16.5 pA the onset is also marked with a phase difference. The 15 - 40 Hz band marks the stimulus offset and when the mean is 125 pA it also marks the post stimulus time. The 8 - 15 Hz band marks the stimulus onset and partially the post stimulus condition. <5 Hz marks the stimulus duration.

Figure 3.24 shows the disconnected network under the same conditions as figure 3.23. The general trend highlighted for the connected network are far more fragmentary, yet the hold.

Figure 3.25 shows the significant differences in the mean phase of the simulated field potential between a 0 Hz and a 80 Hz bottom up input in a network with a white noise input mean of 2100 pA. Figure 3.26 shows the disconnected network. A very similar pattern to that shown with the network where the white noise input standard deviation is 1300 pA can be observed.

Overall there is a greater structure in the mean phase differences between simulations with and without a bottom up input than in the differences in power. A general trend is that there is less structure the higher the input standard deviation, and there is less structure between the connected and disconnected networks.

Stimulus linked events are represented differently in different frequency bands. Of particular note however, is that in the 580 pA input standard deviation condition there is a slower change in the comparative phase angle across time, suggestion a locking of the oscillations.

Each of the measures of network activity, the raw simulated field potential, the firing rates of cells by layer and type, the time frequency power and the time frequency phase have shown a representation of the bottom up

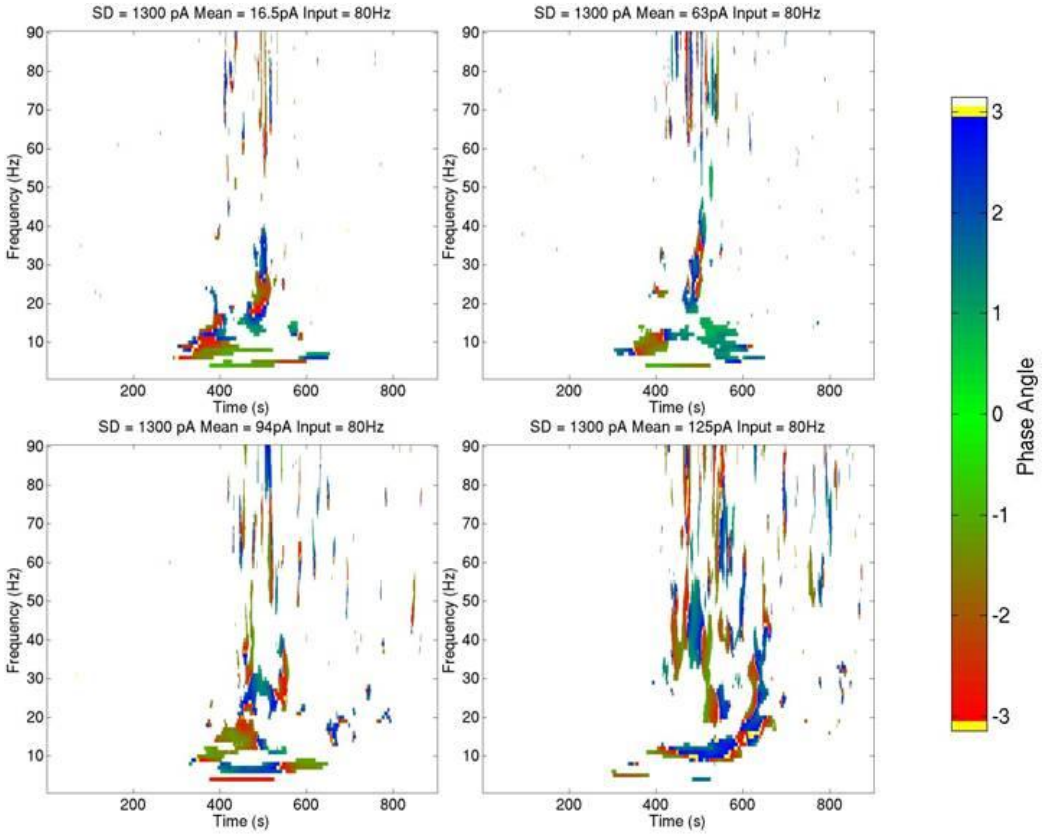

Figure 3.23: **Significant (p <0.01) simulated field potential time frequency mean phase differences between 0 and 80 Hz bottom up input in a connected network with white noise input standard deviation of 1300 pA** *In all figures the colour represents the advance (blue) or lag (red) of the 80Hz input mean phase compared to the 0 Hz input. The input was delivered at 400 ms. The top left shows the input white noise mean condition of 16.5 pA, the top right of 63 pA, the bottom left of 94 pA and the bottom right of 125 pA.*

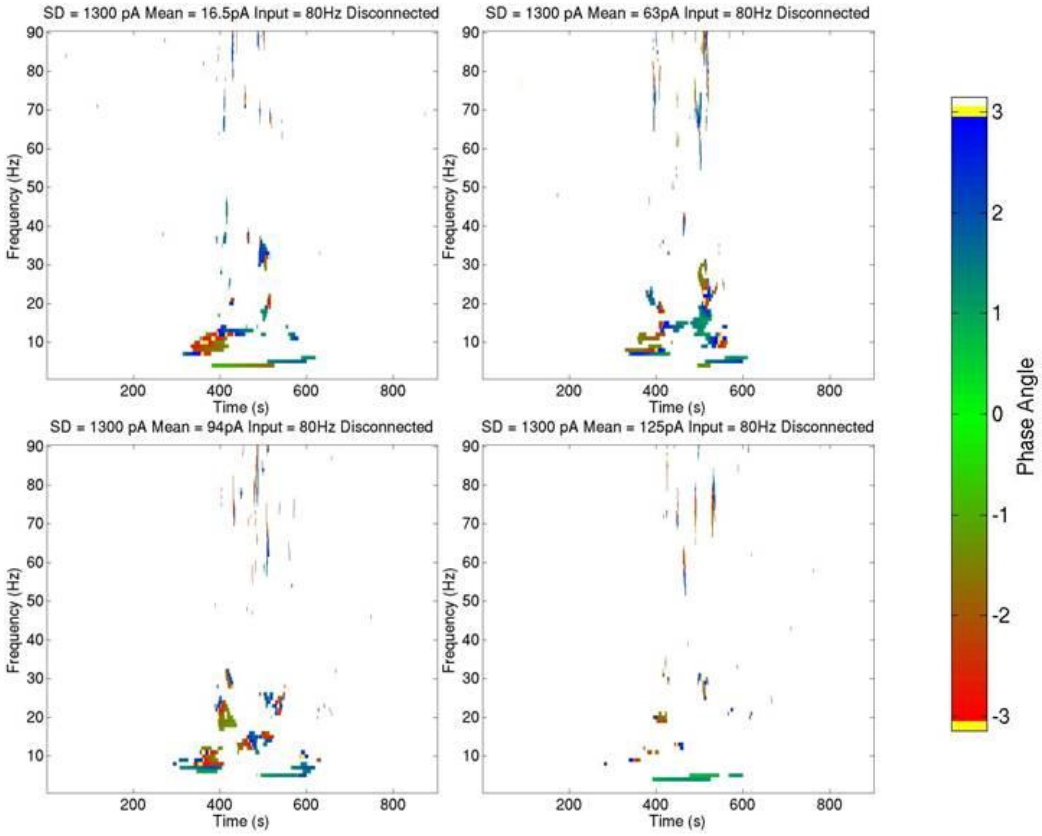

Figure 3.24: **Significant (p <0.01) simulated field potential time frequency mean phase differences between 0 and 80 Hz bottom up input in a disconnected network with white noise input standard deviation of 1300 pA** *In all figures the colour represents the advance (blue) or lag (red) of the 80Hz input mean phase compared to the 0 Hz input. The input was delivered at 400 ms. The top left shows the input white noise mean condition of 16.5 pA, the top right of 63 pA, the bottom left of 94 pA and the bottom right of 125 pA.*

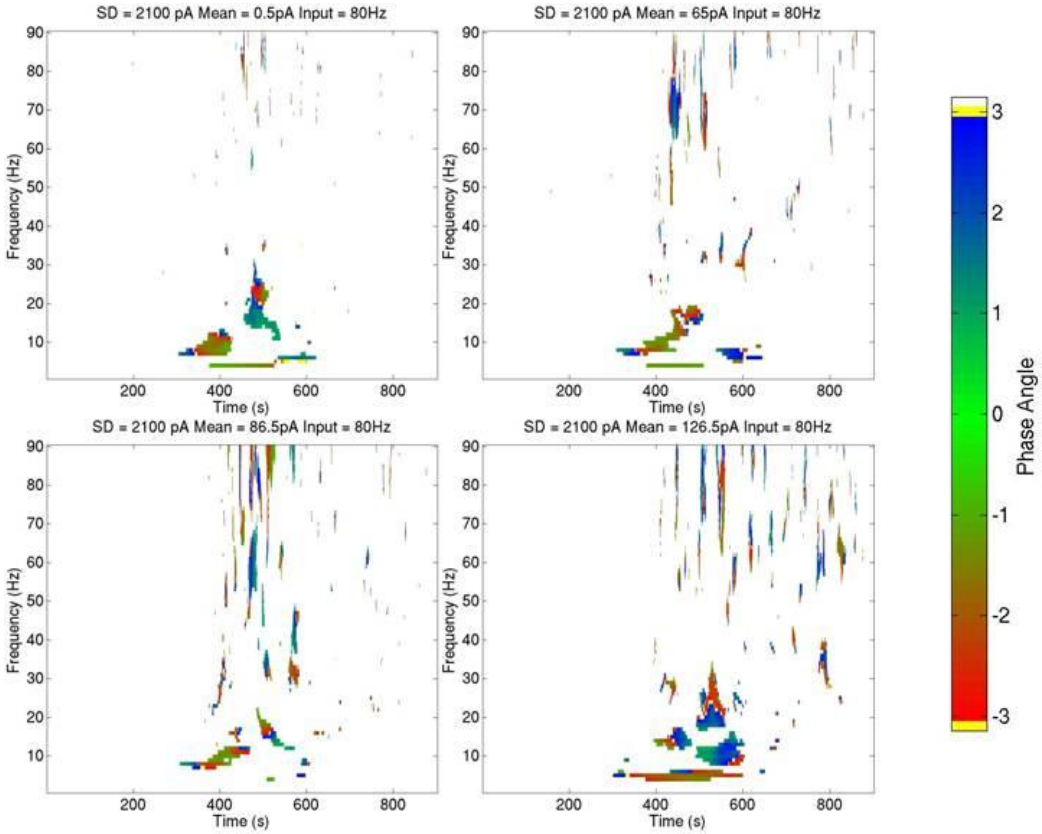

Figure 3.25: **Significant (p <0.01) simulated field potential time frequency mean phase differences between 0 and 80 Hz bottom up input in a connected network with white noise input standard deviation of 2100 pA** *In all figures the colour represents the advance (blue) or lag (red) of the 80Hz input mean phase compared to the 0 Hz input. The input was delivered at 400 ms. The top left shows the input white noise mean condition of 0.5 pA, the top right of 65 pA, the bottom left of 86.5 pA and the bottom right of 126.5 pA.*

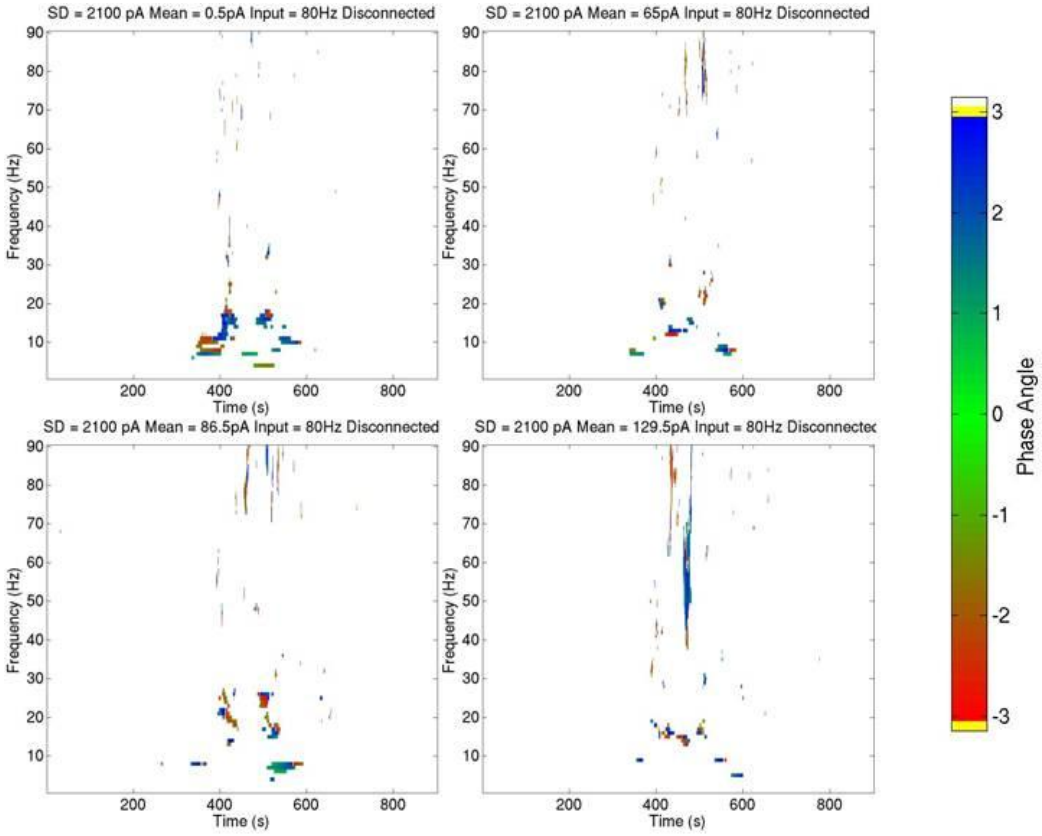

Figure 3.26: **Significant (p <0.01) simulated field potential time frequency mean phase differences between 0 and 80 Hz bottom up input in a disconnected network with white noise input standard deviation of 1300 pA** *In all figures the colour represents the advance (blue) or lag (red) of the 80Hz input mean phase compared to the 0 Hz input. The input was delivered at 400 ms. The top left shows the input white noise mean condition of 0.5 pA, the top right of 65 pA, the bottom left of 86.5 pA and the bottom right of 126.5 pA.*

stimulus in their responses. In the next sections I will present information theory analyses in order to quantify the transmission of information using these experimentally available metrics.

3.2.3.5 Information analysis of the simulated field potential

In this section I present the significant mutual information between eleven bottom up input values of the poisson spike generators set between 0 and 100 Hz firing rates in steps of 10 Hz and the raw simulated field potential magnitude. By inspecting this it looks at the value of using magnitude and rise gradient as experimental metrics.

Figure 3.27 shows the mutual information between the absolute field potential voltage and the stimulus rate for a range of input means across three input standard deviations in connected and disconnected networks at each simulations time step.

When the input white noise standard deviation is 580 pA, between an input mean of 90 and 120 pA, both the connected and disconnected networks show significant stimulus related mutual information values shortly after the stimulus is applied. There is a brief drop at stimulus offset followed by around 30 ms of significant mutual information. The connected network shows a higher value of mutual information than the disconnected network. At input means between 120 and 180 pA only the connected network shows significant mutual information between the stimulus and the response. At 130 pA this is only associated with stimulus onset and offset. At 140 pA the mutual information latency from stimulus onset is greater than in other conditions. At 150 - 180 pA the significant mutual information values reduce towards insignificance.

When the input white noise standard deviation is 1300 pA the connected network mutual information values mark the onset by the appearance of significant mutual information values and the offset with a brief reduction in information values. The disconnected network has lower significant mutual information values. At 30 - 70 pA the connected network stimulus offset period is marked with an increase in mutual information whilst the disconnected network shows a reduction towards insignificance.from 70 - 100 pA there are significant, but reduced mutual information values in the connected network.

When the input white noise standard deviation is 2100 pA a similar pattern at lower input means can be seen where the connected network has a slight increase in mutual information when the input mean reaches -60 pA whilst the disconnected network decays to insignificance.

Overall the measures show that the simulated field potential magnitude

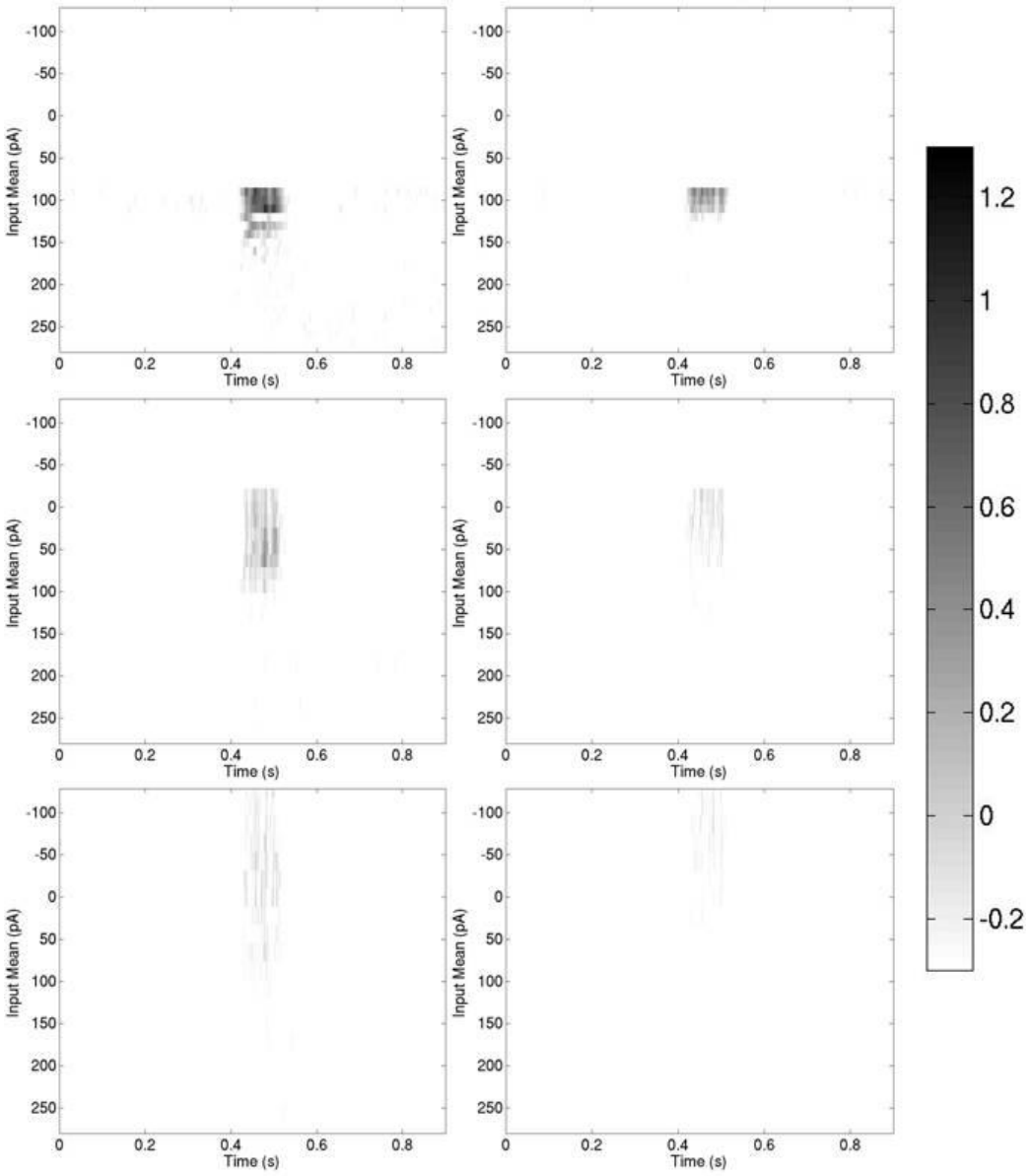

Figure 3.27: **The mutual information between the absolute field potential voltage and the stimulus rate** *in all plots only the information values significantly greater than bootstrapped values are shown. The bottom up stimulus was applied between 0.4 and 0.5 seconds. The left hand plots are connected networks and the right hand plots are disconnected networks. The top plots have an input standard deviation of 580 pA, the middle 1300 pA and the bottom 2100 pA. The mutual information is in bit units*

is only sensitive to input in short regions of input mean values. The highest information values are in the 580 PA range where input means of 90 to 170 pA produce values. This band is not represented in the other white noise input standard deviation conditions. Around 120 pA input mean the information values show a structure where only the onset of the stimulus contains mutual information, rather than the whole duration of the stimulus. This suggests that in the experimentally available signals there may be a value in trying different encoding schemes based upon preceding ongoing activity.

3.2.3.6 Information analysis of the instantaneous firing rate

In this analysis I present the mutual information between the eleven bottom up input conditions and the average spike rate from the average cell in each population. This is in order to characterize the role each population plays in representing a bottom up input according to pre stimulus input means.

Figure 3.28 the mutual information between the instantaneous firing rate of the average cell in each population and the stimulus rate in the connected network with a Gaussian white noise input standard deviation of 580 pA.

The most striking feature of this figure is that there is no stimulus linked increase in mutual information between the stimulus and the firing rate in the layer 3 and layer 5 inhibitory cells. This should be interpreted as a lack of precise spike timing coding. All the other populations show a similar pattern of information values. At low input means there is a longer onset latency of increased information than at higher input means. As the input mean increases there is an extended post stimulus increase in information. The transition from low to higher firing rate is marked by a reduction in onset latency and increasing post stimulus persistence of increased information. Between the population types the latency of layer 4 is shortest, followed by layer 3 then layer 5. Between input means of 120 and 150 pA the maximum information is found in the layer 3 and layer 5 excitatory cells. At 120 pA this is at stimulus offset and at 130 pA it is at stimulus onset.

These results indicate that around 120 - 150 pA input mean the network is in an optimal state for transmitting information about a bottom up input to other cortical or subcortical regions.

3.2.3.7 Information analysis of the time frequency response power

In this analysis I present the significant information values between the eleven bottom up conditions and the time frequency power response of the simulated field potential. This offers a comparison with the significant differences in power presented above.

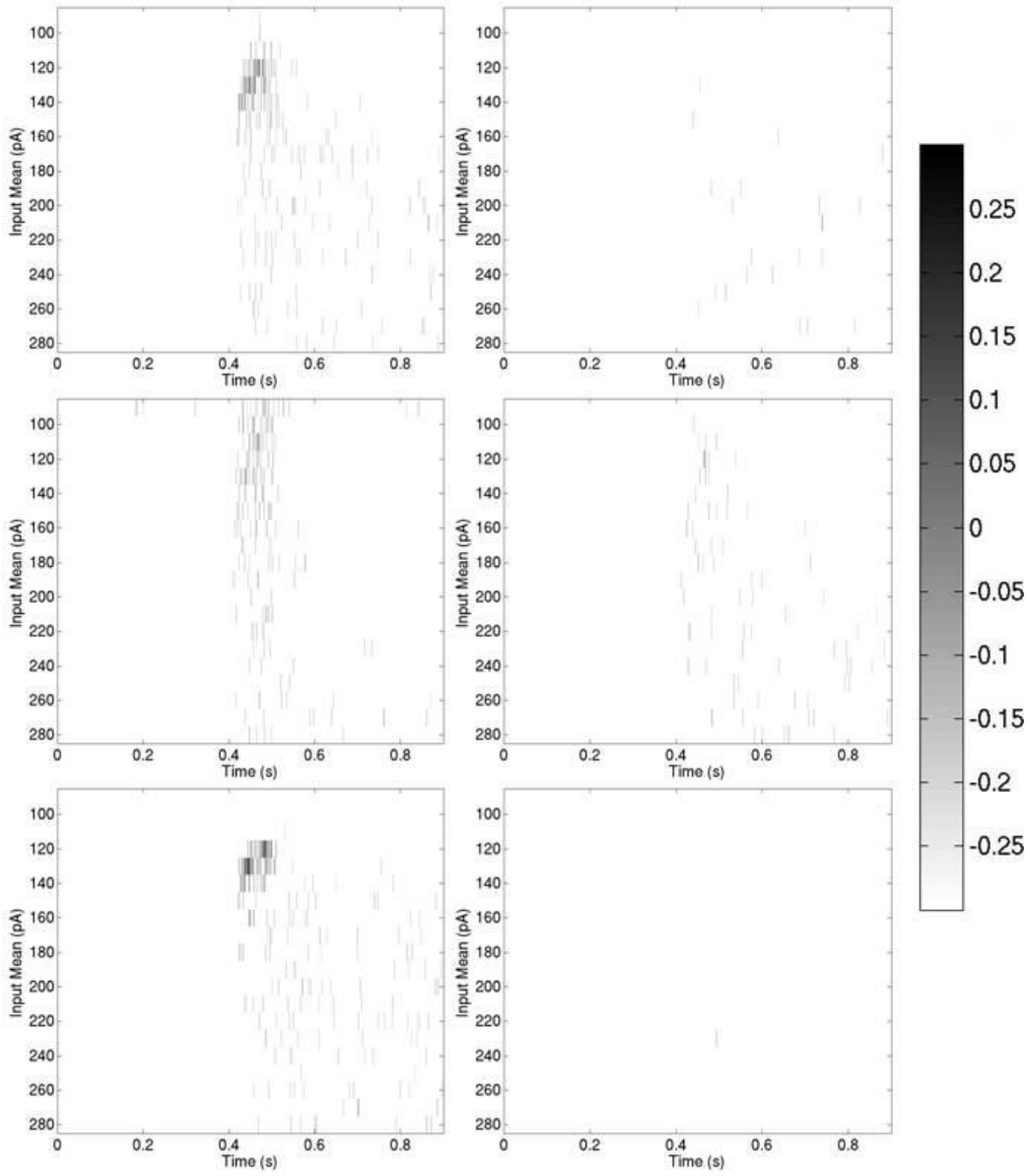

Figure 3.28: **The mutual information between the instantaneous firing rate of the average cell in each population and the stimulus rate** *in all plots only the information values significantly greater than bootstrapped values are shown. The bottom up stimulus was applied between 0.4 and 0.5 seconds. The left hand plots are the excitatory cells, the right the inhibitory cells. The top plots are the layer 3 cells, the middle plots are the layer 4 cells and the bottom are the layer 5 cells.*

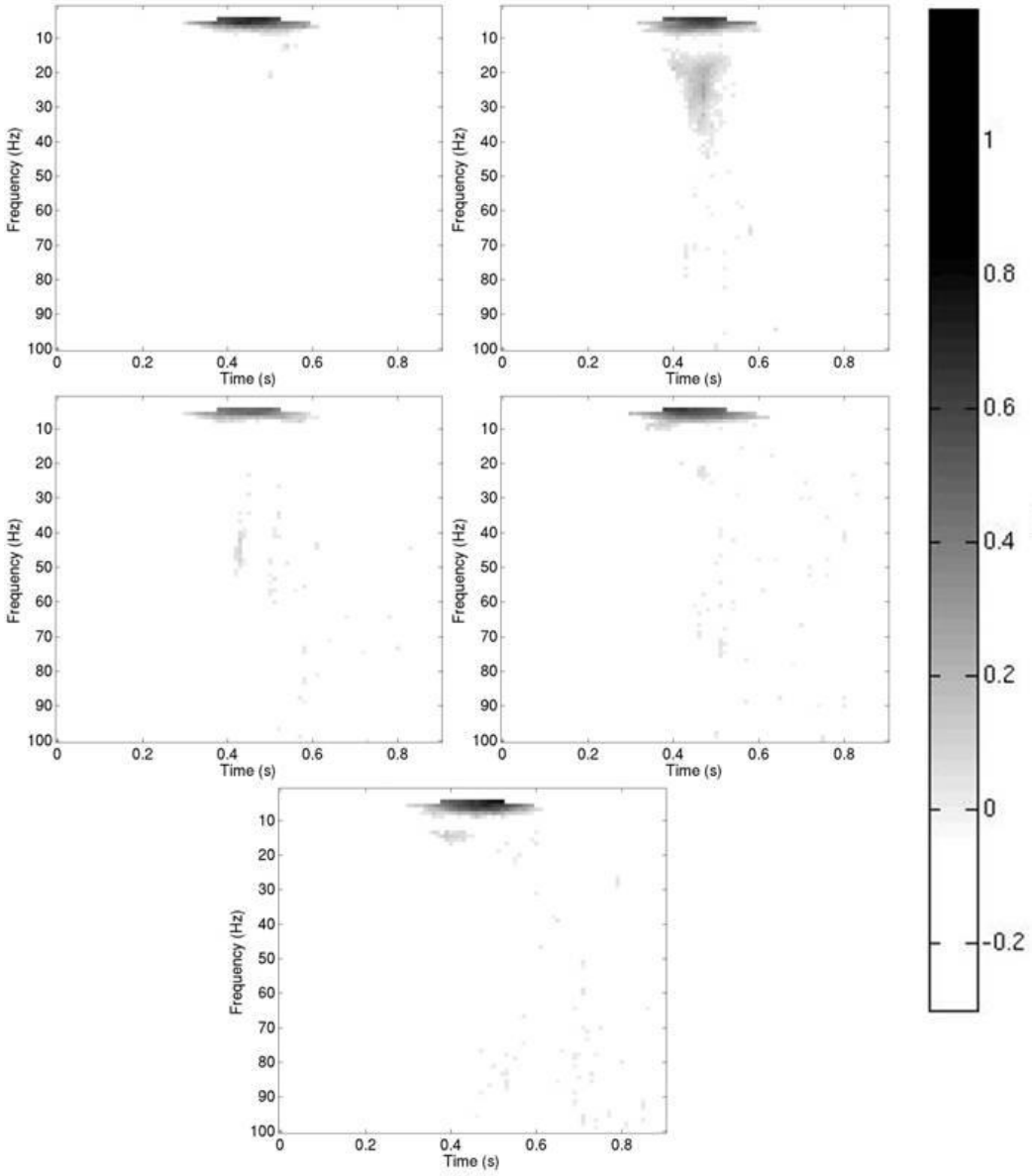

Figure 3.29: **The mutual information between the time frequency response power and the stimulus rate with an input standard deviation of 580 pA** *in each of the subplots only the significant mutual information between the input and response is shown. Mutual information is given in bits. The top left plot shows the response with a white noise input mean of 110pA, the top right 130 pA, the middle left 140pA, the middle right 160 pA and the bottom 180 pA.*

Figure 3.29 the significant mutual information between the time frequency response power and the stimulus rate with an input standard deviation of 580 pA. In all inpt mean conditions there is significant mutual information values in the <10 Hz range. In teh disconnected networks (not shown) there is a slight significant mutual information increase in this band and no other bands showing significant values across simulation time. As the input mean increases there is significant mutual information between the input and other frequency bands.

When the white noise input mean is 110 pA there is a short period of mutual information in the simulated field potential at bottom up stimulus offset in the 15 Hz and 25 Hz range.

When the input mean is 130 pA the onset and offset of the bottom up inputs are marked at the 10 Hz and the 65 - 80 Hz frequencies. There is an significant mutual information in the 15 - 40 Hz for the whole duration of the stimulus and extending up to 50 ms beyond stimulus offset. From 25 - 40 Hz the stimulus onset is not strongly marked, with significant values occurring mid stimulus. The peak mutual information values can be found at the 25 - 30 Hz range at stimulus offset.

When the white noise input mean is 140 pA stimulus onset and off set are marked in the 10 Hz range and in the 35 - 55 Hz range, with onset having slightly higher mutual information values. outside the <10 Hz range there are no mid stimulus significant mutual information values.

When the white noise input mean is 160 pA stimulus onset is marked by significant mutual information in the 10 Hz range. Midstimulus and stimulus offset are not marked in this range. Midstimulus is marked in the 20 - 25 Hz range and at around 70 Hz. Stimulus offset is marked in the >40 Hz range with some features in this range significantly after the stimulus offset.

When the white noise input mean is 180 pA stimulus onset is marked in the 15 Hz range extending to mid stimulus. Stimulus offset is marked around 80 Hz with post stimulus features at 20 Hz, 15 Hz and >30 Hz bands.

Figure 3.30 the significant mutual information between the time frequency response power and the stimulus rate with an input standard deviation of 1300 pA. When the white noise input mean is 16.5 pA the stimulus onset and offset are marked in the 5 Hz range. In all other conditions the whole duration of the stimulus is marked in this range, with the stimulus offset containing slightly more mutual information. The 63 pA condition shows the highest mutual information values. In the 94 pA condition the is also a post stimulus mark in the 80 - 90 Hz range. In the disconnected network there are no significant information values between the stimulus input and the simulated field potential time frequency power values.

In the white noise input standard deviation condition of 2100 pA there is

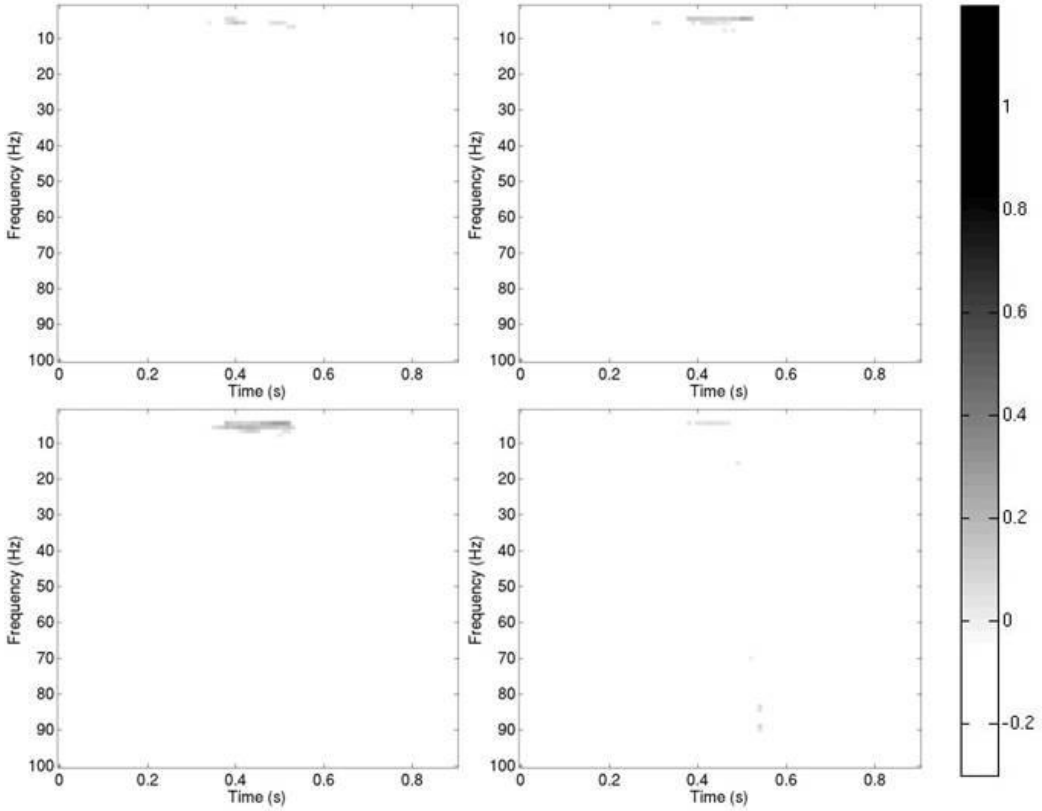

Figure 3.30: **The mutual information between the time frequency response power and the stimulus rate with an input standard deviation of 1300 pA** *in each of the subplots only the significant mutual information between the input and response is shown. Mutual information is given in bits. The top left plot shows the response with a white noise input mean of 16.5pA, the top right 47.5 pA, the bottom left 63pA, the bottom right 94 pA.*

no significant mutual information in any of the conditions.

Overall the best condition for extracting information from the field potential time frequency power is in the white noise input standard deviation 580 pA condition between 110 and 180 pA. The information values are different depending upon prestimulus conditions of the network. these regions of significant information roughly match up with the significant changes in power presented above, although some features are not present in the information analysis. This suggests that although they may show up at extremes of presentation they do not encode the finer scale changes in input values.

3.2.3.8 Information analysis of the time frequency response phase

In this analysis I present the mutual information values between the eleven bottom up stimulus conditions and the phase angle of the time frequency response.

Figure 3.31 the significant mutual information between the time frequency response phase and the stimulus rate with an input standard deviation of 580 pA. When the input mean is 110 Hz the significant mutual information <8 Hz marks the whole bottom up stimulus with more information in stimulus onset. Around 10 Hz there is a marker for stimulus off set.

When the white noise input mean is 130 pA the <8 Hz range favours the offset. The 10 - 15 Hz range marks the duration of the stimulus with the 15 Hz range marking on set and offset. There is a small amount of significant information marking the offset around 70 Hz.

When the white noise input mean is 140 pA the <8 Hz range marks the stimulus duration favouring the onset the 10 Hz range marks mid stimulus through offset to about 100 ms post stimulus. There is a small contribution from the 20 Hz range marking the stimulus off set. The 40 - 60 Hz range has a small mid stimulus marker and there is a small post stimulus representation in the >40 Hz range.

When the white noise input mean is 160 Hz the <8 Hz marks the duration of the stimulus. The 8 - 12 Hz range marks the duration of the input with the highest mutual information values appearing mid stimulus. the 15 Hz range marks stimulus onset and stimulus off set. Around 18 Hz there is a mid stimulus marker with a small post stimulus contribution. About 25 Hz there is a post stimulus marker. At 40 - 55 Hz mid stimulus there is a brief high information marker. At >70 Hz there is a small post stimulus contribution.

When the white noise input mean is 180 pA Hz the <8 Hz marks the duration of the stimulus. The 8 - 12 Hz range marks the duration of the input with the highest mutual information values appearing post stimulus. The 10 Hz range marks stimulus onset and post stimulus periods. around

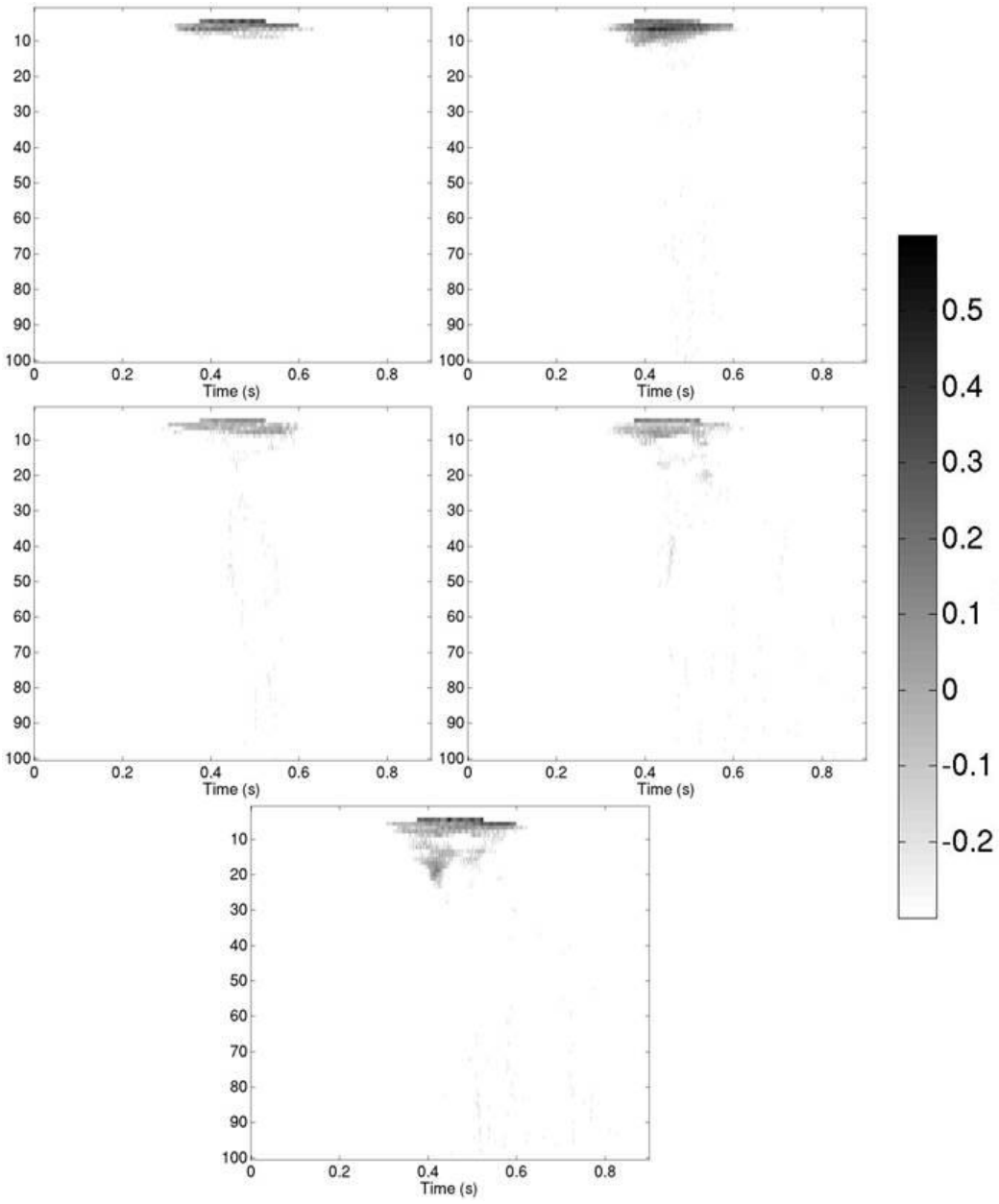

Figure 3.31: **The mutual information between the time frequency response phase and the stimulus rate with an input standard deviation of 580 pA** *in each of the subplots only the significant mutual information between the input and response is shown. Mutual information is given in bits. The top left plot shows the response with a white noise input mean of 110pA, the top right 130 pA, the middle left 140pA, the middle right 160 pA and the bottom 180 pA.*

12 Hz there is a stimulus onset marker. In the 15 Hz range there is a mid stimulus and a post stimulus marker. At 20 Hz there is a strong mid stimulus marker. At the >80 Hz range there is a stimulus offset marker.

In the disconnected network (not shown) there is a slight <5 Hz component in all conditions, but no other features.

Figure 3.32 the mutual information between the time frequency response phase and the stimulus rate with an input standard deviation of 1300 pA. In all subplots there is a <5 Hz increase in mutual information. In each of the subplots the is a 8 Hz component which marks either the stimulus offset (16.5 and 63 pA) or the stimulust offset (47.5 and 94 pA). There is no significant mutual information content in the disconnected network.

In the white noise input condition where the standard deviation is 2100 pA there is no significant mutual information between bottom up input and the time frequency phase response of the simulated field potential.

Overall there is an optimal prestimulus condition influence on the availability of stimulus linked information. The optimal range is in the 580 pA white noise standard deviation condition with a mean between 110 and 180 pA.

3.2.4 Discussion

In this section I have presented a number of complex and potentially realistic responses of a cortical network to a bottom up sensory input. These results show a marked difference in network response below and above the network activation threshold. There is also further evidence to suggest that when local cortical networks are activated there is a suppression of encoding in the surrounding areas. The data presented regarding the spiking activity in laminar cells also strongly supports specific roles in information processing for each population.

The simulated field potential demonstrates that in low local input areas near activation threshold there are a variety of different features that encode stimulus features. The evoked potential in this region of parameter space becomes more complex, the maximal information in the raw signal allows latency encoding, and the stimulus onset, duration and offset are encoded in the power and phase of the time frequency breakdown.

The spiking activity in each of the laminar populations and cell types further demonstrate a different role in information processing. In the evoked instantaneous firing rates there is strong evidence for a rate coding flow of information through the network. In the information content in the instantaneous firing rate there is evidence that each population has a different level of spike timing coding, with it being absent entirely from the layer 3 and

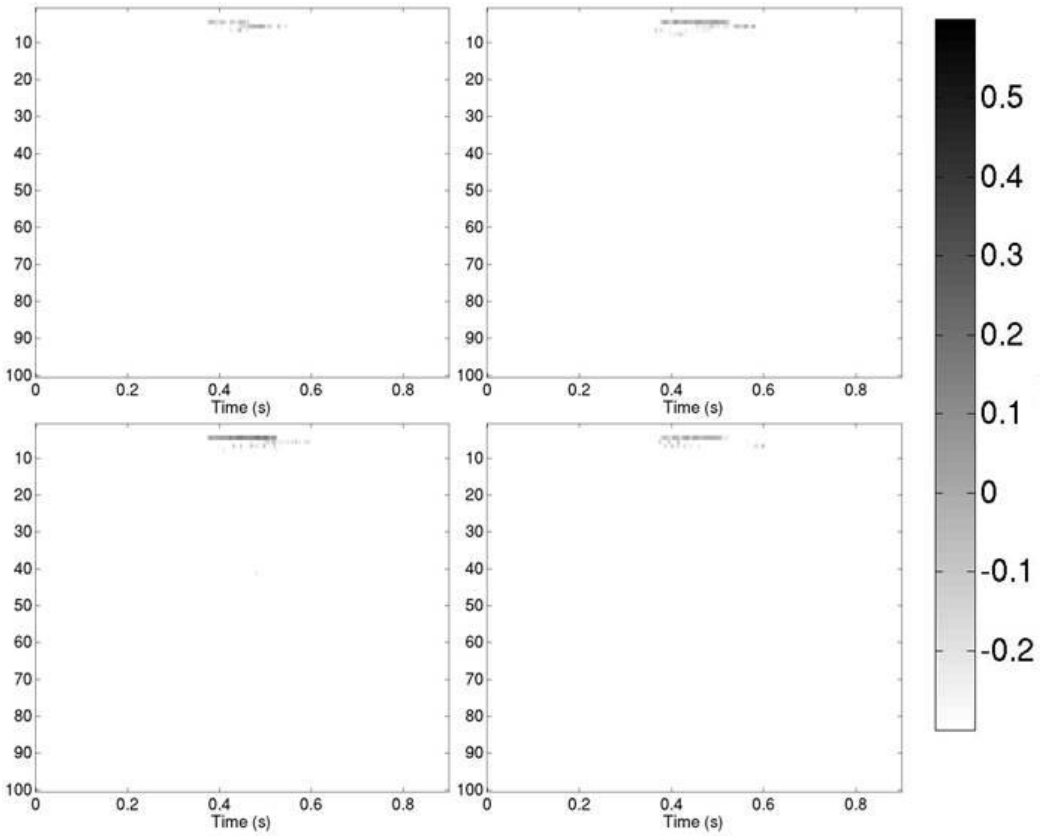

Figure 3.32: **The mutual information between the time frequency response phase and the stimulus rate with an input standard deviation of 1300 pA** *in each of the subplots only the significant mutual information between the input and response is shown. Mutual information is given in bits. The top left plot shows the response with a white noise input mean of 16.5pA, the top right 47.5 pA, the bottom left 63pA, the bottom right 94 pA.*

layer 5 inhibitory cells. It should be born in mind that they show stimulus associated changes in rate. The highest stimulus related information is in the layer 4 excitatory cells, which suggests a strong spike timing regimen.

It is clear from this analysis that in this model there is an optimal region of parameter space where experimentally available information via the simulated field potential and the physiologically available information in the projection neurons maximized. This suggests that any incoming variable synchronized input will result in changes in the coding scheme in the local cortical network. However this does not suggest that in this variable condition these results will hold, as they have been carried out with a static mean value. In the next section I will present a network with a low white noise input standard deviation with a sinusoidal input varying across the range of the mean values that provided the clearest representations of the input in order to investigate this further.

3.3 Oscillatory input with a sensory input

3.3.1 Introduction

In this section I look at simulations with an oscillatory mean representing an oscillatory cortico-cortical input. The frequencies of this sinusoidal input explored are 5 Hz, 10 Hz, 20 Hz and 40 Hz. Within this context I introduce two sensory inputs of 30 ms with frequency values as in the previous section. In addition to this I run 20 batches of simulations with the input time of the bottom up stimulus covering the entire wavelength of the oscillatory input. This is to explore the response of the network under the context of a specific oscillation band of ongoing activity.

Firstly I look at all the evoked potentials under each oscillatory input condition in the connected and disconnected network. I hypothesise that there will be a different EP depending upon whether or not the network is connected or not.

Secondly I look at the evoked instantaneous firing rate in the 5 Hz condition. I hypothesize that this will vary according to the timing of the sensory input, being facilitated depending upon the phase of the ongoing oscillations.

Thirdly I look at the relative mean field potential time frequency response power in all conditions. I hypothesise that there will be a phase dependent variation in response and this will be different in different frequency bands.

Next I perform an information analysis on the response. Firstly I look at the mutual information between input and magnitude at each time step in the simulated field potential for every input time condition. I hypothesise

that there will be a variation in the mutual information depending upon the phase of the ongoing activity at the time of stimulus application. A secondary hypothesis is that this will vary according to the frequency of the oscillatory input.

Secondly I look at the mutual information between the input frequency and the instantaneous firing rate of the average cell from each population at each time step and stimulus time. I hypothesise that there will be a stimulus time related variation in stimulus related information.

Thirdly I look at the mutual information between the time frequency response power and the input frequency. I hypothesise that there will be a variation in information across different frequency bands according to the application time os the stimulus. A secondary hypothesis is that different frequency bands will represent the input differently over time. A tertiary hypothesis is that the information representation will vary according to the oscillatory input frequency.

Finally I look at the mutual information between the time frequency response phase and he input frequency. I hypothesise that there will be a variation in information across different frequency bands according to the application time os the stimulus. A secondary hypothesis is that different frequency bands will represent the input differently over time. A tertiary hypothesis is that the information representation will vary according to the oscillatory input frequency.

3.3.2 Methods

3.3.2.1 Simulations

In this section all simulations were carried out with a Gaussian white noise input standard deviation of 580 pA and a mean of 140 pA. A sinusoidal ac input was applied to all cells with a mean value of 0, and amplitude of 50 pA, phase zero at time zero and a frequency of 5, 10, 20 or 40Hz. An identical 30 ms bottom up spike input was applied at 400 ms and 600 ms. The bottom up input covered the firing rate range 0 - 100 Hz. The stimuli were shifted by 1/20 th of the wavelength of the AC input. The parameter space explored was: AC frequency (4) X bottom up phase shift(20) X bottom up firing rate frequency (11). At each point in the parameter space twenty trials were carried out with a different Gaussian white noise input seed but the same poisson spike generator seed at both bottom up impulses. All simulations were replicated with a disconnected network resulting in a total of 1760 simulations.

3.3.2.2 Analysis

The analysis procedures were carried out in the same way as in the previous section with the exception that the mean time frequency power or phase from the network with no bottom up input was subtracted from the mean values of those with a bottom up input. This served as a baseline to highlight differences due to the bottom up input.

3.3.3 Results

3.3.3.1 The evoked potential

In this section I present the evoked potentials across four input frequencies in the connected and disconnected networks with two bottom up inputs presented at different phases of the injected oscillatory current. This is to establish whether there are visible changes in the evoked potential due to the bottom up input and whether network connectivity yields a different evoked potential shape.

Figure 3.33 shows the evoked potentials from all input phases with oscillatory inputs of 5 and 10 Hz with a bottom up input of 100 Hz. Figure 3.33 shows the evoked potentials from all input phases with oscillatory inputs of 20 and 40 Hz with a bottom up input of 100 Hz.

In the disconnected networks the evoked potentials are simpler than the connected networks. The overall shape is very close to the sinusoidal input. For the 5 and 10 Hz input the initial rise in the first quarter wavelength has a steeper gradient than a sinusoid followed in the second quarter wavelength by a negative deflection and a smaller positive deflection with a trace high frequency component. The second half of the wavelength follows the general shape of a sinusoid. In the 20 and 40 Hz evoked potentials the shape is far closer to the sinusoid, if a little sawtoothed. The introduction of the stimulus input sees an increased standard deviation of the evoked responses for a duration of around one and a half wavelengths. In the 5 Hz input evoked response this can be observed in the second input.

In the connected networks in the first quarter wavelength there is a steep positive deflection followed by a steeper negative deflection. In the second quarter wavelength there is a high frequency oscillation leading to a positive deflection. In the second half wavelength there is a component somewhat matching the trough of the second half of the sinusoidal input. As the frequency increases the complex oscillation component is reduced. The introduction of stimulus input also sees an increased standard deviation of the evoked responses for a duration of around one and a half wavelengths. There is an increase in the magnitude of the negative deflection associated with the

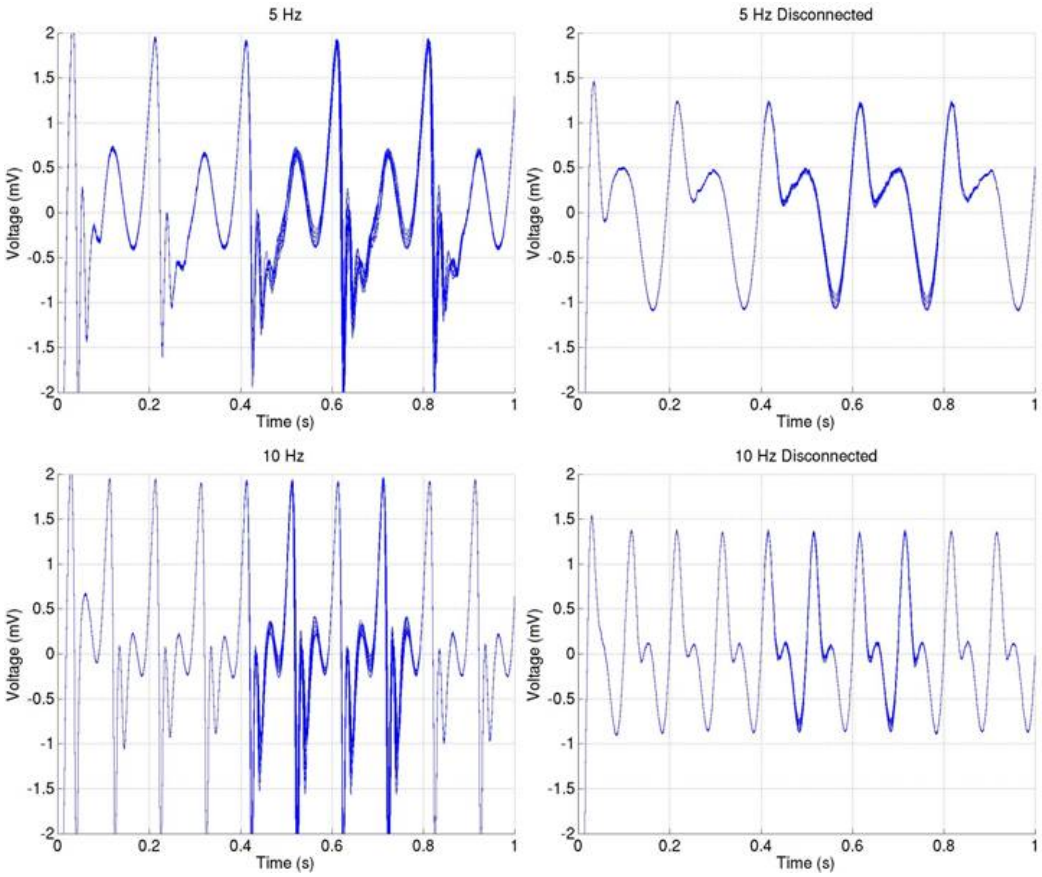

Figure 3.33: **Evoked potentials from all input phases with 5 and 10 Hz oscillatory inputs** *each plot shows an overlay of 20 evoked potentials with a bottom up input presented at 0.4 and 0.6 seconds plus* $\frac{0}{20}\lambda$ *to* $\frac{19}{20}\lambda$*. The left hand plots show the connected networks and the right hand plots show the disconnected networks. The top plots show an a.c. input delivered at 5 Hz and the bottom plots show an a.c. input delivered at 10 Hz.*

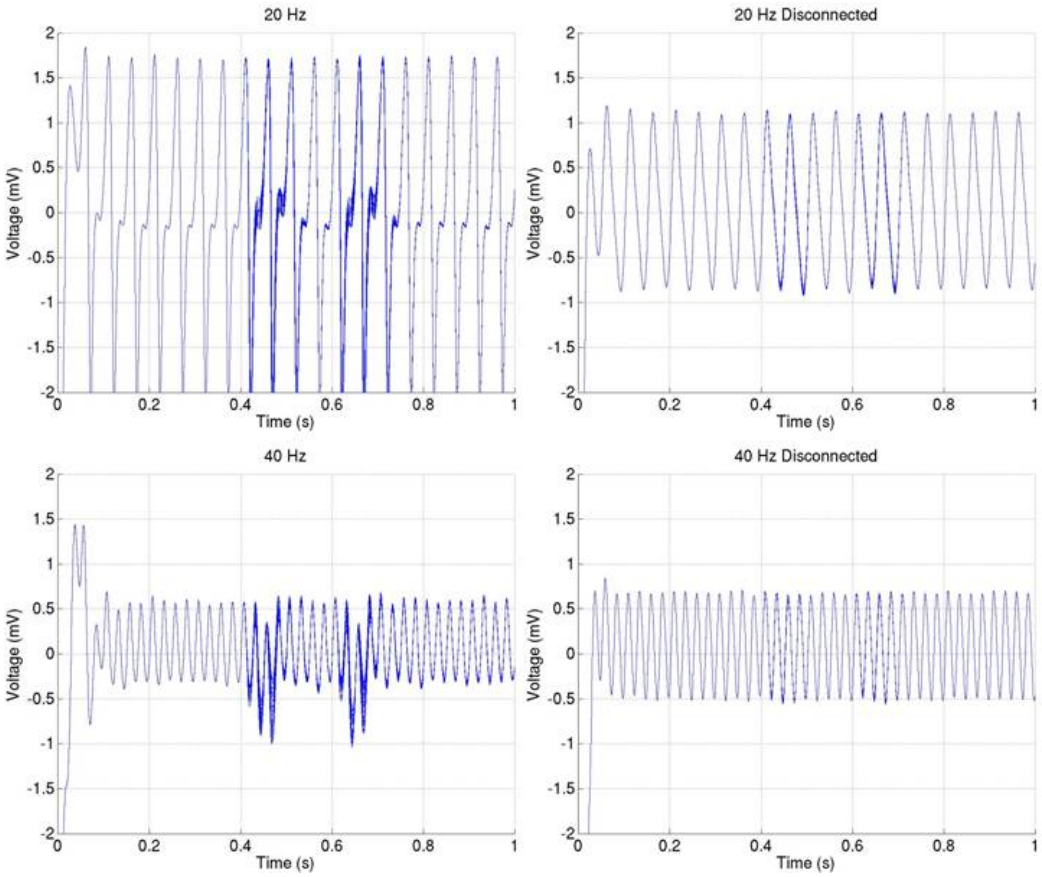

Figure 3.34: **Evoked potentials from all input phases with 20 and 40 Hz oscillatory inputs** *each plot shows an overlay of 20 evoked potentials with a bottom up input presented at 0.4 and 0.6 seconds plus* $\frac{0}{20}\lambda$ *to* $\frac{19}{20}\lambda$*. The left hand plots show the connected networks and the right hand plots show the disconnected networks. The top plots show an a.c. input delivered at 20 Hz and the bottom plots show an a.c. input delivered at 40 Hz.*

stimulus inputs. In the 40 Hz input oscillation the stimulus also produces a reduced positive deflection in the first quarter wavelength.

It should be noted that the complex oscillation in the second quarter wavelength varies in the evoked potential before the first bottom up stimulus input.

Overall there is a significant difference between the evoked potential in the connected and disconnected states. The evoked potentials also, although there is a repeating feature, do not directly represent the sinusoidal shape of the injected input.

3.3.3.2 The evoked instantaneous firing rates

In this section I present the evoked firing potential of the individual cells under the 5 Hz stimulation condition in both the connected and the disconnected networks. This is in order to establish where there are any prominent stimulus related features in the firing rates and whether or not they are cell type specific.

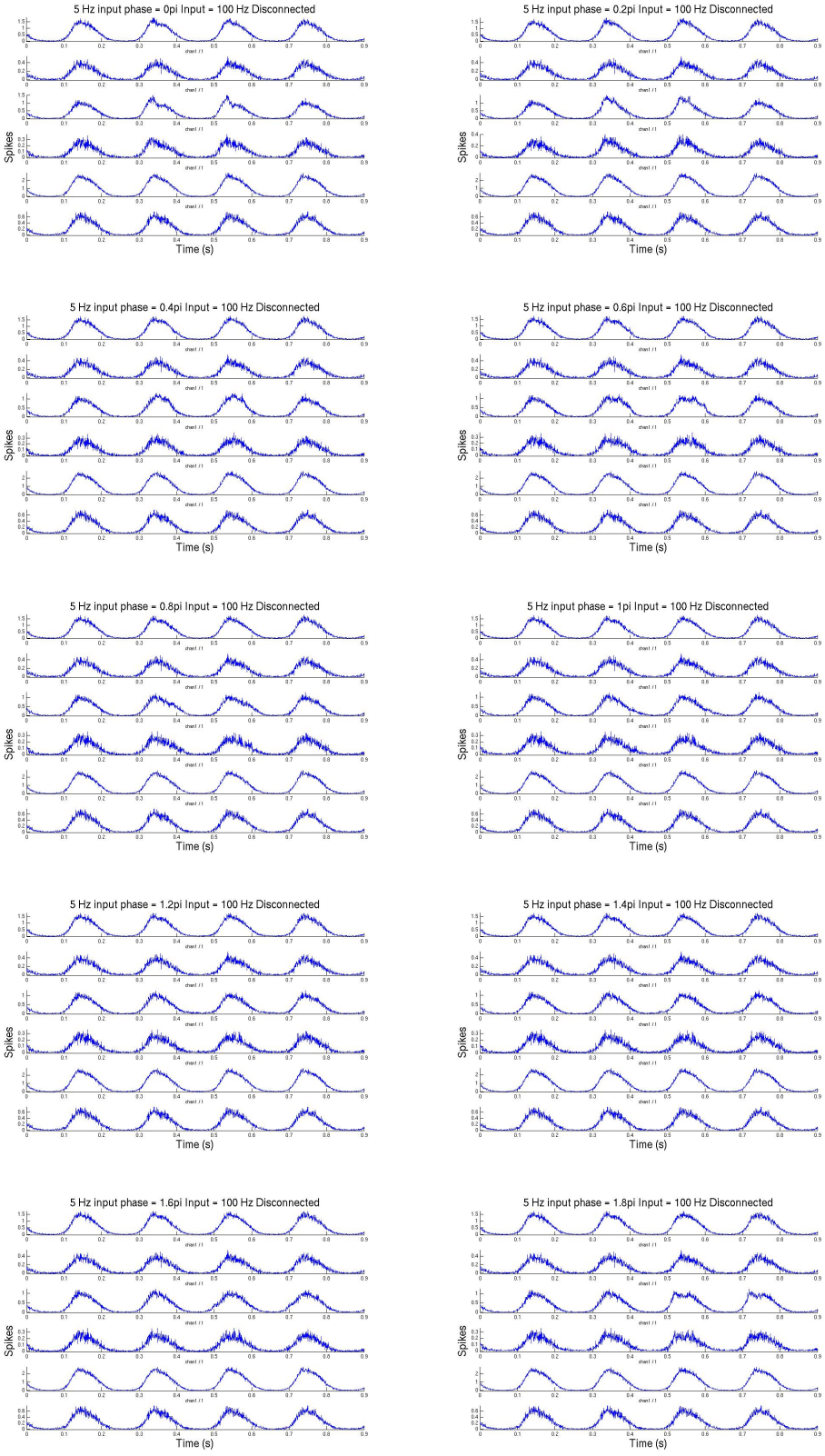

Figure 3.35: **The mean instantaneous spike count of each population with a 5 Hz oscillatory input with a bottom up input at various input times across wavelength in a disconnected network** *Reading left to right top to bottom the plots have the bottom up input at 0, 0.2, 0.4, 0.6, 0.8, 1, 1.2, 1.4, 1.6, 1.8 pi units. Each plot from top to bottom shows the layer 3 excitatory cells, layer 3 inhibitory cells, layer 4 excitatory cells, layer 4 inhibitory cells, layer 5 excitatory cells and layer 5 inhibitory cells. Phase 0 of the second sinusoid begins at 0.1 seconds. The bottom up input is delivered at 0.3 and 0.5 seconds plus the phase shift of each plot.*

Figure 3.35 shows the mean instantaneous spike count of each population with a 5 Hz oscillatory input with a bottom up input at various input times across wavelength in a disconnected network.

The sinusoidal oscillatory input is represented in the firing rate largely in the first half wavelength. The second half wavelength has a relatively flat response. In the first half the sinusoidal shape is slightly skewed to the left. When the bottom up input is presented in the first half there is a slight additive peak in the firing rate.

Figure 3.36 shows the mean instantaneous spike count of each population with a 5 Hz oscillatory input with a bottom up input at various input times across wavelength in a connected network.

The sinusoidal oscillatory input is represented in the firing rate largely in the first half wavelength. The second half wavelength has a relatively flat response. in all layers the first half is characterized by a rise in firing rate with a steeper gradient than the sinusoid. After this there is and oscillatory period in the layer 3 cells and the layer 5 excitatory cells. In the layer 4 cells and the layer 5 inhibitory cells there is an initial peak superimposed on the left skewed sinusoidal shape. With the addition of the bottom up input this pattern is changed depending upon the phase of oscillation at which it is applied. During the second half wavelength there is a small increase in the firing rate, but that portion remains flat. In the first half wavelength the input either facilitates or reduces the oscillation in the oscillatory populations depending in what point it is applied. In the peaked populations it either facilitates the peak, reduces it or introduces a second peak depending upon the time that it is applied. The first and second bottom up inputs have a slightly effect, in particular at 0.2 pi the secondary peak in the second input is far more pronounced.

Overall there is a difference between the connected and disconnected networks, with network contributions to the firing rate structure, particularly in the projection neurons and the layer 3 excitatory cells.

3.3.3.3 The relative mean power

In this analysis I present the significant time frequency mean power difference between the 0 Hz and the 100 Hz bottom up input across different phase input values for stimulus presentation. This is in order to establish whether different frequencies respond differently and input and whether this varies according to the phase of the injected oscillation current at which it is presented.

Figure 3.37 shows the relative difference in power in the time frequency response according to the phase of the input in a connected network with an oscillatory input of 5 Hz.

In each figure a relatively stereotypical response is shown in each stimulus delivery, with slight changes in the second stimulus delivery.

When the stimulus is delivered at 0.1 π there are 5 clear frequency bands with separable significant changes in power. Around 5 Hz there is an increase in power covering the whole stimulus period. In the 8 - 12 Hz band there is a decrease in power associated with each stimulus. In the 20 Hz range there is an increase in power for each stimulus and an increase in the post stimulus

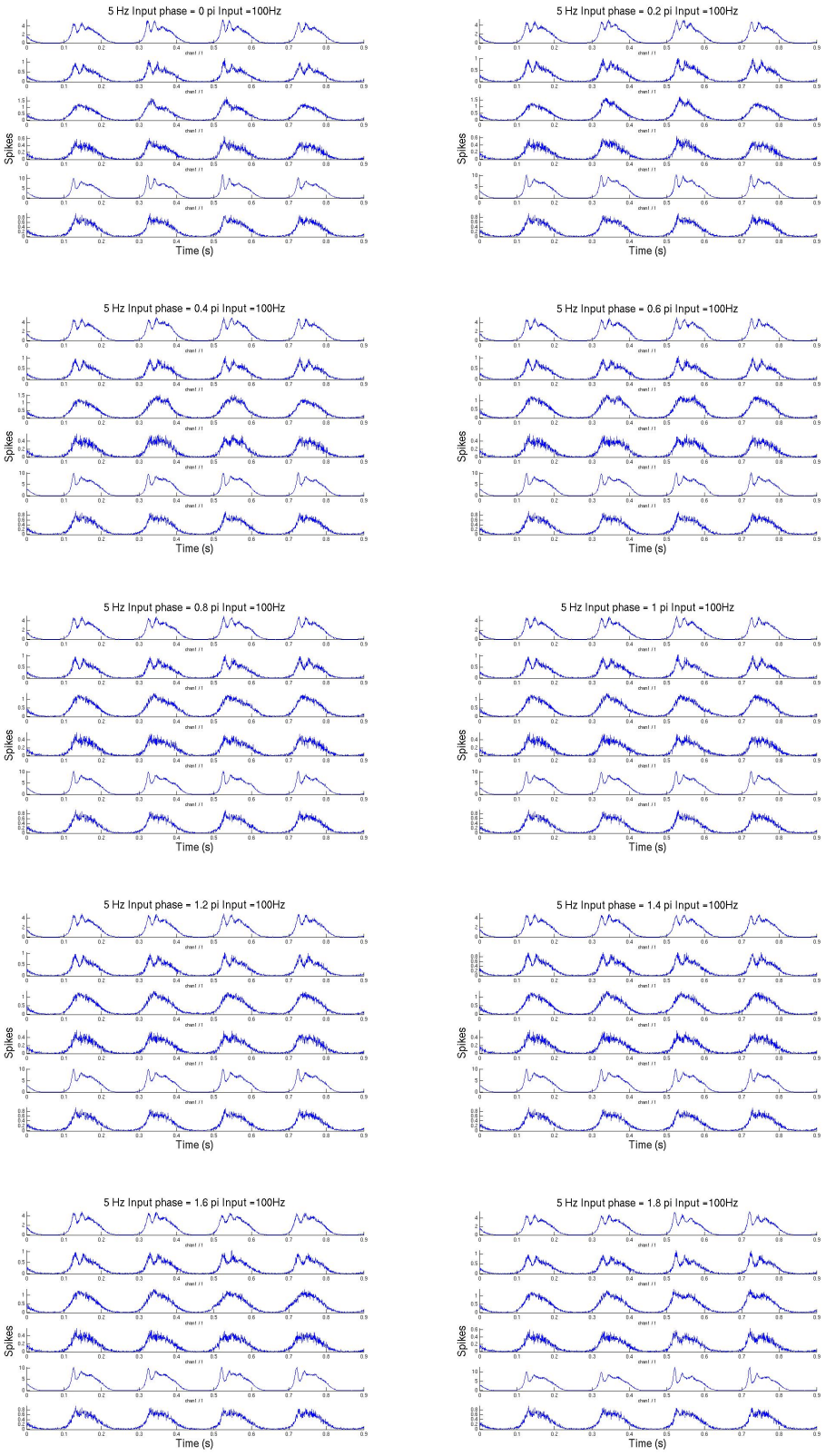

Figure 3.36: **The mean instantaneous spike count of each population with a 5 Hz oscillatory input with a bottom up input at various input times across wavelength in a connected network***Reading left to right top to bottom the plots have the bottom up input at 0, 0.2, 0.4, 0.6, 0.8, 1, 1.2, 1.4, 1.6, 1.8 pi units. Each plot from top to bottom shows the layer 3 excitatory cells, layer 3 inhibitory cells, layer 4 excitatory cells, layer 4 inhibitory cells, layer 5 excitatory cells and layer 5 inhibitory cells. Phase 0 of the second sinusoid begins at 0.1 seconds. The bottom up input is delivered at 0.3 and 0.5 seconds plus the phase shift of each plot.*

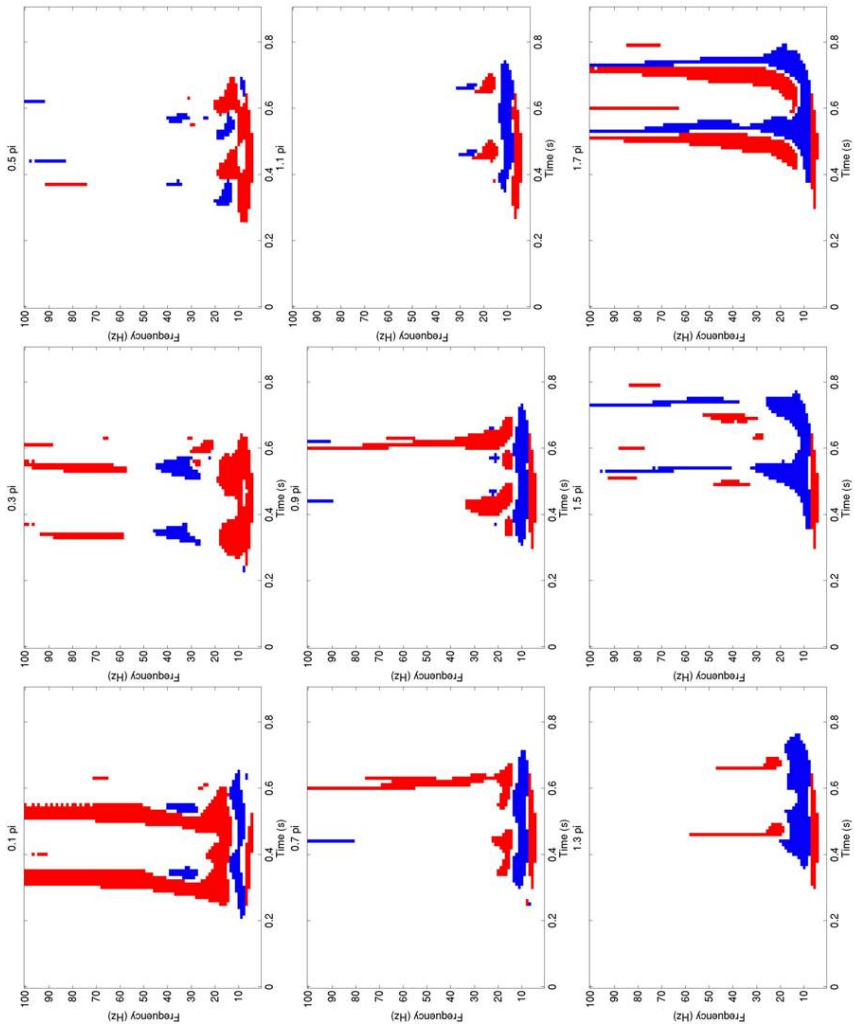

Figure 3.37: **The relative difference in power in the time frequency response between no bottom up input and 100 Hz bottom up input response according to the phase of the input in a connected network. Oscillatory input of 5 Hz** *in all plots red means an increase in power in the 100 Hz input case and blue means a decrease in power. Two inputs are delivered at 0.3 and 0.5 seconds with an offset of, from left to right top to bottom, 0.1, 0.3, 0.5, 0.7, 0.9, 1.1, 1.3, 1.5, 1.7 pi units.*

condition. In the 30 Hz range there is an increase in power during stimulus delivery followed by a post stimulus decrease in power. In the >40 Hz range there is a stimulus linked increase in power.

When the stimulus is delivered at 0.3 π there is a stimulus linked increase in power in the 5 - 20 Hz range. In the 25 - 45 Hz range there is a stimulus linked decrease in power, with a post stimulus increase in power in the 20 -30 Hz range after the second stimulus. In the >50 Hz range there is a stimulus linked increase in power.

When the stimulus is delivered at 0.5 π there is a stimulus linked increase in power in the <10 Hz range. In the 12 - 20 Hz range there is a stimulus linked decrease in power followed by a post stimulus increase in power. In the 40 Hz range there is a stimulus offset decrease in power. In the >70 Hz range there is a stimulus offset increase in power followed by a post stimulus decrease in power on the first stimulus.

When the stimulus is delivered at 0.7 π there is at around 5 Hz an increase in power covering the whole stimulus period. In the 8 - 12 Hz band there is a decrease in power associated with each stimulus, post stimulus this decrease reduces in frequency. In the 20 Hz range there is an increase in power for each stimulus and an increase in the post stimulus condition. In the >80 Hz range there is a stimulus offset decrease in power in the first stimulus. In the second stimulus there is a post stimulus increase in power in the 20 - 50 Hz range and a stimulus linked increase in power in the >50 Hz range.

When the stimulus is delivered at 0.9 π there is a similar response as to when it is delivered at 0.7 π with the exception that there is a a 20 - 30 Hz increase in power during the stimulus and there is a reduction in power at 20 Hz at stimulus onset and offset.

When the stimulus is delivered at 1.1 π there is no >30 Hz component with the lower frequency components having a similar feature make up to the previous two plots. There is an additional stimulus linked decrease in power at 30 Hz.

When the stimulus is delivered at 1.3 π at <8 Hz there is an increase in power. Between 8 and 20 Hz there is a stimulus linked decrease in power. From 20 - 55 Hz there is a stimulus linked increase in power.

When the stimulus is delivered at 1.5 π there is a <8 Hz increase in power. From 10 - 30 Hz there is a stimulus linked decrease in power. There is a stimulus onset increase in power at 30 - 40 Hz, a decrease in power at the >40 Hz range and a post stimulus increase in power around 80 Hz.

When the stimulus is delivered at 1.7 π there is an increase in power at the <8 Hz range. from 8 - 12 Hz there is a decrease in power at stimulus onset there is an increase in power from >12 Hz followed by a stimulus offset decrease in power.

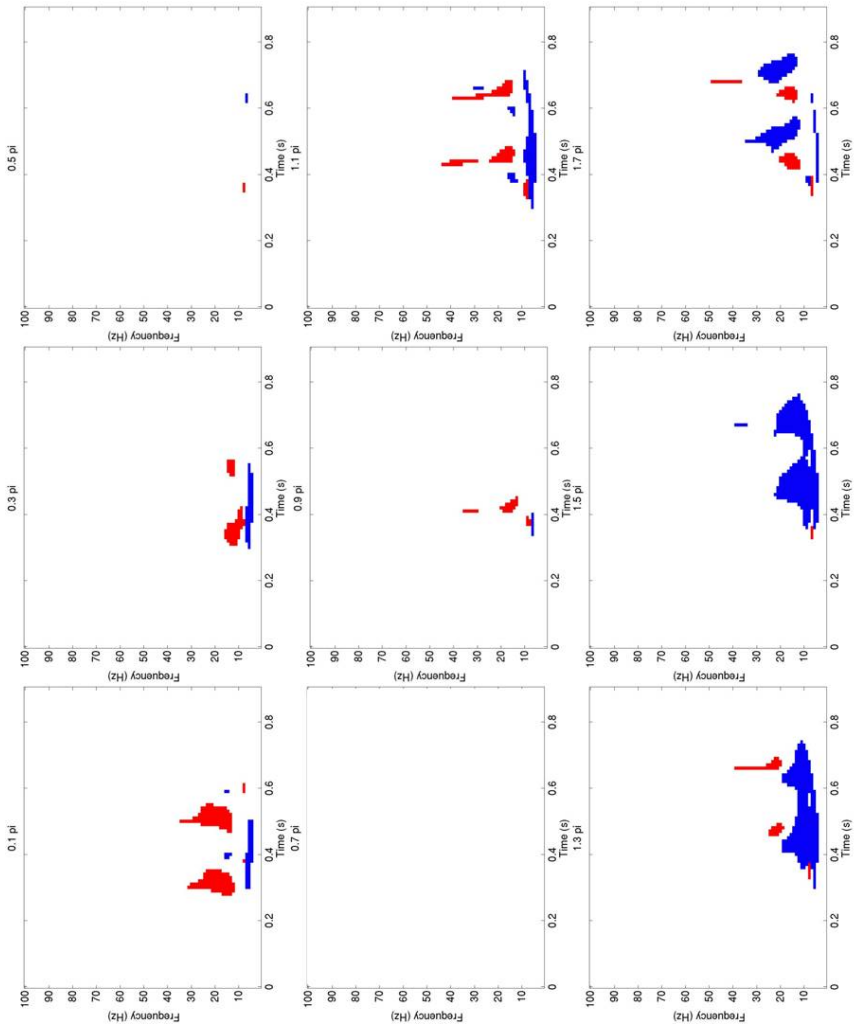

Figure 3.38: **The relative difference in power in the time frequency response between no bottom up input and 100 Hz bottom up input response according to the phase of the input in a disconnected network. Oscillatory input of 5 Hz** *in all plots red means an increase in power in the 100 Hz input case and blue means a decrease in power. Two inputs are delivered at 0.3 and 0.5 seconds with an offset of, from left to right top to bottom, 0.1, 0.3, 0.5, 0.7, 0.9, 1.1, 1.3, 1.5, 1.7 pi units.*

Figure 3.38 shows the relative difference in power in the time frequency response according to the phase of the input in a disconnected network with an oscillatory input of 5 Hz.

In comparison with the connected network, some of the stimulus linked components are present in a simplified way, however none of the >40 Hz components are present. The low frequency increases in power are absent and from 0.5 π to 0.9 π there is virtually no significant difference associated with the stimulus.

Figure 3.39 shows the relative difference in power in the time frequency response according to the phase of the input in a connected network with an oscillatory input of 10 Hz.

Under the 10 Hz oscillatory input condition there is a clear separation of the significant power changes into frequency bands. The <8 Hz band shows an increase in power across the simulation time with the exception of around 1.3 π where is not continuous.

The 8 Hz band shows a significant decrease in power at stimulus onset followed by an increase in power during offset and post stimulus. The decrease in power is dominant from 0.1 π to 0.5 π and between 1.5 π and 1.7 π, with the increase in power being dominant between 0.7 π and 1.3 π.

The 10 - 15 Hz band shows a stimulus related increase in power followed by a decrease in power at 0.1 π and 1.1 π to 1.7 π, with only an increase in power shown when the stimulus is applied between 0.3 π and 0.9 π.

The 15 - 20 Hz band shows a decrease in power followed by an increase in power at 0.1 π and between 1.1 π to 1.7 π. Is shows an increase in power followed by a decrease in power between 0.3 π and 0.5 π. It shows only a decrease in power between 0.7 π and 0.9 π.

The 25 - 40 Hz band shows an increase in power followed by a decrease in power and a post stimulus decrease in power at 0.1 π and from 1.1 π to 1.7 π. From 0.3 π to 0.5 π only the decrease in power is present. At 0.7 π there is a decrease followed by a broader band increase in power and at 0.9 π there is only an increase in power at stimulus onset.

In the >40 Hz band there is a significant increase in power at 0.1 to 0.3 π. This is smaller in breadth at 0.5 π. at 0.7 to 0.9 π it is only present in the first of the two stimulus. From 1.1 π to 1.7 π this increase recovers with a mid stimulus decrease in power.

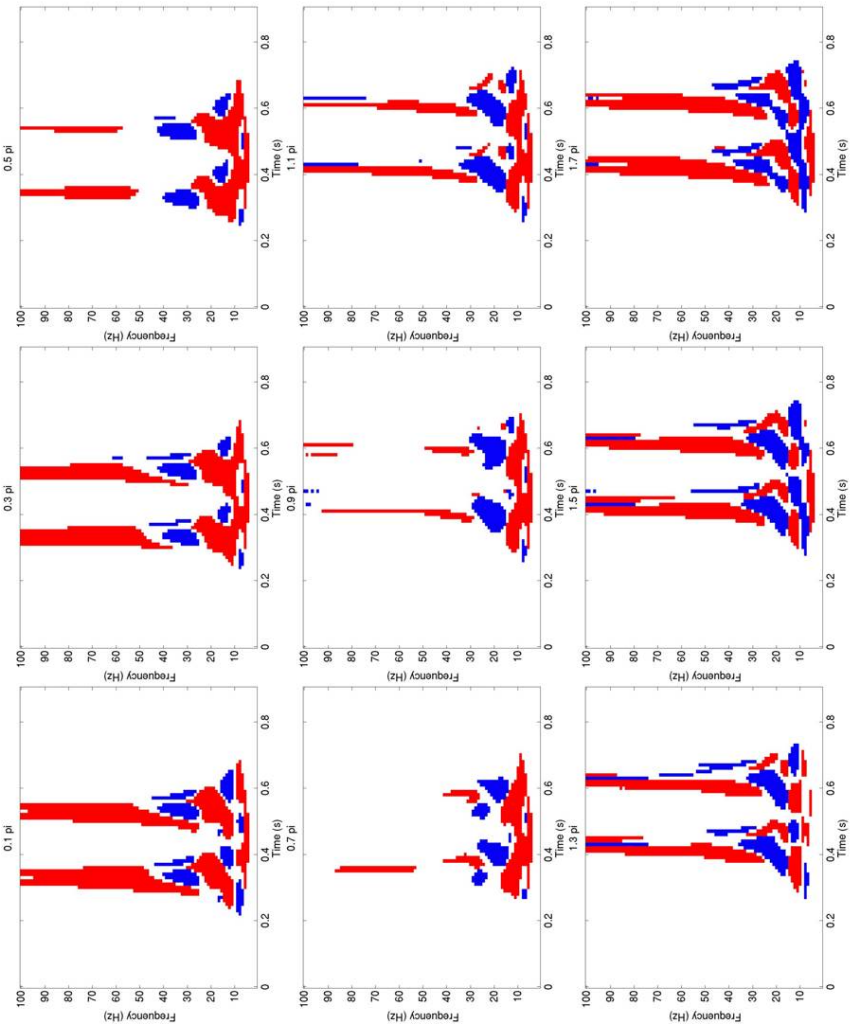

Figure 3.39: **The relative difference in power in the time frequency response between no bottom up input and 100 Hz bottom up input response according to the phase of the input in a connected network. Oscillatory input of 10 Hz** *in all plots red means an increase in power in the 100 Hz input case and blue means a decrease in power. Two inputs are delivered at 0.3 and 0.5 seconds with an offset of, from left to right top to bottom, 0.1, 0.3, 0.5, 0.7, 0.9, 1.1, 1.3, 1.5, 1.7 pi units.*

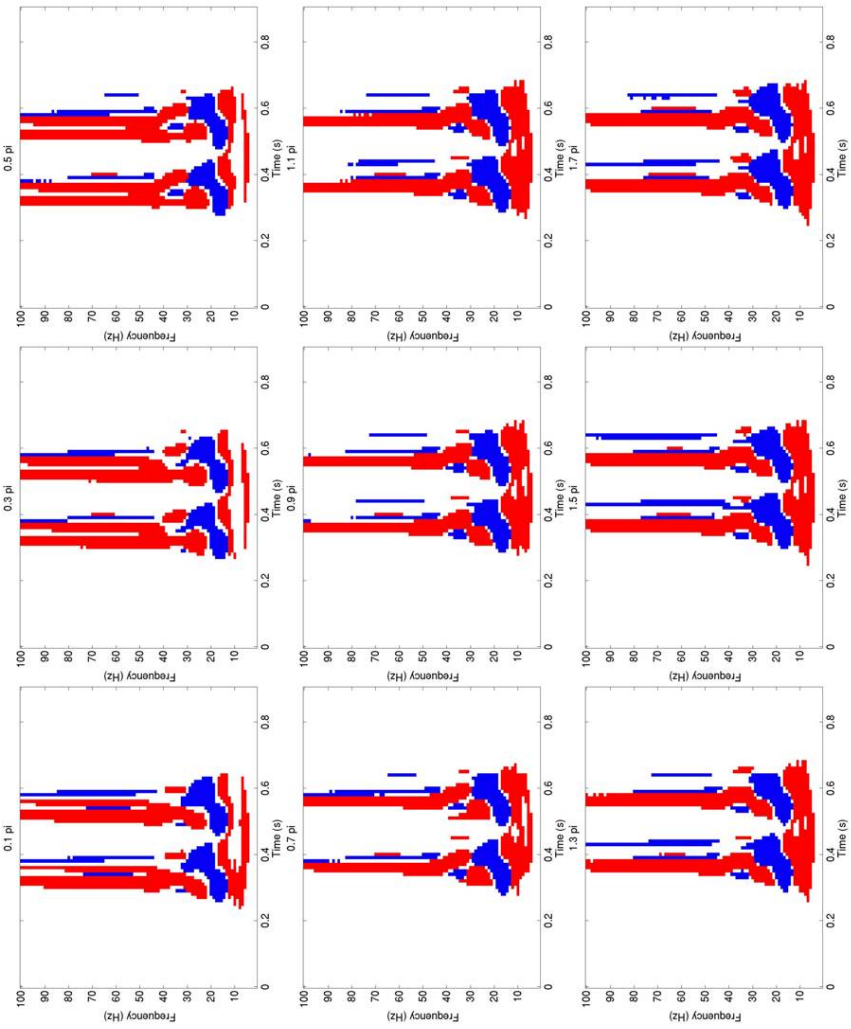

Figure 3.40: **The relative difference in power in the time frequency response between no bottom up input and 100 Hz bottom up input response according to the phase of the input in a connected network. Oscillatory input of 20 Hz** *in all plots red means an increase in power in the 100 Hz input case and blue means a decrease in power. Two inputs are delivered at 0.3 and 0.5 seconds with an offset of, from left to right top to bottom, 0.1, 0.3, 0.5, 0.7, 0.9, 1.1, 1.3, 1.5, 1.7 pi units.*

Figure 3.40 shows the relative difference in power in the time frequency response according to the phase of the input in a connected network with an oscillatory input of 20 Hz.

Under this oscillatory input condition the response is stereotypical across all input phase conditions, with the exception of 10 Hz and 30 Hz. The general condition is that <8Hz there is an increase in power. at 12 Hz there is an increase in power. At 15 - 20 Hz there is a decrease in power followed by an increase in power. at 20 - 30 Hz there is an increase in power followed by a decrease in power. At >40 Hz there is an increase in power followed by a decrease in power, this is variable in structure. In the 10 Hz range there is an increase in power with the exception that between 0.1 π and 0.5 π there is no significant change in power. In the 30 Hz range there is a decrease in power followed by an increase, followed by a decrease in power followed by an increase at 0.1 π and 1.3 to 1.7 π. At 0.3 π to 0.5 π there is an increase, followed by a decrease in power followed by an increase in power. At 0.7 π to 1.1 π there is a decrease in power followed by an increase in power followed by a post stimulus increase in power.

Figure 3.41 shows the relative difference in power in the time frequency response according to the phase of the input in a connected network with an oscillatory input of 40 Hz.

In this oscillatory input condition below 15 Hz shows a stereotypical increase in power around the stimulus across all input phases. In the 15 - 25 Hz range there is a general absence of significant power changes with the exception of 0.3 π to 0.7 π where the second bottom up stimulus shows a stimulus related increase in power followed by on or two post stimulus decreases in power. At 30 Hz from 0.7 π to 1.7 π there is a stimulus related increase in power preceded and then flanked by a short decrease in power in the second bottom up stimulus. above 40 Hz there is a stimulus related increase in powere followed by a post stimulus decrease in power, with the exception of 0.7 π. From 1.3 π to 1.7 π this is followed by another increase in power.

Overall the network clearly splits into frequency bands that are largely stable over the whole stimulus presentation. In each case there is a clear power response dependence upon when the input is presented relative to the oscillatory input. In the lower frequencies of oscillation there is greater variability in the network response with whole frequency ranges being absent particularly around the 1 π period. In the next sections I will present an information analysis of the four metrics used in the static mean section.

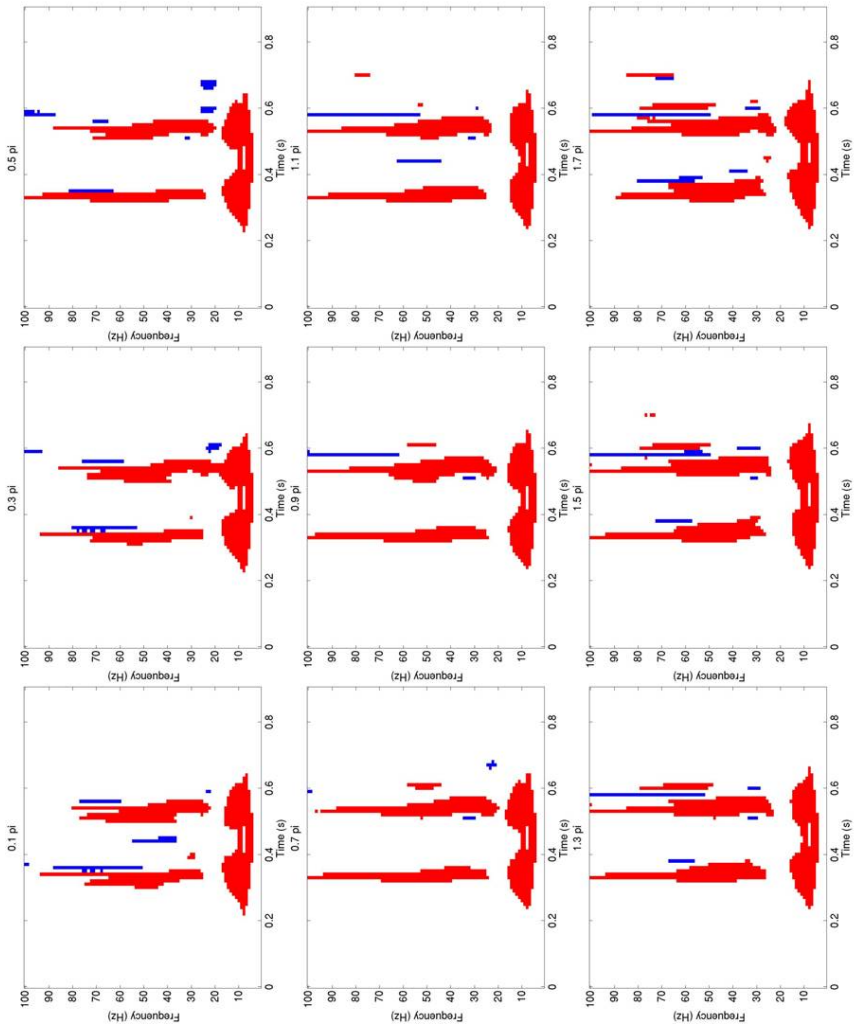

Figure 3.41: **The relative difference in power in the time frequency response between no bottom up input and 100 Hz bottom up input response according to the phase of the input in a connected network. Oscillatory input of 40 Hz** *in all plots red means an increase in power in the 100 Hz input case and blue means a decrease in power. Two inputs are delivered at 0.3 and 0.5 seconds with an offset of, from left to right top to bottom, 0.1, 0.3, 0.5, 0.7, 0.9, 1.1, 1.3, 1.5, 1.7 pi units.*

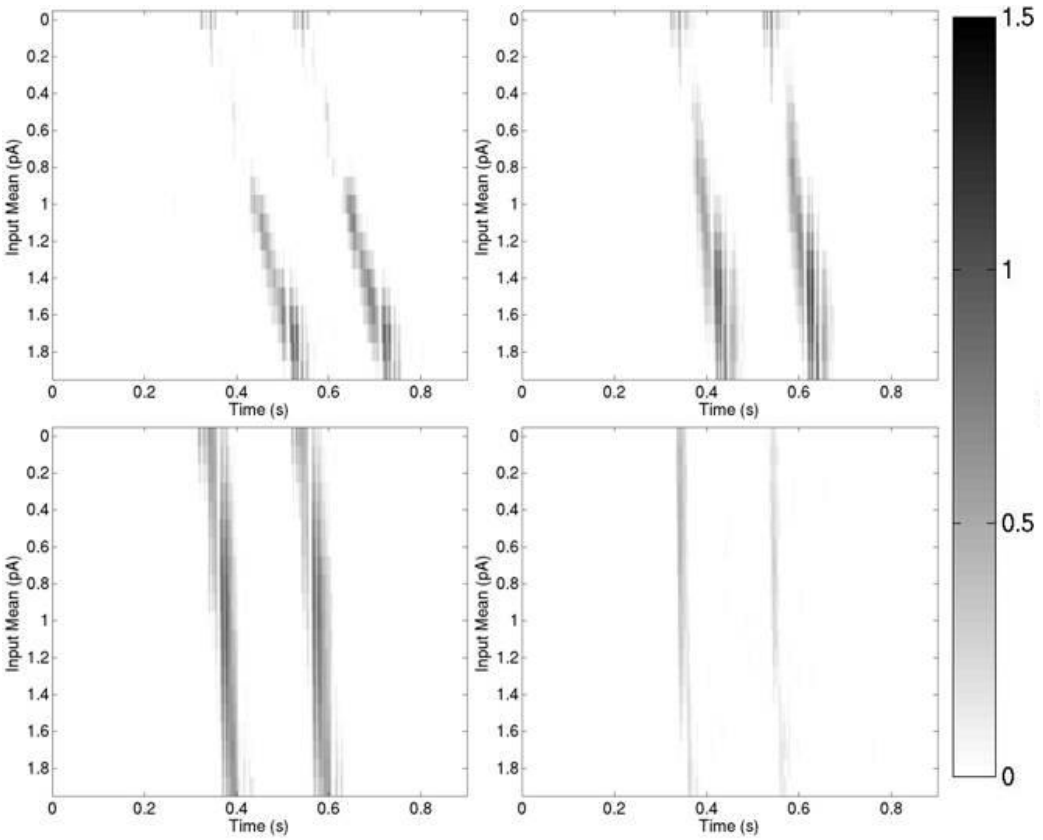

Figure 3.42: **Mutual information between the field potential value and input frequency for all oscillatory frequencies in a connected network** *The top left shows the 5 Hz oscillatory input, the top right shows the 10 Hz input, the bottom left 20 Hz and the bottom right 40 Hz. The information is given in bits.*

3.3.3.4 Mutual information in the raw field potential signal

In this section I present the mutual information between the bottom up input with a range of 0 to 100 Hz firing rate conditions in the poisson spike generators and the raw simulated field potential signal according to the presentation phase of the stimulus. This is in order to establish whether or not there is an optimal phase condition in which the raw signal best represents the input.

Figure 3.42 shows the mutual information between the field potential value and bottom up input frequency for all oscillatory frequencies in the connected network and figure 3.43 shows the disconnected network.

When the oscillatory input frequency is 5 Hz the stimulus duration of the

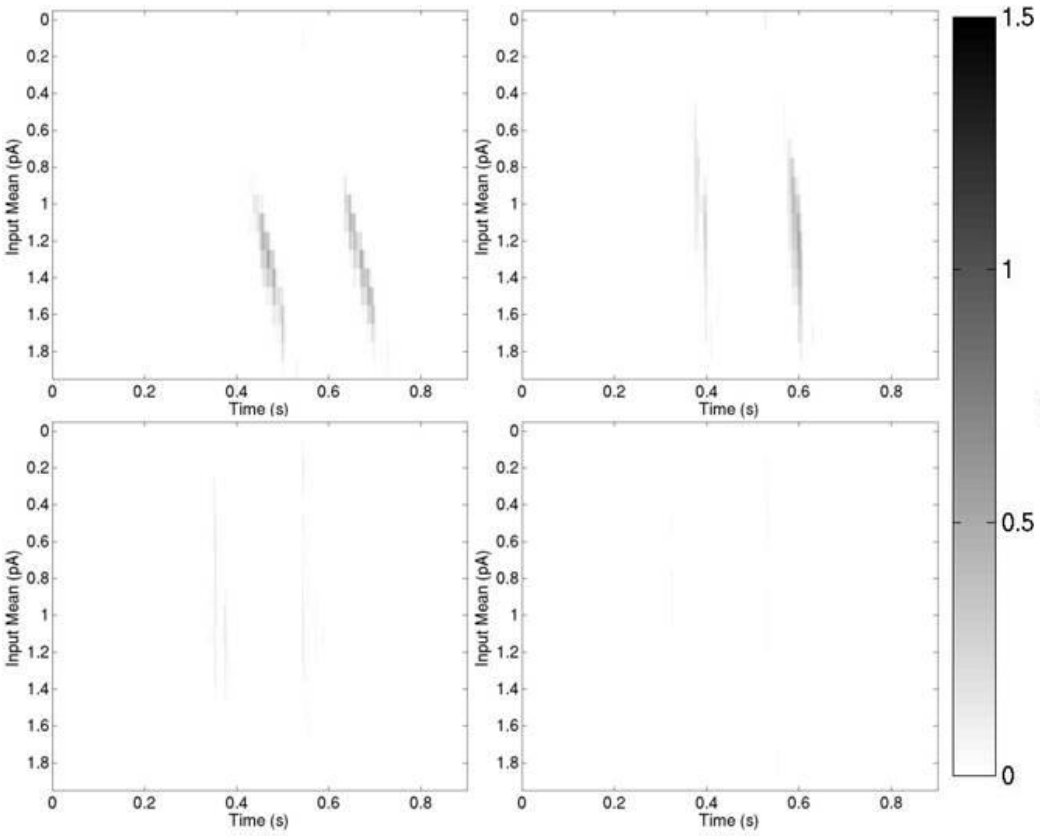

Figure 3.43: **Mutual information between the field potential value and input frequency for all oscillatory frequencies in a disconnected network** *The top left shows the 5 Hz oscillatory input, the top right shows the 10 Hz input, the bottom left 20 Hz and the bottom right 40 Hz. The information is given in bits.*

input is significantly shorter than the oscillatory input wavelength (1/6th). In the disconnected network there is only information about the stimulus in the region where the oscillatory input is at a minimum. In the connected network the information is at a maximum when the stimulus is presented in the earliest quarter of the oscillatory input and the second half of the input. If the input is presented in the final quarter of the wavelength There is information in the subsequent sinusoid. In the first quarter of the subsequent sinusoid there is a short period of no information followed by a maximum of information.

When the oscillatory input frequency is 10 Hz the stimulus input duration is 1/3rd of the oscillatory input wavelength. In the disconnected network there is only information about the stimulus during the lowest values of the oscillatory input. There is a slight representation in the first quarter of the subsequent sinusoid when the input is presented in the last quarter of the first sinusoid. The connected network shows the same pattern of reduced information in the second quarter of the oscillatory input, however due to the stimulus extending beyond this quarter there is a slight representation of the stimulus in the second half of the sinusoid. There is an additional representation in the subsequent oscillatory input sinusoid with zero information at the start of the first quarter and reduced information during the second quarter increasing in the second half of the subsequent sinusoid.

When the oscillatory input frequency is 20 Hz the stimulus input duration is 2/3rds of the oscillatory input wavelength. In the disconnected network the stimulus is represented in the second half of the oscillatory wavelength with some representation in the second sinusoid when the stimulus is presented later. In the connected network the only reduction in information is at the initial portion of the representation in the second sinusoid. There is a step in the latency of the representation of the input when it is presented in the second quarter of the oscillatory input from 0.4 to 1 pi. This shows that the initial portion of the input is not represented in the same way as when the oscillatory input is 5 or 10 Hz.

When the oscillatory input frequency is 40 Hz the stimulus input is 1 and 1/3rd of the oscillatory input wavelength. In the disconnected network the information is marginally present. In the connected network the input is represented in the second and when it's presented later, third post stimulus sinusoids. From 1.2 to 2 pi you can see reduced information in the second quarter of the second stimulus wavelength.

Over all it is clear that the phase of presentation has in impact on the information regarding the input we are able to extract from the simulated field potential, some phases providing no information at all. There are indications that, particularly in the lower frequencies that the network activity

is sustaining information regarding the input, especially around 1.8 π.

3.3.3.5 Mutual Information in firing rate

In this section I present the mutual information between the bottom up input and the firing rate of the mean cell types in the network model. This is in order to establish whether or not each cell type plays a different role in information processing.

Figure 3.45 shows the mutual information between the spike count in each population and bottom up input frequency according to the phase of the input in a connected network with an oscillatory input of 5 Hz. Figure 3.44 shows the disconnected network. In the disconnected network only the layer 4 cells, the main input of the bottom up stimulus, show a mutual information value, with the majority being shown in the excitatory cells. This is present shortly after the stimulus is delivered with a slightly higher value between 1.6 π and 1.8 π.

In the connected network the information structure in the layer 4 cells is similar to that in the disconnected network with a slightly higher information value between 1.4 π and 1.9 π. In the projection neurons, the excitatory cells in layer 3 and 5, there is a strong pattern in the mutual information values. From 0 to 1 π there is stimulus linked mutual information with a stable time lag giving a clear diagonal line. from 1 to 1.5 π there is no mutual information between the stimulus input and the firing rate. From 1.5 to 1.9 π there is the highest mutual information values, with a broader duration than at lower phase offsets. There is also a variable response latency with higher phase offsets having a quicker response latency, this is shown by the near vertical structure of the information content in this range. There is also a small mutual information representation in the inhibitory cells at this phase offset period.

Figure 3.46 shows the mutual information between the spike count in each population and bottom up input frequency according to the phase of the input in a connected network with an oscillatory input of 10 Hz.

In the layer 4 populations there is an increase in mutual information between the firing rate with a relatively fixed latency in the excitatory cells. Between 1.1 π and 1.9 π there is a higher mutual information value.

In the layer 3 and layer 5 excitatory cells there is vertical arrangement of the mutual information suggesting that the maximum information is locked to a fixed phase of the ongoing oscillation. The information is maximal between 1 π and 1.9 π with a lower value between 0 π and 1.5 π. In the layer 5 excitatory cells there is a gap in the maximal information where the mutual information is not significant. In the layer 3 inhibitory cells there is

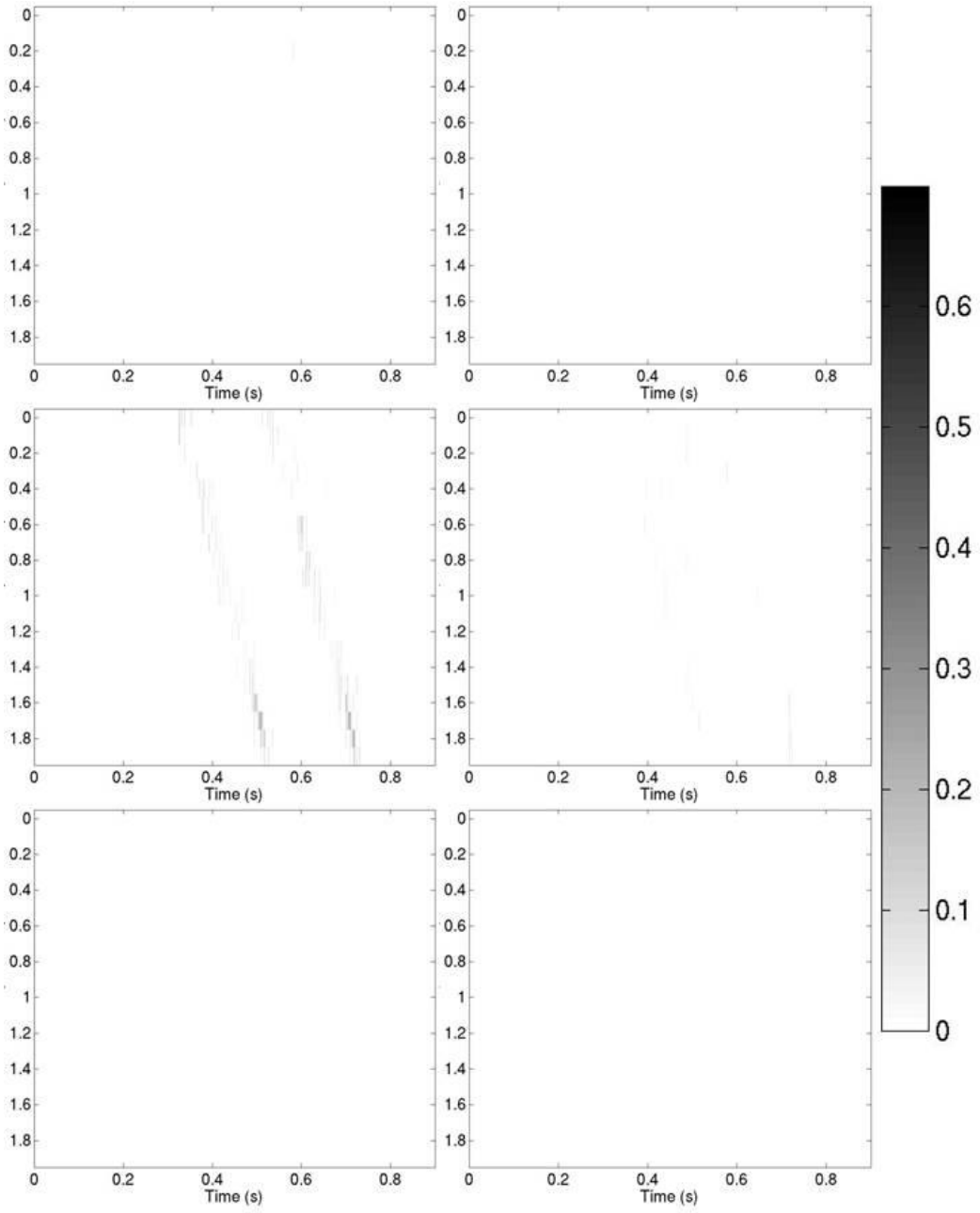

Figure 3.44: **The mutual information between the spike count in each population and bottom up input frequency in a disconnected network with an oscillatory input of 5 Hz** *Each bottom up stimulus is delivered at 0.3 and 0.5 seconds shifted by 0 - 1.9 π. The left hand axis in each figure shows the phase shift of the stimulus. The left hand plots are the excitatory populations and the right hand plots are the inhibitory populations. The top plots are the layer 3 cells, the middle plots are the layer 4 cells and the bottom plots are the layer 5 cells. Information is given in bits.*

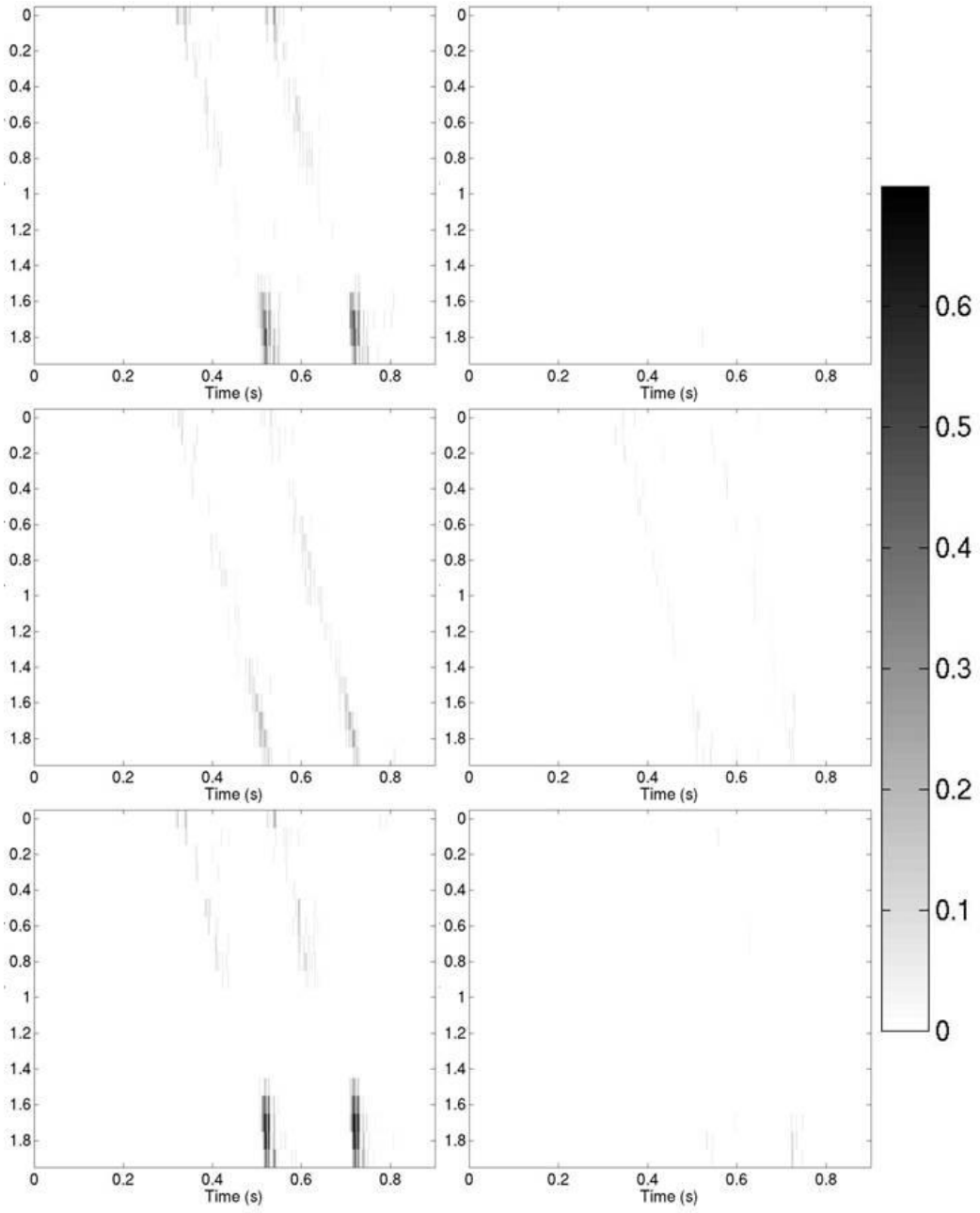

Figure 3.45: **The mutual information between the spike count in each population and bottom up input frequency in a connected network with an oscillatory input of 5 Hz** *Each bottom up stimulus is delivered at 0.3 and 0.5 seconds shifted by 0 - 1.9 π. The left hand axis in each figure shows the phase shift of the stimulus. The left hand plots are the excitatory populations and the right hand plots are the inhibitory populations. The top plots are the layer 3 cells, the middle plots are the layer 4 cells and the bottom plots are the layer 5 cells. Information is given in bits.*

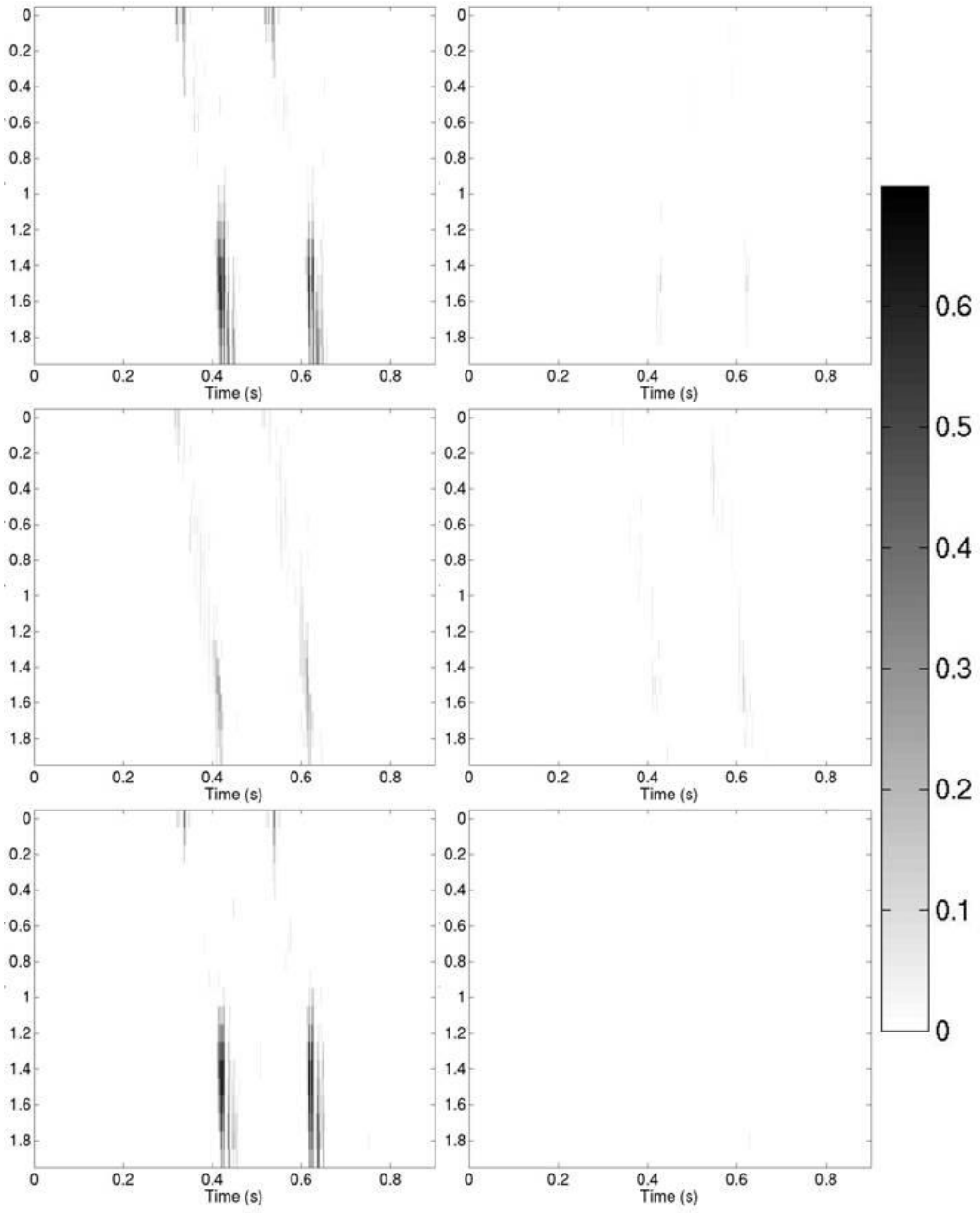

Figure 3.46: **The mutual information between the spike count in each population and bottom up input frequency in a connected network with an oscillatory input of 10 Hz** *Each bottom up stimulus is delivered at 0.3 and 0.5 seconds shifted by 0 - 1.9 π. The left hand axis in each figure shows the phase shift of the stimulus. The left hand plots are the excitatory populations and the right hand plots are the inhibitory populations. The top plots are the layer 3 cells, the middle plots are the layer 4 cells and the bottom plots are the layer 5 cells. Information is given in bits.*

a small mutual information value between 1.4 π and 1.6 π.

Figure 3.47 shows the mutual information between the spike count in each population and bottom up input frequency according to the phase of the input in a connected network with an oscillatory input of 20 Hz. In the layer 4 excitatory cells ther are two vertical arrangements of the mutual information. Between 0 and 0.4 π it comes earlier than between 0.5 π and 1.9 π. There is a band of increased information value between 0.7 and 1.4 π, this region features in the layer 4 inhibitory cells. In the layer 3 and 5 excitatory cells there are three vertical bands in which the mutual information is present. between 0 and 0.2 π the information is in the first two bands. Between 0.2 π and 1.6 π the information is only in the middle band. This region contains the highest mutual information values. Between 1.6 π and 1.9 π the information is in the middle and the third band. The layer 4 inhibitory cells show mutual information content between 0.6 and 1.3 π arranged vertically.

Figure 3.48 shows the mutual information between the spike count in each population and bottom up input frequency according to the phase of the input in a connected network with an oscillatory input of 40 Hz. This shows a very similar arrangement of the information to the 20 Hz condition With the exception that the information content is maximal towards the 0 to 0.7 π stimulus offset phase.

Overall there is a clear picture that the presentation phase has a strong impact on the mutual information values in the projection neurons. In particular where the stimulus duration is much less than the duration of one cycle of oscillatory input. There appears to be a point in the oscillation where if the stimulus is delivered near it the information is packaged and locked to the phase of the oscillation regardless of when it was delivered. The phase of 1.8 π appears to give the maximal information at 5 Hz and around 1.6 π at 10 Hz.

3.3.3.6 Mutual Information in time frequency power

In this analysis I present the mutual information between the bottom up stimulus and the time frequency power according to probe phase. This is in order to establish whether on not the phase dependence shown in the raw signal and in the firing rates is contained in the power of particular frequency bands.

Figure 3.49 shows the mutual information between power in the time frequency power response and bottom up input frequency according to the phase of the input in a disconnected network with an oscillatory input of 5 Hz. With the exception of the 1 π to 1.4 π input range there is no significant mutual information between the stimulus and the power of the simulated field

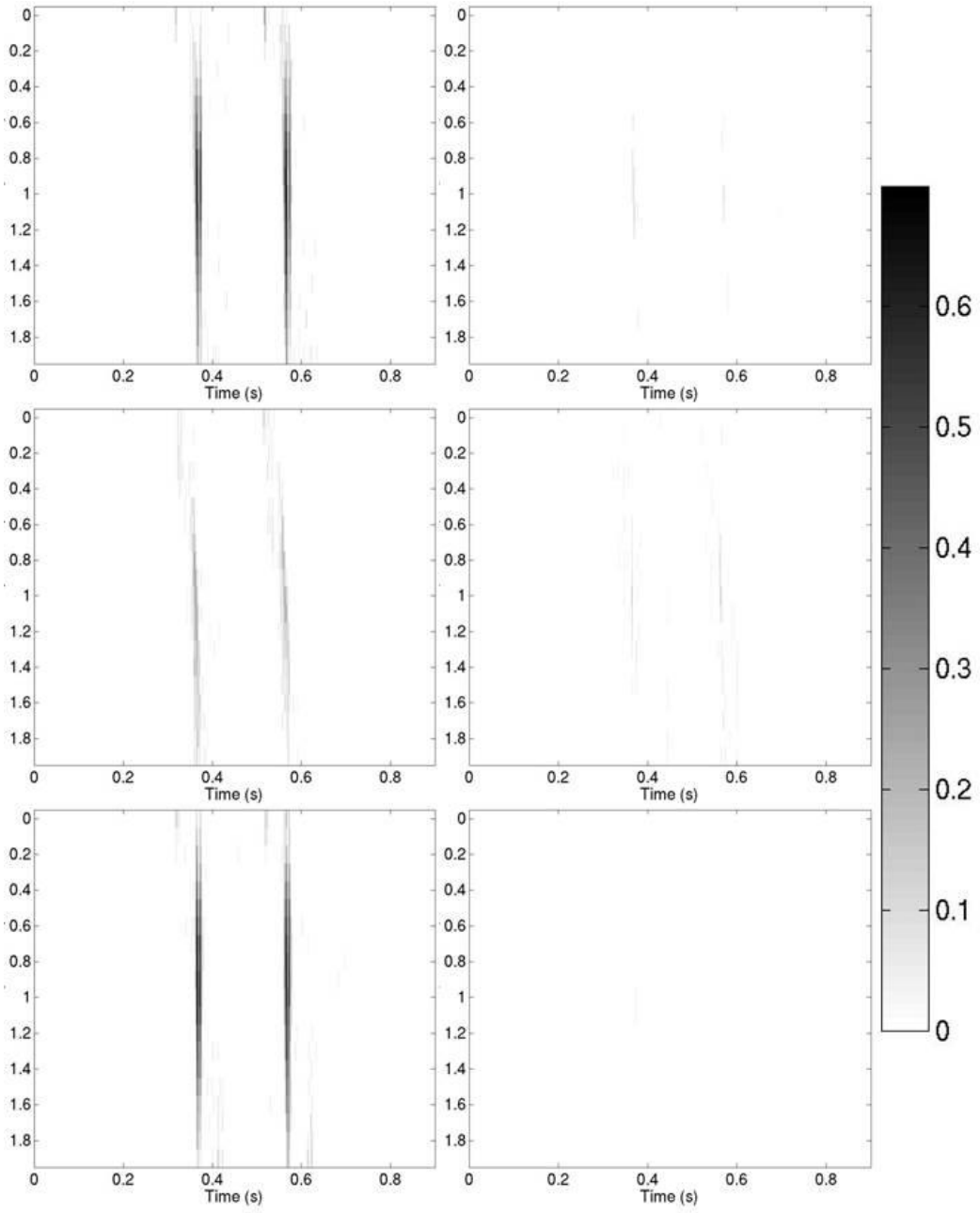

Figure 3.47: **The mutual information between the spike count in each population and bottom up input frequency in a connected network with an oscillatory input of 20 Hz** *Each bottom up stimulus is delivered at 0.3 and 0.5 seconds shifted by 0 - 1.9* π*. The left hand axis in each figure shows the phase shift of the stimulus. The left hand plots are the excitatory populations and the right hand plots are the inhibitory populations. The top plots are the layer 3 cells, the middle plots are the layer 4 cells and the bottom plots are the layer 5 cells. Information is given in bits.*

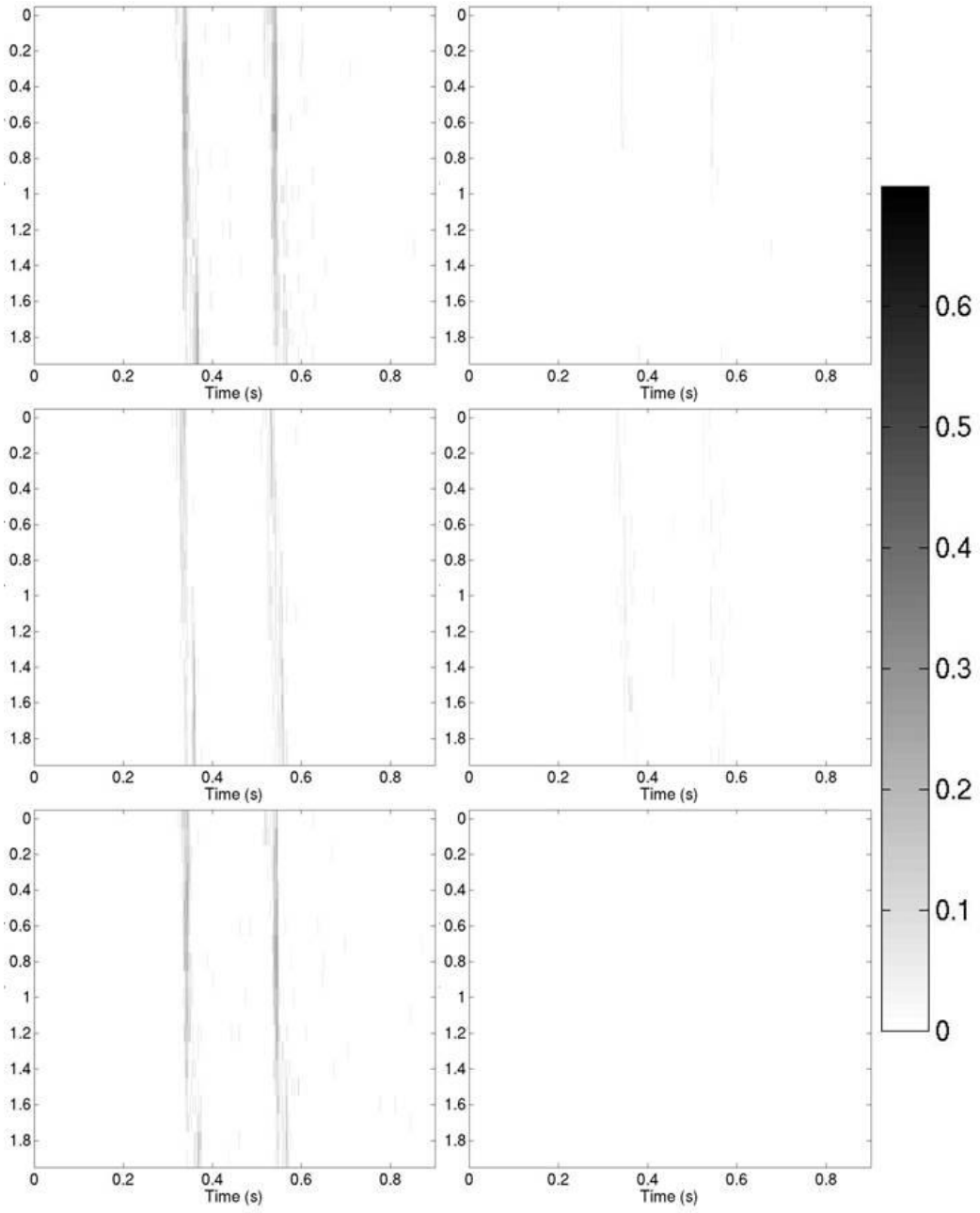

Figure 3.48: **The mutual information between the spike count in each population and bottom up input frequency in a connected network with an oscillatory input of 40 Hz** *Each bottom up stimulus is delivered at 0.3 and 0.5 seconds shifted by 0 - 1.9 π. The left hand axis in each figure shows the phase shift of the stimulus. The left hand plots are the excitatory populations and the right hand plots are the inhibitory populations. The top plots are the layer 3 cells, the middle plots are the layer 4 cells and the bottom plots are the layer 5 cells. Information is given in bits.*

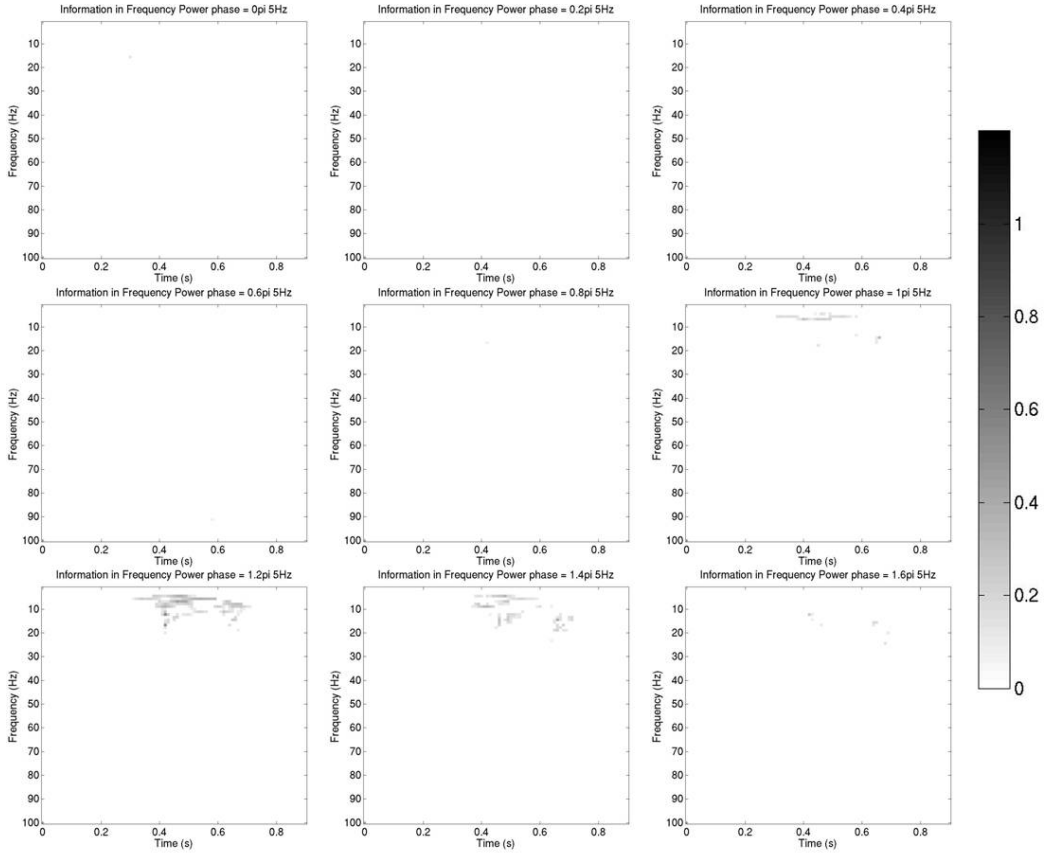

Figure 3.49: **The mutual information between power in the time frequency response and bottom up input frequency according to the phase of the input in a disconnected network with an oscillatory input of 5 Hz** *Two inputs are delivered at 0.3 and 0.5 seconds with an offset of, from left to right top to bottom, 0, 0.2, 0.4, 0.6, 0.8, 1, 1.2, 1.4, 1.6 pi units. Mutual information is in units of bits.*

potential. In teh excepted region of input there is a broad mutual information representation in the <8 Hz region. There is a stimulus linked feature in the 10 - 20 Hz range.

Figure 3.50 shows the mutual information between power in the time frequency response power and bottom up input frequency according to the phase of the input in a connected network with an oscillatory input of 5 Hz. There is a general stimulus linked mutual information value at the <8 Hz range with the exception of 0 to 0.2 π input phase. in the 10 Hz range there is occasional mutual information representation at the presentation of the first stimulus. in the 15 Hz range there is a stimulus linked mutual information value.in the 30 - 40 Hz range there is representation of the stimulus at 0 - 0.2 π and at 1.6 π. In the later case it marks both stimulus onset and offset. In the >40 Hz range stimulus representation is only present in the 0 π and the 1.6 π condition, however between 1.6 and 0 π there is also representation in this frequency range too.

Figure 3.51 shows the mutual information between power in the time frequency response and bottom up input frequency according to the phase of the input in a connected network with an oscillatory input of 10 Hz. In this group there is a somewhat stereotypical representation of the stimulus fixed to the rising phase of the ongoing stimulus. Features of this pattern are enhanced or lost depending upon what phase the input is delivered. Of particular not is the >40 Hz component which is absent from 0.4 to 1 π. This is also the case for the 30 Hz component. There is no mutual information in the 10 Hz range. The <8 Hz range is not present between 1 and 1.4 π, exclusive.

Figure 3.52 shows the mutual information between power in the time frequency response and bottom up input frequency according to the phase of the input in a connected network with an oscillatory input of 20 Hz. Again this condition produces a stereotypical input oscillation phase locked response. Between 0 and 0.4 π the information is minimal. At 0 π you can see the locked response of the high frequency component has a secondary representation on full cycle after the first stronger representation. At 0.2 π the secondary representation is stronger and at 0.4 π the second phase lock becomes the position the remainder of the plots are locked to. 0.8 to 1.2 π show the highest valuse for the mutual information in all bands.

Figure 3.53 shows the mutual information between power in the time frequency response and bottom up input frequency according to the phase of the input in a connected network with an oscillatory input of 40 Hz. This again shows a stereotypical response to both inputs with information representation in the <8 Hz, 8 -15 Hz band and the 30 -60 Hz band. In the 30 - 60 Hz band there is an increase in the range and value of the representa-

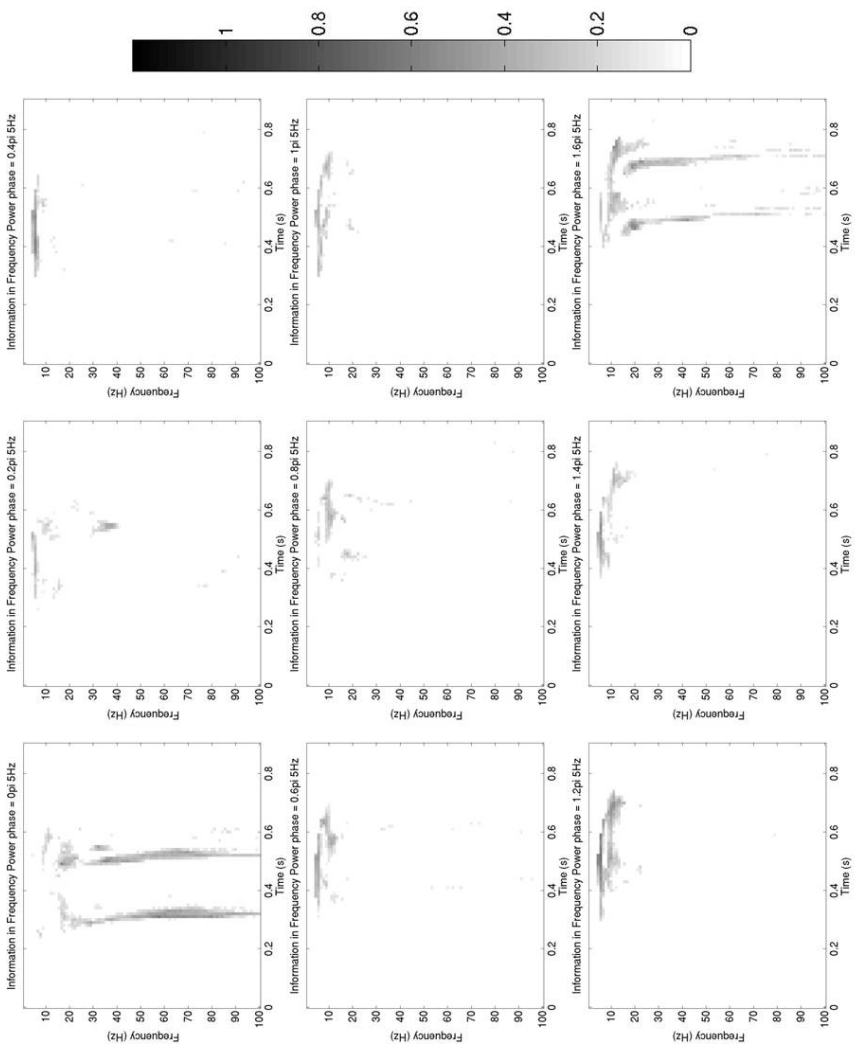

Figure 3.50: **The mutual information between power in the time frequency response and bottom up input frequency according to the phase of the input in a connected network with an oscillatory input of 5 Hz** *Two inputs are delivered at 0.3 and 0.5 seconds with an offset of, from left to right top to bottom, 0, 0.2, 0.4, 0.6, 0.8, 1, 1.2, 1.4, 1.6 pi units. Mutual information is in units of bits.*

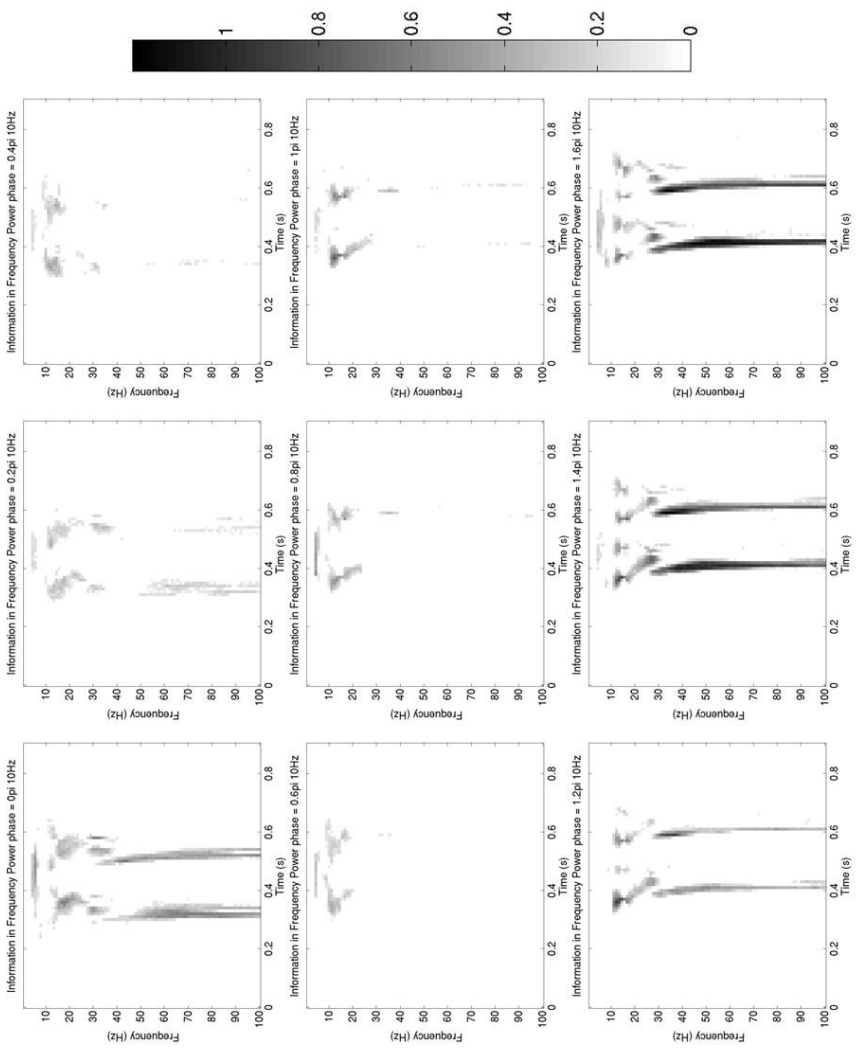

Figure 3.51: **The mutual information between power in the time frequency response and bottom up input frequency according to the phase of the input in a connected network with an oscillatory input of 10 Hz** *Two inputs are delivered at 0.3 and 0.5 seconds with an offset of, from left to right top to bottom, 0, 0.2, 0.4, 0.6, 0.8, 1, 1.2, 1.4, 1.6 pi units. Mutual information is in units of bits.*

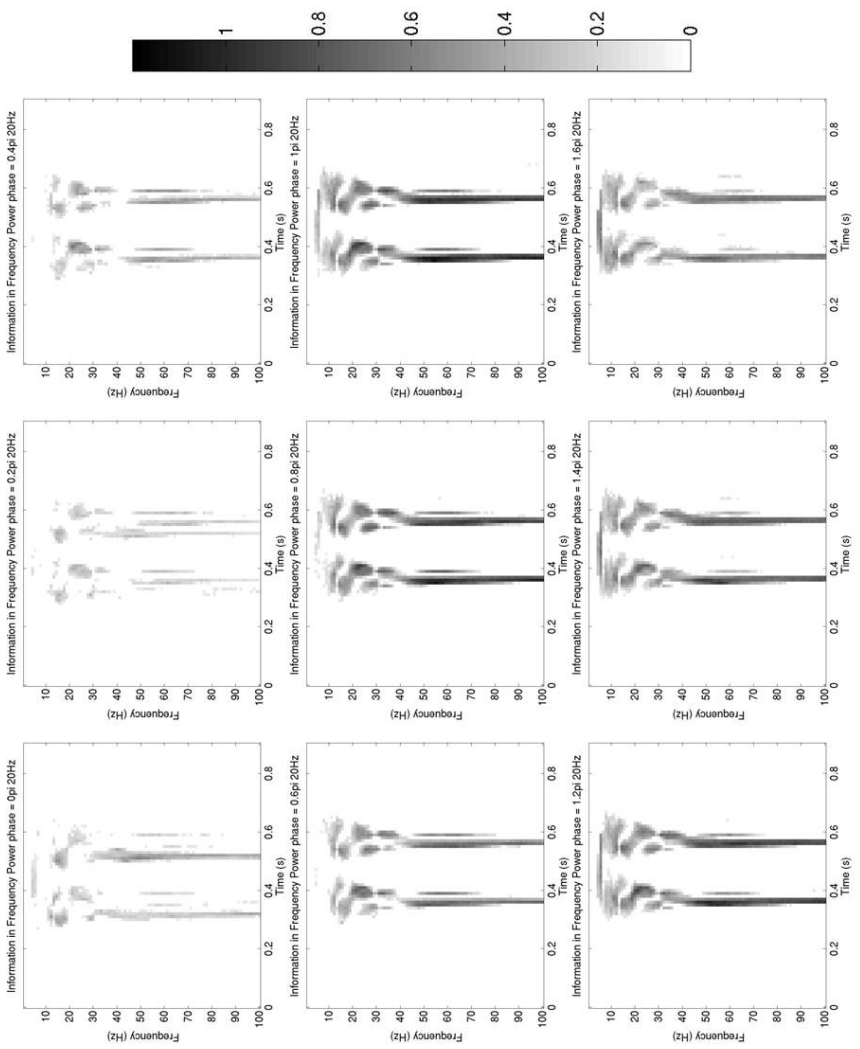

Figure 3.52: **The mutual information between power in the time frequency response and bottom up input frequency according to the phase of the input in a connected network with an oscillatory input of 20 Hz** *Two inputs are delivered at 0.3 and 0.5 seconds with an offset of, from left to right top to bottom, 0, 0.2, 0.4, 0.6, 0.8, 1, 1.2, 1.4, 1.6 pi units. Mutual information is in units of bits.*

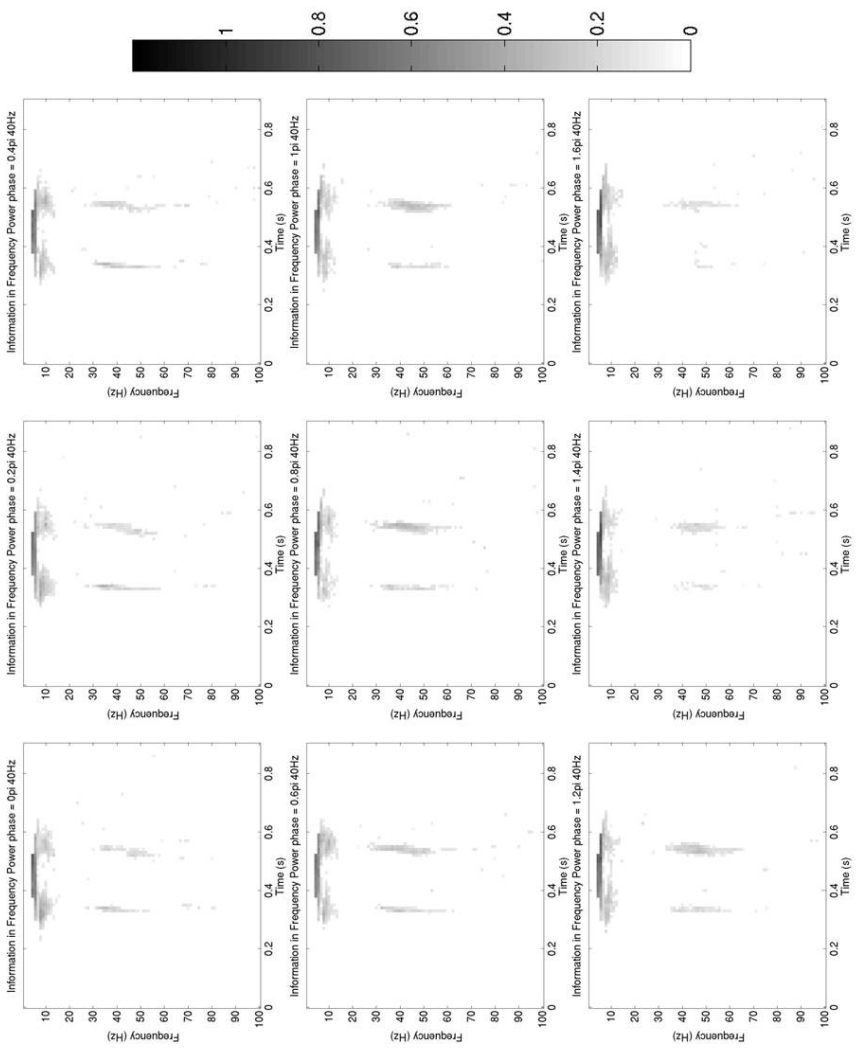

Figure 3.53: **The mutual information between power in the time frequency response and bottom up input frequency according to the phase of the input in a connected network with an oscillatory input of 40 Hz** *Two inputs are delivered at 0.3 and 0.5 seconds with an offset of, from left to right top to bottom, 0, 0.2, 0.4, 0.6, 0.8, 1, 1.2, 1.4, 1.6 pi units. Mutual information is in units of bits.*

tion in the second stimulus presentation phase. This is highest where the presentation is between 0.8 π and 1.2 π. In the first presentation there is a weaker representation in this frequency range when the stimulus is delivered between 1.4 an 1.9 π.

Overall there is a demonstrable phase dependence on the representation of the stimulus according to the phase at which the bottom up input is delivered. In the higher frequencies this modulates a pattern of representation fixed to the phase of the injected sinusoid. In the lower frequencies this changes the frequency bands in which information is carried. This shows up particularly in the gamma range, with a sensitivity to transmitting maximal information between 1.6 and 1.8 π.

In the next analysis I explore the time frequency phase as a basis of comparison.

3.3.3.7 Mutual information and phase

In this analysis I present the mutual information between the bottom up stimulus and the time frequency phase according to probe phase. This is in order to establish whether on not the phase dependence shown in the raw signal and in the firing rates is contained in the phase of particular frequency bands.

Figure 3.54 shows the mutual information between phase in the time frequency response and bottom up input frequency according to the phase of the input in a disconnected network with an oscillatory input of 5 Hz. Between 1 π and 1.6 π there is a small mutual information representation in the <25 Hz range, otherwise there is no significant information in any frequency band.

Figure 3.55 shows mutual information between phase in the time frequency response and bottom up input frequency according to the phase of the input in a connected network with an oscillatory input of 5 Hz. Between 0.4 π and 1.2 π there is a small mutual information representation of the stimulus in the time frequency phase in the 20 and 10 Hz ranges. Between 1.4 π and 0 π there is a wide broad band phase linked representation in the time frequency phase.

Figure 3.56 shows the mutual information between phase in the time frequency response and bottom up input frequency according to the phase of the input in a connected network with an oscillatory input of 10 Hz. There is a stereotypical pattern of significant information that is phase locked to the input stimulus here. The magnitude of the information is dependent upon the oscillatory phase the bottom up input is applied, with the maximal values at between 1.4 and 1.6 π. between 0.2 π and 0.8 π the >25 Hz component

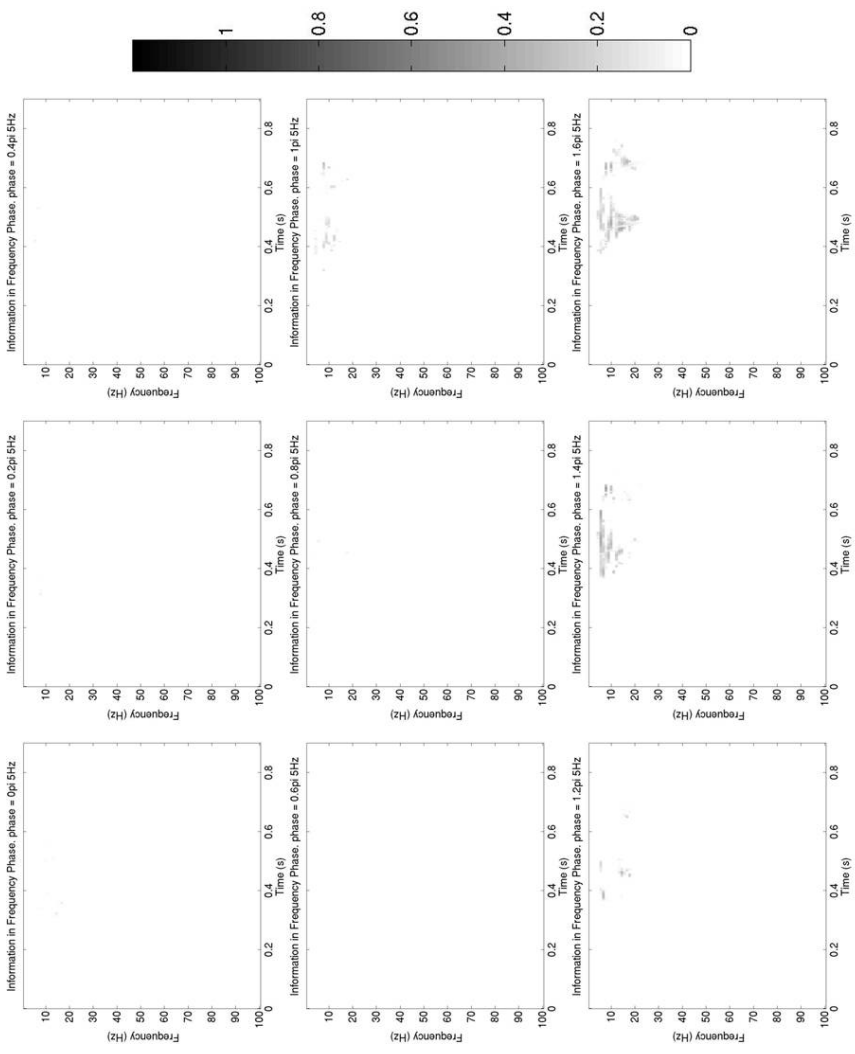

Figure 3.54: **The mutual information between phase in the time frequency response and bottom up input frequency according to the phase of the input in a disconnected network with an oscillatory input of 5 Hz** *Two inputs are delivered at 0.3 and 0.5 seconds with an offset of, from left to right top to bottom, 0, 0.2, 0.4, 0.6, 0.8, 1, 1.2, 1.4, 1.6 pi units. Mutual information is in units of bits.*

Figure 3.55: **The mutual information between phase in the time frequency response and bottom up input frequency according to the phase of the input in a connected network with an oscillatory input of 5 Hz** *Two inputs are delivered at 0.3 and 0.5 seconds with an offset of, from left to right top to bottom, 0, 0.2, 0.4, 0.6, 0.8, 1, 1.2, 1.4, 1.6 pi units. Mutual information is in units of bits.*

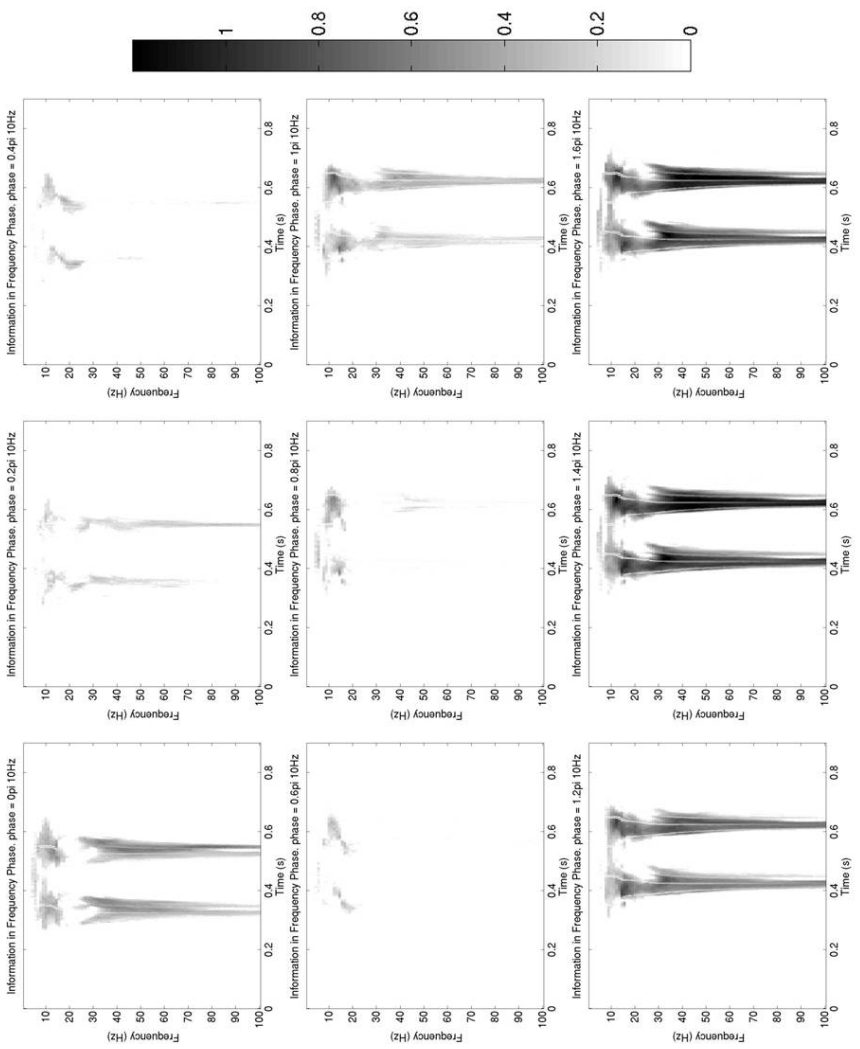

Figure 3.56: **The mutual information between phase in the time frequency response and bottom up input frequency according to the phase of the input in a connected network with an oscillatory input of 10 Hz** *Two inputs are delivered at 0.3 and 0.5 seconds with an offset of, from left to right top to bottom, 0, 0.2, 0.4, 0.6, 0.8, 1, 1.2, 1.4, 1.6 pi units. Mutual information is in units of bits.*

is absent. Another point to note is that in the 20 - 30 Hz range there is a gap in mid to post stimulus significance, with the whole band being absent in the 0 π stimulus phase.z feature

Figure 3.57 shows the mutual information between phase in the time frequency response and bottom up input frequency according to the phase of the input in a connected network with an oscillatory input of 20 Hz. There is a stereotypical stimulus locked mutual information pattern across all input phase conditions. There appears to be two components, a 15 - 30 Hz feature and a >30Hz feature. Phase locking can be seen in the 0 π and 1.6 π plots where the >30 Hz component splits across two oscillatory input cycles. The highest mutual information values can be seen in the 0.6 - 1 π bottom up input conditions.

Figure 3.58 shows the mutual information between phase in the time frequency response and bottom up input frequency according to the phase of the input in a connected network with an oscillatory input of 40 Hz. This is similar to the mutual information in the time frequency power plot with the exception that the 30 -60 Hz band is split in half into two segments where the lower frequencies phase lock on the cycle preceding that of the higher frequency range. The first and second stimulus are represented in an opposite way here when the stimulus is delivered at 1.4 to 1.6 π. Whereas in the power's case the first stimulus is not represented, in the phase it's the second stimulus that is not represented.

Overall there is a similar, although more broadband, response profile of the mutual information between input and time frequency phase as with the time frequency power.

3.3.4 Discussion

In this section I have demonstrated that oscillatory long range inputs are able to alter the encoding of a bottom up stimulus in the field potential and in the spiking activity. It is also apparent that the stimulus information may be eliminated dependent on the phase of the top down input. The information is also packaged by the oscillation, in that maximal information is locked to the phase of the long range input oscillation.

The strongest determinant of the information processing of the entire network is the point where the oscillatory input drives the network into network activation, when is crosses the activation threshold. This resets the information in the spiking activity of the network to zero or near zero. This is also marked by a resetting of information in the field potential power and phase.

The role of different laminar populations in the network for computation is sharply brought into focus. Whilst there is a similar information content

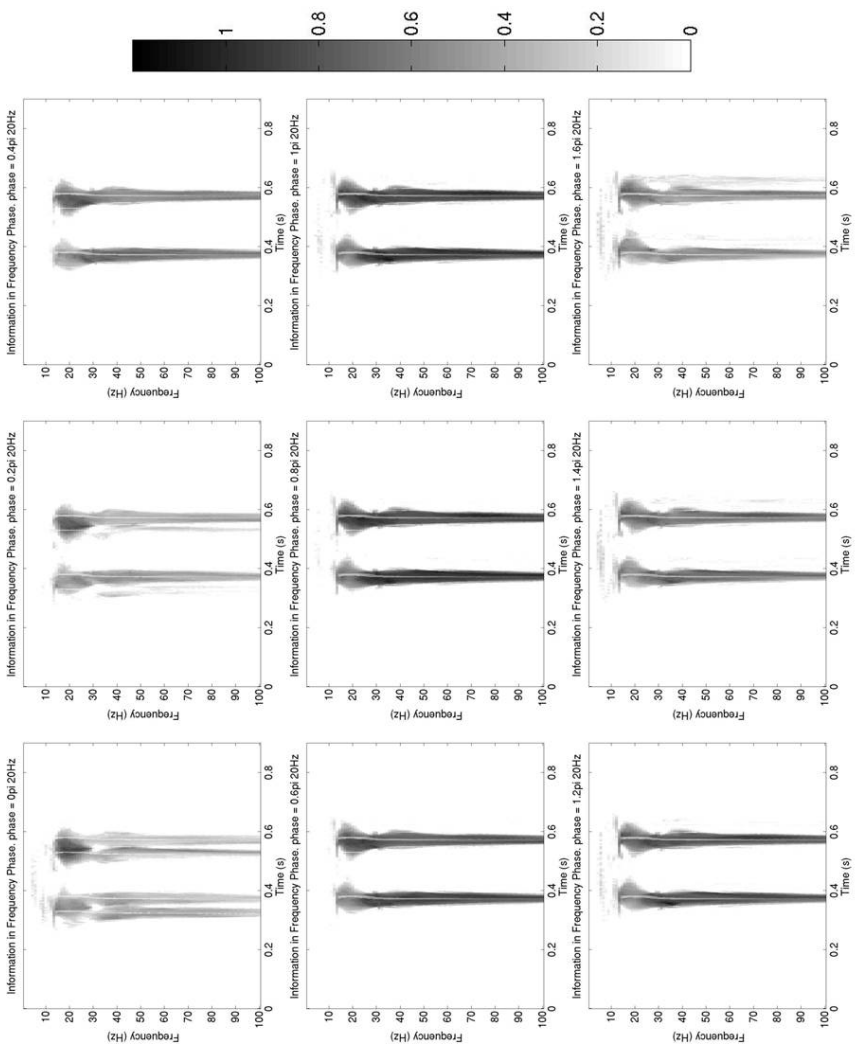

Figure 3.57: **The mutual information between phase in the time frequency response and bottom up input frequency according to the phase of the input in a connected network with an oscillatory input of 20 Hz** *Two inputs are delivered at 0.3 and 0.5 seconds with an offset of, from left to right top to bottom, 0, 0.2, 0.4, 0.6, 0.8, 1, 1.2, 1.4, 1.6 pi units. Mutual information is in units of bits.*

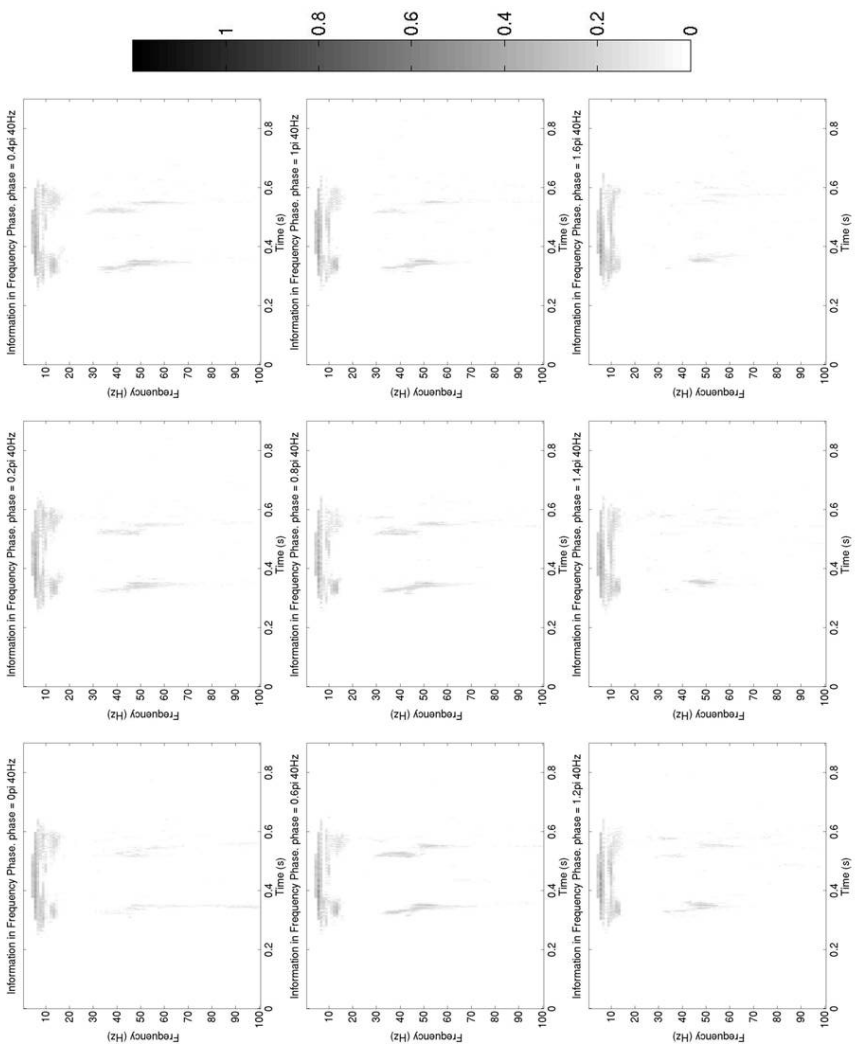

Figure 3.58: **The mutual information between phase in the time frequency response and bottom up input frequency according to the phase of the input in a connected network with an oscillatory input of 40 Hz** *Two inputs are delivered at 0.3 and 0.5 seconds with an offset of, from left to right top to bottom, 0, 0.2, 0.4, 0.6, 0.8, 1, 1.2, 1.4, 1.6 pi units. Mutual information is in units of bits.*

in most layers related to the stimulus no matter what time it is applied, even for the duration of the stimulus when applied during the network activation period, in the layer 3 and layer 5 excitatory cells there is a strong increase in information for stimulus immediately following the crossing of the network threshold.

3.4 Chapter Summary

In this chapter I have shown the network behaviour over an increasingly realistic range of inputs. I have identified a number of input and stimulus encoding features in the discussion of each section. I have shown the laminar organisation of the network to carry out different and important roles for encoding of stimulus information. And I have identified a potential gating mechanism for the communication of computation performed upon stimulus information to long distance areas within the cortical hierarchy.

This phase dependent gating mechanism is the strongest testable hypothesis to be derived from the simulation results presented in this work. Plainly stated an ongoing or induced oscillation in a sensory network will change the state of a primary sensory cortical area and thus its response to bottom up information from a stimulus that's duration is shorter than the wavelength. There is a point during the rise time of the oscillation where the local network enters the activated state. Stimuli presented immediately after this point will be facilitated. Stimulus presented closely preceding this point will be attenuated. This effect will be independent of the ongoing or induced oscillation frequency. This effect will also be represented in a concurrently recorded field potential measurement.

In the next chapter I will derive and carry out a number of experiments to test this hypothesis.

Chapter 4

Behavioural and MEG studies

4.1 Chapter introduction

In this chapter I will present two behavioural studies and two MEG studies whose paradigms were derived from the results of the modelling study. The modelling study suggests that the information relating to a bottom up input or stimulus available to experimenters from recorded field potential activity and the information available to higher and lower areas of the brain are dependent on the coincidence with the phase of a cortico-cortical oscillatory input.

To investigate this experimentally I was presented with two options, to come up with a simple sensory task and analyse the field potential state preceding a stimulus or to induce oscillations in the cortex and control the relative timing of a sensory stimulus. I decided to pursue both approaches.

Firstly, to investigate endogenous oscillations presents the problem that there can be no behavioural pilots without recording neural oscillations. Secondly, repeated stimuli are likely to induce task related anticipatory oscillations(Worden et al., 2000; Kelly et al., 2006; Thut et al., 2006). Nonetheless, this presents a simpler set of tasks available for investigation when measuring field potentials.

A simple task had to be devised in order to be considered equivalent at both the small scale and the large scale level. Areili et al (Arieli et al., 1996) showed that variability in the optical dye and local field potential (LFP) event related potential (ERP) response to repeated stimulus in the cat visual cortex depended upon the amplitude of the LFP. Haslinger et al (Haslinger et al., 2006) demonstrated that the phase of a 1 Hz LFP oscillation in the barrel cortex of the rat predicts the spiking response of that area to whisker deflection. Linkenkaer-Hansen et al (Linkenkaer-Hansen et al., 2004)

have shown that the amplitude of prestimulus oscillations 10, 20 and 40Hz influences the detection of near threshold stimuli in human somatosensation. These results suggested a simple near threshold perception task would be an appropriate paradigm to investigate the interaction between information flow and cortical oscillations.

I was then presented with the challenge of selecting a method of reliably inducing oscillations. Oscillatory input has been shown to induce phase locked neural oscillation in a number of sensory modalities (Nakayama and Mackeben, 1982; Tobimatsu et al., 1999; Bergholz et al., 2008; Manganotti et al., 2009). Upon consideration of ease of delivery, cortical localization and the limited number of studies in this modality I decided on using the auditory steady state response. This response is easily reproduced and utilized in audiology, neurology and in surgery to ascertain depth of anaesthesia(Azzena et al., 1995; Santarelli et al., 1995; John and Picton, 2000; Ross et al., 2000).

The effects of oscillatory input and facilitation of perceptual response have been shown in a number of recent studies (Fries, 2005; Schnitzler and Gross, 2005; Schoffelen et al., 2005). Their potential for use investigation of endogenous brain rhythms has recently been discussed by Thut, Schyns and Gross(Thut et al., 2011).

Thus I derived the three experimental paradigms presented in this study. The first is the detection of a near threshold auditory stimulus in the context of a steady state stimulus. This is closest to the paradigm explored in the final section of the second modelling chapter. Four auditory steady state frequencies were explored in a behavioural study and in an MEG study.

The second paradigm was based on the assumption that entrained endogenous rhythms would persist beyond the offset of an auditory steady state stimulus. Thus a steady state stimulus would be played long enough to induce the entrainment of a rhythm and then near threshold perception would be measured post stimulus.

The third paradigm was a simple near threshold detection task of an auditory stimulus to be performed in the MEG.

Each of these experiments and their results will now be presented.

4.2 A behavioural study of ongoing auditory steady state

In this behavioural study participants undertook a near threshold perception test in the presence of a continuous auditory steady state stimulus. Four entrainment frequencies were employed, 4 Hz, 10 Hz, 20 Hz and 39 Hz. Each

stimulus lasted 200 seconds and each frequency was presented three times.

I hypothesise that there will be a phase dependent change in the perception of a stimulus. A secondary hypothesis is that it will be facilitated during the rising phase of the stimulus and inhibited during the falling phase. A tertiary hypothesis is that the perception relationship to the phase will be independent of the frequency.

4.2.1 Methods

4 participants with an average age of 29 took part in this study. There were 2 males and 2 females. Participants reported no known hearing problems. The study was approved by the local ethics committee (University of Glasgow Faculty of Information and Mathematical Sciences) and conducted in conformity with the declaration of Helsinki. Each subject provided informed consent.

The experiment was carried out in a quiet lab. Participants used a dell laptop computer and Sennheiser HD 205-II Headphones.

The experiment was a within subjects design with two factors. The first factor was a 200 second presentation of a 250 Hz sinusoidal tone. This had four conditions. It was either played with amplitude modulated with a sinusoid with a modulation depth of 100 per cent. The modulation frequency was 4, 10, 20 or 39 Hz. The second factor was a 5 ms burst of Gaussian white noise presented at near 50 percent perception level. The noise probe was presented 99 times in the context of the sinusoidal tone with a 2 second interstimulus time plus a random duration of between 0 and 1 seconds. Each modulation frequency was presented three times.

The experimental procedure was as follows. The participant was seated in front of the computer screen with the headphones on. The experimenter initialised the program and asked the participant to follow the on screen instructions. The white noise probe was played and the participant was asked to adjust this to a barely audible level by adjusting it until they couldn't hear it, then increasing it to the first stepwise point where it was audible. This level was then used to determine the perception threshold psychometric curve.

The white noise probe was played 100 times with the amplitude randomly adjusted each time to cover the range of 0 - 100 percent perceived levels. After each presentation there was a pause where the participant was asked to respond whether or not they heard the probe by entering a keystroke. The responses were binned according to 10 amplitude levels and plotted in a Matlab figure. This was sufficient to produce the classical sigmoid threshold response. The experimenter then determined the 50 percent threshold level

and entered it into the computer. This level was used to set the 0 decibel level and determine the level of the ongoing sinusoidal carrier wave.

The probe perception threshold was the determined in the context of the carrier wave. The 250 Hz carrier wave was set at 70 dB. A 200 ms carrier wave was played with the white noise probe played 99 times with the amplitude randomly adjusted each time to cover the range of 0 - 100 percent perceived levels. The noise probe was presented in the context of the sinusoidal tone with a 2 second interstimulus time plus a random duration of between 0 and 1 seconds. The participant was asked to respond by a keystroke whenever they hear a probe stimulus. The responses were binned according to 10 amplitude levels and plotted in a Matlab figure. This was sufficient to produce the classical sigmoid threshold response. The experimenter then determined the 50 percent threshold level and entered it into the computer. This level was used to set the threshold level of the noise probe in the context of the sinusoidal signal.

The experiment was as follows. The participant was presented with three blocks of four trials with the participant able to determine the start of each block and trial. Each block consisted of a trial at each of the modulation frequencies. Each trial consisted of a 200 ms amplitude modulated 250 Hz carrier wave with 99 presentations of the noise probe at 50 percent perception level. The noise probes were presented with a 2 second interstimulus time plus a random duration of between 0 and 1 seconds.The participant responded with a key stroke each time the probe was perceived. The time of each keystroke was recorded. After the experiment the participants were fully debriefed.

4.2.2 Results

Figures 4.1, 4.2, 4.3 and 4.4 show the perception response for all participants. These results demonstrate that there is a significant difference in the mean phase angle at which the probe stimulus is applied. Although non of the participants have a significant difference for all probe frequencies, three of the participants show a significant difference in three of the four conditions and the remaining participant in two of the four. The mean angle for a correct response is approximately 1.8 π, the mean angle for an incorrect response is approximately 0.8 π, although this is more variable. There is not a significant difference in the mean angle according to steady state stimulus frequency.

Figures 4.5, 4.6, 4.7 and 4.8 show the reaction time histograms and the median and mean values for each correct response at each of the steady state probe frequencies. Although testing for statistical significance does not

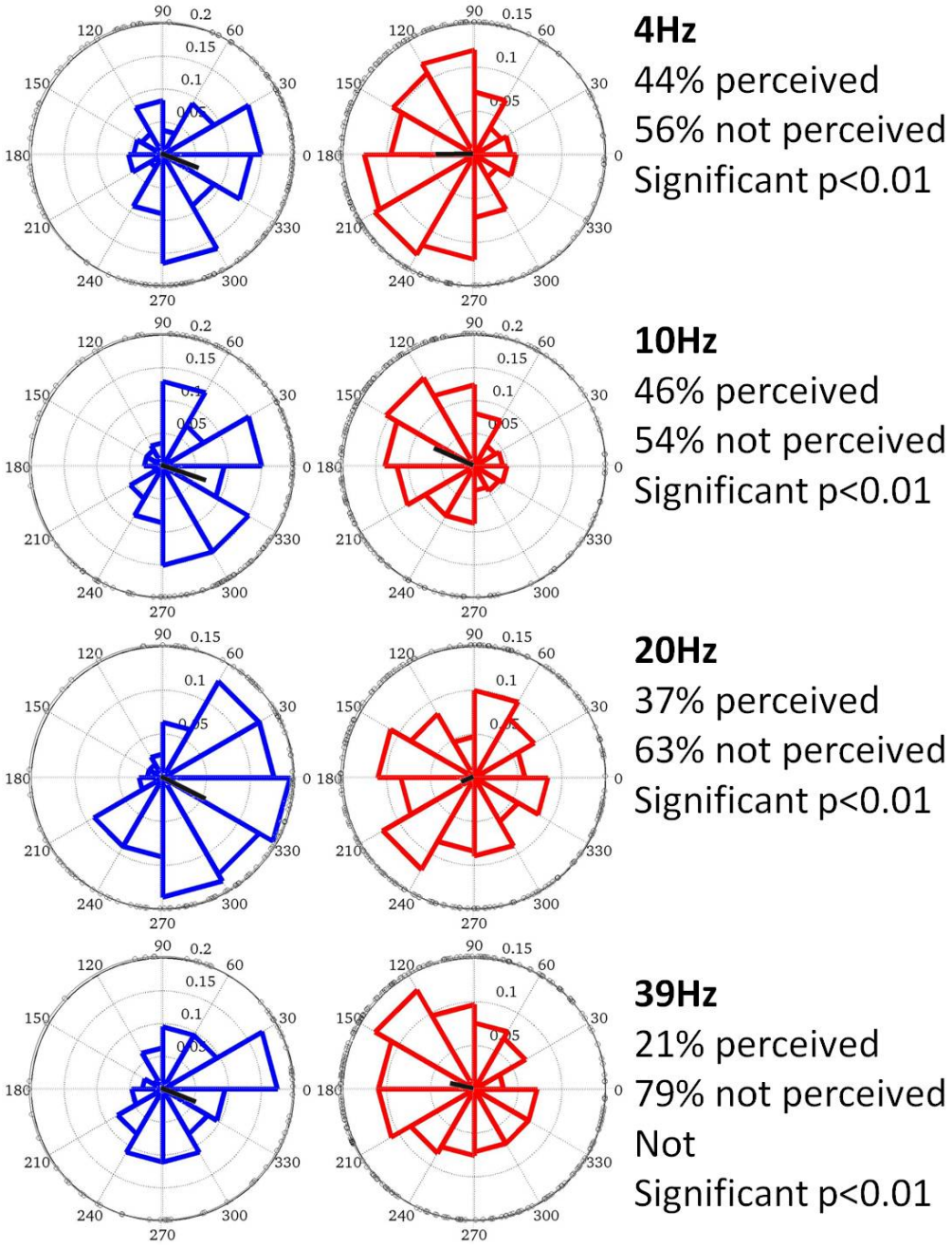

Figure 4.1: **The mean correct and incorrect response mean phase and the normalized summery of results - participant 1** *the blue plots show the normalized correct responses by the phase at which they were applied. The red plots show the normalized incorrect responses by the phase at which they were applied. The black centre vector in each plot is the mean phase angle for the given response. The text gives the percentage of perceived and unperceived trials and whether or not the difference between the two mean angles are significant. From top to bottom the 4 Hz, 10 Hz, 20 Hz and 39 Hz condition is presented.*

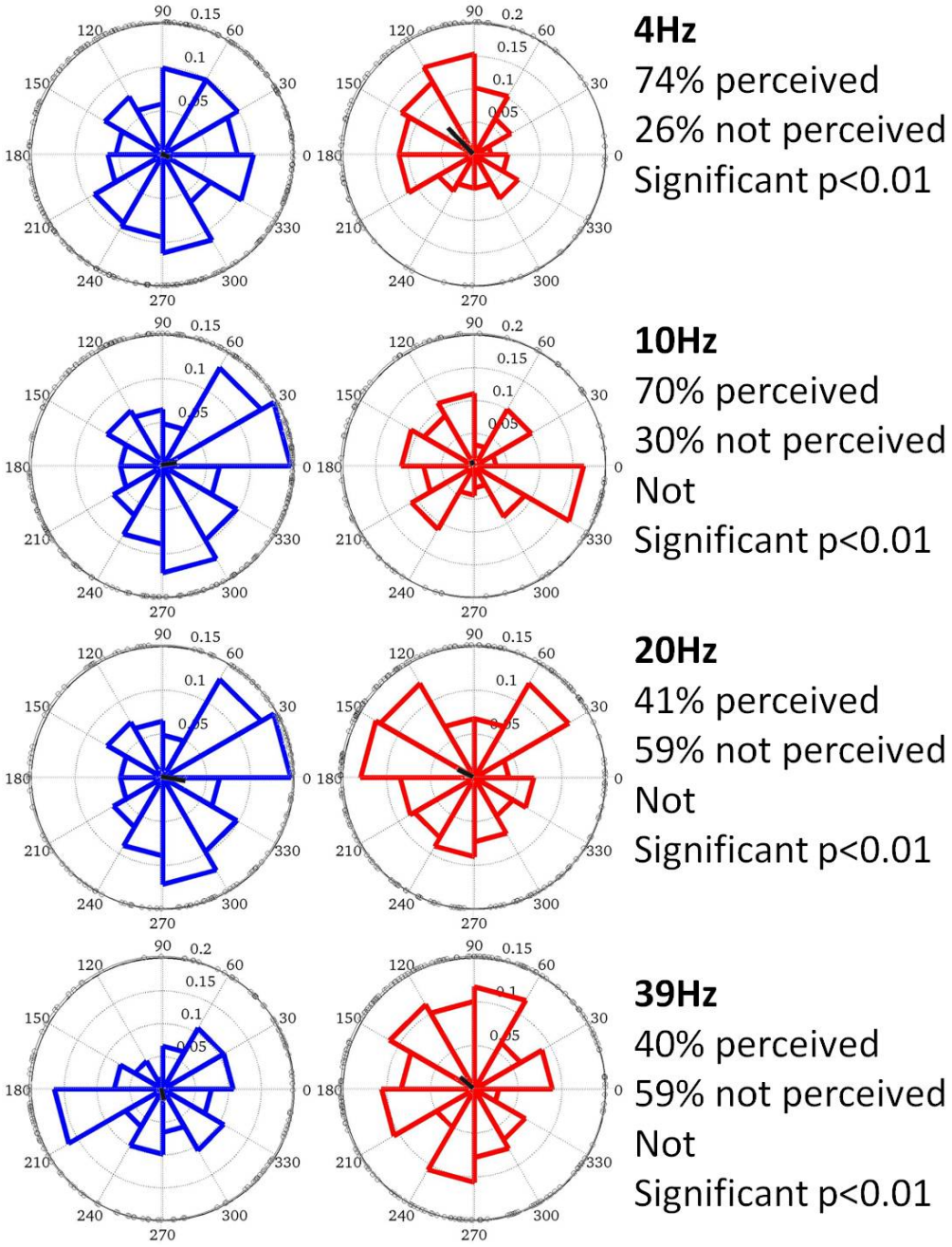

Figure 4.2: **The mean correct and incorrect response mean phase and the normalized summery of results - participant 2** *the blue plots show the normalized correct responses by the phase at which they were applied. The red plots show the normalized incorrect responses by the phase at which they were applied. The black centre vector in each plot is the mean phase angle for the given response. The text gives the percentage of perceived and unperceived trials and whether or not the difference between the two mean angles are significant. From top to bottom the 4 Hz, 10 Hz, 20 Hz and 39 Hz condition is presented.*

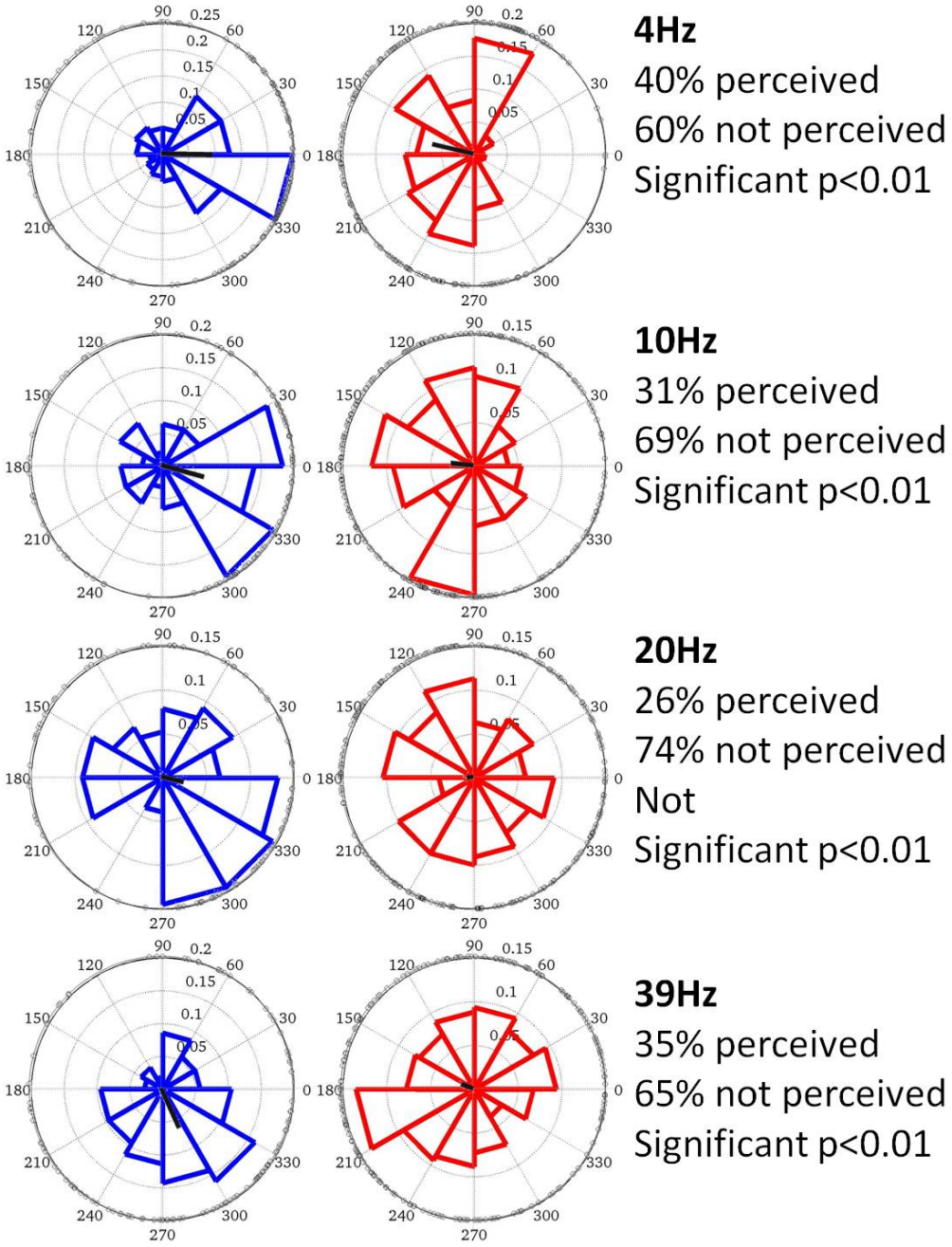

Figure 4.3: **The mean correct and incorrect response mean phase and the normalized summery of results - participant 3** *the blue plots show the normalized correct responses by the phase at which they were applied. The red plots show the normalized incorrect responses by the phase at which they were applied. The black centre vector in each plot is the mean phase angle for the given response. The text gives the percentage of perceived and unperceived trials and whether or not the difference between the two mean angles are significant. From top to bottom the 4 Hz, 10 Hz, 20 Hz and 39 Hz condition is presented.*

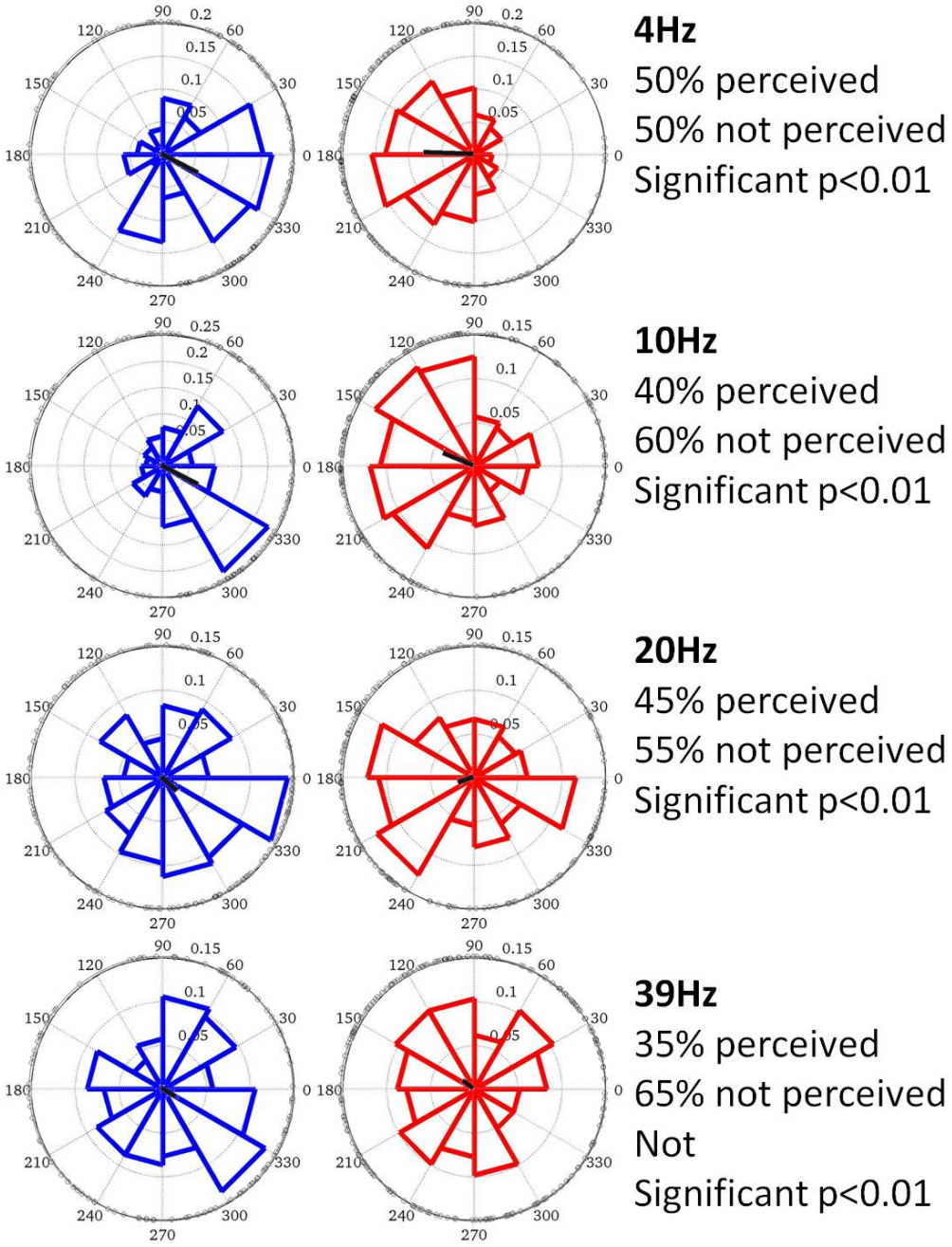

Figure 4.4: **The mean correct and incorrect response mean phase and the normalized summery of results - participant 4** *the blue plots show the normalized correct responses by the phase at which they were applied. The red plots show the normalized incorrect responses by the phase at which they were applied. The black centre vector in each plot is the mean phase angle for the given response. The text gives the percentage of perceived and unperceived trials and whether or not the difference between the two mean angles are significant. From top to bottom the 4 Hz, 10 Hz, 20 Hz and 39 Hz condition is presented.*

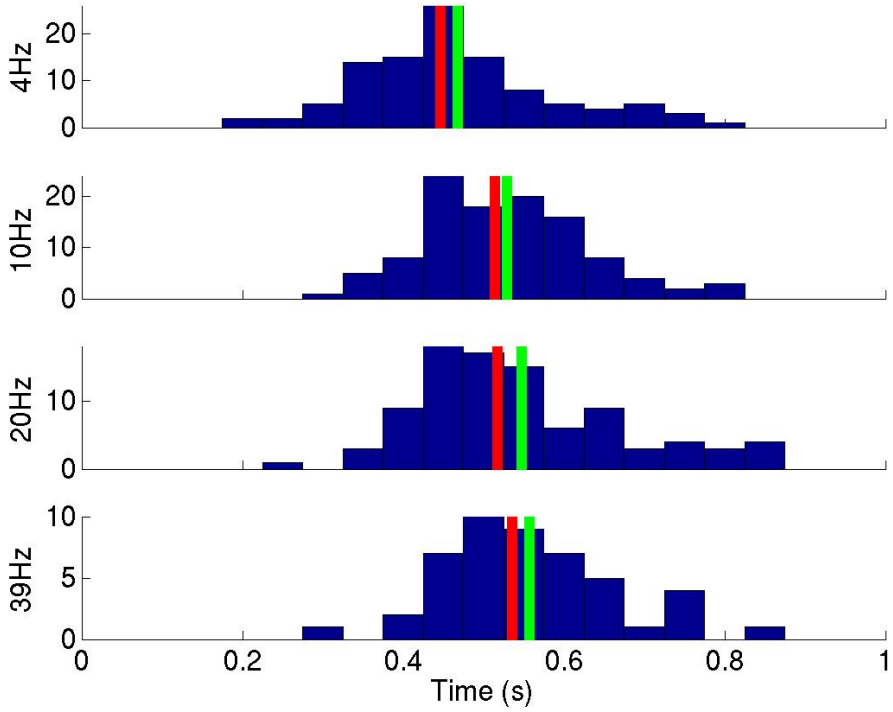

Figure 4.5: **The reaction time histogram for each stimulus condition - participant 1** *the red line shows the median reaction time and the green shows the mean. From top to bottom the 4 Hz, 10 Hz, 20 Hz and 39 Hz condition is presented.*

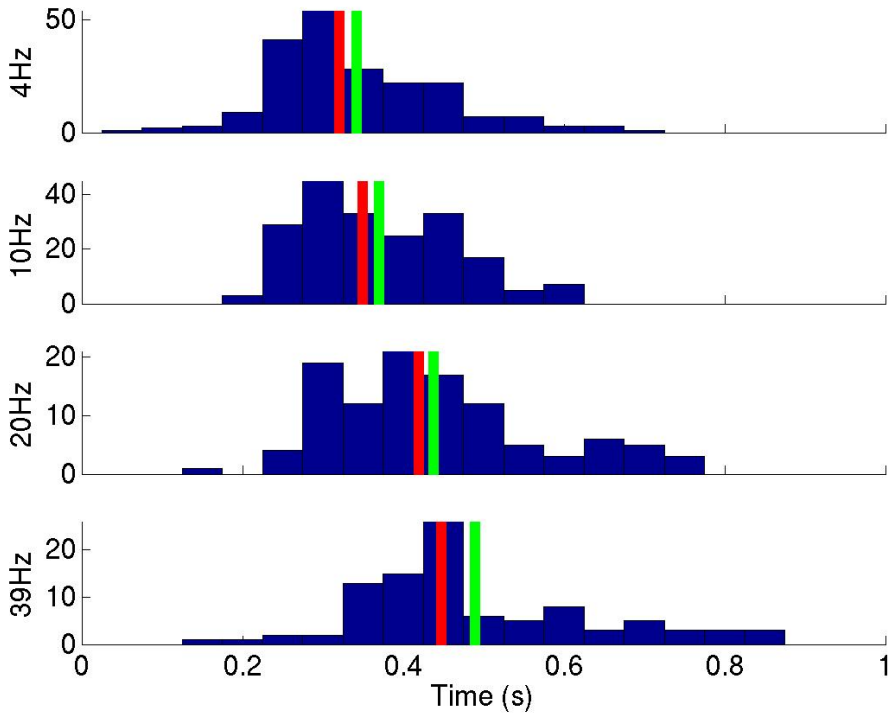

Figure 4.6: **The reaction time histogram for each stimulus condition - participant 2** *the red line shows the median reaction time and the green shows the mean. From top to bottom the 4 Hz, 10 Hz, 20 Hz and 39 Hz condition is presented.*

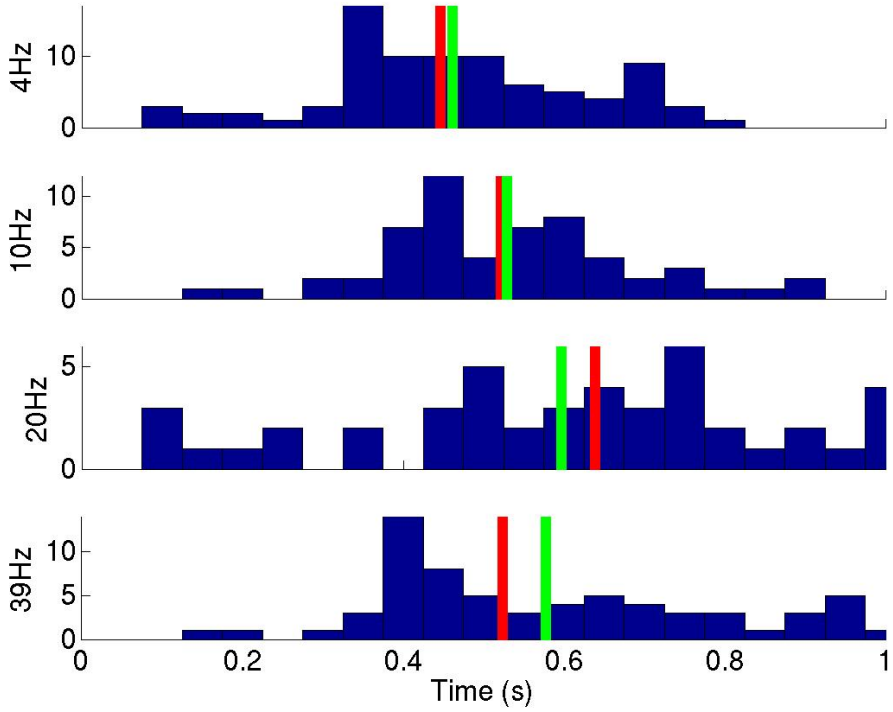

Figure 4.7: **The reaction time histogram for each stimulus condition - participant 3** *the red line shows the median reaction time and the green shows the mean. From top to bottom the 4 Hz, 10 Hz, 20 Hz and 39 Hz condition is presented.*

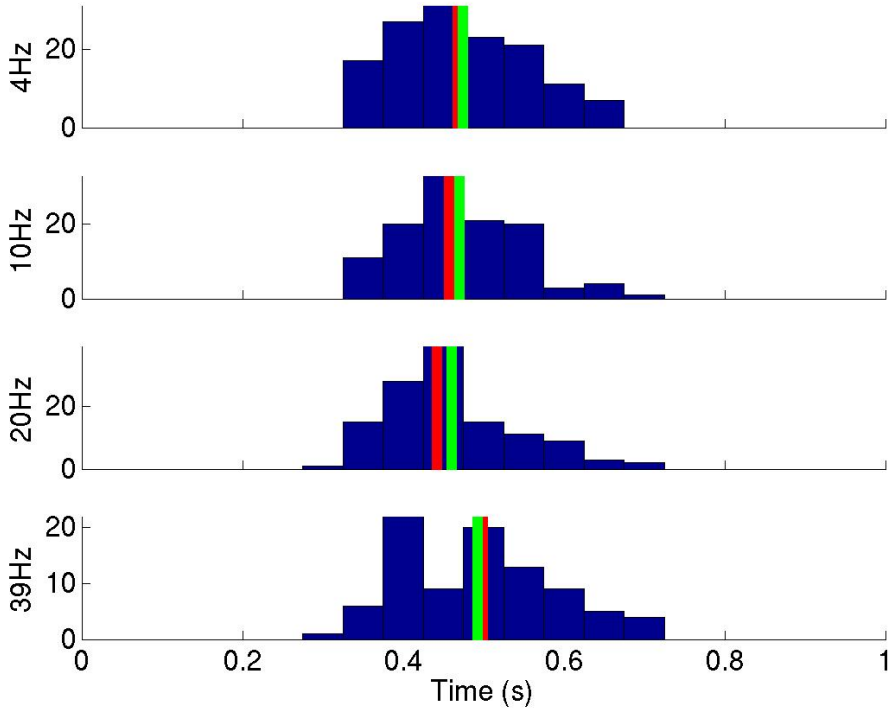

Figure 4.8: **The reaction time histogram for each stimulus condition - participant 4** *the red line shows the median reaction time and the green shows the mean. From top to bottom the 4 Hz, 10 Hz, 20 Hz and 39 Hz condition is presented.*

yield any clear answers, in the first three of the four participants there is a suggestion that as the probe frequency increases reaction time is longer. Further experimentation would be required to confirm this.

4.2.3 Discussion

The behavioural results response probabilities show a strong correlation with the mechanism identified through the modelling study. The phase dependence in both is independent of the induced frequency. There is a point during the rise time of the sinusoid after which there is greater information about the stimulus available. Preceding this there is a period where information about the sensory input is reduced. This lends strong support for the mechanism of network activation identified in the model.

4.3 A behavioural study of auditory steady state phase

In this experiment 25 participants were presented with either a one second auditory steady state stimulus modulated at 10 Hz or an unmodulated carrier wave followed by a 50% perception level probe stimulus with a post stimulus delay of one of eight equally spaced levels within a single wavelength.

I hypothesise that there will be an effect on perception level related to the phase of the absent auditory steady state cycle.

4.3.1 Methods

25 participants with an average age of 21 took part in this study. There were 10 males and 15 females. Participants reported no known hearing problems. The study was approved by the local ethics committee (University of Glasgow Faculty of Information and Mathematical Sciences) and conducted in conformity with the declaration of Helsinki. Each subject provided informed consent.

The experiment was carried out in a quiet lab. Participants used a dell desktop computer and Sennheiser HD 205-II Headphones.

The experiment was a within subjects design with two factors. The first factor was a 1 second presentation of a 250 Hz sinusoidal tone. This had two conditions. It was either played unmodulated or amplitude modulated with a 10 Hz sinusoid with a modulation depth of 0.8. The second factor was a 5 ms burst of Gaussian white noise presented at near 50 percent perception level. This had eight conditions. The noise probe was presented after the

modulated or unmodulated sinusoidal stimulus with a time delay of 1 - 8 eighths of the amplitude modulation frequency wavelength.

The experimental procedure was as follows. The participant was seated in front of the computer screen with the headphones on. The experimenter initialised the program and asked the participant to follow the on screen instructions. The initial stimulus level was set by playing the unmodulated sinusoidal tone and asking the participant to adjust it to a loud, but not uncomfortable level. This level was saved for future factor 1 presentation.

The white noise probe was played and the participant was asked to adjust this to a barely audible level by adjusting it until they couldn't hear it, then increasing it to the first stepwise point where it was audible. This level was then used to determine the perception threshold psychometric curve in the context of the sinusoidal input.

To determine the curve there 50 presentations of the unmodulated 1 sec sinusoidal tone followed by a probe tone of varying amplitude levels. For each presentation the participant was asked to respond by a key press 'y' if perceived and 'n' if not perceived. The responses were binned according to 10 amplitude levels and plotted in a Matlab figure. This was sufficient to produce the classical sigmoid threshold response. The experimenter then determined the 50 percent threshold level and entered it into the computer. This level was used for factor 2 presentation.

The experiment was as follows. The participant was presented with two blocks of 160 trials. Each trial consisted of a sinusoidal tone, either modulated or unmodulated, followed by a noise probe played with one of the eight time delays. All possible combinations of tone and delay were presented 10 times with random presentation. Between blocks the participant was asked to sit quietly and begin the second block with a keystroke. After the second block the participants were fully debriefed.

4.3.2 Results

Figure 4.9 shows the mean response across participants to the probe stimulus at different phases for modulated and unmodulated auditory steady state stimulus. The top plot shows the number of positive responses to ten presentations of the probe at each post condition delay time. The delay data point times each represent an increase of 1/8 th of the auditory steady state stimulus wavelength. The blue plot is teh modulated carried wave and the green plot is the unmodulated carrier wave. The bottom plot shows the values of the modulated carrier wave responses minus the responses following the unmodulated carrier wave.

Both lines in the top plot show a sigmoidal increase in perception rate

Figure 4.9: The mean response across participants to the probe stimulus at different phases for modulated and unmodulated auditory steady state stimulus

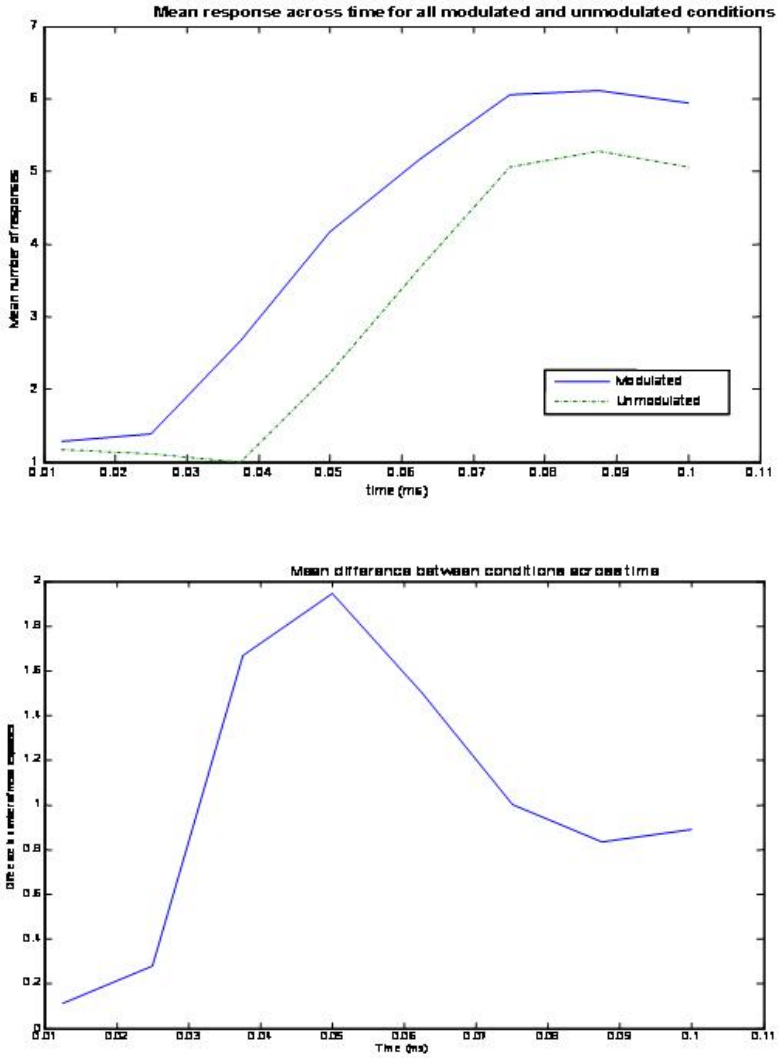

following the pre probe stimulus. The 50 percent perception rate is reached by approximately one wavelength post condition. The perception rate is facilitated by the 10 Hz auditory steady stimulus at all time points. The central section of the modulated carrier wave condition is not linear.

The bottom plot shows the difference between the modulated and unmodulated response. It is clear that the facilitation is phase dependent upon the post auditory steady state stimulus. Facilitation is maximal in the anticipated falling section of the modulating sinusoid.

4.3.3 Discussion

This study supports the hypothesis that induced oscillations alter post stimulus responses. That the curve in the second plot is the opposite of that found in the previous behavioural experiment suggests that there may be some adaptive compensation to the ASSR stimulus from a higher area in the cortex.

4.4 An MEG study of auditory steady state signals

In this study a similar paradigm to the first behavioural experiment was presented in the MEG. The paradigm was altered slightly to accommodate restrictions presented by the MEG set up. The frequencies of the auditory steady state stimuli were changed to avoid interference from the mains electricity artefact.

There were significant problems delivering the auditory stimulus to the participant in the magnetically shielded room (MSR). In initial runs there was a strong temporal response to the auditory steady state stimulus, however upon further investigation it was found that this was an artefact from the headset speakers. At the volume required to induce an auditory steady state response the headset shielding proved infective in removing any related magnetic contribution to the signal.

In response to this I sourced an alternative delivery system which consisted of speakers external to the MSR driving a column of air in a ten foot silicone tube connected with the participants ear canal through an in ear device. This system produced a filtering effect on the low and high frequencies, however this was not in effect in the frequency of the carrier wave. It did attenuate the white noise stimulus to the point where in the context of the auditory steady state response it could not be perceived at its highest

volume. As such the probe stimulus was replaced with a 1 kHz burst which was able to be perceived very close to maximum volume.

This system resulted in an over all reduction in volume, with the maximum volume only at the lowest limits reported to produce an auditory steady state response.

4.4.1 Methods

3 right handed participants with an average age of 30 took part in this study. There were 2 males and 1 female. Participants reported no known hearing problems. The study was approved by the local ethics committee (University of Glasgow Faculty of Information and Mathematical Sciences) and conducted in conformity with the declaration of Helsinki. Each subject provided informed consent. All subjects participated in the behavioural experiment presented in 4.2.1 and were familiar with the paradigm.

The recording session consisted of two auditory experiments. All stimuli were presented binaurally. The first experiment was a within subject design with one factor. The subject had to respond with a button press when a 5 ms burst of a 1000 Hz sinusoid presented at near 50 percent perception level. The noise probe was presented 99 times over 200 seconds with a 2 second interstimulus time plus a random duration of between 0 and 1 seconds. This was carried out three times.

The second experiment was a within subjects design with two factors. The first factor was a 200 second presentation of a 250 Hz sinusoidal tone. This had four conditions. It was either played with amplitude modulated with a sinusoid with a modulation depth of 100 per cent. The modulation frequency was 4, 9, 19 or 39 Hz. The second factor was a 5 ms burst of a 1000 Hz sinusoid presented at near 50 percent perception level. The noise probe was presented 99 times in the context of the sinusoidal tone with a 2 second interstimulus time plus a random duration of between 0 and 1 seconds. Each modulation frequency was presented three times.

Brain activity was recorded with a 248-magnetometer whole-head MEG system (MAGNES 3600 WH, 4-D Neuroimaging) confined in a magnetically shielded room. The MEG signal was high-pass filtered at 0.1 Hz and digitized at 508 Hz. Before starting the recording session, five coils were positioned on the participant's head. These coils, together with three fiducial points and the subject's head shape, were digitized using a Polhemus Fastrak system. At the beginning and end of each run the five coils were activated to localise the participants head with respect to the MEG sensor array. During the recording session, subjects were seated in a reclining chair and supported their head against the back and top of the magnetometer. Some of them

opted for using an additional neck support to increase their comfort. Participants were asked to remain as still as possible during the recording session and were continuously monitored by a video camera.

Instruction was presented through a DLP projector (PT-D7700E-K, Panasonic) placed outside the shielded room onto a screen situated 1.90 m away from participants via an in-room mirror. All stimuli were generated off-line using Matlab 7.5 (The MathWorks) and were presented using Psychtoolbox (Brainard, 1997). Auditory stimulus was presented using a Behringer POWERPLAY PRO-XL HA4700 amplifier delivered by Etymotics ER30 dual mono headphones with 20 ft silicone delivery tubes feeding to moulded ear inserts within the magnetically shielded room. Participants responded using one non-magnetic response pad (Lumitouch) held in the right hand. Responses during the setup phase were using the right index finger or the right ring finger. Responses during the experimental phase were the right index finger only.

The experimental procedure was as follows. The experimenter initialised the program and asked the participant to follow the on screen instructions. The 1000 Hz burst probe was played and the participant was asked to adjust this to a barely audible level by adjusting it until they couldn't hear it, then increasing it to the first stepwise point where it was audible. This level was then used to determine the perception threshold psychometric curve.

The 1000 Hz burst probe was played 100 times with the amplitude randomly adjusted each time to cover the range of 0 - 100 percent perceived levels. After each presentation there was a pause where the participant was asked to respond whether or not they heard the probe by entering a keystroke. The responses were binned according to 10 amplitude levels and plotted in a Matlab figure. This was sufficient to produce the classical sigmoid threshold response. The experimenter then determined the 50 percent threshold level and entered it into the computer. This level was used to set the 0 decibel level and determine the level of the ongoing sinusoidal carrier wave in experiment 2.

The first experiment was as follows. The participant was presented with three blocks of 200 ms with 99 presentations of the 5 ms 1000 Hz sinusoid probe. The 1000 Hz sinusoid probes were presented with a 2 second interstimulus time plus a random duration of between 0 and 1 seconds.The participant responded with a key stroke each time the probe was perceived. The time of each keystroke was recorded. The participant determined the onset of each block.

In preparation for the second experiment the probe perception threshold was the determined in the context of the carrier wave. The 250 Hz carrier wave was set at 70 dB. A 200 ms carrier wave was played with the 1000 Hz

burst probe played 99 times with the amplitude randomly adjusted each time to cover the range of 0 - 100 percent perceived levels. The 1000 Hz burst was presented in the context of the sinusoidal tone with a 2 second interstimulus time plus a random duration of between 0 and 1 seconds. The participant was asked to respond by a keystroke whenever they hear a probe stimulus. The responses were binned according to 10 amplitude levels and plotted in a Matlab figure. This was sufficient to produce the classical sigmoid threshold response. The experimenter then determined the 50 percent threshold level and entered it into the computer. This level was used to set the threshold level of the 1000 Hz sinusoid probe in the context of the sinusoidal signal.

The second experiment was as follows. The participant was presented with three blocks of four trials with the participant able to determine the start of each block and trial. Each block consisted of a trial at each of the modulation frequencies. Each trial consisted of a 200 ms amplitude modulated 250 Hz carrier wave with 99 presentations of the 1000 Hz sinusoid probe at 50 percent perception level. The 1000 Hz sinusoid probes were presented with a 2 second interstimulus time plus a random duration of between 0 and 1 seconds. The participant responded with a key stroke each time the probe was perceived. The time of each keystroke was recorded. After the experiment the participants were fully debriefed.

4.4.2 Results

After a number of pilots only one participant was determined to be able to perceive the probe stimulus in the context of the ASSR stimulus when the probe was at maximum volume. Upon investigation of the MEG signal there was no evidence of auditory steady state entrainment. The behavioural results presented below indicate that there was not the same effect as the participant's behavioural results presented above.

Figures 4.10 and 4.11 show the two equivalent graphs from the MEG study to the behavioural study carried out in section 4.2.2. Both figures demonsrate that there is no significant difference in the steady state response phase probe angle, and no trend in the reaction times according to stimulus frequency.

4.4.3 Discussion

The negative behavioural results and the absence of a recorded steady state response to a stimulus level that was thought to be at the threshold of a measurable effect support the hypothesis that induced cortical oscillation is

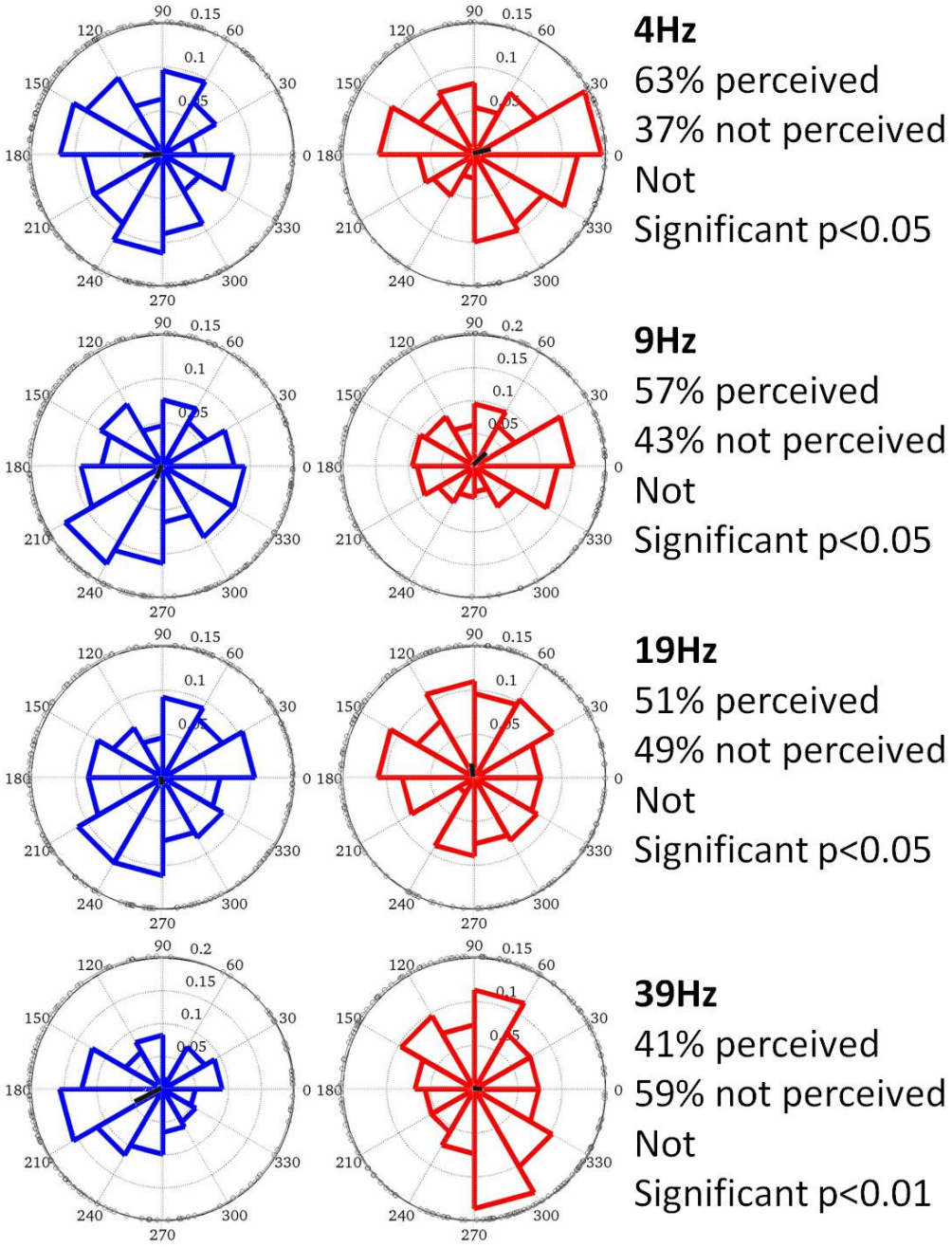

Figure 4.10: **The mean correct and incorrect response mean phase and the normalized summery of results** *the blue plots show the normalized correct responses by the phase at which they were applied. The red plots show the normalized incorrect responses by the phase at which they were applied. The black centre vector in each plot is the mean phase angle for the given response. The text gives the percentage of perceived and unperceived trials and whether or not the difference between the two mean angles are significant. From top to bottom the 4 Hz, 9 Hz, 19 Hz and 39 Hz condition is presented.*

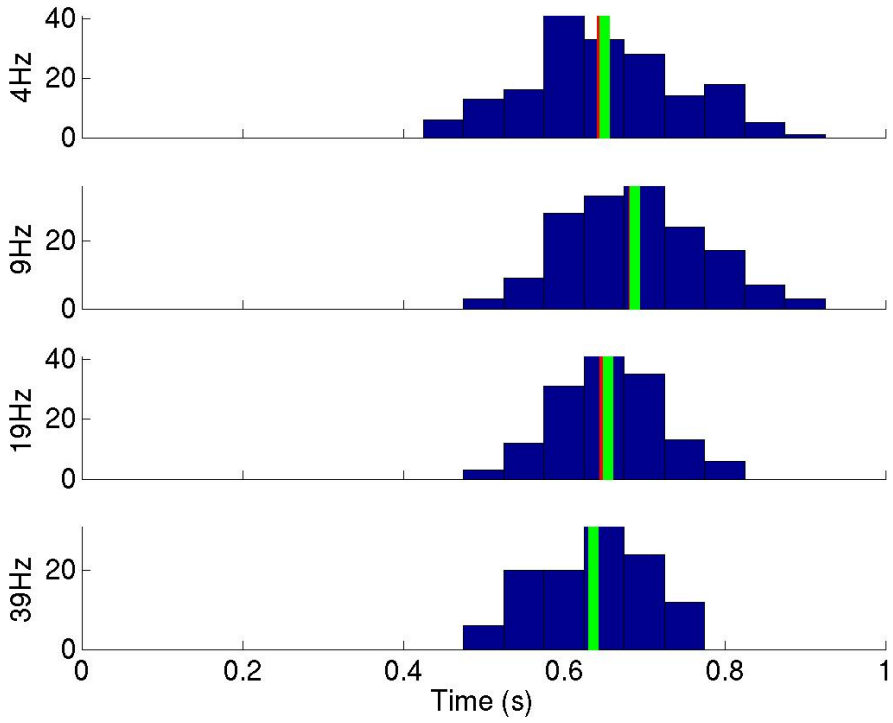

Figure 4.11: **The reaction time histogram for each stimulus condition** *the red line shows the median reaction time and the green shows the mean. From top to bottom the 4 Hz, 10 Hz, 20 Hz and 39 Hz condition is presented.*

required for the effect, rather than just a conflicting osculating stimulus in the same modality.

4.5 An MEG study of near threshold stimuli and ongoing activity

In this study the results from a single participant to repeated presentations of a 1 kHz tone at 50 % perception level are presented. The participant was given 297 probe stimuli and responded with a right index finger button press when the tone was perceived. The probes were presented every two seconds with a randomized offset of between zero and one second.

In the analysis the MEG recordings were segmented according to stimulus presentation time. The raw signal was dominated by a strong occipital alpha signal. The signal was analysed using independent component analysis to extract whole brain components that would be most likely to contain a representation of the primary auditory cortices, rather than using a sensor based analysis (Ramkumar, 2012). The signals underwent dimensional reduction and were sorted into independent components using the fieldtrip ICA algorithm (Oostenveld, 2011). The components were then ranked according to variance. Here I present an analysis of the three strongest dipole components from the occipital and both temporal regions. The signals were then further sorted into positive and negative responses.

I hypothesise that there will be a prestimulus frequency power and phase dependence upon perception.

First I present the components under investigation. Next I present the mean power spectral distribution of the positive and negative responses. Thirdly I look at the time frequency power response of the positive response. Then I look at the positive response time frequency response relative to baseline. This is followed by the time frequency power response of the positive trials minus the negative trials. Finally I present the time frequency power response of the positive trials minus the negative trials relative to baseline.

This is followed by an information theory analysis first into the mutual information between time frequency power and correct or incorrect response. And secondly to the mutual information in the time frequency phase.

4.5.1 Methods

The experiment was carried out concurrently with the experiment on auditory steady state responses and the methods are described in that section.

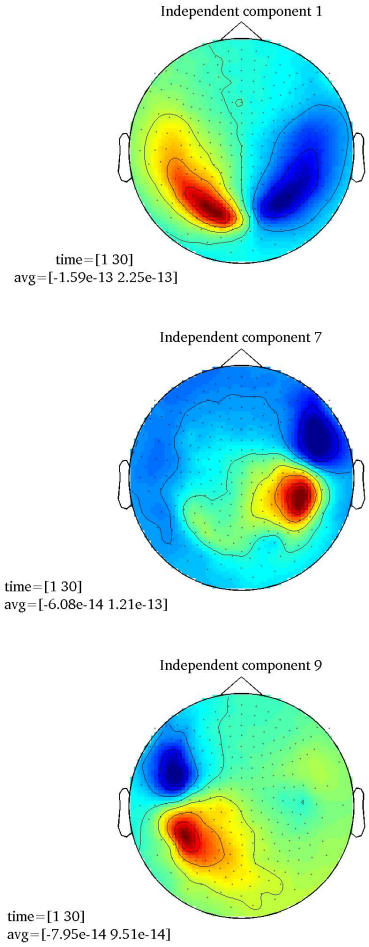

Figure 4.12: **3 independent components of the MEG response**

4.5.2 Results

In all figures in the results section there are three figures from top to bottom they are independent components representing from top to bottom the primary occipital component, the primary right temporal component and the primary left temporal component.

4.5.2.1 Independent components

Figure 4.12 shows the three independent components that will be investigated in this MEG study. Dimension reduction was performed using PCA and sorted according to variance. Components were selected for their anatomical location and whether or not they represented a dipole. The top plot is the component ranked with highest variance. This shows a dipole in the occipital

region. The middle plot is the component ranked 17th according to variance. This shows a dipole in the right temporal region. The bottom plot is the component ranked 20th according to variance. This shows a dipole in the left temporal region.

4.5.2.2 Independent components' power spectra

Figure 4.13 shows the power spectral distributions for the independent components sorted according to positive or negative response. The blue line shows the correct response; the green line shows the incorrect response.

The top plot represents the normalised power spectral distribution in the occipital component. There is an higher proportion of the normalised power for the positive response in the lowest frequency band, the 5 Hz band and the 10 Hz band. There is a reduced proportion of normalised power at 15 Hz.

The middle plot represents the normalised power spectral distribution in the right temporal component. There is an higher proportion of the normalised power for the positive response at 7 Hz, 10 Hz and 20 Hz. There is a reduced proportion of normalised power at all frequencies less than 6 Hz.

The bottom plot represents the normalised power spectral distribution in the left temporal component. There is an higher proportion of the normalised power for the positive response at 13 - 17 Hz. There is a reduced proportion of normalised power at all frequencies less than 12 Hz and at 20 Hz.

4.5.2.3 Independent components time frequency response for positive response

Figure 4.14 shows the mean time frequency response for positive response in the independent components. The probe stimulus was applied at time equal to zero. All three show a dominant power around 10 Hz.

The top plot represents the occipital component. The dominant frequency is the 10 -12 Hz range. There is a peak in power preceding the stimulus to -0.2 seconds with a reduction in power post stimulus.

The middle plot represents the right temporal component. The dominant frequency range is the 6 - 11 Hz range. There is a prestimulus peak in power to -0.4 seconds. There is a post stimulus reduction in power from 0.1 seconds.

The bottom plot represents the left temporal component. There are two prominent frequency ranges, the 5 - 11 Hz range and the less than 3 Hz range. In the 10 Hz range there is a stimulus related increase in power that extends 0.1 seconds either side of the stimulus. There is a post stimulus decrease in this range from 0.2 seconds. There is a post stimulus increase in power in

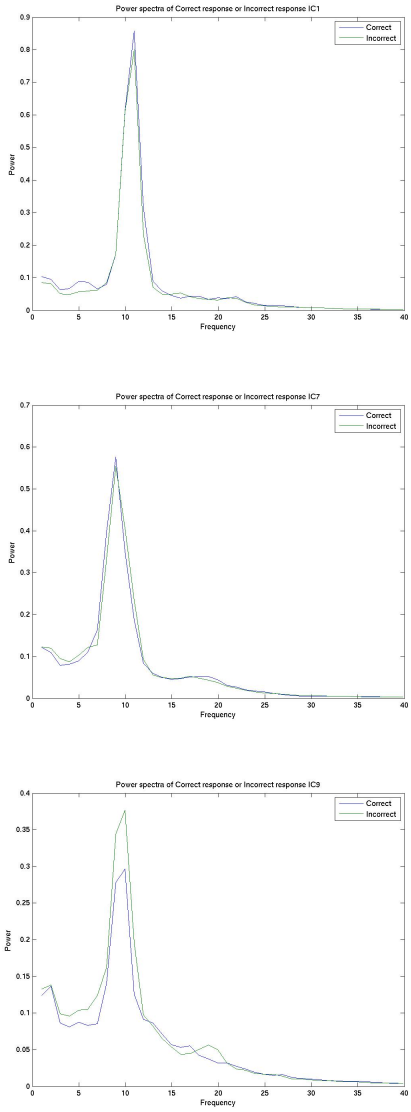

Figure 4.13: **Independent components' power spectral distribution positive and negative response**

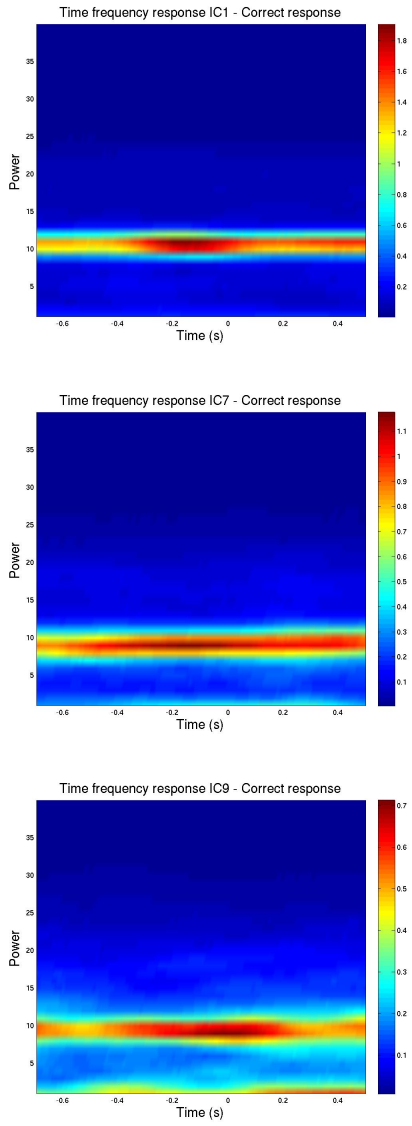

Figure 4.14: **Time frequency response for positive response**

the 7-5 Hz range from around 0.1 Hz. There is a prestimulus reduction in power in the 5 Hz range and in the less than three Hz range. There is a slight increase in power in the 4 Hz range pre stimulus. There is a post stimulus increase in power in the less than 3 Hz from about 0.1 Hz.

4.5.2.4 Independent components time frequency relative response for positive response

Figure 4.15 shows the time frequency relative response for positive response in the independent components. The probe stimulus was applied at time equal to zero.

The top plot shows the occipital component. Prestimulus shows an increase in the 10 Hz and the 22 Hz bands extending to -0.2 seconds. There is a reduction in power in the 5 Hz, 7 Hz, 15 Hz and 25 Hz bands. Post stimulus there is an increase in power in the 15 Hz, 20 Hz, 30 - 34 Hz and 36 Hz bands. There is a reduction in power in the less than 5 Hz, 13 Hz and 25 Hz range.

The middle plot shows the right temporal component. Pre stimulus there is an increase in power in the 10 Hz and 30 Hz bands. There is reduced power in all other bands. Post stimulus there is an increase in power 3 Hz, 10 Hz, 20 Hz and in particular the 30 Hz range.

The bottom plot shows the left temporal cortex. Pre stimulus there is an increase in the 3 Hz, 9 Hz and 20 Hz range. There is a reduction in power in the less than 3 Hz, 6 Hz and the 25 - 35 Hz range. At stimulus there is an increase in power at the 9 Hz range. Post stimulus there is an increase in power in the 6 Hz, 12 Hz and 19 Hz range.

4.5.2.5 Independent components time frequency response for positive response minus negative response

Figure 4.16 shows time frequency response for positive response minus negative response in the independent components. The probe stimulus was applied at time equal to zero. This should increase the components that are associated with positive responses.

The top plot shows the occipital component. There is a strong 10 Hz component preceding the stimulus followed by a reduction in this component post stimulus.

The middle plot shows the right temporal component. There is a strong 9- 10 Hz component peaking at -0.2 prestimulus. There is a reduction in 5 - 6 Hz prestimulus that extends to the post stimulus time. There is a prestimulus increase in the less than 3 Hz range.

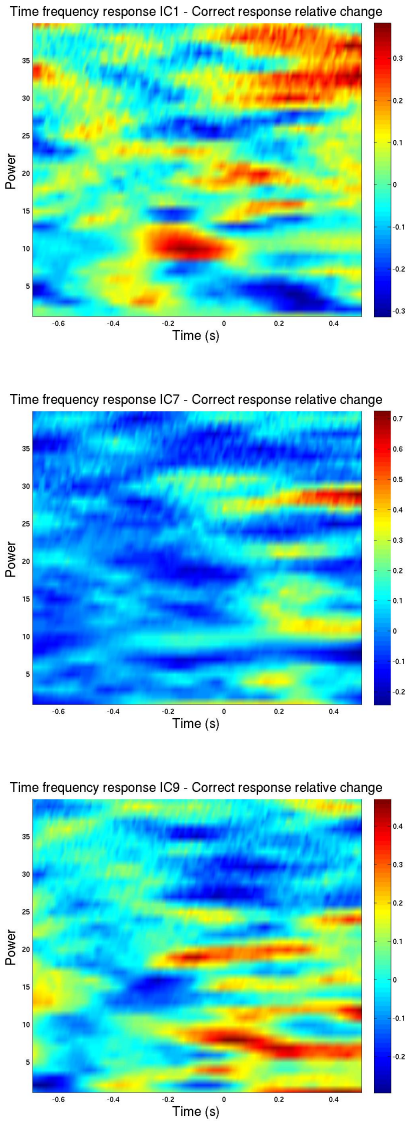

Figure 4.15:
Time frequency relative response for positive response

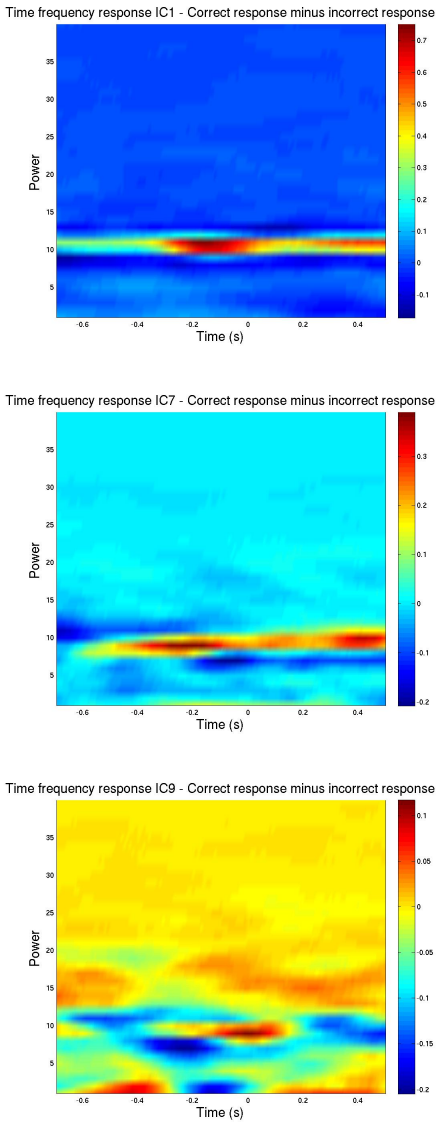

Figure 4.16: **Time frequency response for positive response minus negative response**

The bottom plot is the left temporal component. There is a prestimlus increase in power in the 28 Hz range. There is a pre stimulus reduction in power in the less than 3 Hz range and in the 6 Hz range. There is an increase in 10 Hz around the stimulus. There is a post stimulus increase in power in the less than 3 Hz and 15 Hz range.

4.5.2.6 Time frequency relative response for positive response minus negative response

Figure 4.17 shows relative time frequency response for positive response minus negative response in the independent components. The probe stimulus was applied at time equal to zero. This should increase the components that are associated with positive responses.

The top plot shows the occipital component. There is a pre stimulus increase in power in the 10 Hz and 28 Hz range. There is a post stimulus increase in power in the 15 Hz, 30 Hz and 40 Hz range. There is a post stimulus reduction in power in the less than 5 Hz range.

The middle plot shows the right temporal component. There is a pre stimulus increase in power in the 10 Hz range around -0.2 seconds. There is a prestimulus decrease in power in the 5Hz, 20 Hz and 30 Hz range. There is a post stimulus increase in power in the 3 Hz, 10 Hz, 25 and 40 Hz ranges. There is a post stimulus decrease in power in the 5 Hz and 30 Hz range.

The bottom plot shows the left temporal component. There is a strong prestimulus increase in power in the 20 Hz range. There is a prestimulus decrease in power in the less than 3 Hz, 5-7 Hz and 15 Hz range. There is a stimulus linked increase in power in the 9 Hz range. There is a post stimulus increase in power in the 15 and 20 Hz ranges. There is a post stimulus decrease in power in the 30 -35 Hz range.

4.5.2.7 Mutual information between time frequency power and response

Figure 4.18 shows the mutual information between time frequency power and response in three independent components. The probe stimulus was applied at time equal to zero.

The top plot shows the occipital component. There is a significant mutual information value in the pre stimulus 10 Hz range There is a significant mutual information value post stimulus in the 22 Hz range extending for 0.4 seconds. after this there is an high information value in the 38 Hz range. There is a post stimulus increase in information in the less than 3 Hz range from 0.2 seconds.

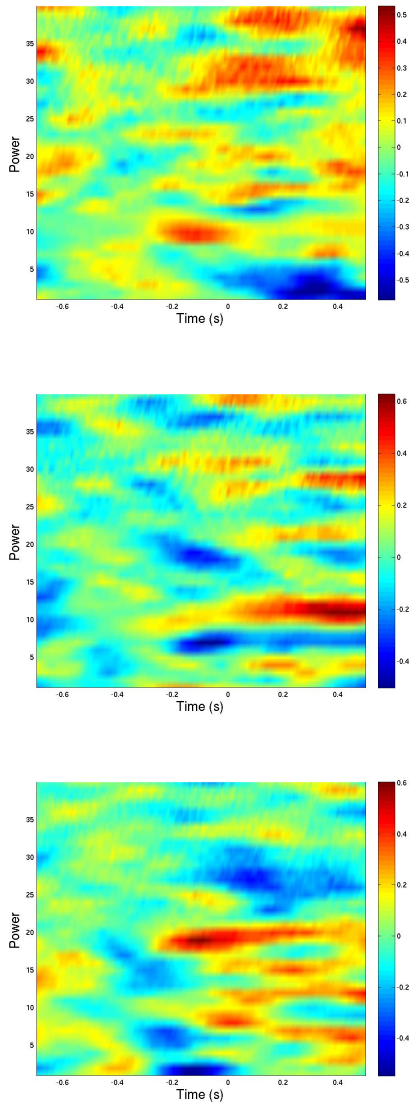

Figure 4.17: **Time frequency relative response for positive response minus negative response**

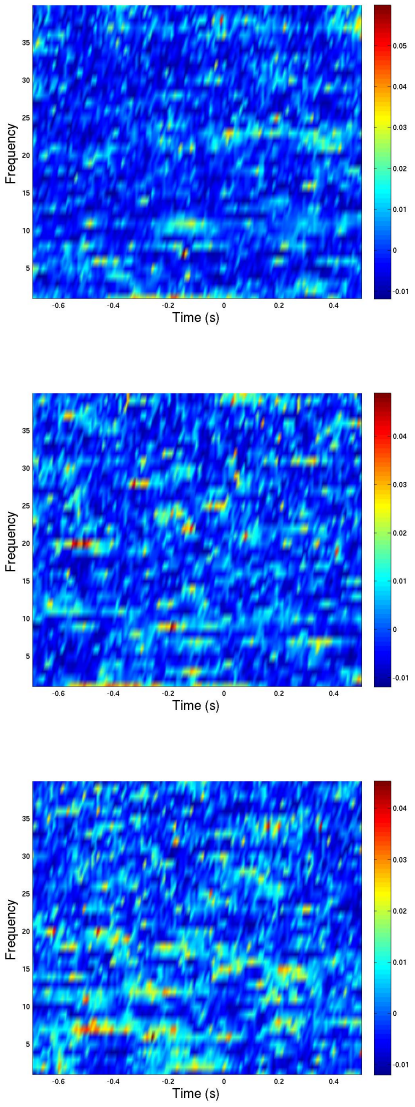

Figure 4.18: **The mutual information between time frequency power and response**

The middle plot shows the right temporal component. There is a high information value around -0.2 seconds at 10 Hz. There is a post stimulus increase in information in the 40 Hz range. There is an increase in information in the 5 Hz range from 0.2 seconds post stimulus.

The bottom plot shows the left temporal component. There is a 10 Hz increase in information between -0.4 and -0.2 seconds prestimulus. There is an increase in information in the less than 3 Hz and the 17 Hz range immediately prestimulus. There is a stimulus increase in information in the 15 Hz range. There is a post stimulus increase in information in the 25 Hz range. At around 0.2 seconds post stimulus there is an increase in information in the 7 Hz and 13 Hz range.

4.5.2.8 Mutual information between time frequency phase and response

Figure 4.19 shows the mutual information between time frequency phase and response in three independent components. The probe stimulus was applied at time equal to zero.

The top plot shows the occipital component. There is an increase in information around -0.4 seconds prestimulus in the 10 Hz and 40 Hz range. There is an increase in information in the less than 3 Hz range around -0.2 seconds prestimulus. There is a prestimulus increase in information around 10 Hz. There is a post stimulus increase in information in the 20 Hz 27 Hz and 38 Hz ranges. After 0.2 seconds there is an increase in information in the less than 3 Hz, 10 Hz, 15 Hz and 35 Hz range.

The middle plot shows the right temporal component. There is a pre stimulus increase in information in the 10 Hz range leading up to -0.3 seconds prestimulus. From -0.3 to -0.1 Hz there is increased information in the 15 Hz and 40 Hz ranges. Crossing stimulus time there is increased information in the 38 Hz range. post stimulus there is an increase in power in the 10 Hz range. at around 0.1 seconds post stimulus there is an increase in information in the less than 3 Hz and the 25 Hz range followed by an increase in information in the 20 Hz range.

The bottom plot shows the left occipital component. There is a strong prestimulus increase in information in the 32 Hz range until -0.4 seconds. At -0.3 seconds there is a strong increase in information in the less than 3 Hz range. Immediately pre stimulus there is a strong increase in information in the 13 Hx and 25 Hz range, these extend beyond the stimulus time. After 0.2 seconds post stimulus there is an increase in information in the 15 Hz and 28 Hz ranges.

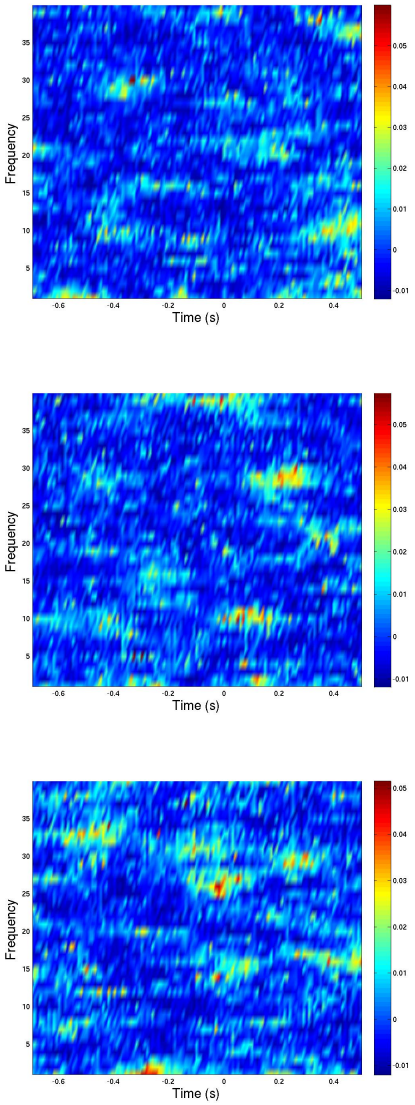

Figure 4.19: **Mutual information between time frequency phase and response**

4.5.3 Discussion

The information analysis of the pre and post stimulus time frequency power and phase suggest interaction between the auditory and early visual cortices. Immediately preceding the stimulus in the occipital component the power in the alpha band, 10 Hz, to - 0.2 seconds contains the most information about the perception of the stimulus. Increased alpha in this region has been associated with decreased visual attention, this suggests that visual suppression facilitates the perception of near threshold auditory stimuli. The right temporal component shows increased information in the same band and time scale. However the power shows that there is a reduction in alpha preceding the positive stimuli. This suggests that attention is also associated with the perception of auditory stimuli. In the left temporal component there is most information in the less than three Hz range. Immediately before this increase in power there is a peak in information in the phase in this band. Preceding the occipital pre stimulus alpha there is a prolonged period of increased information in the phase of alpha in the right temporal region. This may be a candidate for future investigation of connectivity and causation.

Post stimulus there is increased information in the 15 - 20 Hz range phase and power in the left temporal component. This is reminiscent in frequency and duration of the stimulus response of the near network activation threshold simulation in the static mean condition.

The right temporal shows information in 4 Hz power and phase that would place the stimulus time at the point around which there is maximum receptivity to an input in the 5 Hz oscillatory model. The response frequencies in both the model and the right temporal component are alpha and gamma.

4.6 Chapter summary

In this chapter I have investigated three experimental paradigms developed from hypotheses derived from my mechanistic cortical model. One of the behavioural experiment's results was predicted by the model. And the others produced data that could be interpreted in terms of the model.

Chapter 5

Conclusions and further work

In this work I have presented a novel mechanistic model based upon the best obtainable cortical laminar connectivity statistics. I characterized the model according to rough expectations using a simple white noise stimulus and found an area in parameter space where complex oscillatory activity occurred. Using these parameters I was able to explore the model's response properties to a simulated bottom up input. At this point an injected oscillatory current was found to illicit a strong variability of the transmission of information through the network, in particular at lower frequency values, and a variability in the information available from the experimentally available simulated field potential. This reduction occurred at around 180 degrees phase angle, and at around 330 degrees there was an increase in information in the both the projection neurons and the simulated field potential.

I used these results to design a behavioural experiment within which I obtained the result that a near threshold auditory stimulus delivered at the same time as an oscillatory steady state will be more, or less likely to be perceived according to the phase of the auditory steady state stimulus. Upon comparison the same phase value, 330 degrees for increased information representation in the model projection neurons and that found in the behavioural experiment matched. Subsequent MEG experimentation did not yield clear results, however as the behavioural results were unable to be replicated in the MEG experimental setup it would be worth pursuing further experiments where the behavioural results could be replicated.

In the visual domain Busch (Busch, 2009) found that the phase of ongoing EEG oscillations predicts perception of a near threshold stimulus. There is not a clear indication that the phase values are equivalent to those found my model or behavioural study, but the effects may be related. A problem with comparison does arrive however regarding whether or not you can get a clear estimate of the time a stimulus related signal is available at the cortical level

using only a recorded EEG signal locked to stimulus delivery. An additional problem with my study is that although the ASSR signal is locked with the probe, I was unable to obtain the MEG signal to determine the lag of the phase. So for a full comparison further experimentation is necessary.

In the introduction I identified three challenges in experimental neuroscience associated with experimental design and data interpretation, namely : the inverse problem and source localization; the integration of experimental results across scales and paradigms; and the variability associated with ongoing activity. I will now summarize my results in relation to these issues.

Firstly the integration of experimental results across scales and paradigms. In this thesis I have developed and presented a novel cellular level mechanistic cortical model derived from the most up to date anatomical and physiological statistics. I have applied abstract inputs to the model representing the three main classes of input to a given cortical area, namely: subcortical input; local cortical input; and long range cortico-cortical input. I have characterized the model's response properties across a range of combinations of these inputs. I have analysed these response properties at the cellular level and at a field potential level, which may be considered to represent a local field potential or a cortical source in MEG/EEG experiments. I have used this cellular level model to simulate a psychophysical paradigm and analysed it using information theory. From this I derived a testable hypothesis relating to the transfer of sensory information through subpopulations of cortical neurons. I have shown only the subpopulations of neurons responsible for long distance communications use network activity in association with ongoing activity to maximise and package the transfer of information. From this model I have derived an experimental paradigm, carried out the experiment and found the results of a behavioural experiment are predicted by the model. I am able to offer a cellular level mechanism to explain a psychophysical result. Although I was not able to complete the MEG study, the paradigm is available to be investigated in terms of non-invasive recording of field potentials.

Secondly, experimental variability and ongoing activity. I have demonstrated that applying white noise, synaptic and oscillatory input at the cellular level to the model is able to produce field potential power spectral distributions comparable to biologically recorded ongoing activity. I have shown that the response properties of the model produce stimulus related frequency events in separable frequency bands and power and phase properties similar to recorded field potentials. I have shown in the model properties of sensory integration in relation to ongoing activity similar to reported experimental results. I have shown that the model predicts perception variability in the same relationship to phase as in my behavioural results. I am able to offer a mechanistic interpretation of this relationship. This interpretation suggests

analysis approaches not fully explored in the literature.

Thirdly, the inverse problem and source localization. I have demonstrated that there are stereotypical responses to input in relation to ongoing activity. Using independent component analysis I have localised potential cortical sources. The experimental MEG data I have presented has demonstrated potential comparison with the simulated network stereotypical responses over time. Should there be a strong correspondence between the biological and simulated responses, the model is suited as a test bed to suggest further paradigms for experimental exploration.

Each of the assertions made in this thesis must of course be taken in the context of the limitations of the study and, of course, suggest further work. The model utilises the best mean properties of the cortical microcircuit, layer 6 is not represented, and as such makes a wide number of assumptions. The input used in this study is also generalised to the point where some interpretations are somewhat stretched. For example that increasing the standard deviation is equivalent to synchronised local input, that long range excitatory input is either a DC or a sinusoidal AC current, or that bottom up input is suitably represented by a population of rate coding Poisson spiking neurons. The field potential output is a first approximation taken from a model with no spatial extension. The complexities in the field potential's multiple subcellular sources can not be encompassed in the LIF model.

Whilst the behavioural results do strongly support the model, I have been unable to successfully verify it using field potential recordings, nor have I been able to strongly identify a stereotypical stimulus response between my MEG data and the model. I have also not yet attempted to verify the model at a cellular level.

That being said, these limitations do not reduce the level of verification I have achieved with the model, or its central role in the successful experimental design, prediction of results and derivation of a hypothesised underlying mechanism. All these limitations suggest further work. The model may also be able to be compared with simpler cortical models used to explain large scale dynamics, such as that used in dynamic causal modelling and the dynamical systems model presented by Curto(David 2006a; David, 2006b; Curto, 2009)

Further work could take three courses : Deeper analysis of the existing data; further behavioural and MEG experimentation; and development of the model.

Further analysis of the behavioural data could include an investigation into the apparent response time dependence upon ASSR frequency. It has been shown that there is a resonance response to the auditory steady state stimulus at 40 Hz that may suggest a stronger network effect upon infor-

mation transfer in the cortical network(Azzena et al., 1995; Santarelli et al., 1995; John and Picton, 2000; Ross et al., 2000). There are variations in the latency of maximal information in the simulation data that may support this. An analysis of the independent information in spike train and field potential responses could go further towards verification of the model at the local level. As could an investigation into correlations between individual cells. The MEG data could be explored further to investigate communication and causality between the areas represented by the independent components. This could also be extended to the other independent components not investigated here.

Further behavioural and MEG experimentation could include finding a solution to the delivery of the auditory steady state stimulus. This could involve an ambient presentation of the stimulus. Should a solution be found a study of the second behavioural experiment could suggest the source of the inverse phase relationship when the ASSR stimulus is absent. Pilot data also suggested that the response probability phase dependence extended into the second post stimulus wavelength. This would demonstrate a persistent induced cortical osculation. There effect shown here was only investigated for a 10 Hz condition, it would be worth pursuing an investigation into other frequencies to determine whether the response was frequency independent. If this was the case it may suggest that the same mechanism is involved for both effects.

Further development of the model could in the first instance be an improvement in the realism of the input. Recorded thalamic stimulus responses could be used rather than the Poisson spike generators. For long range inputs two models could be coupled together to investigate intracortical interactions. The simulation environment is able to communicate with other simulation environments, so it would be possible to couple the model with neuronal mass models with parameters derived using dynamic causal modelling to attempt to fit simulations with experimental data. Alternatively multiscale modelling could be employed to obtain a more biophysically realistic spatially extended field potential signal.

Appendix A

Additional components from the MEG study

A.0.0.1 Independent components

A.0.0.2 Independent components power spectra

A.0.0.3 Independent components time frequency response for positive response

A.0.0.4 Independent components time frequency relative response for positive response

A.0.0.5 Independent components time frequency response for positive response minus negative response

A.0.0.6 Independent components time frequency relative response for positive response minus negative response

A.0.0.7 Independent components Mutual information between time frequency power and response

A.0.0.8 Independent components Mutual information between time frequency phase and response

Figure A.1: Independent components

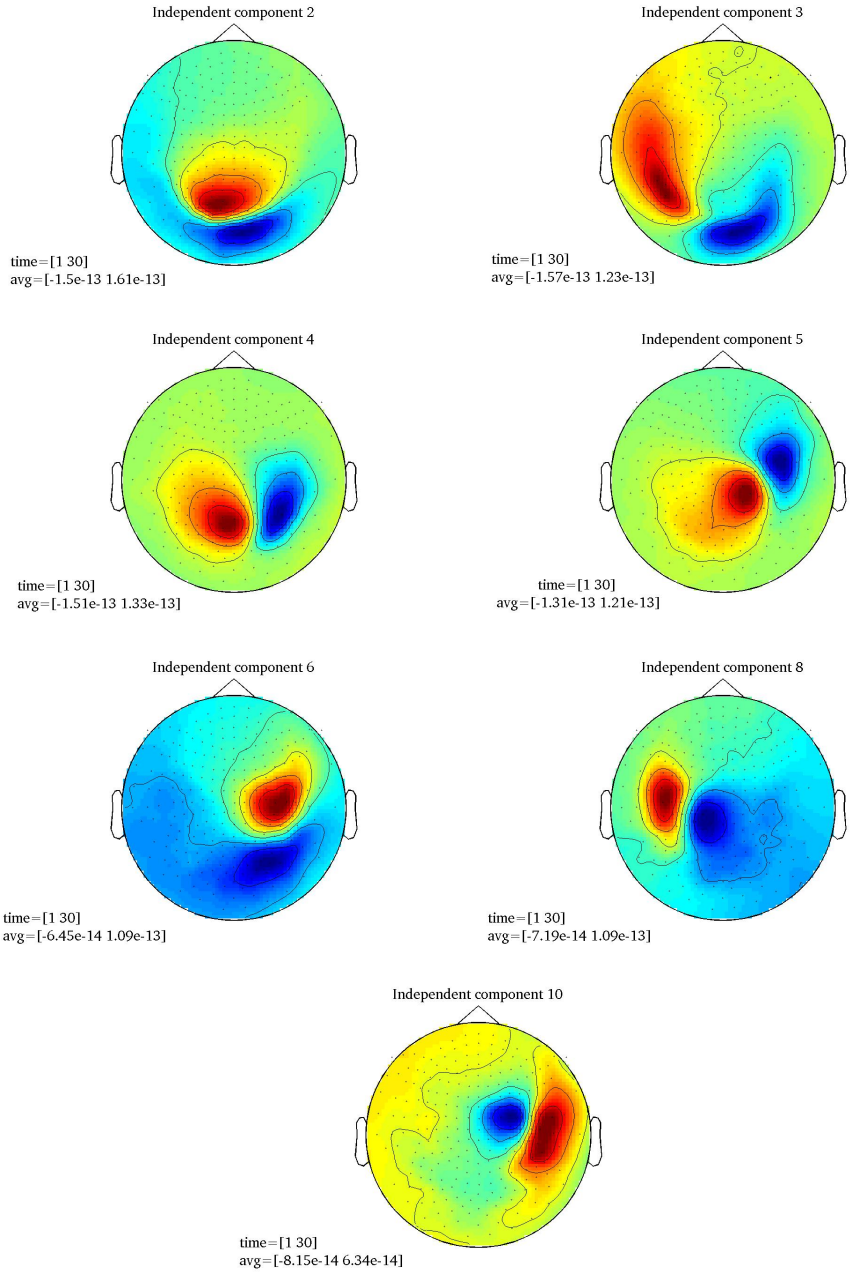

Figure A.2: Independent components power spectra

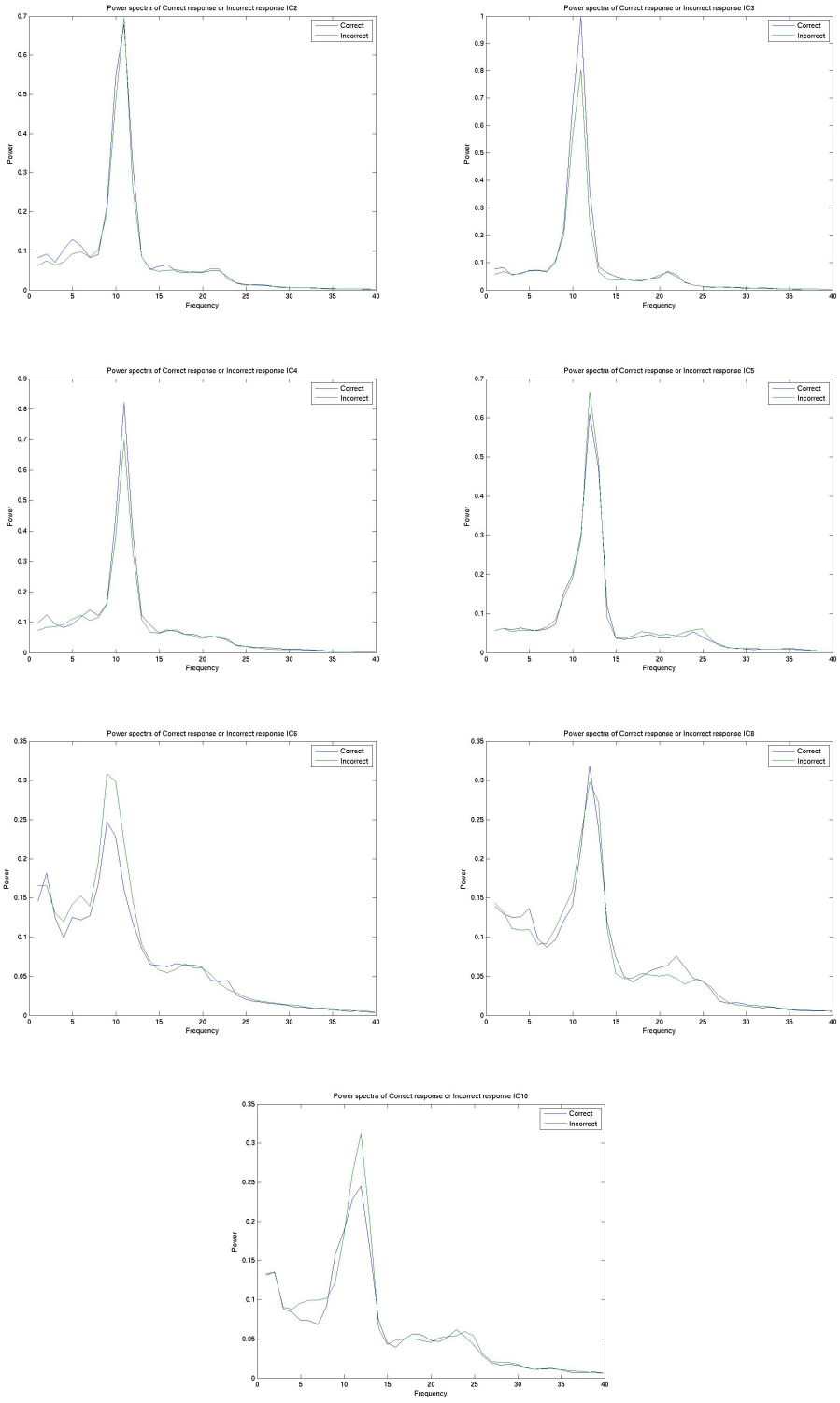

Figure A.3: Independent components time frequency response for positive response

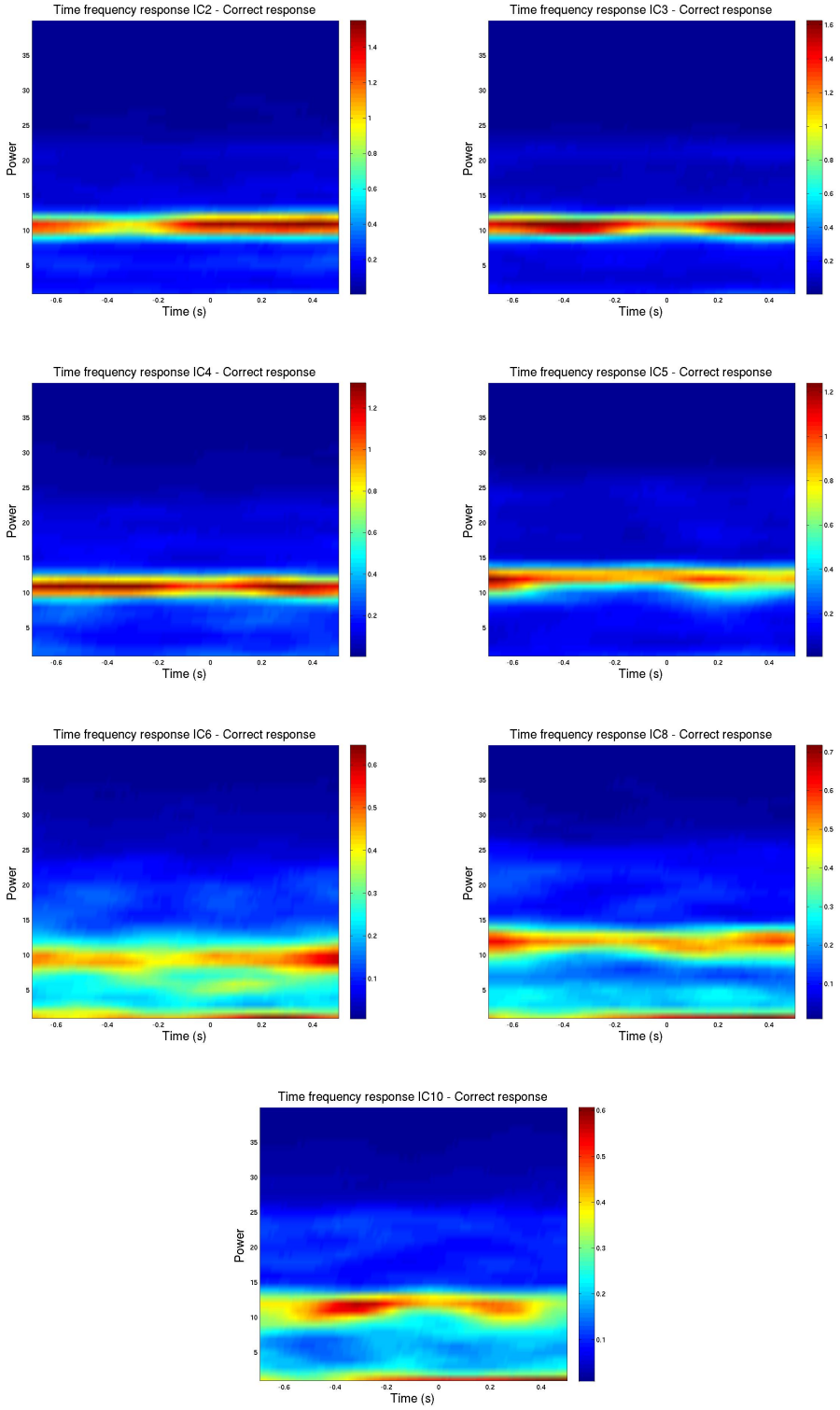

Figure A.4: Independent components time frequency relative response for positive response

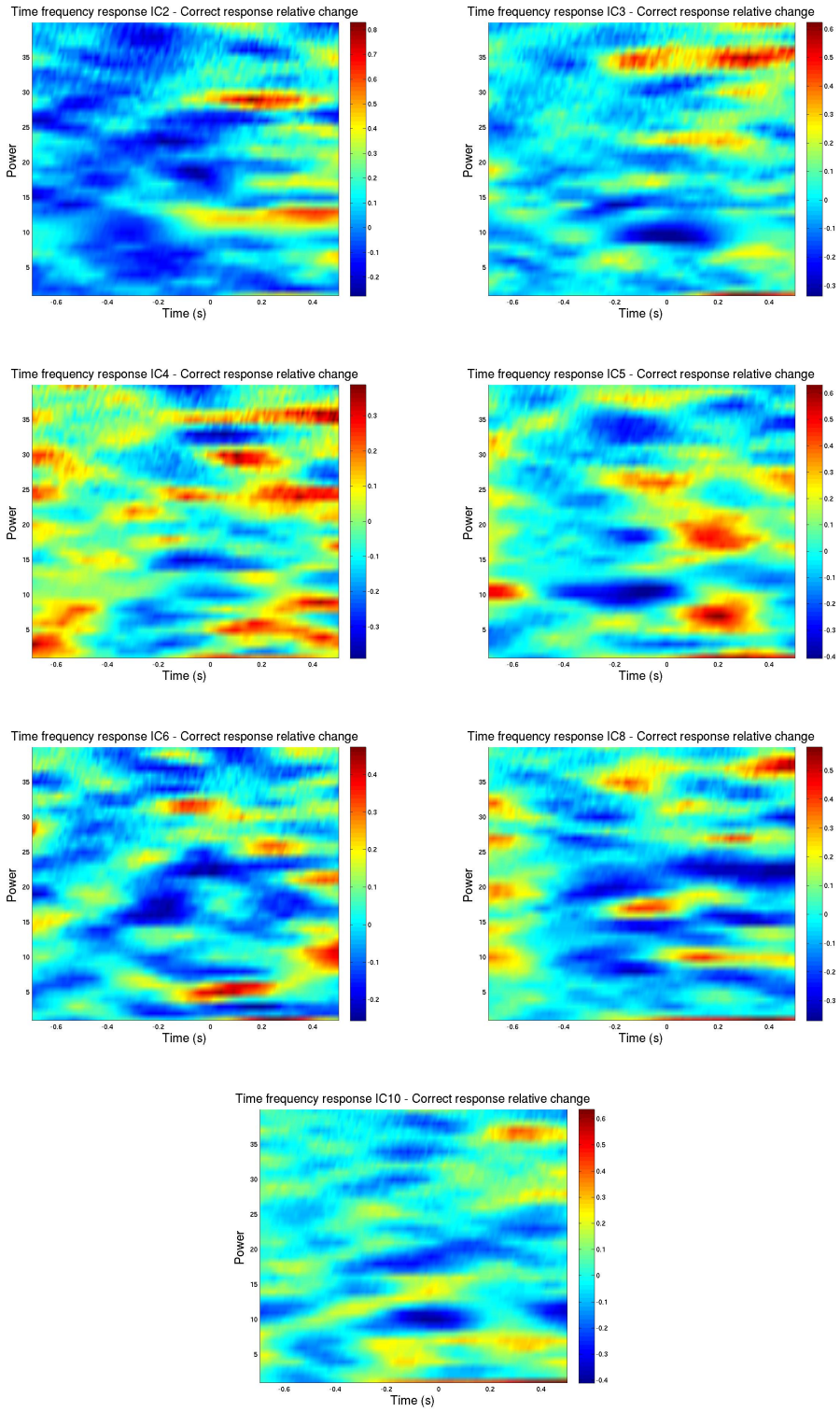

Figure A.5: Independent components time frequency response for positive response minus negative response

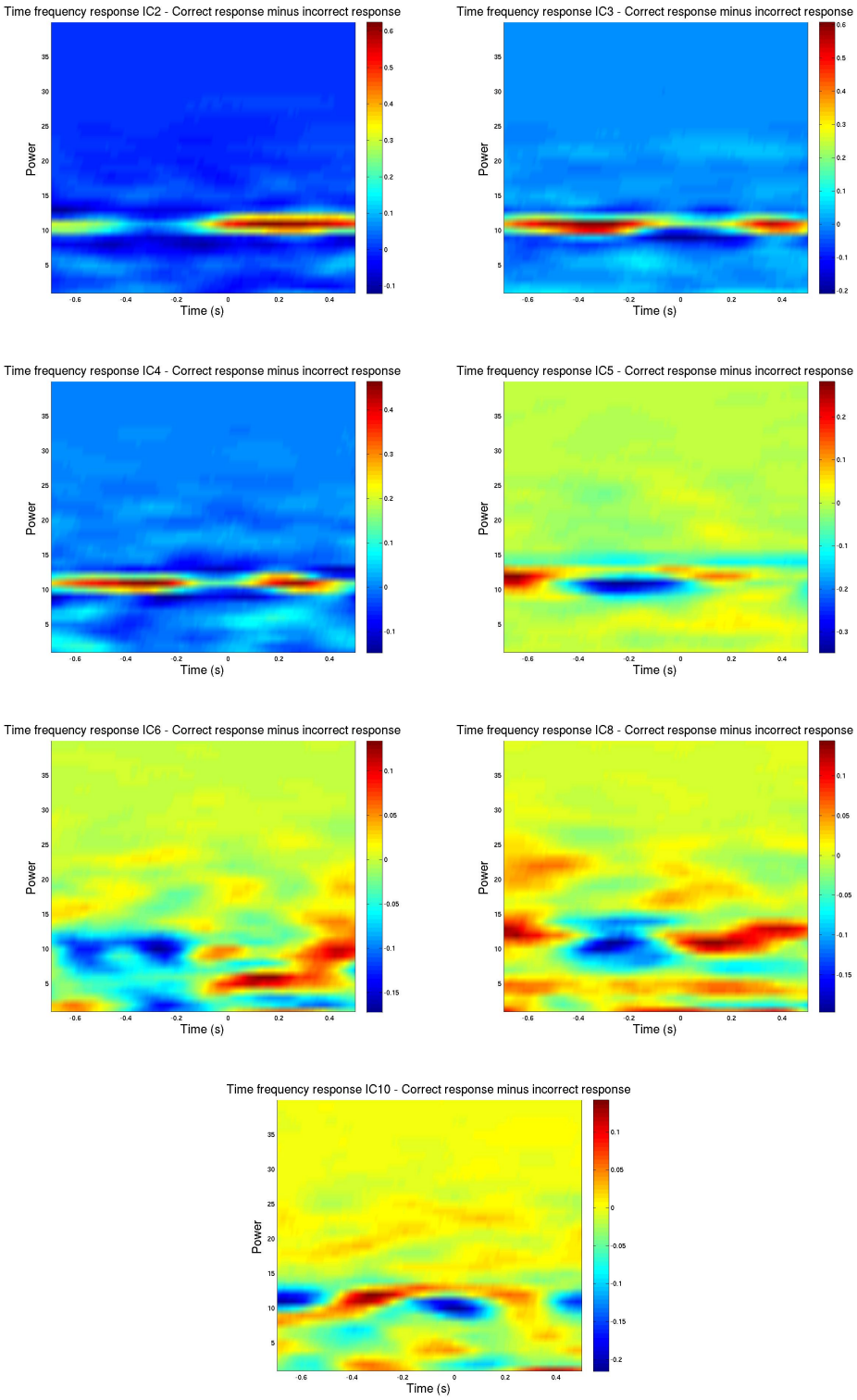

Figure A.6: Independent components time frequency relative response for positive response minus negative response

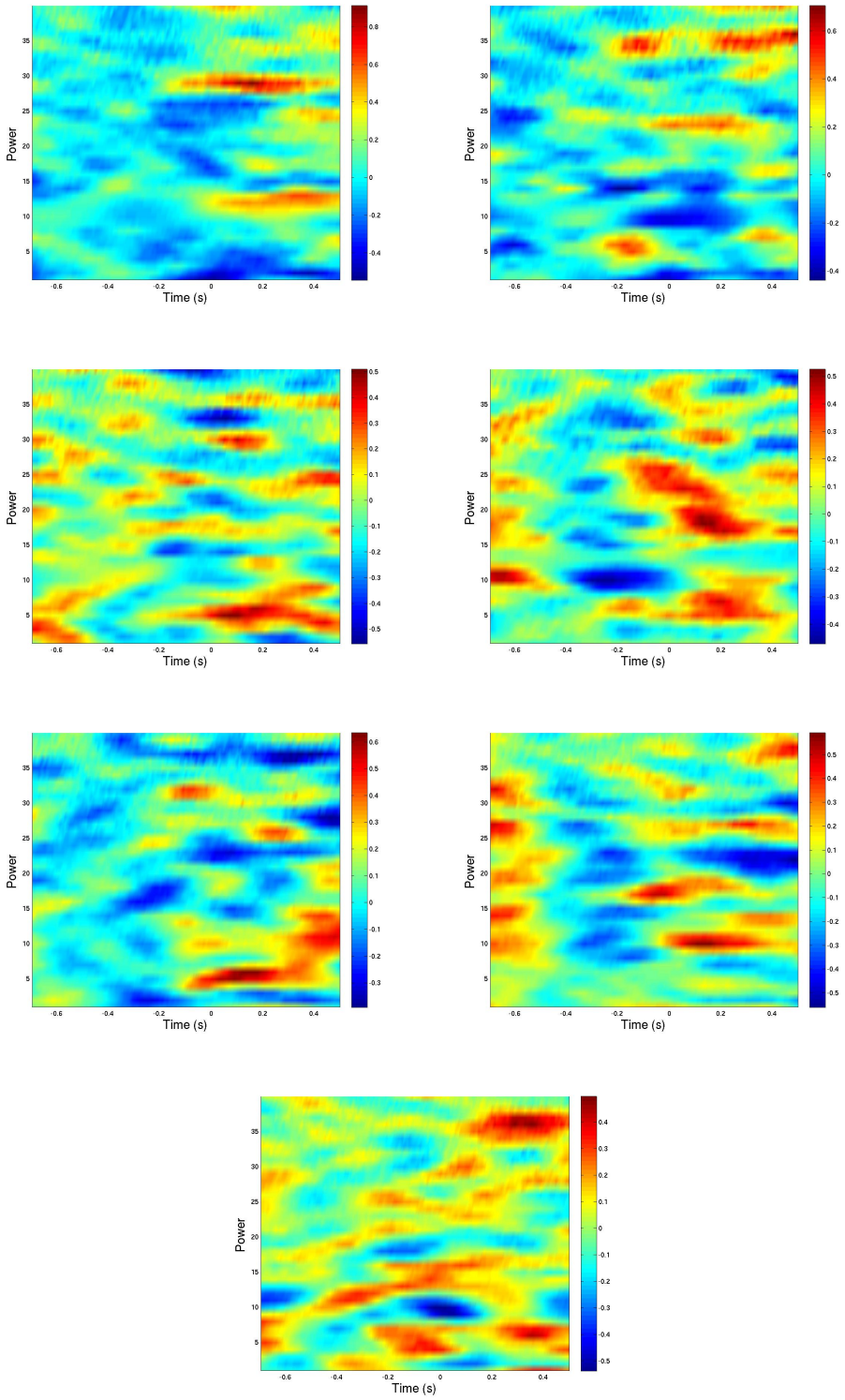

Figure A.7: Independent components Mutual information between time frequency power and response

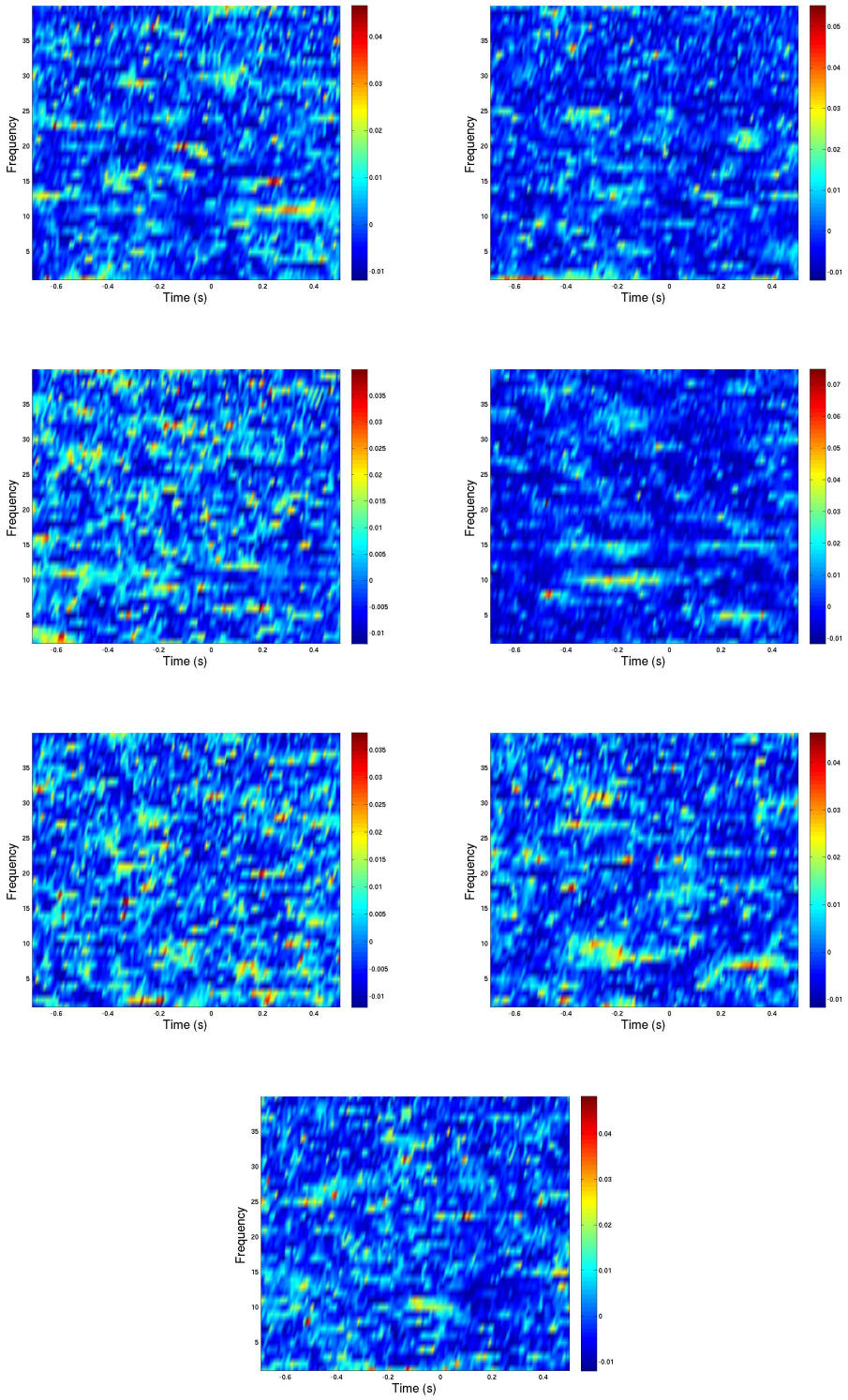

Figure A.8: Independent components Mutual information between time frequency phase and response

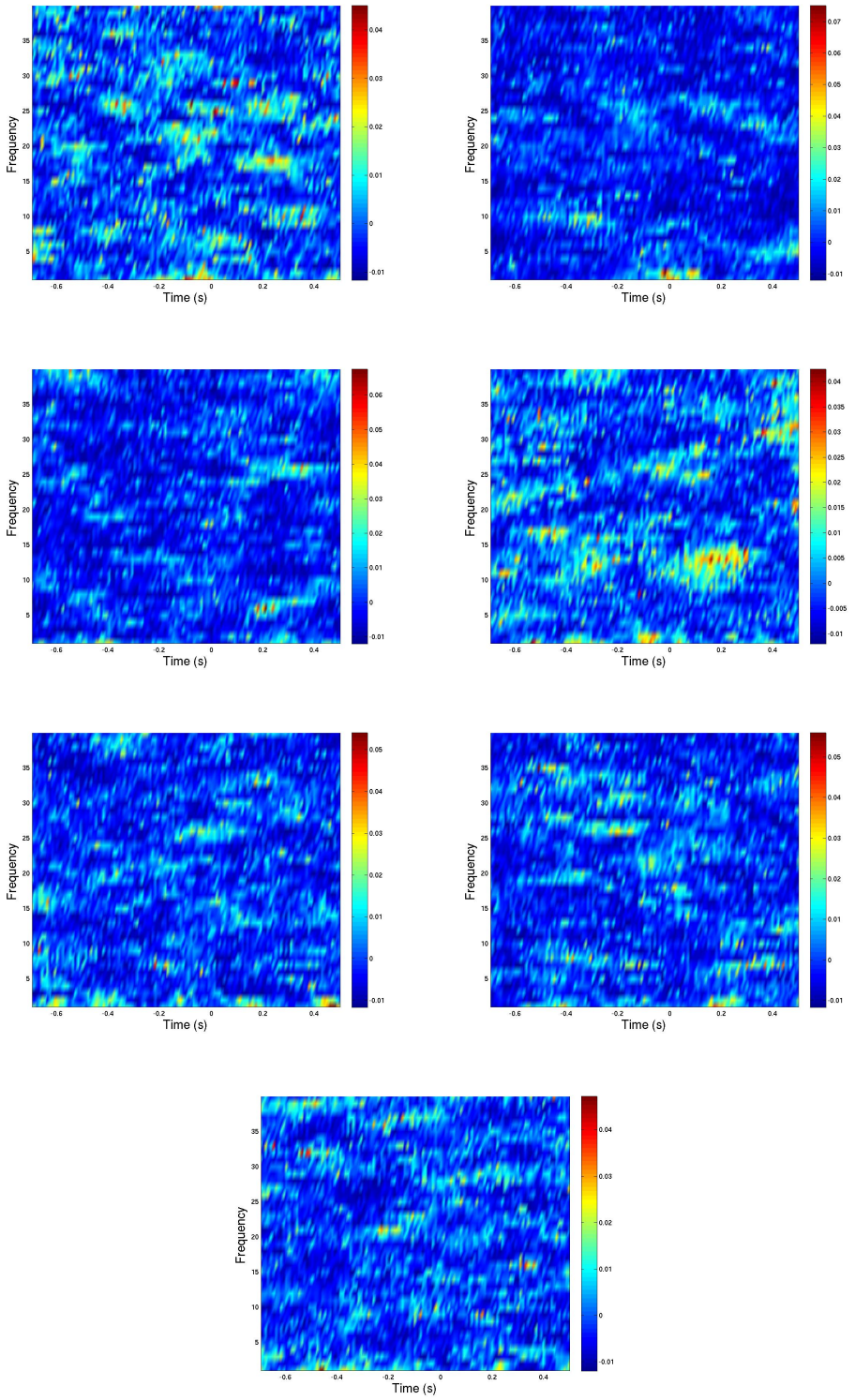

Appendix B

List of references

Arabzadeh E, Panzeri S, Diamond ME(2004) Whisker vibration information carried by rat barrel cortex neurons. Journal of Neuroscience. 24(26):6011-6020.

Arieli A, Sterkin A, Grinvald A, Aertsen A (1996) Dynamics of ongoing activity: explanation of the large variability in evoked cortical responses. Science 273:1868-1871.

Bedard C. Kroger H. Destexhe A. (2006) Does the 1/f frequency scaling of brain signals reflect self-organized critical states Phys. Rev. Lett., 97: 118102.

Azzena GB, Conti G, Santarelli R, Ottaviani F, Paludetti G, Maurizi M (1995) Generation of human auditory steady-state responses (SSRs). I: Stimulus rate effects. Hear Res 83:1-8.

Berens P, CircStat (2009) A Matlab Toolbox for Circular Statistics, Journal of Statistical Software, Volume 31, Issue 10,

Bergholz R, Lehmann TN, Fritz G, Ruther K (2008) Fourier transformed steady-state flash evoked potentials for continuous monitoring of visual pathway function. Doc Ophthalmol 116:217-229.

Brunel N (2000) Dynamics of sparsely connected networks of excitatory and inhibitory spiking neurons. J Comput Neurosci 8:183-208.

Brunel N, Hakim V (1999) Fast global oscillations in networks of integrate-and-fire neurons with low firing rates. Neural Comput 11:1621-1671.

Brunel N, Wang XJ (2003) What determines the frequency of fast network oscillations with irregular neural discharges? I. Synaptic dynamics and excitation-inhibition balance. J Neurophysiol 90:415-430.

Buzsaki G (2006) Rhythms of the brain (Oxford, Oxford university press)

Burkitt AN (2006a) A review of the integrate-and-fire neuron model: I. Homogeneous synaptic input. Biol Cybern 95:1-19.

Burkitt AN (2006b) A review of the integrate-and-fire neuron model: II.

Inhomogeneous synaptic input and network properties. Biol Cybern 95:97-112.

Busch N, Dubois J, VanRullen R (2009) The phase of ongoing EEG oscilations predicts visual perception. The Journal of Neuroscience 29(24):7869-7876

Curto C, Sakata S, Marguet S, Itskov V, Harris K (2009) A simple model of cortical dynamics explains variability and state dependence of sensory responses in Urethane Anesthitized auditory cortex. The Journal of Neuroscience 29(34):10600-10612

David O, Friston KJ (2003) A neural mass model for MEG/EEG: coupling and neuronal dynamics. Neuroimage 20:1743-1755.

David O, Harrison L, Friston KJ (2005) Modelling event-related responses in the brain. Neuroimage 25:756-770.

David O, Kilner JM, Friston KJ (2006a) Mechanisms of evoked and induced responses in MEG/EEG. Neuroimage 31:1580-1591.

David O, Kiebel SJ, Harrison LM, Mattout J, Kilner JM, Friston KJ (2006b) Dynamic causal modeling of evoked responses in EEG and MEG. Neuroimage 30:1255-1272.

Dempster M, A (2006) Understanding the specific neural mechanisms underlying Local Field Potentials by means of computer simulation. In: Optometry and Neuroscience. Manchester: The University of Manchester Institute of Science and Technology.

Dempster M, A (2007a) An analysis of electrophysiological recording from the rat somatosensory cortex. In: The Faculty of Life Science. Manchester: The University of Manchester.

Dempster M, A (2007b) A new mechanistic model for the exploration of cortical Local Field Potentials. In: Faculty of Life Sciences. Manchester: The University of Manchester.

Dyan P, Abbot L F (2001) Theoretical neuroscience: computational and mathematical modeling of neural systems. (Cambridge, Mass MIT Press)

Fries P (2005) A mechanism for cognitive dynamics: neuronal communication through neuronal coherence. Trends Cogn Sci 9:474-480.

Fries P, Nikolic D, Singer W (2007) The gamma cycle. Trends Neurosci 30:309-316. Gewaltig M-O and Diesmann M (2007) NEST (Neural Simulation Tool) Scholarpedia 2(4):1430.

Haeusler S, Maass W (2007) A statistical analysis of information-processing properties of lamina-specific cortical microcircuit models. Cereb Cortex 17:149-162.

Hanuschkin A, Kunkel S, Helias M, Morrison A, Diesmann M (2010) A general and efficient method for incorporating precise spike times in globally time-driven simulations. Front Neuroinform 4:113.

Haslinger R, Ulbert I, Moore CI, Brown EN, Devor A (2006) Analysis of LFP phase predicts sensory response of barrel cortex. J Neurophysiol 96:1658-1663.

Herron J (1980) Neuropsychology of left-handedness. New York ; London: Academic Press.

Hines, M.L. and Carnevale, N.T(2003) The NEURON simulation environment. In: The Handbook of Brain Theory and Neural Networks, 2nd ed, edited by M.A. Arbib. Cambridge, MA: MIT Press, pp. 769-773.

Hodgkin AL, Huxley AF (1952a) The dual effect of membrane potential on sodium conductance in the giant axon of Loligo. J Physiol 116:497-506.

Hodgkin AL, Huxley AF (1952b) Currents carried by sodium and potassium ions through the membrane of the giant axon of Loligo. J Physiol 116:449-472.

Hodgkin AL, Huxley AF (1952c) A quantitative description of membrane current and its application to conduction and excitation in nerve. J Physiol 117:500-544.

Hodgkin AL, Huxley AF (1952d) Propagation of electrical signals along giant nerve fibers. Proc R Soc Lond B Biol Sci 140:177-183.

Hodgkin AL, Huxley AF (1952e) Movement of sodium and potassium ions during nervous activity. Cold Spring Harb Symp Quant Biol 17:43-52.

Hodgkin AL, Huxley AF (1952f) The components of membrane conductance in the giant axon of Loligo. J Physiol 116:473-496.

Hodgkin AL, Huxley AF, Katz B (1952) Measurement of current-voltage relations in the membrane of the giant axon of Loligo. J Physiol 116:424-448.

Jansen BH, Rit VG (1995) Electroencephalogram and visual evoked potential generation in a mathematical model of coupled cortical columns. Biol Cybern 73:357-366.

Jansen BH, Zouridakis G, Brandt ME (1993) A neurophysiologically-based mathematical model of flash visual evoked potentials. Biol Cybern 68:275-283.

John MS, Picton TW (2000) Human auditory steady-state responses to amplitude-modulated tones: phase and latency measurements. Hear Res 141:57-79.

Kamondi A, Acsady L, Buzsaki G (1998a) Dendritic spikes are enhanced by cooperative network activity in the intact hippocampus. J Neurosci 18:3919-3928.

Kamondi A, Acsady L, Wang XJ, Buzsaki G (1998b) Theta oscillations in somata and dendrites of hippocampal pyramidal cells in vivo: activity-dependent phase-precession of action potentials. Hippocampus 8:244-261.

Kandel ER, Schwartz JH, Jessell TM (2000) Principles of neural science, 4th ed. Edition. New York ; London: McGraw-Hill, Health Professions

Division.

Kelly SP, Lalor EC, Reilly RB, Foxe JJ (2006) Increases in alpha oscillatory power reflect an active retinotopic mechanism for distracter suppression during sustained visuospatial attention. J Neurophysiol 95:3844-3851.

Kobayashi M, Inoue T, Matsuo R, Masuda Y, Hidaka O, Kang Y, Morimoto T (1997) Role of calcium conductances on spike afterpotentials in rat trigeminal motoneurons. J Neurophysiol 77:3273-3283.

Koch C, Davis JL (1994a) Large-scale neuronal theories of the brain. Cambridge, Mass. ; London: MIT Press.

Koch CE, Davis JLE (1994b) Large-scale neuronal theories of the brain : Workshop : Papers. Cambridge, MA: MIT Press.

Linden H, Tetzlaff T, Potjans TC, Pettersen KH, Grun S, Diesmann M, Einevoll GT (2010) Modeling the spatial reach of the LFP. Neuron 72:859-872.

Linkenkaer-Hansen, K. Nikouline, V.V. Palva, J.M. Ilmoniemi, R.J. (2001). Long-range temporal correlations and scaling behavior in human brain oscillations. J. Neurosci., 21:1370-1377.

Linkenkaer-Hansen K, Nikulin VV, Palva S, Ilmoniemi RJ, Palva JM (2004) Prestimulus oscillations enhance psychophysical performance in humans. J Neurosci 24:10186-10190.

Lopes da Silva FH, Hoeks A, Smits H, Zetterberg LH (1974) Model of brain rhythmic activity. The alpha-rhythm of the thalamus. Kybernetik 15:27-37.

Magri C, Whittingstall K, Singh V, Logothetis NK, Panzeri S (2009) A toolbox for the fast information analysis of multiple-site LFP, EEG and spike train recordings. BMC Neurosci 10:81.

Manganotti P, Formaggio E, Storti SF, Avesani M, Acler M, Sala F, Magon S, Zoccatelli G, Pizzini F, Alessandrini F, Fiaschi A, Beltramello A (2009) Steady-state activation in somatosensory cortex after changes in stimulus rate during median nerve stimulation. Magn Reson Imaging 27:1175-1186.

Mazzoni A, Brunel N, Cavallari S, Logothetis N, Panzeri (2011) Cortical dynamics during sensory simulations: Experiments and Models. Journal of Physiology 2 - 15

Mitzdorf U (1985) Current source-density method and application in cat cerebral cortex: investigation of evoked potentials and EEG phenomena. Physiol Rev 65:37-100.

Mitzdorf U (1987) Properties of the evoked potential generators: current source-density analysis of visually evoked potentials in the cat cortex. Int J Neurosci 33:33-59.

Montemurro MA, Senatore R, Panzeri S (2007) Tight data-robust bounds to mutual information combining shuffling and model selection techniques. Neural Computation . 19(11):2913-57.

Montemurro MA, Rasch MJ, Murayama Y, Logothetis NK, Panzeri S (2008) Phase-of-firing coding of natural visual stimuli in primary visual cortex. Curr Biol 18:375-380.

Nakayama K, Mackeben M (1982) Steady state visual evoked potentials in the alert primate. Vision Res 22:1261-1271.

Nemenman I, Bialek W, de Ruyter van Steveninck R (2004) Entropy and information in neural spike trains: progress on the sampling problem. Physical review E, Statistical, nonlinear, and soft matter physics. 69(5 Pt 2):056111.

Nordlie E, Gewaltig MO, Plesser HE (2009) Towards reproducible descriptions of neuronal network models. PLoS Comput Biol 5:e1000456.

Novikov E. Novikov A. Shannahoff-Khalsa D. Schwartz B Wright J. (1997) Scale-similar activity in the brain. Phys. Rev. E, 56:R2387-R2389.

Okun M, Naim A, Lampl I (2010) The subthreshold relation between cortical local field potential and neuronal firing unveiled by intracellular recordings in awake rats. J Neurosci 30:4440-4448.

Oostenveld R, Fries P, Maris E, and Schoffelen J, (2011) FieldTrip: Open Source Software for Advanced Analysis of MEG, EEG, and Invasive Electrophysiological Data, Computational Intelligence and Neuroscience, vol. 2011, Article ID 156869, 9 pages, 2011. doi:10.1155/2011/156869

Paninski L(2003) Estimation of Entropy and Mutual Information. Neural Computation, 15:1191-1253.

Panzeri S, Senatore R, Montemurro MA, Petersen RS (2007) Correcting for the sampling bias problem in spike train information measures. J Neurophysiol , 98:1064-1072.

Panzeri S, Treves A (1996) Analytical estimates of limited samplingbiases in different information measures. Network: Computation in Neural Systems, 7:87-107.

Panzeri S, Magri C, Logothetis NK (2008) On the use of information theory for the analysis of the relationship between neural and imaging signals. Magn Reson Imaging 26:1015-1025.

Phillips WA, Singer W (1997) In search of common foundations for cortical computation. Behav Brain Sci 20:657-683; discussion 683-722.

Ramkumar P, Parkkonen L, Hari R, Hyvrinen A.(2012) Characterization of neuromagnetic brain rhythms over time scales of minutes using spatial independent component analysis. Human Brain Mapping 33(7):1648-62.

Ross B, Borgmann C, Draganova R, Roberts LE, Pantev C (2000) A high-precision magnetoencephalographic study of human auditory steady-state

responses to amplitude-modulated tones. J Acoust Soc Am 108:679-691.

Rotter S, Diesmann M (1999) Exact Digital Simulation of Time-Invariant Linear Systems with Applications to Neuronal Modeling Biological Cybernetics 81:381-402

Santarelli R, Maurizi M, Conti G, Ottaviani F, Paludetti G, Pettorossi VE (1995) Generation of human auditory steady-state responses (SSRs). II: Addition of responses to individual stimuli. Hear Res 83:9-18.

Schlaggar BL, O'Leary DD (1991) Potential of visual cortex to develop an array of functional units unique to somatosensory cortex. Science 252:1556-1560.

Schnitzler A, Gross J (2005) Normal and pathological oscillatory communication in the brain. Nat Rev Neurosci 6:285-296.

Schoffelen JM, Oostenveld R, Fries P (2005) Neuronal coherence as a mechanism of effective corticospinal interaction. Science 308:111-113.

Steriade M, McCormick DA, Sejnowski TJ (1993) Thalamocortical oscillations in the sleeping and aroused brain. Science 262:679-685.

Sur M (1988) Visual projections induced into auditory thalamus and cortex: implications for thalamic and cortical information processing. Prog Brain Res 75:129-136.

Sur M, Garraghty PE, Roe AW (1988) Experimentally induced visual projections into auditory thalamus and cortex. Science 242:1437-1441.

Thomson AM, Bannister AP (2003) Interlaminar connections in the neocortex. Cereb Cortex 13:5-14.

Thomson AM, Lamy C (2007) Functional maps of neocortical local circuitry. Front Neurosci 1:19-42.

Thomson AM, West DC, Wang Y, Bannister AP (2002) Synaptic connections and small circuits involving excitatory and inhibitory neurons in layers 2-5 of adult rat and cat neocortex: triple intracellular recordings and biocytin labelling in vitro. Cereb Cortex 12:936-953.

Thut G, Schyns PG, Gross J (2011) Entrainment of perceptually relevant brain oscillations by non-invasive rhythmic stimulation of the human brain. Front Psychol 2:170.

Thut G, Nietzel A, Brandt SA, Pascual-Leone A (2006) Alpha-band electroencephalographic activity over occipital cortex indexes visuospatial attention bias and predicts visual target detection. J Neurosci 26:9494-9502.

Tobimatsu S, Zhang YM, Kato M (1999) Steady-state vibration somatosensory evoked potentials: physiological characteristics and tuning function. Clin Neurophysiol 110:1953-1958.

Trappenberg T P (2002) Fundementals of computational neuroscience (Oxford, Oxford university press)

Ursino M, La Cara G E (2006) Travelling waves and EEG patterns during epileptic seizure: analysis with an integrate and fire neural network. Journal of theoretical biology 242, 171-187

Vanrullen R, Busch NA, Drewes J, Dubois J (2011) Ongoing EEG Phase as a Trial-by-Trial Predictor of Perceptual and Attentional Variability. Front Psychol 2:60.

Vinck M, Lima B, Womelsdorf T, Oostenveld R, Singer W, Neuenschwander S, Fries P (2010) Gamma-phase shifting in awake monkey visual cortex. J Neurosci 30:1250-1257.

Wilson M, Bower JM (1992) Cortical oscillations and temporal interactions in a computer simulation of piriform cortex. J Neurophysiol 67:981-995.

Wolfe J, Hill DN, Pahlavan S, Drew PJ, Kleinfeld D, Feldman DE (2008) Texture coding in the rat whisker system: slip-stick versus differential resonance. PLoS Biol 6:e215.

Worden MS, Foxe JJ, Wang N, Simpson GV (2000) Anticipatory biasing of visuospatial attention indexed by retinotopically specific alpha-band electroencephalography increases over occipital cortex. J Neurosci 20:RC63.